REPORT DOCUMENTATION PAGE

Form Approved
OMB No. 0704-0188

1. AGENCY USE ONLY (Leave Blank)	2. REPORT DATE	3. REPORT TYPE AND DATES COVERED
	September 1994	Final

4. TITLE AND SUBTITLE
Improved Design of Microphone-Array Hearing Aids

5. FUNDING NUMBERS

6. AUTHORS
Julie Elise Greenberg

AFRL-SR-BL-TR-98-
0038

7. PERFORMING ORGANIZATION NAME(S) AND ADDRESS(ES)
Massachusetts Institute of Technology

TION

9. SPONSORING/MONITORING AGENCY NAME(S) AND ADDRESS(ES)
AFOSR/NI
110 Duncan Avenue, Room B-115
Bolling Air Force Base, DC 20332-8080

10. SPONSORING/MONITORING AGENCY REPORT NUMBER

11. SUPPLEMENTARY NOTES

12a. DISTRIBUTION AVAILABILITY STATEMENT
Approved for Public Release

12b. DISTRIBUTION CODE

13. ABSTRACT *(Maximum 200 words)*
See attached.

14. SUBJECT TERMS

15. NUMBER OF PAGES

16. PRICE CODE

17. SECURITY CLASSIFICATION OF REPORT	18. SECURITY CLASSIFICATION OF THIS PAGE	19. SECURITY CLASSIFICATION OF ABSTRACT	20. LIMITATION OF ABSTRACT
Unclassified	Unclassified	Unclassified	UL

Improved Design of Microphone-Array Hearing Aids

by

Julie Elise Greenberg

B.S.E., University of Michigan, Ann Arbor (1985)

S.M., Massachusetts Institute of Technology (1989)

Submitted to the Harvard-MIT Division of
Health Sciences and Technology
in Partial Fulfillment of the Requirements
for the Degree of

Doctor of Philosophy

at the

MASSACHUSETTS INSTITUTE OF TECHNOLOGY

September 1994

Signature of Author Julie Elise Greenberg
Harvard-MIT Division of Health Sciences and Technology
August 31, 1994

Certified by Pat Zurek
Patrick M. Zurek
Principal Research Scientist, Research Laboratory of Electronics
Thesis Supervisor

Accepted by _____
Roger G. Mark
Chairman, Departmental Committee on Graduate Students

Improved Design of Microphone-Array Hearing Aids

by

Julie Elise Greenberg

Submitted to the Harvard-MIT Division of Health Sciences and Technology
on August 31, 1994, in partial fulfillment of the requirements
for the Degree of Doctor of Philosophy

Abstract

A common complaint of hearing-aid users is the difficulty encountered when listening to a talker in a noisy environment. Conventional hearing aids amplify all sounds without discriminating between the desired source (target) and background noises (jammers). These devices increase the overall sound levels, but do nothing to improve target-to-jammer ratio (TJR). Research on microphone-array hearing aids is motivated by the lack of success of single-microphone systems, as well as the documented advantages of binaural hearing and multiple-element sensing systems.

Array processing can be classified as either fixed (time invariant) or adaptive (time varying). Previous work on microphone-array hearing aids has demonstrated that under certain conditions, adaptive arrays can provide significantly better performance than simpler fixed arrays. The benefit of adaptive systems is realized when the input TJR is low and when the signals arriving via direct paths are stronger than the reflections. This benefit is reduced or eliminated at high TJR or in strong reverberation. This work studies modified adaptive algorithms to improve performance at high TJR and in reverberation; it also provides complete specifications for the design of an adaptive microphone-array hearing aid.

In particular, two previously proposed *ad hoc* methods for controlling adaptation at high TJR are analyzed and evaluated. The results confirm the usefulness of these methods and provide guidelines for selecting relevant parameters in anechoic and reverberant environments. In addition, an analysis of the specific causes of target cancellation in reverberation reveals that a simple set of parameter choices can solve this problem.

Computer simulations of the complete system demonstrate its benefits in a variety of acoustic environments. Steady-state results show that the system provides very large improvements in relatively anechoic environments. Substantial benefits are provided in moderate reverberation, particularly if relatively long filters ($\sim$ 100 ms) are used. In extreme reverberation, performance is comparable to that obtained with the underlying non-adaptive microphone array. Transient results indicate that convergence is sufficiently rapid for processing speech signals. The number of microphones required in a practical system and the use of directional microphones are discussed.

Thesis Supervisor: Patrick M. Zurek
Title: Principal Research Scientist, Research Laboratory of Electronics

Acknowledgements

This research was supported by the National Institute on Deafness and Other Communication Disorders grant number DC00270, the Air Force Office of Scientific Research Laboratory Graduate Fellowship Program, and the Harvard-MIT Division of Health Sciences and Technology Medical Engineering and Medical Physics Fellowship.

I was fortunate to do this research in the supportive atmosphere of the Sensory Communication Group, surrounded by a number of extraordinarily talented people. I am especially grateful to Pat Zurek, who supervised this thesis. He was always available for discussion, and this work would not have been possible without his ideas, advice, and guidance. Thanks are due to Lou Braida, who chaired the thesis committee, and Bill Rabinowitz and Derek Rowell, who served as readers. This work benefited greatly from their technical expertise. In addition, I had the pleasure of working with a number of fellow multimikers over the years; Pat Peterson, Wolf Knecht, Rob Stadler, Jay Desloge, Mike O'Connell and Dan Welker all contributed to various stages of this research.

I could not have completed this thesis without the support, both technical and moral, of many wonderful folks on the seventh floor. They are too numerous to list here, but Rosalie, Lorraine, Ann, and Louise deserve special mention. Many thanks to Danielle for her careful proofreading of a draft of this document. I am indebted to Joe, for expertly answering all of my computer questions and for organizing diverting expeditions, and to my former (and future?) officemate Paul, from whom I have learned many useful things, including how to answer questions when giving a talk.

I thank my parents, brother, and sister for their perpetual encouragement and belief in my abilities. Finally, I want to express my gratitude to Ron, for his unwavering confidence in me and for his help with the little things, as well as the big ones.

Contents

Chapter 1

Introduction

A common complaint of hearing-aid users is the difficulty encountered in listening to talkers in noisy environments (Plomp, 1978; Smedley and Schow, 1990). Conventional hearing aids amplify all sounds without discriminating between the desired source (target) and background noises (jammers). These devices increase the overall sound levels, but do nothing to improve target-to-jammer ratio (TJR). A variety of techniques have been investigated for single-microphone speech enhancement, but none of these techniques has improved speech intelligibility in the presence of broadband jammers such as competing speech (Lim and Oppenheim, 1979; Weiss and Neuman, 1993; Dillon and Lovegrove, 1993). The lack of success of single microphone systems, together with the documented advantages of binaural hearing and, more generally, multiple-element sensing systems, has led to substantial research interest in microphone-array hearing aids.

The ideal hearing aid is one that replaces the functions of normal binaural hearing, providing a signal or signals that allow the listener to focus on one source while simultaneously monitoring other directions (Durlach and Colburn, 1978). An artificial system to replace binaural capabilities could be composed of two stages. The first stage would decompose the acoustic environment into directional channels, each containing an isolated signal emanating from a particular direction. The second stage then consists of a coding scheme that would allow the user to focus on any single channel while simultaneously monitoring all other channels.

A necessary component of the ideal hearing aid, and one that would be useful in its own right, is a system that maximizes the target-to-jammer ratio (TJR) assuming a known target direction. Even in the absence of schemes for separating and coding multiple directional sources, this component of the first stage could be incorporated in a system with user controls for steering to a selected target direction, or in which the target direction is fixed.

Previous research has demonstrated that adaptive microphone-array systems have potential as an effective way to perform this signal extraction (Greenberg and Zurek, 1992). However, several pressing problems remain that must be addressed before microphone arrays can perform successfully in a variety of acoustic environments. This thesis proposes solutions to those problems and demonstrates their effectiveness with computer simulations. The goal of this work is the development of a practical system for microphone-array hearing aids.

Although the focus of this thesis is the improvement of conventional hearing aids, the results are applicable to other aids such as cochlear implants. More generally, the system described in this thesis may be of use in any situation where reduction of interference from spatially-separated sound sources is required. Examples of such situations include general microphone systems, hands-free telephones, teleconference systems, and automatic speech recognition devices.

The remainder of this thesis is organized as follows. Chapter 2 reviews relevant signal processing concepts and previous work on microphone-array hearing aids. It also contains a summary of problems identified by previous work and motivations for the solutions investigated in the following chapters. Chapter 3 describes methods common to several aspects of the current work, including source materials, simulated rooms, and the performance metric. Chapters 4–6 each address a particular issue with implications for designing microphone-array hearing aids. The results of these three chapters specify a modified adaptive algorithm that is subsequently implemented in computer simulations. The results of those simulations are presented in Ch. 7, illustrating the performance that can be obtained with adaptive microphone-array systems in a variety of acoustic environments. Chapter 8 contains a discussion that

includes recommendations for future work, and Ch. 9 consists of a summary and conclusions.

Chapter 2

Background

2.1 Array Processing

This section provides a brief description of signal processing concepts and terminology relevant to this work. A thorough presentation of array processing, beamforming, and adaptive signal processing can be found in the extensive literature available on these subjects (e.g., Van Veen and Buckley, 1988; Widrow and Stearns, 1985; Monzingo and Miller, 1980; Haykin, 1985; Haykin, 1986; Johnson and Dudgeon, 1993).

The bulk of research concerning the design and analysis of array processors has been for applications in radar, sonar, and geophysics. Although the basic principles and some algorithms from these fields are applicable to the hearing-aid problem, several significant differences exist. First, in hearing aids the signals are speech, a broadband signal, while much of the array processing literature is restricted to the somewhat simpler narrowband case. Second, assuming that cosmetic considerations limit the design to head-sized arrays, for the hearing-aid problem the spatial aperture will be small relative to the wavelengths of interest. Furthermore, whereas in some fields the concept of multipath refers to a small number of reflections with substantially less energy than the direct signal, in a typical room the reverberant sound arrives from countless directions and may have significantly more energy than the direct sound. And finally, although this work does not directly address the issues of implementing an algorithm in a practical hearing aid, necessary restrictions on

processor size and power consumption will ultimately impose severe limitations on computational complexity in a wearable device.

Recent literature does contain some applications of microphone arrays to speech processing. In addition to hearing aids, these applications include hands-free telephony (Goulding and Bird, 1990; Claesson et al., 1991; Grenier, 1993), preprocessing for speech recognition (Van Compernolle et al., 1991; Parry, 1990), cockpit communication systems (Harrison et al., 1986), and general microphone systems (Kaneda and Ohga, 1986; Lu and Clarkson, 1993; Flanagan et al., 1991).

Array processors can be classified as either fixed or adaptive. Fixed or data-independent processing applies fixed filters to each microphone signal and sums the results to produce a single output. The weights are typically selected to optimize a quantity such as directivity (the array's response to a signal from straight ahead relative to its diffuse-field response). On the other hand, adaptive processors utilize time-varying filters that are adjusted to approach a statistical optimum (in a least-squares sense) while tracking changes in the environment. Adaptive processing usually requires more intensive computation than fixed processing, but may provide better performance against directional and time-varying jammers. The advantage of adaptive processing is realized if the underlying optimum processor outperforms a fixed processor with an equal number of sensors and if the non-stationarity in the environment is slow relative to the time required for the adaptive algorithm to converge.

The choice of the optimality criterion for an adaptive system is dictated by the information assumed to be available about the signals and the environment. Peterson (1989) showed that many different optimum processors (minimum mean-square error, maximum *a posteriori* probability, maximum likelihood, and minimum variance) are identical to within a scalar function of frequency dependent only on the assumed *a priori* knowledge of the target and jammer spectra. Two adaptive systems often considered for use in the hearing aid application are the adaptive noise canceller (Widrow, et al., 1975) and the linearly constrained minimum variance (LCMV) beamformer (Frost, 1972). The adaptive noise canceller (ANC) requires a reference

signal related to the jammer, but free of target. The LCMV beamformer requires that the target direction is known and that the target signal is uncorrelated with all jammer signals.

A block diagram of the adaptive noise canceller is shown in Figure 2.1. This system requires two inputs, a primary signal that contains target plus jammer and a reference signal that ideally contains a filtered version of the jammer only. An adaptive filter then operates on the reference input using the LMS algorithm (Widrow and Stearns, 1985) to minimize the total output power of the system. If the reference contains no target and if the target and jammer are uncorrelated, minimizing the total output power is equivalent to minimizing the jammer power. For the hearing-aid application, it is usually not possible to obtain a reference signal that is perfectly free of target. Instead, the reference signal is obtained from either a directional microphone pointed away from the target or a remote microphone placed close to the noise source. Any 'leakage' of the target into the reference channel can lead to cancellation of the target, a situation to be avoided. Although the results of previous work with adaptive noise cancellers can provide insight into issues relevant to the design of microphone-array hearing aids, this work will only consider systems that do not require a 'target-free' reference signal.

The LCMV beamformer assumes that the direction of the target signal is known, and that the target and jammer signals are uncorrelated. The weights are adjusted to minimize output power subject to constraints that apply a specified filter to the signal arriving from the target direction. The two basic structures used to implement LCMV beamforming are the linearly constrained adaptive array processor (Frost, 1972) and the generalized sidelobe canceller (Griffiths and Jim, 1982), shown in Figs. 2.2 and 2.3. For simplicity, the implementations in the figures do not show the initial stage of time-delay steering required to align the array to the target signal.

The structure used to implement Frost's linearly constrained adaptive array processor consists of a tapped delay line for each microphone signal. There is a single adaptive weight associated with each tap, and the output consists of the sum of all weighted tap values. The adaptive weights are updated by an iterative constrained

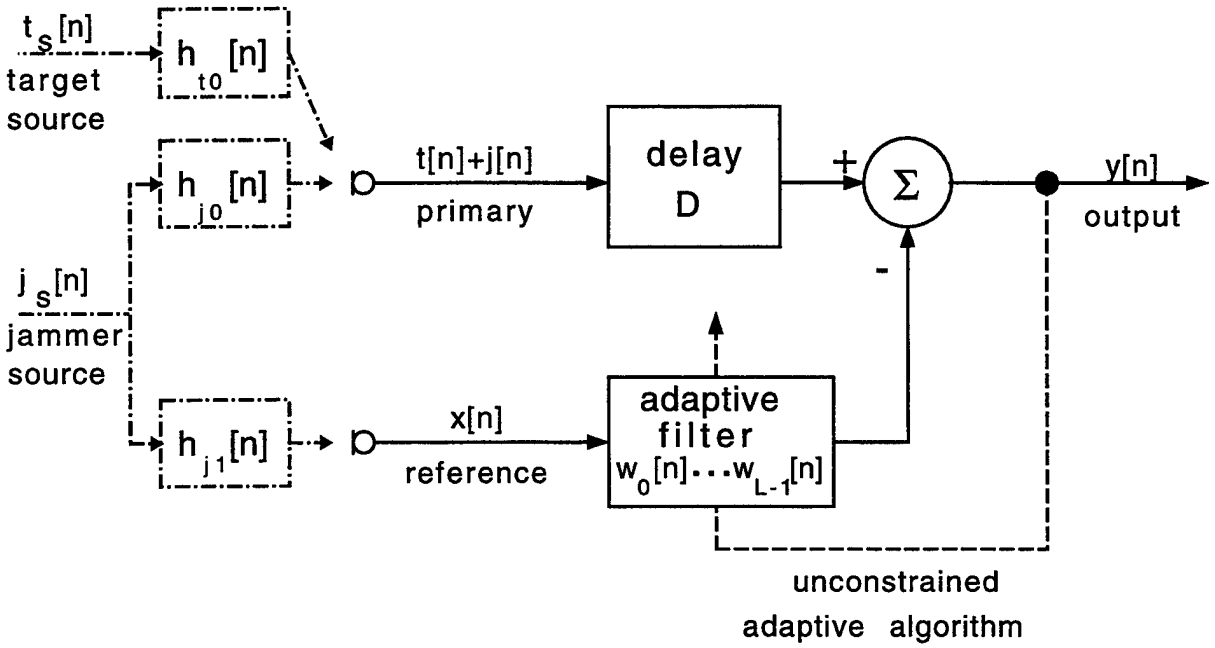

Figure 2-1: Block diagram of adaptive noise canceller. The two inputs are a primary signal, containing filtered versions of the target and jammer sources, and a reference signal, containing a different filtered version of the jammer. The reference signal is the input to an L-point adaptive filter. The adaptive noise canceller output, $y[n]$, is the difference between the delayed primary signal and the output of the adaptive filter. The adaptive weights, $w_k[n]$ for $k = 0, \cdots, L-1$, are adjusted to minimize the total output power, which, under ideal conditions, preserves the target signal and minimizes the jammer output power.

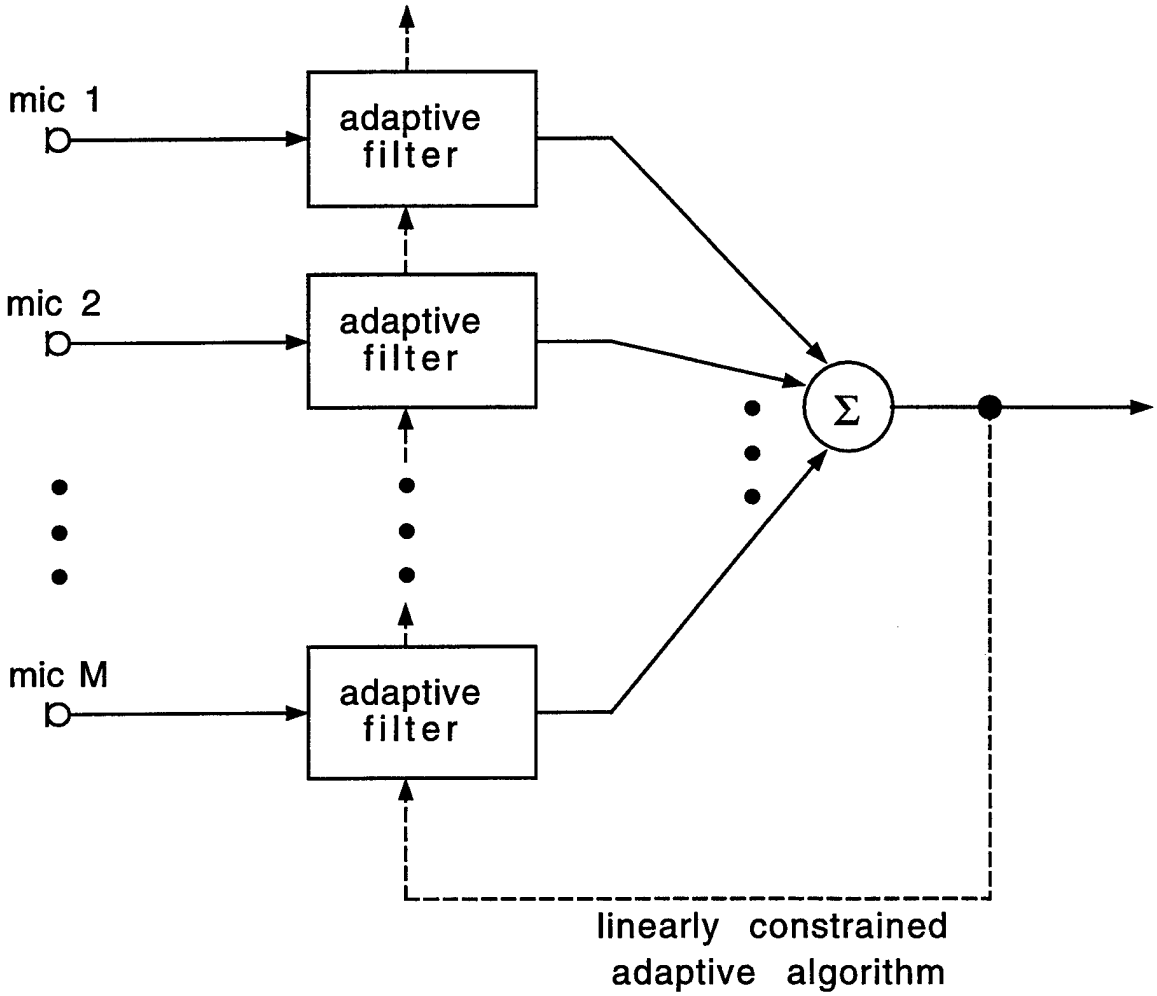

Figure 2-2: Block diagram of linearly constrained adaptive array processor. Each microphone signal is processed by a tapped delay line with adaptive weights updated by an iterative constrained minimization algorithm.

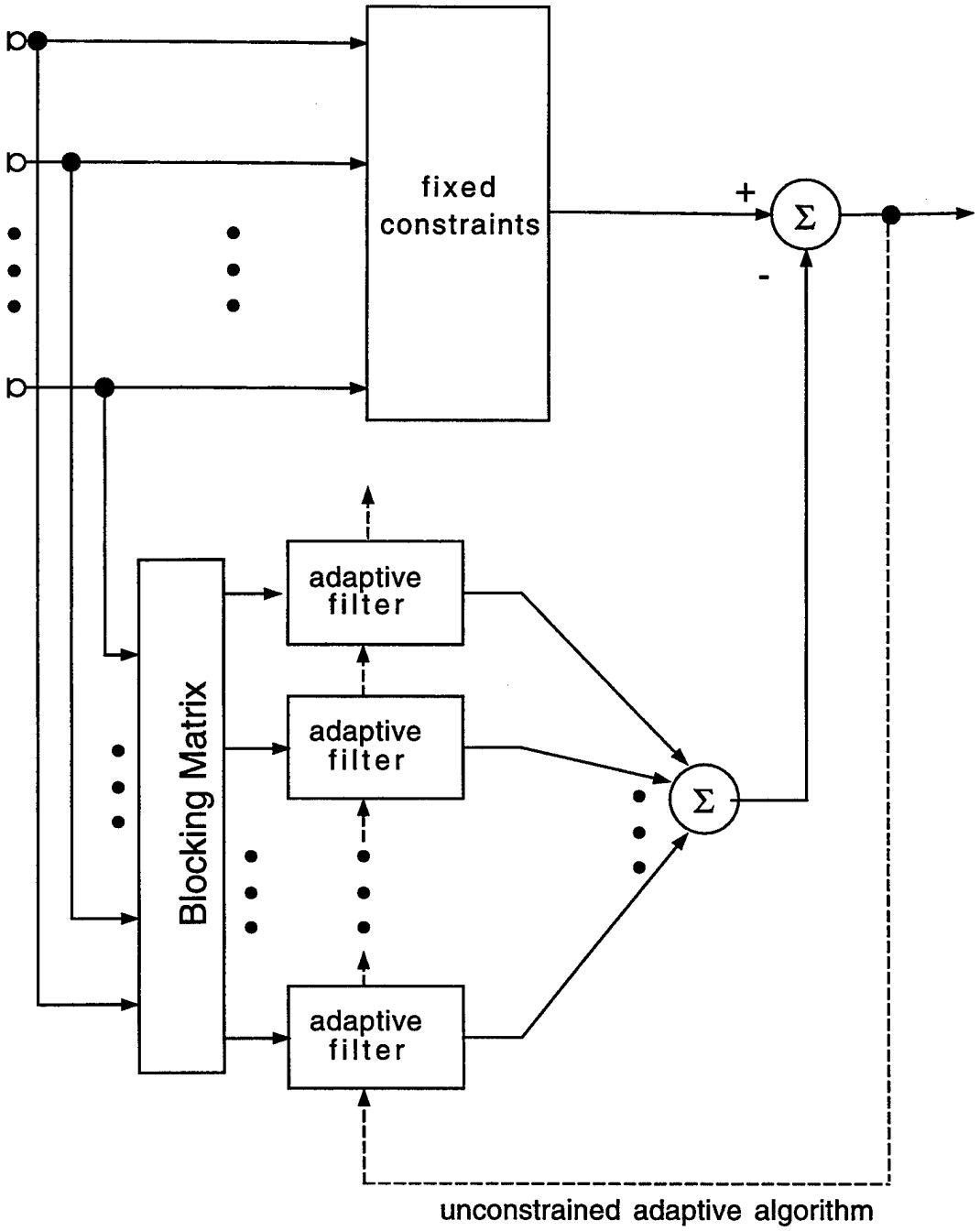

Figure 2-3: Block diagram of generalized sidelobe canceller. The upper channel imposes fixed constraints, while the lower channel consists of a blocking matrix that removes the target signal, followed by adaptive filters that perform unconstrained minimization on the remaining signals.

minimization algorithm. The constraints are selected to provide the desired response for signals arriving from the target direction (typically unity gain).

The generalized sidelobe canceller proposed by Griffiths and Jim (1982) consists of two substructures that together act to minimize the total output power subject to the constraints. The upper channel forms a weighted sum of the sensor signals (essentially a fixed array processor), and then processes this sum by an FIR filter that imposes the desired filtering described by the constraints (again, typically unity gain). The lower channel consists of a blocking matrix that combines the sensor signals so as to remove the target signal, followed by an adaptive algorithm that performs unconstrained minimization on the remaining signals. Equivalence of the Frost and Griffiths-Jim processors can be shown for a variety of conditions (Griffiths and Jim, 1982).

Figure 2.4 shows a simple and useful form of the generalized sidelobe canceller, again assuming that the target signal was previously equalized across microphones. In this case, the constraints consist of averaging the M microphone signals and then delaying that primary signal by D samples. The purpose of the delay is to permit the adaptive filter in the lower channel to form non-causal responses (Widrow and Stearns, 1985). The blocking matrix consists of taking the difference between pairs of microphone signals to produce $M-1$ target-free reference signals. For any combination of pairs selected so that the blocking matrix has full rank, the optimal solution for the adaptive weights will be identical.

There is a wide variety of adaptive algorithms available for implementing the unconstrained minimization required by the generalized sidelobe canceller. The LMS algorithm is often used because of its simplicity. When the LMS algorithm is used in conjunction with a two-microphone version of the generalized sidelobe canceller shown in Fig. 2.4, the system is equivalent to a preprocessor consisting of taking the sum and difference of the microphone signals, followed by an adaptive noise canceller. In any case, steering errors or imperfections in the blocking matrix can cause leakage of the target signal into the reference signal, resulting in target cancellation as described above in conjunction with the adaptive noise canceller.

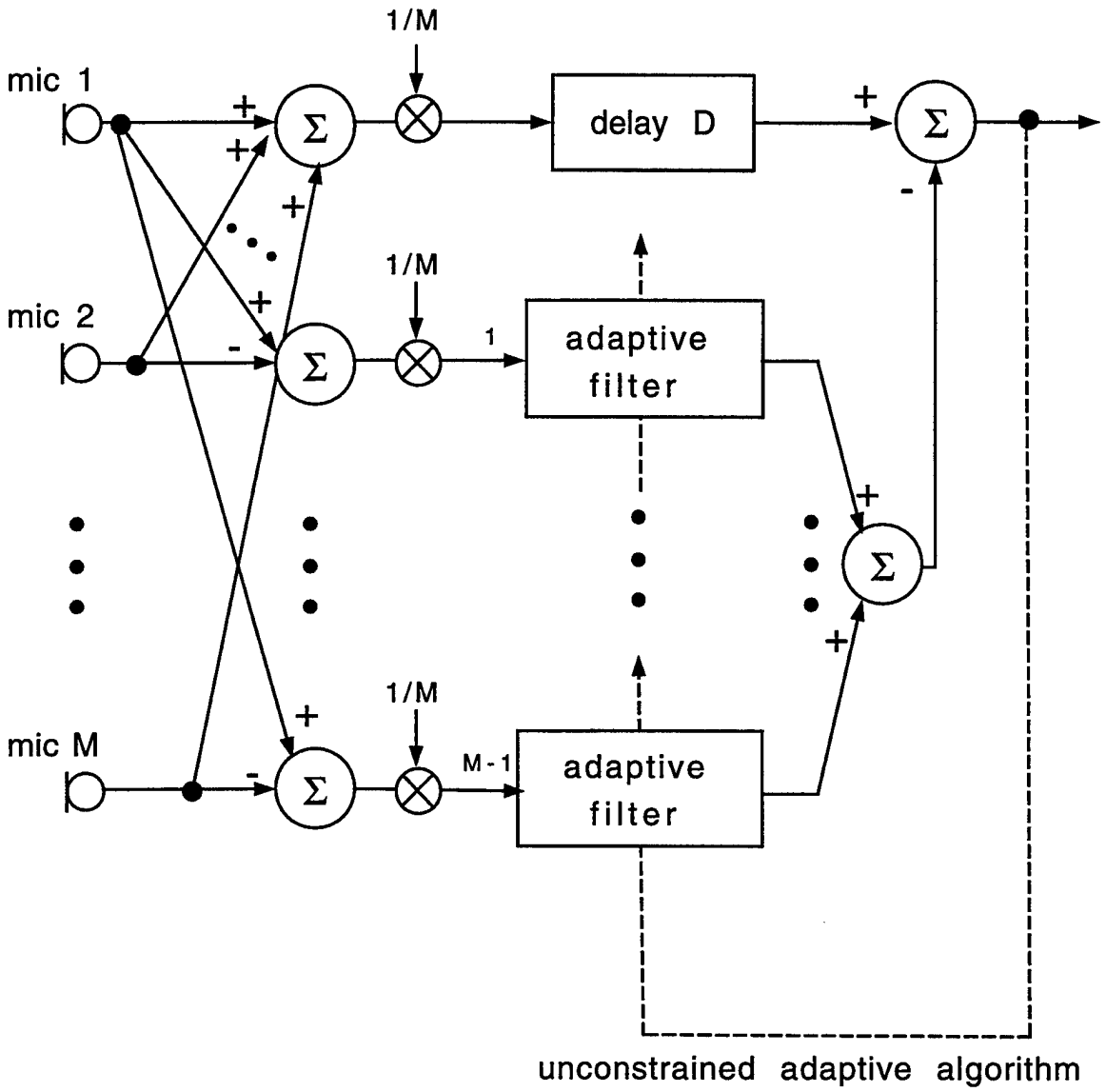

Figure 2-4: Block diagram of a simple generalized sidelobe canceller with M microphones. The fixed constraints in the upper channel preserve the target by averaging the microphone signals and delaying the result. The blocking matrix is implemented in the lower channel by taking the difference between pairs of microphone signals.

2.2 Microphone-array hearing aids

2.2.1 Fixed array processors

Previous work has established the potential benefits of fixed arrays for the hearing-aid application (Peterson, 1989; Soede et al., 1993a,b; Stadler and Rabinowitz, 1993; Kates, 1993). Peterson (1989) considered the performance of both fixed and adaptive arrays; that work is discussed in Sec. 2.2.2.

Soede et al. (1993a,b) designed, constructed, and evaluated fixed arrays for use as hearing aids. They considered linear arrays consisting of five evenly-spaced cardioid microphones mounted on eyeglass frames in both broadside and endfire configurations.[1] Physical measurements showed that these arrays provide gains in signal-to-noise ratio of 6–7 dB in diffuse noise. Intelligibility tests with hearing-impaired listeners showed improvements of 7 dB in the speech reception threshold.

Stadler and Rabinowitz (1993) also considered linear broadside and endfire arrays. They applied sensitivity-constrained optimum beamforming (Cox et al., 1986) to fixed arrays with directional microphone elements, providing a design method that controls the tradeoff between directionality and noise sensitivity. They computed the theoretical performance of these arrays in free space for various numbers and types of microphones. Their results predict gains comparable to those seen by Soede et al. (1993a,b) for the same array configurations. For endfire arrays, their results show that using frequency-dependent weights with four or five microphones provides directivities of 8–10 dB, regardless of the type of microphone. For broadside arrays, directional microphones provide a clear advantage, but there is little advantage to using frequency-dependent weights. A broadside array of two or five cardioid or supercardioid elements with uniform weights (simply averaging the microphone signals) provides directivities of 7–8 dB. Although the directivity of these broadside arrays is roughly constant for 2–5 microphones, increasing the number of microphones reduces the noise sensitivity, making the system more robust.

[1] Microphones in a broadside array form a line perpendicular to the target direction, while microphones in an endfire array are colinear with the target direction.

2.2.2 Adaptive array processors

A number of researchers have considered adaptive microphone-array systems for application to hearing aids (Weiss, 1987; Schwander and Levitt, 1987; Chabries et al., 1987; Brey et al., 1987; Chazan et al., 1987; Peterson, 1989; Peterson et al., 1990; Van Compernolle, 1990a; Farassopoulos, 1992; Greenberg and Zurek, 1992; Dillier et al., 1993; Kohlmeier et al., 1993; Hoffman et al., 1994; Link, 1994). Unlike fixed arrays, there are a variety of ways to design, implement, and evaluate these adaptive processors, which hinders comparisons among the different studies. Some of these systems are based on the adaptive noise canceller and require a target-free reference signal, and many are restricted to two-microphone arrays. In general, the results of these studies indicate that adaptive microphone array systems provide substantial benefits under certain conditions.

Peterson (1989) calculated the optimum performance of LCMV beamformers in the presence of directional and isotropic noise for head-sized free-space arrays based on unlimited filter length. He considered how performance varies with the number of sensors, internal sensor noise, array dimension, and array orientation. His results show that in general, the performance of arrays *designed to provide equal noise sensitivity* increases with the number of microphones, but, for head-sized arrays and realistic levels of sensor noise, performance saturates and the improvement is negligible beyond 4–6 microphones. Once the number of microphones exceeds the number of directional jammers, little or no additional benefit is obtained from adding more microphones. Performance also increases with array length, except for arrays with a small number of microphones where spatial undersampling occurs in the long arrays.

Most previous studies have considered relatively simple adaptive systems based on two microphones. The performance of two-microphone systems decreases dramatically when a second jammer source is introduced (Weiss, 1987; Peterson et al., 1990). In theory, a system with M microphones can create $M-1$ independent broadband nulls, and therefore can effectively cancel $M-1$ independent directional jammers. As a result, a two-microphone array is only expected to perform well against a single directional jammer.

Initial assessments have demonstrated the potential benefits of adaptive systems based on the generalized sidelobe canceller. (Peterson et al., 1990; Greenberg and Zurek, 1992). These studies have shown that adaptive systems operating in anechoic environments can provide 20–30 dB improvement based on both physical measurements and intelligibility tests with normal-hearing listeners. Improvements of 3–15 dB have been reported for a variety of moderately reverberant environments.

2.3 Problems and proposed solutions

Previous studies have identified a number of problems with adaptive array systems, and some have proposed solutions to those problems. The problems include misadjustment of the adaptive algorithm, misalignment due to nonideal conditions, and problems caused by reverberation.

2.3.1 Misadjustment and misalignment

Misadjustment of adaptive weights is an unavoidable result of any adaptive process using a stochastic gradient search such as the LMS algorithm. The misadjustment is defined as the ratio of mean-squared error caused by the adaptive process to the minimum mean-squared error produced by the optimal filter (Widrow and Stearns, 1985). Because the adaptive weights are driven by the output of the system, when a strong target signal is present there are large steps in the weight update uncorrelated with the jammer being cancelled. This leads to reduced jammer cancellation at high TJRs. The effects of misadjustment are described in Peterson et al. (1990) and Greenberg and Zurek (1992).

Another degrading effect is caused by *misalignment* of the array to the target source. If the array is not perfectly aligned to the target, then some target signal will leak through the constraints or the blocking matrix and can subsequently be cancelled by the adaptive process. Even if the target direction is known exactly and the array is perfectly steered, mismatched sensors and errors in sensor placement will cause misalignment. The importance of target leakage was described by Widrow et

al. (1975) who showed that, for an unconstrained adaptive filter (one whose impulse response can extend infinitely in both time directions), the target-to-jammer ratio at the output equals the jammer-to-target ratio at the reference input. With any fixed, non-zero transfer function in the leakage path, the problem clearly worsens as the input TJR increases, leading to more target cancellation at higher TJRs. This degradation caused by target leakage is seen with TJRs as low as 0 dB, and is clearly detrimental at 10-20 dB (Peterson et al., 1990; Greenberg and Zurek, 1992).

The degradations due to misadjustment and misalignment are both proportional to the TJR. Therefore, a general solution to these problems is based on controlling the adaptive process so that adaptation occurs only when the target signal is weak or absent. Greenberg and Zurek (1992) accomplish this with two methods for controlling adaptation at high TJR. Both methods exploit the fact that the target signal in this application – speech – exhibits a high degree of fluctuation, and, in fact, has pause periods when the target is absent. Both attempt to sense the TJR and to adapt only in intervals when the TJR is small.

The first method is only effective when there is negligible leakage of the target signal. When this condition is met and the input TJR is high, the system output power will be greater than the power of the reference signal. The LMS weight update equation is modified to normalize the step-size parameter with the sum of the reference signal and output signal powers[2] in order to reduce the size of target-induced weight fluctuations. (This method is explained in detail in Ch. 4.) The approach is similar to that taken by Duttweiler (1982) and Jeyendran and Reddy (1990).

The second method employs intermicrophone correlation to determine the range of TJR . The straight-ahead target contributes a signal with correlation near unity, and off-axis jammers have a correlation that is less than unity and depends on frequency and direction. A running measure of the correlation between microphone signals will vary with TJR and can be used as an indicator of relative target strength. For each cycle of the adaptive algorithm, the correlation measure is compared to a threshold and the adaptive process is inhibited (the weights are frozen at their current values)

[2]Traditionally, the step-size parameter is normalized by the reference signal power alone.

if the correlation exceeds the threshold. Other researchers have proposed similar mechanisms to disable the adaptive process in the presence of strong target signals (Van Compernolle, 1990a,b; Harrison et al., 1986; Kaneda and Ohga, 1986; Sondhi and Berkley, 1980; Dillier et al., 1993); they use various methods of estimating signal powers to determine when adaptation should be disabled.

Both of these methods for controlling adaptation at high TJR were shown to be effective with a two-microphone generalized sidelobe canceller in an anechoic environment. Using the two methods together significantly improved performance at high TJRs and eliminated degrading target cancellation. Although these two methods were shown to be effective, the resulting algorithms were not subject to thorough analysis and many of the parameters were selected in an *ad hoc* manner. In the current work, the two previously proposed methods of controlling adaptation are analyzed individually, formal methods are developed for parameter selection in anechoic and reverberant environments, and the performance of these methods is predicted and verified under simplified conditions before application to the more complex situation of speech in reverberation. Alternative methods for normalizing the step-size parameter are analyzed in Ch. 4, and the use of intermicrophone correlation to determine the range of TJR is analyzed in Ch. 5.

Hoffman (1992) proposed an alternate technique to prevent target cancellation due to misalignment, without addressing the problem of misadjustment. He developed a method for determining linear constraints plus a quadratic constraint for Frost's linearly constrained adaptive array processor to prevent target cancellation beyond an acceptable level (e.g., 3 dB). The constraints are based on a model of the sources of misalignment that the system must accommodate, for example, errors due to microphone locations. He demonstrates arrays of three, five, and seven microphones with 8 and 16 taps per filter. Simulation results show gains of 10–20 dB in an anechoic environment and 5–10 dB in moderate reverberation.

2.3.2 Reverberation

Previous work has shown that adaptive array processors provide some improvement in reverberant environments, but that the benefit decreases as the degree of reverberation increases. For some conditions, performance also decreases dramatically with increasing TJR. Reverberation limits adaptive system performance in two ways. The first is target cancellation resulting from violation of the system's fundamental assumptions. The second is reduced jammer cancellation due to increased complexity of the acoustic environment.

Target cancellation

As discussed in Sec. 2.1, the LCMV beamformer assumes that the target direction is known and that target and jammer are uncorrelated. Target signal reflections violate one of these two assumptions. If the reflected target signal is considered target, then the assumption of known target direction is violated. On the other hand, if the reflected target is considered jammer, the assumption of uncorrelated target and jammer is violated. Taking the latter view, it is instructive to consider the optimum performance of the LCMV beamformer in the presence of correlated interference. Reddy et al. (1987) considered the case of a narrowband target with a single jammer that is either partially or fully correlated with the target. Zoltowski (1988) extended the analysis to include multiple partially-correlated narrowband jammers. Their results provide general expressions for the steady-state output power and quantify the target cancellation due to correlated jammers. In general, as the correlation increases between target and jammer signals, the LCMV beamformer exhibits progressive deterioration in performance due to both diminished jammer rejection and increased target cancellation.

Some researchers have proposed methods to overcome the problem of multipath or correlated jammers, but for the most part they have addressed the simpler problem of a small number of reflections encountered in other applications. For example, one approach is to include a model of the multipath in the design and null the reflections before they enter the adaptive processor (Owsley, 1985). Obviously, this is only

appropriate when an accurate model of the multipath exists and is not applicable to acoustic reflections in arbitrary rooms.

A more general approach to the problem of correlated jammers is spatial dithering, intended to eliminate the correlation between the on-axis target and its off-axis reflections. This was first suggested by Widrow et al. (1982) who proposed mechanically moving the sensor array along a line perpendicular to the direction of arrival of the desired signal. Shan and Kailath (1985) proposed a method called spatial smoothing to accomplish the dithering. Spatial smoothing uses subarrays of the total sensors and requires twice as many sensors as correlated signal sources, meaning that in theory the system requires twice as many microphones as the number of target reflections. Hoffman et al. (1991) propose a method of virtual dithering that performs spatial smoothing by applying matrix transformations to a number of sensor signals and therefore does not require extra physical sensors. However, their work does not indicate how many virtual transformations need to be performed or if that number is related to the number of target reflections as in spatial smoothing. Both spatial smoothing and virtual dithering were demonstrated to work for a small number of narrowband correlated jammers. The problem is that in a reverberant environment, the number of reflections will outnumber the number of microphones or, in the case of virtual dithering, the number of matrix transformations that can feasibly be performed. In order to demonstrate that these techniques have any potential for the hearing aid application, they must first be analyzed in situations where the target reflections outnumber the microphones.

Hoffman et al. (1994) suggest a simple solution to the problems caused by target reflections; they note that appropriate selection of the parameters of the generalized sidelobe canceller (in particular, setting the primary delay to zero) will prevent target cancellation. This idea will be analyzed and extended in Ch. 6.

Reduced jammer cancellation

Reduced jammer cancellation can be examined by considering the performance of LCMV beamformers against a single reverberant jammer in the absence of a target

signal. Because the system can operate only over the time-span of the adaptive filter, jammer cancellation is impaired when the room impulse response exceeds that span.[3] This effect is illustrated in Greenberg and Zurek (1992) for a two-microphone generalized sidelobe canceller with two filter lengths in a variety of reverberant environments. The results show that although extremely long filters may provide substantial improvement in strong reverberation, the filter lengths currently attainable with a practical system only provide significant improvements at source-to-array distances less than the critical distance of the room.

When the filter length is short relative to the impulse response of the room, late reflections arriving at the array will be uncorrelated with the data in the filter. Therefore, the adaptive filter will not be of any use in cancelling the late reflections. Furthermore, it is reasonable to assume that the late reflections are equally likely to arrive from all directions. In this situation, the late reflections can be modeled accurately as isotropic noise (Beranek, 1954; Cremer and Müller, 1982). An array designed to perform optimally against isotropic noise has maximum directivity (Peterson, 1989), which is typically the design criterion for fixed array processors.

In terms of the generalized sidelobe canceller (Figs. 2.3 and 2.4), as reverberation increases, the reference signals at the adaptive filter inputs become progressively less correlated with the primary signal in the upper channel. In the extreme, they are completely uncorrelated and the adaptive filter weights tend to zero. In this case, the system output simply equals the primary signal, and the performance of the system depends on the fixed processor defined by the constraints. Therefore, in order to design an adaptive system that performs optimally in extreme reverberation, the constraints should define an underlying fixed processor with maximum directivity. The design choices that affect the fixed processor performance are the number of microphones, their directional characteristics, and the weights implemented in the constraints. These issues will be discussed in Chs. 7 and 8.

[3]Strictly speaking, the impulse response is infinitely long for any real room. Here, the length of the room impulse response refers to the length of time that non-negligible reflections continue to propagate after the direct sound. For example, this measure could be the reverberation time of the room (time required for reflections to decay 60 dB relative to the direct power).

It is important to note that obtaining the benefits of the underlying fixed processor in extreme reverberation does not require any additional processing effort; rather, it is obtained automatically when the adaptive weights cannot further minimize the output power. In some sense, the system can be thought of as a hybrid fixed/adaptive array processor, where the fixed weights (constraints) provide a desired default response in the absence of directional jammers, while the adaptive process utilizes the degrees of freedom in the adaptive weights to reduce directional jammers when possible. The result is a system that maximizes directivity when reverberation is strong, yet allows adaptation to provide the additional benefit obtained from cancelling directional jammers in less reverberant environments.

2.4 Goals

The goals of this work are to completely specify the algorithm for use in adaptive microphone-array hearing aids and to demonstrate the benefits provided by such systems in a variety of acoustic environments. The algorithm includes several features to ensure robustness at high TJR and in reverberation. In particular, the goals of this work are:

- To provide a thorough analysis of the two *ad hoc* methods for controlling adaptation proposed by Greenberg and Zurek (1992). This analysis will result in guidelines for selecting relevant parameters and also will facilitate comparison to similar methods proposed by other researchers.

- To analyze the specific causes of target cancellation in reverberation and to explain and extend previously suggested (Hoffman et al., 1994) parameter choices to eliminate this problem.

- To establish the usefulness of each of these methods individually via simple simulations that isolate the relevant effects.

- To demonstrate the effectiveness of the modified algorithm by combining these methods in computer simulations and evaluating performance under a range of

acoustic conditions. These simulations will also investigate selection of design parameters such as the adaptive filter length and the number of microphones.

Chapter 3

Methods

The purpose of this chapter is to introduce several elements that are common to the analyses and simulations performed in Chs. 4–7.

3.1 Source materials

Since speech is the signal of interest in the hearing aid application, it will be necessary to evaluate systems using speech or speech-like signals. When possible, initial assessments use uncorrelated zero-mean white Gaussian noise for the target and jammer signals. When more realistic source signals are required, the target signal consists of a series of phonetically-balanced sentences (IEEE, 1969) spoken by a single male talker and the jammer signal consists of 12-talker SPIN babble (Kalikow et al., 1977). These sources were obtained from anechoic recordings that were digitized, sampled at 10 kHz, and approximately whitened with high frequency emphasis of 6 dB/octave (Link and Buckley, 1993).

3.2 Room simulations

Convolving the source materials with source-to-microphone impulse responses produces microphone signals appropriate for input to the systems of interest. Those impulse responses can be obtained from recordings made in real rooms, or from a

room simulation. This work uses source-to-microphone impulse responses generated by a simulation of free-space microphones in a rectangular room with specifiable dimensions and uniform surface absorption (Peterson, 1986).

The following analyses and simulations utilize a single room. Its dimensions are $5.2 \times 3.4 \times 2.8$ meters. This is slightly larger than the 'living room' used by Peterson (1989). One corner of the room is the origin of a three dimensional coordinate system with the room oriented squarely with three orthogonal planes. The center of the array is at (2.755, 1.380, 1.600) meters, and the array is oriented along the straight line defined by the array center and the point (2.685, 1.400, 1.600) meters. All sources are located around the array center in a circle in the horizontal plane with radius 0.9 meters at a height of 1.7 meters. A source at zero degrees is located at array broadside in the direction of positive coordinates from the array, and positive source angles refer to clockwise progression from zero when viewed from above.

Two linear broadside arrays of omnidirectional elements will be investigated. The first is 7 cm in length with two microphones. This array was selected because of its promising performance in earlier work (Greenberg and Zurek, 1992), and because of a desire to investigate a relatively simple system (two microphones). The second array is 16 cm in length with 5 microphones uniformly spaced, resulting in 4 cm intermicrophone spacing. The array length was selected to be roughly 'head-sized', and the number of microphones was selected to prevent spatial undersampling for frequencies below 5 kHz when evenly spaced throughout that length.

These arrays are simulated in free space, but in real applications they will be placed on or near the listener's head. Although the presence of the head affects the structure of the signals received at the array, it has little effect on the resulting performance of broadside arrays (Greenberg and Zurek, 1992; Soede et al., 1993a). Previous work (Greenberg and Zurek, 1992) has shown that endfire arrays are much more sensitive to the presence of the head; therefore this work only considers broadside arrays.

For both the two- and five-microphone arrays described above, three values of the uniform surface absorption are used in the room simulation to generate source-to-microphone impulse responses with different degrees of reverberation. The three

absorption values are 1.0 (anechoic), 0.6, and 0.2. For the room described above, the moderately reverberant room had a direct-to-reverberant ratio of +6 dB and a reverberation time of 150 ms, while the more strongly reverberant room had a direct-to-reverberant ratio of −2 dB and a reverberation time of 620 ms. Representative source-to-microphone impulse responses are shown in a later chapter (Fig. 6.2).

3.3 Performance metric

Since the purpose of these systems is to improve the intelligibility of speech, the ultimate test of their effectiveness comes from tests of intelligibility with human subjects. However, such tests are time-consuming and do not allow rapid evaluations of many algorithms and parameter choices. For efficiency, previous work has used a physical measure, the intelligibility-weighted gain, for preliminary assessment of system performance. This section summarizes the computation of the intelligibility-weighted gain, denoted G_I, as described elsewhere (Peterson, 1989; Greenberg and Zurek, 1992; Greenberg et al., 1993).

G_I is based on the intelligibility-weighted level, $\Gamma(s)$, given by

$$\Gamma(s) = \sum_j a_j B_j(s), \tag{3.1}$$

where $B_j(s)$ is the decibel level in the j^{th} frequency band of the signal s and a_j is the weight reflecting the contribution of that band to intelligibility. In principle, these measures can be based on any index designed to predict intelligibility. In this work, G_I is based on the Articulation Index (ANSI, 1969; Kryter, 1962) with the weights, a_j, reflecting the contribution of each one-third-octave band to intelligibility.

The absolute values of these intelligibility-weighted levels depend on the reference level and are therefore arbitrary. However, they can be used to make comparisons between signals. For these comparisons, there are four signals of interest: target input, T_i; target output, T_o; jammer input, J_i; jammer output, J_o. The *improvement*

from input to output in target and jammer is given by

$$\Delta\Gamma(T) = \Gamma(T_o) - \Gamma(T_i) \tag{3.2}$$

and

$$\Delta\Gamma(J) = \Gamma(J_i) - \Gamma(J_o). \tag{3.3}$$

Positive values indicate improved intelligibility (amplification of the target or attenuation of the jammer), while negative values indicate degraded intelligibility (attenuation of the target or amplification of the jammer). G_I is then given by the overall intelligibility-weighted gain in TJR from input to output,

$$\begin{aligned} G_I &= \Delta\Gamma(T) + \Delta\Gamma(J) && (3.4) \\ &= \Gamma(T_o) - \Gamma(T_i) + \Gamma(J_i) + \Gamma(J_o). && (3.5) \end{aligned}$$

Other useful measures are obtained by combining values of Γ for the input and output components separately, resulting in measures of intelligibility-weighted target-to-jammer ratio at the input and output of the system. These measures are given by

$$\mathrm{TJR}_{I,\mathrm{in}} = \Gamma(T_i) - \Gamma(J_i) \tag{3.6}$$

and

$$\mathrm{TJR}_{I,\mathrm{out}} = \Gamma(T_o) - \Gamma(J_o), \tag{3.7}$$

and can also be combined to determine the intelligibility-weighted gain according to

$$G_I = \mathrm{TJR}_{I,\mathrm{out}} - \mathrm{TJR}_{I,\mathrm{in}}. \tag{3.8}$$

In order to calculate G_I, it is necessary to obtain separate target and jammer signals at the system output. This is accomplished with a controlling processor and two yoked processors (Greenberg and Zurek, 1992). The controlling processor operates on the total input signal (target plus jammer) while each yoked processor has the

same structure as the controller, and processes either the target or jammer signal, T_i or J_i. The adaptive filter weights of the yoked processor are copied exactly from the controlling processor. Because the filtering operation is linear, superposition holds and the total system output provided by the controlling processor equals the sum of the two yoked processor outputs, T_o and J_o.

Using additional yoked processors, this approach can be extended to investigate the effect of the system on other components of the input signals. For instance, by separating the direct wave from the reflections of the source-to-microphone impulse responses and convolving them individually with the same target source material, it is possible to obtain the direct and reflected target at the inputs, $T_{d,i}$ and $T_{r,i}$, where $T_i = T_{d,i} + T_{r,i}$. Using these signals as the inputs to additional yoked processors produces the direct and reflected target at the output, $T_{d,o}$ and $T_{r,o}$, where $T_o = T_{d,o} + T_{r,o}$. Applying intelligibility weighting to these signals provides an indication of how the system affects the direct target and the reflected target individually, that is,

$$\Delta\Gamma(T_d) = \Gamma(T_{d,o}) - \Gamma(T_{d,i}) \tag{3.9}$$

and

$$\Delta\Gamma(T_r) = \Gamma(T_{r,o}) - \Gamma(T_{r,i}). \tag{3.10}$$

However, even though $T_i = T_{d,i} + T_{r,i}$ and $T_o = T_{d,o} + T_{r,o}$, $\Delta\Gamma(T) \neq \Delta\Gamma(T_d) + \Delta\Gamma(T_r)$ because $\Gamma(s)$ is a nonlinear function of the signal s. Also, these values will not be meaningful if the output includes cancellation of direct target based on target reflections.

As defined here, the sign of $\Delta\Gamma(T_r)$ suggests that target reflections contribute to intelligibility. In fact, early reflections (arriving within up to 50–95 ms of the direct wave) tend to improve intelligibility while later reflections tend to be detrimental to intelligibility (Cremer and Müller, 1982). To obtain more accurate treatment of the effect of late reflections, the calculation of intelligibility-weighted levels (3.1) could be modified to include the Speech Transmission Index (Steeneken and Houtgast, 1980; Houtgast et al., 1980). Using the Articulation Index and computing G_I according

to (3.5) treats all target reflections as if they contribute to intelligibility. If only early reflections exist, then G_I is an accurate measure of the effect of the system on intelligibility. On the other hand, if only late reflections exist, then G_I underestimates intelligibility if the system attenuates the reflections ($\Delta\Gamma(T_r) < 0$), and overestimates intelligibility if the system amplifies the reflections ($\Delta\Gamma(T_r) > 0$). In reality, the target reflections consist of both early and late reflections, and the results in Ch. 7 show that $\Delta\Gamma(T_r)$ is typically negative. Therefore, G_I is at best accurate, and at worst a conservative estimate of system performance.

Finally, for assessing the performance of fixed systems in extreme reverberation approaching an isotropic field, it is useful to apply intelligibility-weighting to the directivity index (Peterson, 1989). The directivity index is defined as the ratio of the output power due to sounds from the target direction to the average output power due to sounds incident from all directions. Since the directivity index typically varies with frequency, a useful measure is the broadband intelligibility-weighted directivity,

$$D_I = \sum_j a_j D_j, \tag{3.11}$$

where D_j is the directivity index corresponding to the j^{th} frequency band in units of decibels and a_j is the weight reflecting the contribution of that band to intelligibility as in (3.1).

Chapter 4

Optimal step-size parameter for the LMS algorithm.

4.1 Introduction

This chapter is concerned with determining the optimal step-size parameter to use with the LMS algorithm. For simplicity, the analysis is performed for an adaptive noise canceller, but the results apply to the generalized sidelobe canceller implementation of LCMV beamforming, because, as explained in Sec. 2.1, the generalized sidelobe canceller can be thought of as a preprocessor followed by an adaptive noise canceller.

The optimal time-varying step-size parameter is defined as one that minimizes the steady-state excess mean-squared error (mse) due to the adaptive process. Realizable expressions for the step-size parameter based on quantities available to the adaptive processor are developed and their performance is compared to that obtained with the optimal (non-realizable) step-size parameter result. In addition, the resulting convergence time is determined for the optimal and realizable step-size parameters.

The analysis begins with expressions for the behavior of the LMS algorithm that are available in the literature; these expressions are modified to include the effects of the target signal in the primary input to the adaptive noise canceller. It is shown that the traditional method of normalizing the step-size parameter leads to poor per-

formance in the presence of strong target signals. Next, an expression is derived for the step-size parameter that minimizes the steady-state excess mse of the adaptive noise canceller's output. However, this optimal step-size parameter cannot be implemented in a real system, since it requires knowledge of quantities that are not available. Instead, simplifying assumptions are made about the unknown quantities in order to obtain expressions for the step-size parameter that can be implemented in a real system. Three different expressions for the step-size parameter result from different sets of assumptions.

The analysis described above produces five candidates for the step-size parameter in the LMS algorithm. The first is the value traditionally used, which ignores the presence of the target signal in the adaptive noise canceller's primary input. The second is the optimal value, which is of theoretical interest but cannot be implemented in a real system. The last three are the step-size parameters derived from the optimal expression based on different simplifying assumptions. For each of these five expressions for the step-size parameter (traditional, optimal, and three methods based on simplifying assumptions) expressions are derived to characterize the steady-state excess mse and the transient behavior.

The results are summarized in Table 4.1 on page 53. They show that the optimal step-size parameter results in a steady-state excess mse equal to zero. The traditional step-size parameter results in a steady-state excess mse that increases linearly with target signal power. The three new expressions for the step-size parameter result in values of steady-state excess mse that are nonzero, but preferable to the traditional method. Iterative expressions are determined to characterize the transient behavior of the adaptive process. These expressions permit comparisons between the different step-size parameter algorithms, but the expressions depend on relative signal strengths and the spread of the eigenvalues of the autocorrelation matrix of the reference signal. For the most promising method, time constants are determined for exponential decays that approximate the transient behavior.

4.2 Background

4.2.1 The adaptive noise canceller

A block diagram of the adaptive noise canceller was shown in Fig. 2.1.[1] The adaptive noise canceller requires two inputs. The primary input contains target plus jammer, denoted by $t(n) + j(n)$, where n is the discrete-time index. The reference input contains a filtered version of the jammer, $x(n)$, and is (ideally) free of target. The reference signal passes through an L-tap adaptive FIR filter, whose weights, $w_k(n)$ for $k = 0, \ldots, L-1$, are adjusted to minimize the power in the output signal. This minimization is achieved by filtering $x(n)$ to approximate $j(n)$ and subtracting it from the primary signal. With the primary delay equal to zero, the output of the adaptive noise canceller, $y(n)$, is given by

$$y(n) = t(n) + j(n) - \sum_{k=0}^{L-1} w_k(n)x(n-k). \tag{4.1}$$

If the target and jammer are uncorrelated and the reference input contains no target, then minimizing the power in $y(n)$ results in an output signal with $t(n)$ perfectly preserved and the jammer power minimized.

The analysis presented here is based on the following assumptions:

1. The primary target and jammer signals are uncorrelated; $t(n)$ is uncorrelated with $j(n)$.

2. There is no leakage of target signal into the reference input; $t(n)$ is uncorrelated with $x(n)$.

3. The signals $t(n)$, $j(n)$, and $x(n)$ are all real and zero-mean.

4. The signals $t(n)$, $j(n)$, and $x(n)$ are wide-sense stationary, that is, their second-order statistics are constant. This restriction is necessary to simplify the derivation, but will be lifted in the subsequent interpretation of the results.

[1] In the following analysis, the primary channel delay, D, is set to zero, but the results are applicable when the delay is nonzero as well.

The following definitions will simplify notation. Boldface lowercase and uppercase letters represent vectors and matrices, respectively, while ^{T} denotes transpose and $E[\ ]$ denotes expected value. The signal powers are defined as

$$\sigma_t^2 = E[t^2(n)] \tag{4.2}$$

$$\sigma_j^2 = E[j^2(n)] \tag{4.3}$$

$$\sigma_x^2 = E[x^2(n)]. \tag{4.4}$$

The data vector is

$$\mathbf{x}(n) = [x(n)\ \ x(n-1)\ \ \cdots\ \ x(n-(L-1))]^T \tag{4.5}$$

with elements equal to the values in the tapped delay line of the adaptive filter. The weight vector is

$$\mathbf{w}(n) = [w_0(n)\ \ w_1(n)\ \ \cdots\ \ w_{L-1}(n)]^T \tag{4.6}$$

The data autocorrelation matrix and cross-correlation vector are given by

$$E[\mathbf{x}(n)\mathbf{x}^T(n)] = \mathbf{R} \tag{4.7}$$

and

$$E[\mathbf{x}(n)j(n)], = \mathbf{p}, \tag{4.8}$$

while from the second assumption,

$$E[\mathbf{x}(n)t(n)] = \mathbf{0}, \tag{4.9}$$

where $\mathbf{0}$ is the vector of L zeros. The autocorrelation matrix $\mathbf{R}$ is symmetric, Toeplitz, and positive definite (Haykin, 1986). The eigenvalues of $\mathbf{R}$ are positive and are denoted λ_i for $i = 1, \ldots, L$. The diagonal entries of $\mathbf{R}$ equal σ_x^2 and, from the

definition of the trace of a matrix (Strang, 1988),

$$\sum_{i=1}^{L} \lambda_i = \mathrm{tr}[\mathbf{R}] = L\sigma_x^2, \tag{4.10}$$

where tr[ ] denotes the trace of a matrix.

The optimal values for the adaptive weights, $\mathbf{w}^*$, are given by the solution to the Wiener-Hopf equation (Widrow and Stearns, 1985),

$$\mathbf{w}^* = \mathbf{R}^{-1}\mathbf{p}. \tag{4.11}$$

The error signal, $e(n)$, is the difference between the actual output and the desired output, that is,

$$e(n) = y(n) - t(n) = j(n) - \mathbf{w}^T(n)\mathbf{x}(n), \tag{4.12}$$

where vector multiplication has replaced the summation in (4.1). The minimum error (in the mean-squared sense) is obtained when the adaptive weights are fixed at their optimal values so that

$$e_{\min}(n) = j(n) - \mathbf{w}^{*T}\mathbf{x}(n). \tag{4.13}$$

The minimum error is uncorrelated with the reference input, that is,

$$E[\mathbf{x}(n)e_{\min}(n)] = \mathbf{0} \tag{4.14}$$

(Haykin, 1986). The mean-squared error associated with a particular weight vector, $J(\mathbf{w})$, is given by

$$J(\mathbf{w}) = E[e^2(n)|_{\mathbf{w}(n)=\mathbf{w}}] = \sigma_j^2 - 2\mathbf{p}^T\mathbf{w} + \mathbf{w}^T\mathbf{R}\mathbf{w} \tag{4.15}$$

and the minimum mse is

$$J_{\min} = E[e^2(n)|_{\mathbf{w}(n)=\mathbf{w}^*}] = E[e_{\min}^2(n)] = \sigma_j^2 - \mathbf{p}^T\mathbf{w}^* \tag{4.16}$$

(Haykin, 1986).

4.2.2 The LMS algorithm

Definitions

The problem of determining the optimal value of the adaptive weight vector, $\mathbf{w}^*$, can be interpreted geometrically by considering the mean-squared error as a function of the filter weights, $J(\mathbf{w})$. This results in a concave-upward hyperparaboloid in $(L+1)$-dimensional space (Widrow and Stearns, 1985). The minimum of the hyperparaboloid corresponds to $J_{\min}$. Gradient search algorithms operate by determining or estimating the gradient of the error surface for the current value of the adaptive weights and iteratively modifying the weights to travel in the direction of the negative gradient in an attempt to reach the "bottom of the bowl". The (real) LMS algorithm (Widrow and Stearns, 1985) is a simple gradient search that uses the instantaneous value $y^2(n)$ as an estimate of $E[e^2(n)]$, which is equivalent to using the instantaneous values of $\mathbf{x}(n)\mathbf{x}^T(n)$ and $\mathbf{x}(n)(t(n)+j(n))$ as crude estimates of their expected values, $\mathbf{R}$ and $\mathbf{p}$, respectively, required for the true gradient. The resulting weight update equation for the LMS algorithm is

$$\mathbf{w}(n+1) = \mathbf{w}(n) + \mu y(n)\mathbf{x}(n), \tag{4.17}$$

where $y(n)\mathbf{x}(n)$ is an estimate of the negative gradient, and the parameter μ controls the size of the adaptive steps and has units of inverse power.

Despite the widespread use of the LMS algorithm, there is no unconditional proof of its convergence (Widrow and Stearns, 1985). All known convergence proofs for the LMS algorithm require certain assumptions about the statistics of the inputs in order to make analysis of the algorithm mathematically tractable. One widely used set of assumptions is *independence theory*, which assumes the independence of successive data vectors. Using independence theory, it follows that the current weight vector depends on past values of the inputs, but is independent of the current inputs. The assumptions of independence theory are violated for many practical problems, including the adaptive noise canceller. Despite the violation of these assumptions, results predicted using independence theory are usually found to be in excellent agreement

with experiments and computer simulations (Haykin, 1986, p. 239). The assumptions of independence theory are used as needed throughout the remainder of this work. Using independence theory, the LMS algorithm converges if

$$0 < \mu < \frac{2}{L\sigma_x^2} \tag{4.18}$$

(Widrow and Stearns, 1985). Typically, the step-size parameter is defined in terms of the dimensionless step-size parameter, α, which is related to μ_{trad},[2] by

$$\mu_{\text{trad}} = \frac{\alpha}{L\sigma_x^2}. \tag{4.19}$$

Combining (4.18) and (4.19), the LMS algorithm converges for values of the dimensionless step-size parameter in the range

$$0 < \alpha < 2. \tag{4.20}$$

A closely related method is the normalized LMS (NLMS) algorithm, proposed by Nagumo and Noda (1967). The weights of the NLMS algorithm are updated according to

$$\mathbf{w}(n+1) = \mathbf{w}(n) + \alpha y(n) \frac{\mathbf{x}(n)}{\mathbf{x}^T(n)\mathbf{x}(n)}, \tag{4.21}$$

where α is the dimensionless step-size parameter. The algorithm converges for values of the step-size parameter in the range $0 < \alpha < 2$. Comparing (4.21) to (4.17) reveals that the two algorithms are equivalent when

$$\mu = \frac{\alpha}{\mathbf{x}^T(n)\mathbf{x}(n)}. \tag{4.22}$$

Noting that $E[\mathbf{x}^T(n)\mathbf{x}(n)] = L\sigma_x^2$ and comparing (4.22) with (4.19) reveals that the NLMS algorithm is equivalent to the LMS algorithm with the step-size parameter normalized according to (4.19) if the reference signal power, σ_x^2, is estimated from the

[2]The subscript is used to distinguish the traditional method of computing μ from the methods that will be proposed in Sec. 4.3.

current data vector, $\mathbf{x}(n)$, at each iteration.

Performance analysis

When any adaptive algorithm is used, the weights vary with time, as does the associated mse. An expression for $J(n)$, the mse due to the LMS algorithm at time n, can be found by squaring (4.12) and taking its expected value,[3] producing

$$J(n) = E[e^2(n)] = J_{\min} + E[\mathbf{v}^T(n)\mathbf{R}\mathbf{v}(n)], \tag{4.23}$$

where the weight error vector, $\mathbf{v}(n)$ is defined as

$$\mathbf{v}(n) = \mathbf{w}(n) - \mathbf{w}^*. \tag{4.24}$$

The excess mse, $J_{\text{ex}}(n)$, is

$$J_{\text{ex}}(n) = J(n) - J_{\min} = E[\mathbf{v}^T(n)\mathbf{R}\mathbf{v}(n)]. \tag{4.25}$$

and is nonzero when the weights deviate from their optimal values.[4] Defining the weight error correlation matrix,

$$\mathbf{K}(n) = E[\mathbf{v}(n)\mathbf{v}^T(n)], \tag{4.26}$$

and using the property $\text{tr}[\mathbf{AB}] = \text{tr}[\mathbf{BA}]$, yields

$$J_{\text{ex}}(n) = \text{tr}[\mathbf{R}\mathbf{K}(n)] \tag{4.27}$$

[3]Although (4.15) and (4.23) are both derived from (4.12), the two equations differ in that (4.15) is the constant mse based on an arbitrary, fixed weight vector, while (4.23) is the time-varying mse corresponding to the sequence of weight vectors determined by the LMS algorithm.

[4]Note that the expectations in (4.23) and (4.25) are not expectations over time. Rather, they correspond to an ensemble average based on different input sequences selected at random from the same statistical population. Haykin (1986) uses the notation $J(n)$ and $J_{\text{ex}}(n)$ to denote the value of the error based on the instantaneous weight vector and the expected value of the input vector, that is, $J_{\text{ex}}(n) = \mathbf{v}^T(n)\mathbf{R}\mathbf{v}(n)$, and then gives later results in terms of $E[J_{\text{ex}}(n)]$. In a subsequent edition, Haykin (1991) defines $J(n) = E[e^2(n)]$, which leads to $J_{\text{ex}}(n) = E[\mathbf{v}^T(n)\mathbf{R}\mathbf{v}(n)]$. The latter definition is used in this work, and appropriate substitutions are made when reproducing expressions from Haykin (1986).

(Haykin, 1986, Eq. 5.80). It can be shown that the expected value of the system output equals the sum of the target signal power, the minimum mse, and the excess mse, that is,

$$E[y^2(n)] = \sigma_t^2 + J_{\min} + J_{\text{ex}}(n). \tag{4.28}$$

A useful measure of steady-state performance is the steady-state excess mse, $J_{\text{ex}}(\infty)$. This quantity is non-zero for the LMS algorithm, because it reflects the error due to the ongoing adaptive process, that is, the fluctuation of the weights about their optimal values after they have converged in the mean. The steady-state ratio of excess mse to minimum mse $\frac{J_{\text{ex}}(\infty)}{J_{\min}}$ is referred to as *misadjustment*. When the step-size parameter, μ, is small, both $J_{\text{ex}}(\infty)$ and misadjustment are proportional to μ. However, it is not possible to make these quantities arbitrarily small by reducing μ, because the convergence time of the LMS algorithm is inversely proportional to μ. Selection of the step-size parameter, μ, in the LMS algorithm represents a fundamental tradeoff between convergence time and steady-state error (Widrow and Stearns, 1985).

An expression for the steady-state excess mse, $J_{\text{ex}}(\infty)$, for the traditional LMS algorithm with no target signal present is given by

$$J_{\text{ex}}(\infty) = \frac{J_{\min}\mu \sum_{i=1}^{L} \lambda_i}{2 - \mu \text{tr} \sum_{i=1}^{L} \lambda_i} = \frac{J_{\min}\mu \text{tr}[\mathbf{R}]}{2 - \mu \text{tr}[\mathbf{R}]} \tag{4.29}$$

(Nehorai and Malah, 1980; Haykin, 1986, Eq. 5.108). One modification to (4.29) is required before it can be applied to the adaptive noise canceller. The presence of the target signal, $t(n)$, is standard for the adaptive noise canceller configuration, but is in contrast to the typical problem formulation for adaptive transversal filters and the usual assumptions governing derivation of the LMS algorithm. It can be shown that the presence of target in the primary signal does not affect the convergence of the mean weights to their optimal values, but the target signal does introduce additional noise in the gradient estimates, thereby affecting the weight-error correlation matrix and the steady-state excess mse. Following a derivation similar to the one in Haykin

(1986) but including the target signal, $t(n)$, produces

$$J_{\text{ex}}(\infty) = \frac{\mu L \sigma_x^2 (J_{\min} + \sigma_t^2)}{2 - \mu L \sigma_x^2}. \tag{4.30}$$

This expression differs from (4.29) only by the inclusion of σ_t^2. It is intuitively satisfying to see that the effects of the target signal and the minimum error signal (represented by $J_{\min}$) are the same, since both of these signals are uncorrelated with the reference input [(4.9) and (4.14)], and both appear as noise in the adaptive process.

For the traditional method of calculating the step-size parameter, replacing μ in (4.30) with (4.19) yields

$$J_{\text{ex}}(\infty) = \frac{\alpha (J_{\min} + \sigma_t^2)}{2 - \alpha}. \tag{4.31}$$

This result shows that for the traditional method of calculating the step-size parameter, the steady-state excess mse is proportional to the target signal power, rendering the LMS algorithm ineffective in the presence of strong target signals. Although this is recognized as a shortcoming of the LMS algorithm in applications with strong target signals, the explicit relationship described by (4.31) is not well-known.

4.3 Proposed methods of calculating the step-size parameter

4.3.1 Derivation of the optimal step-size parameter

Choice of quantity to optimize

The goal is to optimize, in some sense, the step-size parameter, μ, in equation (4.17). This requires replacing the constant parameter, μ, with a time-varying quantity $\mu(n)$. The time-varying step-size parameter will be derived to minimize the expected value of an error measure at each iteration. Selection of the particular error measure is discussed below.

This approach is based on the modification commonly made when σ_x^2 is unknown *a priori* or when the second-order statistics of $x(n)$ exhibit nonstationarities that vary

slowly with respect to n. In those cases, σ_x^2 is replaced by a running estimate of the power in the reference signal, $\hat{\sigma}_x^2(n)$, and the constant μ in (4.17) is replaced by the time-varying quantity

$$\mu(n) = \frac{\alpha}{L\hat{\sigma}_x^2(n)} \tag{4.32}$$

where the dimensionless step-size parameter, α, remains constant. The proposed modifications will use a similar approach, employing estimates of additional signal powers as necessary.

Another motivation for this approach is the effect of strong target signals on the performance of the adaptive noise canceller. As shown in Sec. 4.2.2, the steady-state excess mse, $J_{\text{ex}}(\infty)$, is proportional to the target power, σ_t^2, as well as to the step-size parameter, μ. If the target signal exhibits short-term power fluctuations (as is characteristic of speech, for example), then the degrading effect of strong target signals can be mitigated by normalizing the step-size parameter with a short-time estimate of target power, so that the incremental adjustments to the adaptive weights are larger in intervals when the target is weak and smaller when the target is strong.

In the following derivation, the error measure to be minimized is the expected value of the total weight error power, $E[\mathbf{v}^T(n)\mathbf{v}(n)]$, or equivalently $\text{tr}[\mathbf{K}(n)]$, which is L times the mean-squared weight error. Rather than minimizing this quantity, it might be preferable to minimize the excess mean-squared output error $J_{\text{ex}}(n)$, which, from (4.25) and (4.27), corresponds to minimizing $E[\mathbf{v}^T(n)\mathbf{R}\mathbf{v}(n)]$, or equivalently, $\text{tr}[\mathbf{K}(n)\mathbf{R}]$. However, the expression for μ obtained by minimizing either $E[\mathbf{v}^T(n)\mathbf{v}(n)]$ or $E[\mathbf{v}^T(n)\mathbf{R}\mathbf{v}(n)]$ is only of theoretical interest, since it will require quantities not available to the adaptive processor. These two error measures have similar structures and are equivalent when $\mathbf{R} = \mathbf{I}$,[5] where $\mathbf{I}$ is the $L \times L$ identity matrix. It will be shown that the step-size parameter that minimizes $E[\mathbf{v}^T(n)\mathbf{v}(n)]$ produces the minimum possible steady-state excess mse, that is, $J_{\text{ex}}(\infty) = 0$, so any differences that arise from minimizing the weight error power instead of the excess mse only affect the transient behavior of $J_{\text{ex}}(n)$.

[5]If the reference input is a sequence of independent, identically-distributed random variables, as explicitly assumed by Duttweiler (1982), then $\mathbf{R} = c\mathbf{I}$, where c is an arbitrary constant.

Similar approaches designed to minimize the mean-squared weight error or mean-squared output error have been proposed for other applications of the LMS algorithm (Duttweiler, 1982; Sondhi and Berkley, 1980; Mikhael, 1986; Yassa, 1987). These methods optimize the steady-state performance when the system is operating in a stationary environment, that is, when the optimal weights, $\mathbf{w}^*$, do not vary with time. They do not attempt to optimize performance in the presence of nonstationarities or during transients. Because the system is continuously adapting, this results in nearly optimal performance in slowly varying nonstationary environments, providing that the degree of nonstationarity is slow relative to the convergence time of the adaptive filter.

Optimal step-size parameters based on error criteria that include performance during transients and in nonstationary environments are available in the literature for some cases. Examples of step-size parameters selected to optimize performance during transients are presented by Horowitz and Senne (1981), Feuer and Weinstein (1985), and Hsia (1983). Horowitz and Senne (1981) select the step-size parameter to provide "fastest initial convergence." Feuer and Weinstein (1985) derive a step-size parameter that minimizes the quantity

$$C = \sum_{n=0}^{\infty} (J(n) - J(\infty)). \tag{4.33}$$

where small values of C correspond to rapid convergence. Hsia (1983) minimizes the convergence ratio,

$$\frac{\mathrm{tr}[\mathbf{v}^T(n+1)\mathbf{v}(n+1)]}{\mathrm{tr}[\mathbf{v}^T(n)\mathbf{v}(n)]}. \tag{4.34}$$

In nonstationary environments, an additional source of error arises from the weight vector lag, that is, the difference between the current weights, $\mathbf{w}(n)$, and the optimal weights, $\mathbf{w}^*(n)$, due to changes in the optimal weights. Optimized step-size parameters for nonstationary environments are presented by Widrow et al. (1976), Hsia (1983), and Gardner (1987). These methods minimize the total weight vector error due to both weight vector lag and misadjustment from the noisy gradient estimate.

Finally, Fisher and Bershad (1983) and Bershad (1987) advocate selecting the

step-size parameter to provide "the smallest misadjustment error at the end of the observation interval," that is, number of iterations. They determine the optimal value of the step-size parameter empirically by plotting misadjustment as a function of step-size parameter for a variety of observation intervals, filter lengths, signal powers, and values of minimum mse. The approach taken in the current work can be considered an analytical means of satisfying Bershad's (1987) criterion, providing that the 'observation interval' is sufficiently long that the system has converged.

Optimization based on weight error power

Derivation of the optimal step-size parameter based on minimizing the trace of the weight error correlation matrix, $\mathrm{tr}[\mathbf{K}(n)]$, at each iteration, first requires an expression for the time evolution of $\mathbf{K}(n)$. The derivation of this expression is omitted here, but can be found in Haykin (1986, pp. 221–225). The general idea is to use (4.1), (4.17), and (4.24) to determine the time evolution of the weight error vector, $\mathbf{v}(n)$, and then take the outer product of both sides of the equation according to (4.26). With no target signal present, the resulting time evolution of the weight-error correlation matrix is

$$\mathbf{K}(n+1) = \mathbf{K}(n) - \mu[\mathbf{R}\mathbf{K}(n) + \mathbf{K}(n)\mathbf{R}] + \mu^2\mathbf{R}\mathrm{tr}[\mathbf{R}\mathbf{K}(n)] + \mu^2 J_{min}\mathbf{R} \qquad (4.35)$$

(Haykin, 1986, 5.74). Including the target signal and following the steps used to derive (4.35) yields

$$\mathbf{K}(n+1) = \mathbf{K}(n) - \mu[\mathbf{R}\mathbf{K}(n) + \mathbf{K}(n)\mathbf{R}] + \mu^2\mathbf{R}\mathrm{tr}[\mathbf{R}\mathbf{K}(n)] + \mu^2(J_{\min} + \sigma_t^2)\mathbf{R}. \quad (4.36)$$

Again, as discussed following (4.30), the effect of the target signal is the same as the effect of the minimum error.

Given the state of the system at time n, minimization of the expected value of the total weight error power at time $(n+1)$, $E[\mathbf{v}^T(n+1)\mathbf{v}(n+1)]$ or equivalently

$\mathrm{tr}[\mathbf{K}(n+1)]$, begins by taking the trace of (4.36), yielding

$$\mathrm{tr}[\mathbf{K}(n+1)] = \mathrm{tr}[\mathbf{K}(n)] - 2\mu\mathrm{tr}[\mathbf{RK}(n)] + \mu^2\mathrm{tr}\mathbf{R}(\mathrm{tr}[\mathbf{RK}(n)] + J_{\min} + \sigma_t^2) \quad (4.37)$$

where the properties $\mathrm{tr}[\mathbf{A}+\mathbf{B}] = \mathrm{tr}[\mathbf{A}] + \mathrm{tr}[\mathbf{B}]$ and $\mathrm{tr}[\mathbf{AB}] = \mathrm{tr}[\mathbf{BA}]$ have been used. The value of μ that minimizes the total power in the weight error at each iteration, denoted $\mu^*(n)$, is found by taking the first derivative of (4.37) with respect to μ, setting it equal to zero, and solving for μ, resulting in

$$\mu^*(n) = \frac{\mathrm{tr}[\mathbf{RK}(n)]}{(\mathrm{tr}\mathbf{R})(\mathrm{tr}[\mathbf{RK}(n)] + J_{\min} + \sigma_t^2)} \quad (4.38)$$

It can be verified that this is in fact a minimum, because the second derivative is positive.

Substituting (4.10), (4.27), and (4.28) into (4.38) yields

$$\mu^*(n) = \frac{J_{\mathrm{ex}}(n)}{L\sigma_x^2(\sigma_t^2 + J_{\min} + J_{\mathrm{ex}}(n))} = \frac{J_{\mathrm{ex}}(n)}{L\sigma_x^2 E[y^2(n)]}. \quad (4.39)$$

Finally, the constant α is introduced in (4.39) to facilitate comparison with other algorithms, producing

$$\mu^*(n) = \frac{\alpha J_{\mathrm{ex}}(n)}{L\sigma_x^2(\sigma_t^2 + J_{\min} + J_{\mathrm{ex}}(n))} = \frac{\alpha J_{\mathrm{ex}}(n)}{L\sigma_x^2 E[y^2(n)]}. \quad (4.40)$$

This constant affects the convergence of the adaptive algorithm with optimized step-size parameter, but does not affect the steady-state performance, as will be shown below. Substituting (4.19) into (4.40) reveals that

$$\mu^*(n) = \mu_{\mathrm{trad}} \frac{J_{\mathrm{ex}}(n)}{E[y^2(n)]}. \quad (4.41)$$

$J_{\mathrm{ex}}(n)$ represents output signal power that potentially could be cancelled, but remains because the weights are at suboptimal values. Therefore, (4.41) can be interpreted as stating that *the optimal step-size parameter at each iteration equals the traditional step-size parameter adjusted by the ratio of cancellable output signal power to total*

output signal power.

For the optimal method of calculating the step-size parameter, substituting (4.40) for $n = \infty$ into (4.30) and rearranging terms yields

$$(2 - \alpha)J_{\text{ex}}(\infty)(J_{\text{ex}}(\infty) + J_{\min} + \sigma_t^2) = 0. \tag{4.42}$$

The nonnegative solution of (4.42) is

$$J_{\text{ex}}(\infty) = 0. \tag{4.43}$$

This result proves that, in the steady state, the method of calculating the step-size parameter described by (4.40) truly is optimal.

4.3.2 Modifications to the optimal step-size parameter

The expression for the optimal step-size parameter given by (4.40) cannot be implemented in a real system, since it requires exact knowledge either of $J_{\text{ex}}(n)$ or equivalently of the autocorrelation matrix, $\mathbf{R}$, and the current weight error correlation matrix $\mathbf{K}(n)$. None of these quantities is known. $\mathbf{R}$ is implicitly estimated by the LMS algorithm, and $\mathbf{K}(n)$ can be computed from the current weights only if the optimal weights, $\mathbf{w}^*$, are known. Obviously, if the optimal weights were known, there would be no need for any adaptive algorithm. The dependence on these quantities is not surprising, however, since $J_{\text{ex}}(n)$ and $\mathbf{K}(n)$ both measure the deviation of the current weights from the optimal weights, and intuitively, the "best" size step to take at any point depends on the magnitude of that deviation.

In order to determine an expression for the step-size parameter that can be implemented in a real system, additional assumptions are required. The first approach approximates the optimal method derived in the previous section by using (4.40) with an estimate for the excess mse, that is,

$$\hat{\mu}^*(n) = \frac{\alpha\widehat{J_{\text{ex}}}(n)}{L\sigma_x^2(\sigma_t^2 + J_{\min} + J_{\text{ex}}(n))} = \frac{\alpha\widehat{J_{\text{ex}}}(n)}{L\sigma_x^2 E[y^2(n)]}. \tag{4.44}$$

The estimate of the excess mse is based on powers of signals available to the adaptive processor, specifically,

$$\widehat{J_{\text{ex}}}(n) = E[y^2(n)] + \sigma_x^2 - \sigma_{\text{pri}}^2, \tag{4.45}$$

where σ_{pri}^2 is the power of the primary input signal. Implementing this method in a real system requires estimating the power of three signals, the primary input, the reference input, and the system output, to produce the time-varying estimates $\widehat{\sigma_{\text{pri}}^2}(n)$, $\widehat{\sigma_x^2}(n)$, and $\widehat{\sigma_y^2}(n)$. The estimate of the primary input power can be considered the sum of time-varying estimates of σ_t^2 and σ_j^2, while the estimate of the system output power can be considered the sum of a time-varying estimate of σ_t^2, and two terms due to the jammer, J_{min} and $J_{\text{ex}}(n)$. Mathematically,

$$\widehat{\sigma_{\text{pri}}^2}(n) = \sigma_{t,p}^2(n) + \sigma_{j,p}^2(n) \tag{4.46}$$

and

$$\widehat{\sigma_y^2}(n) = \sigma_{t,y}^2(n) + J_{\text{min}} + J_{\text{ex}}(n), \tag{4.47}$$

where $\sigma_{t,y}^2(n)$ is the estimate of target power derived from the system output, $\sigma_{t,p}^2(n)$ is the estimate of target power derived from the primary input, and $\sigma_{j,p}(n)$ is the estimate of jammer power derived from the primary input. Substituting the estimates given by (4.46) and (4.47) into (4.45) and rearranging yields

$$\widehat{J_{\text{ex}}}(n) = J_{\text{ex}}(n) + J_{\text{min}} + \widehat{\sigma_x^2}(n) - \sigma_{j,p}^2(n) + \sigma_{t,y}^2(n) - \sigma_{t,p}^2(n). \tag{4.48}$$

This shows that $\widehat{J_{\text{ex}}}(n)$ is a good estimate of $J_{\text{ex}}(n)$ when the minimum mse, J_{min}, is small and the power estimates are accurate, that is, $\widehat{\sigma_x^2}(n) \approx \sigma_{j,p}^2(n)$ and $\sigma_{t,y}^2(n) \approx \sigma_{t,p}^2(n)$. In a real system, the value of $\widehat{J_{\text{ex}}}(n)$ may be negative due to fluctuations in the power estimates. When this occurs, $\widehat{J_{\text{ex}}}(n)$ can be replaced with zero for that iteration.

To determine the steady-state excess mse associated with this approximation-to-optimal method, it is necessary to make some assumptions about the estimation error.

The estimation error, Δ, is defined by

$$\Delta = \widehat{J_{\text{ex}}}(n) - J_{\text{ex}}(n) \tag{4.49}$$

and is related to the output error power associated with the weight error vector implicitly defined by $\widehat{J_{\text{ex}}}(n)$. In order to simplify the following analysis, it is assumed that Δ is a positive constant. Substituting (4.44) and (4.49) at $n = \infty$ into (4.30) and rearranging yields

$$((2-\alpha)J_{\text{ex}}(\infty) - \alpha\Delta)(J_{\text{ex}}(\infty) + J_{\min} + \sigma_t^2) = 0, \tag{4.50}$$

with the positive solution

$$J_{\text{ex}}(\infty) = \frac{\alpha\Delta}{2-\alpha}. \tag{4.51}$$

If $\widehat{J_{\text{ex}}}(n)$ is exactly equal to $J_{\text{ex}}(n)$, then this method is equivalent to the optimal method, the estimation error, Δ, is zero, and the steady state performance is optimal, that is, $J_{\text{ex}}(\infty) = 0$. From (4.48), this only occurs if $J_{\min} = 0$, $\widehat{\sigma_x^2}(n) = \sigma_{j,p}^2(n)$, and $\sigma_{t,y}^2(n) = \sigma_{t,p}^2(n)$. Any error in the estimate of $\widehat{J_{\text{ex}}}(n)$ will cause the steady state excess mse to be nonzero and proportional to the estimate error, Δ. Defining constants c_x and c_t to indicate the fractional error in the estimates,

$$c_x = \frac{\widehat{\sigma_x^2}(n) - \sigma_{j,p}^2(n)}{\sigma_x^2} \tag{4.52}$$

$$c_t = \frac{\sigma_{t,y}^2(n) - \sigma_{t,p}^2(n)}{\sigma_t^2}, \tag{4.53}$$

and using (4.48) and (4.49), it can be seen that the estimation error, Δ, is composed of three quantities, proportional to the powers $J_{\min}$, σ_x^2, and σ_t^2,

$$\Delta = J_{\min} + c_x\sigma_x^2 + c_t\sigma_t^2. \tag{4.54}$$

Substituting this expression for Δ into (4.51) shows that the approximation-to-optimal method described by (4.44) and (4.45) results in a steady state excess mse that in-

creases with target signal power.

A second candidate for adjusting the step-size parameter can be obtained by making assumptions about the weight error correlation matrix. If the individual weight errors are independent, identically-distributed random variables with variance c,[6] then $\mathbf{K}(n) = c\mathbf{I}$. Using this assumption and (4.10) in (4.27) gives

$$J_{\text{ex}}(n) = \text{tr}[\mathbf{R}\mathbf{K}(n)] = c\text{tr}[\mathbf{R}] = cL\sigma_x^2, \tag{4.55}$$

and (4.40) becomes

$$\mu(n) = \frac{\alpha c}{\sigma_t^2 + J_{\min} + J_{\text{ex}}(n)} = \frac{\alpha c}{E[y^2(n)]}. \tag{4.56}$$

Since c and α are both constants and the value of c is arbitrary, it can be eliminated without loss of generality. Furthermore, to simplify comparisons with other methods, it will be useful to include a factor of $\frac{1}{L}$, yielding

$$\mu_{\text{out}}(n) = \frac{\alpha}{L(\sigma_t^2 + J_{\min} + J_{\text{ex}}(n))} = \frac{\alpha}{LE[y^2(n)]}. \tag{4.57}$$

the output method for calculating the step-size parameter. Note that the quantity $E[y^2(n)]$ can be estimated from the output of the system and that no assumptions have been made about the autocorrelation matrix, $\mathbf{R}$.

Even if individual weight errors are independent, identically-distributed random variables as assumed above, their variance will not remain constant as the LMS algorithm converges in response to new inputs. As a result, the output method produces a steady-state excess mse that is nonzero, but independent of the target power. This can be seen by substituting (4.57) for $n = \infty$ into (4.30) and rearranging terms, yielding

$$(2J_{\text{ex}}(\infty) - \alpha\sigma_x^2)(J_{\text{ex}}(\infty) + J_{\min} + \sigma_t^2) = 0. \tag{4.58}$$

[6]The entries of the weight error correlation matrix, $\mathbf{K}(n)$, are dimensionless, because the weights themselves are dimensionless.

The positive solution to (4.58) is

$$J_{\text{ex}}(\infty) = \frac{\alpha\sigma_x^2}{2}, \tag{4.59}$$

which is independent of the target power.

The final method proposed for calculating the step-size parameter is obtained by combining the advantages of the traditional and output methods. Recall that for the traditional method, the step-size parameter is normalized by the reference input power, σ_x^2, producing a steady-state excess mse that is proportional to the target signal power. For the output method, the step-size parameter is normalized by the system output power, $E[y^2(n)]$, producing a steady-state excess mse that is independent of the target signal power. Therefore, the advantage of the traditional method is that the steady-state excess mse is very small in the presence of weak target signals, while the advantage of the output method is that the steady-state excess mse is constant in the presence of strong target signals. Both of these advantages can be obtained by normalizing by the sum of the reference input and system output powers, according to

$$\mu_{\text{sum}}(n) = \frac{\alpha}{L(\sigma_x^2 + \sigma_t^2 + J_{\min} + J_{\text{ex}}(n))} = \frac{\alpha}{L(\sigma_x^2 + E[y^2(n)])}. \tag{4.60}$$

This method of calculating the step-size parameter was used by Greenberg and Zurek (1992).

The steady-state performance of the sum method can be determined by substituting (4.60) for $n = \infty$ into (4.30) and rearranging, which yields

$$2(J_{\text{ex}}(\infty))^2 + [2(J_{\min} + \sigma_t^2) + (2-\alpha)\sigma_x^2]J_{\text{ex}}(\infty) - \alpha\sigma_x^2(J_{\min} + \sigma_t^2) = 0. \tag{4.61}$$

The positive solution of (4.61) is

$$J_{\text{ex}}(\infty) = \frac{\sqrt{[(2-\alpha)\sigma_x^2 + 2(J_{\min} + \sigma_t^2)]^2 + 8\alpha\sigma_x^2(J_{\min} + \sigma_t^2)} - (2-\alpha)\sigma_x^2 - 2(J_{\min} + \sigma_t^2)}{4}. \tag{4.62}$$

	traditional	optimal	optimal approx	output	sum
adaptive step-size parameter	$\mu = \frac{\alpha}{L\sigma_x^2}$	$\mu^*(n) = \frac{\alpha J_{ex}(n)}{L\sigma_x^2 E[y^2(n)]}$	$\widehat{\mu^*}(n) = \frac{\alpha \widehat{J_{ex}}(n)}{L\sigma_x^2 E[y^2(n)]}$	$\mu_{out}(n) = \frac{\alpha}{LE[y^2(n)]}$	$\mu_{sum}(n) = \frac{\alpha}{L(\sigma_x^2+E[y^2(n)])}$
convergence	$0 < \alpha < 2$	$0 < \alpha < 2$	$0 < \alpha < 2$ if $\Delta \ll \sigma_t^2 + J_{min}$	$0 < \alpha < 2\frac{E[y^2(n)]}{\sigma_x^2}$	$0 < \alpha < 2$
steady-state excess mse $J_{ex}(\infty)$	$\frac{\alpha(J_{min}+\sigma_t^2)}{2-\alpha}$	0	$\frac{\alpha\Delta}{2-\alpha}$	$\frac{\alpha\sigma_x^2}{2}$	$\lim_{(J_{min}+\sigma_t^2)\to 0} = 0$ $\lim_{(J_{min}+\sigma_t^2)\to\infty} = \frac{\alpha\sigma_x^2}{2}$

Table 4.1: Summary of results for five methods of adjusting the step-size parameter described in the text.

It can be shown that

$$\lim_{(J_{min}+\sigma_t^2)\to 0} J_{ex}(\infty) = 0 \tag{4.63}$$

and

$$\lim_{(J_{min}+\sigma_t^2)\to\infty} J_{ex}(\infty) = \frac{\alpha\sigma_x^2}{2}, \tag{4.64}$$

confirming that the sum method has the advantages of both the traditional and output methods at the two extremes of target signal power.

The five methods of calculating the step-size parameter presented above are summarized in Table 4.1. For each of these methods, it is necessary to consider the limits on α required for the adaptive algorithm to converge. From Widrow and Stearns (1985), the algorithm converges for $0 < \mu < \frac{2}{\lambda_{max}}$, and a conservative upper bound can be found by replacing the maximum eigenvalue, λ_{max}, with the sum of all eigenvalues, $\sum_{i=1}^{L} \lambda_i$, which, from (4.10), equals $L\sigma_x^2$. Using this conservative upper bound, the condition required for convergence is $0 < \mu < \frac{2}{L\sigma_x^2}$. Equations (4.19), (4.40),

(4.44), (4.57), and (4.60) were each substituted for μ in this inequality, and the resulting limits on the dimensionless step-size parameter, α, are included in Table 4.1. The limit given for the sum method represents an extremely conservative upper bound based on the assumption that $E[y^2(n)] = 0$. The limit given for the output method reveals a potential problem, since the upper bound on α will be very small when the algorithm has converged and the target signal is weak. In a practical system this could be overcome by selecting α assuming a minimum power level for $E[y^2(n)]$ and then substituting the minimum value into (4.57) whenever that minimum exceeds the current estimate of $E[y^2(n)]$.

4.3.3 Comparison of methods for calculating the step-size parameter.

The five methods described above for calculating the step-size parameter (traditional, optimal, approximation-to-optimal, output, and sum) are compared on the basis of steady-state performance and transient behavior.

Steady-state performance

The measure of steady-state performance is the steady-state excess mse, $J_{ex}(\infty)$, which reflects the error due to the ongoing adaptive process, that is, the fluctuation of the weights about their optimal values after they have converged in the mean. The steady state excess mse was calculated for each of the five methods in the previous sections, and the results are included in Table 4.1.

Figure 4.1 shows the steady-state performance for all but the optimal method in terms of the jammer gain due to the system ($\frac{J(\infty)}{\sigma_j^2}$) as a function of the input TJR ($\frac{\sigma_t^2}{\sigma_j^2}$). This is similar to the normalized residual noise used by Lu and Clarkson (1993). Values of jammer gain less than unity (0 dB) indicate beneficial performance due to the adaptive noise canceller, while values of the jammer gain that exceed unity indicate that the output of the system is degraded relative to the input. The excess mse for the different methods was calculated according to (4.31), (4.43), (4.51), (4.59),

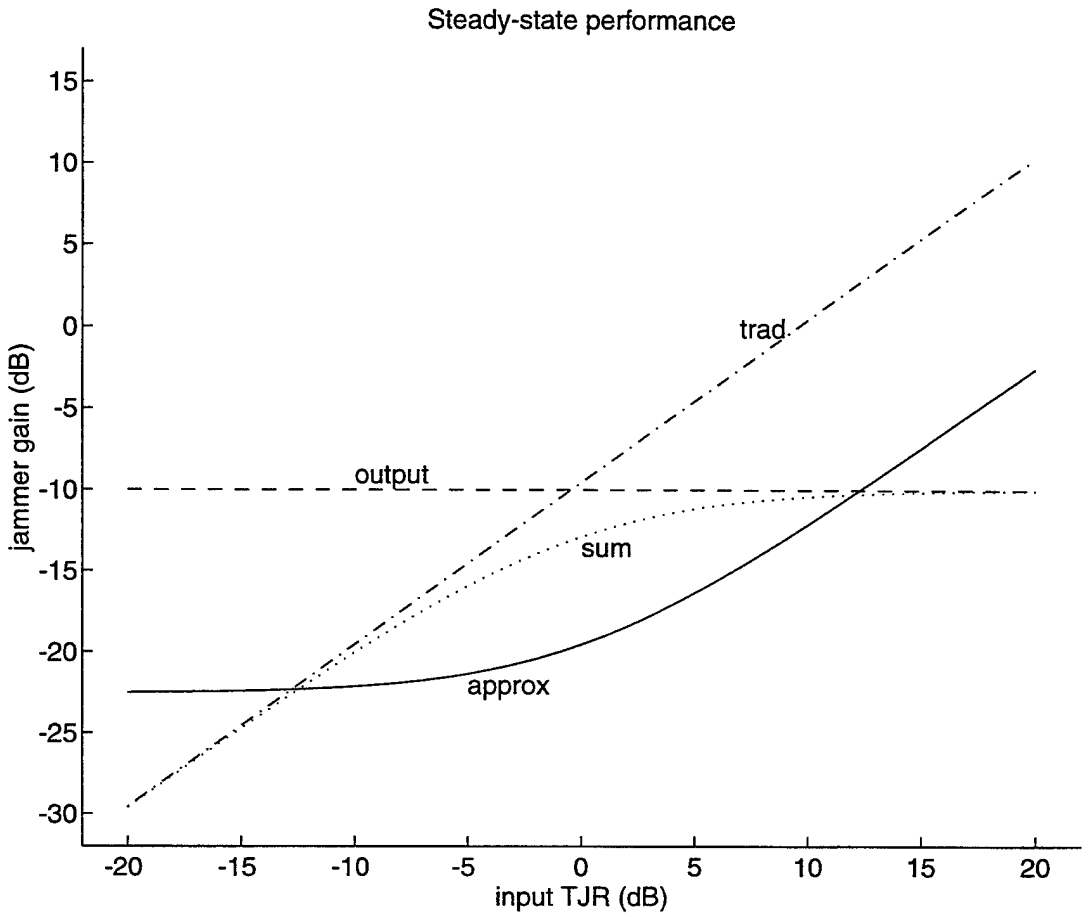

Figure 4-1: Steady-state performance for four methods of computing the step-size parameter. The plot shows the jammer gain due to the system as a function of the input TJR. The four methods are the traditional method, the approximation-to-optimal method, the output method, and the sum method, labeled *trad*, *approx*, *output*, and *sum*, respectively. The curves are based on (4.31), (4.51), (4.59) (4.62) from the text.

and (4.62), for $\alpha = 0.2$, $L = 10$, and $J_{\min} = 0$. Figure 4.2 shows the steady-state performance for all five methods with the same parameter values as Fig. 4.1, except that $\frac{J_{\min}}{\sigma_j^2} = 0.33$. For both figures, the estimation error, Δ, in (4.51) was computed according to (4.54), with $c_x = c_y = 0.05$, corresponding to 5 percent error in the power estimates. Results for the optimal method are not shown in Fig 4.1, since, with $J_{\min} = 0$, the jammer gain is zero ($-\infty$ dB).

For the optimal method of calculating the step-size parameter, the steady-state excess mse is zero. This verifies that, at least in the steady-state, the method derived

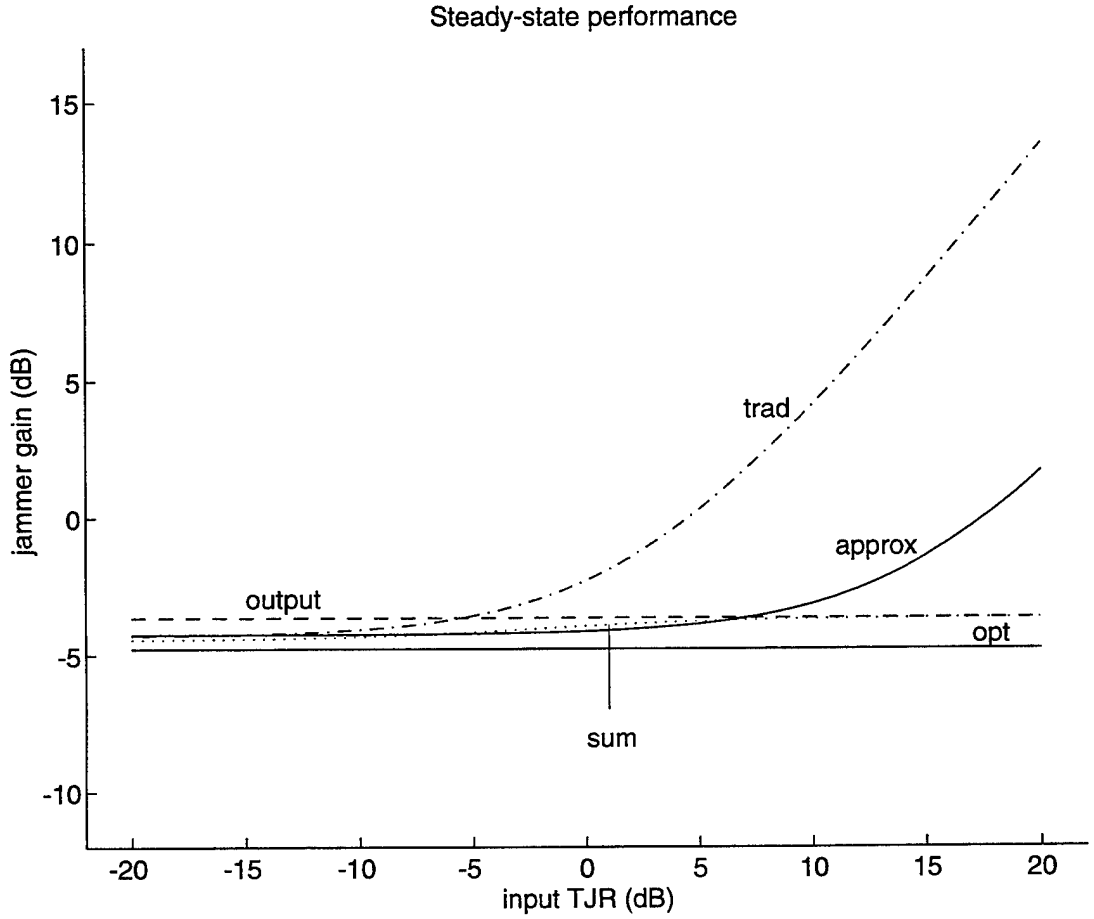

Figure 4-2: Steady-state performance for five methods of computing the step-size parameter. The plot shows the jammer gain due to the system as a function of the input TJR. The five methods are the traditional method, the optimal method, the approximation-to-optimal method, the output method, and the sum method, labeled *trad*, *opt*, *approx*, *output*, and *sum*, respectively. The curves are based on (4.31), (4.43), (4.51), (4.59) (4.62) from the text.

in Section 4.3.1 truly is optimal. However, the optimal method requires knowledge of quantities that are not available to a real system. Because of the assumptions made to derive the approximation-to-optimal, output, and sum methods, the resulting steady-state performance is suboptimal, with nonzero values of steady-state excess mse. However, from Figs. 4.1 and 4.2, it is clear that all three of these methods are preferable to the traditional method in the presence of appreciable target signal power. The performance of the sum method is particularly attractive, since excess jammer power both approaches zero for weak target signals and remains limited for strong target signals.

Transient behavior

In this section, expressions are derived to characterize the transient behavior of the LMS algorithm with the five different methods of calculating the step-size parameter. First, iterative expressions are determined for the method of steepest descent, whose transient behavior is considerably easier to analyze than that of the LMS algorithm. Then, those results are related to the transient behavior of the LMS algorithm. Finally, additional assumptions are used to determine the time constants of simple exponential decays that approximate the transient behavior of the sum method of calculating the step-size parameter.

Expressions for the transient behavior of the LMS algorithm with a constant (traditional) step-size parameter are available in the literature (e.g. Haykin, 1986, Eq. 5.111), but these expressions are quite complicated and do not lend themselves to intuitive interpretations of convergence time. However, under independence theory, the ensemble average of the weights (for identical initial conditions and different input sequences) is equivalent to the weights obtained by the method of steepest descent, which uses the exact gradient at each iteration. Therefore, the expressions derived here are based on the method of steepest descent, and they characterize the mean transient behavior of the weights (Alexander, 1986) and provide a lower bound on the transient behavior of the excess mse (Widrow and Stearns, 1985).

The transient properties of the steepest descent algorithm are analyzed by con-

sidering the decay of different modes associated with the different eigenvalues and eigenvectors of $\mathbf{R}$ as in Widrow and Stearns (1985) and Haykin (1986). The autocorrelation matrix is decomposed to

$$\mathbf{R} = \mathbf{Q}\mathbf{\Lambda}\mathbf{Q}^T \tag{4.65}$$

where the columns of $\mathbf{Q}$ are the normalized eigenvectors of $\mathbf{R}$, and $\mathbf{\Lambda}$ is a diagonal matrix with diagonal elements equal to λ_i, the eigenvalues of $\mathbf{R}$. $\mathbf{Q}$ is orthonormal, and its geometrical interpretation is a rotation that aligns the coordinate space with the principle axes of the hyperparaboloid representing the error surface. This rotation can be applied to the weight error vector to produce a rotated weight error vector,

$$\boldsymbol{\nu}(n) = \mathbf{Q}^T\mathbf{v}(n), \tag{4.66}$$

with the behavior of the individual modes decoupled. This permits the description of the excess mse as

$$J_{\text{ex}}(n) = \sum_{i=1}^{L} \lambda_i(1-\mu\lambda_i)^{2n}|\nu_i(0)|^2 \tag{4.67}$$

(Haykin, 1986, Eq. 5.28) where $\nu_i(0)$ is the i^{th} element of the initial rotated error vector, $\boldsymbol{\nu}(0)$. Because the method of steepest descent uses the exact gradient, the performance is characterized by the weight error vector, $\mathbf{v}(n)$, and the rotated vector $\boldsymbol{\nu}(n)$. It is not necessary to take the expected value, as it was in the analysis of the LMS algorithm.

For the traditional method of calculating the step-size parameter, (4.67) represents a sum of exponential decays. Each mode is associated with its own time constant,

$$\tau_i = \frac{-1}{2\ln(1-\mu\lambda_i)} \tag{4.68}$$

(Haykin, 1986, Eq. 5.30), which is approximated as

$$\tau_i \approx \frac{1}{2\mu\lambda_i} \tag{4.69}$$

for $\mu\lambda_i \ll 1$ (Haykin, 1986, Eq. 5.31). Substituting (4.19) into (4.69) yields

$$\tau_i \approx \frac{L\sigma_x^2}{2\alpha\lambda_i} \tag{4.70}$$

for $\alpha\lambda_i \ll L\sigma_x^2$. Haykin (1986, p. 236) points out that although small eigenvalues of $\mathbf{R}$ lead to slowly converging terms in the transient component of $J_{\text{ex}}(n)$, these small eigenvalues also correspond to modes that make a relatively small contribution to $J_{\text{ex}}(n)$.

The transient behavior of the proposed methods for calculating the step-size parameter can be characterized using the above approach. However, since μ in (4.67) is replaced by the time-varying $\mu(n)$, the resulting decay is not necessarily exponential. Further, μ in (4.67) may depend on $J_{\text{ex}}(n)$, so that the form of the decay may change as the power of the excess mse changes with respect to other power levels. Therefore, it will be useful to consider the change in $J_{\text{ex}}(n)$ at each iteration. This requires defining the components of $J_{\text{ex}}(n)$ attributable to the individual modes, $J_{\text{ex},i}(n)$, so that

$$J_{\text{ex}}(n) = \sum_{i=1}^{L} J_{\text{ex},i}(n). \tag{4.71}$$

With this definition and (4.67)

$$J_{\text{ex}}(n+1) = \sum_{i=1}^{L} J_{\text{ex},i}(n+1) = \sum_{i=1}^{L} (1-\mu(n)\lambda_i)^2 J_{\text{ex},i}(n). \tag{4.72}$$

Substituting the appropriate expressions for $\mu(n)$ into (4.72), it is possible to obtain a recursive formula for the excess mse associated with each of the proposed methods of calculating the step-size parameter. For example, for the sum method, substituting (4.60) into (4.72) gives

$$J_{\text{ex}}(n+1) = \sum_{i=1}^{L} J_{\text{ex},i}(n+1) = \sum_{i=1}^{L} \left(1 - \frac{\alpha\lambda_i}{L(\sigma_x^2 + J_{\text{ex}}(n) + J_{\min} + \sigma_t^2)}\right)^2 J_{\text{ex},i}(n). \tag{4.73}$$

Similarly, substituting (4.40), (4.44), and (4.57) into (4.72) produces iterative formulas for the excess mse associated with the optimal, approximation-to-optimal, and

output methods, respectively. Iterating these recursive formulas for known parameter values produces a smooth decay curve that corresponds to the transient behavior of the steepest descent algorithm. The relation to the transient behavior of the LMS algorithm is discussed below.

Figure 4.3 shows the transient behavior predicted by (4.72) for the five methods of calculating the step-size parameter. The three parts of the figure show the transient behavior for input TJRs of -10, 0, and $+10$ dB. The parameter values used to generate these curves were $\alpha = 0.2$, $L = 10$, $J_{\min} = 0$, $\sigma_x^2 = \sigma_j^2$, $J_{\text{ex}}(0) = \sigma_j^2$, and $\lambda_i = \sigma_x^2$ for all i.

The curves shown in Fig. 4.3 describe the transient behavior of the steepest descent algorithm and can be interpreted to provide some understanding of the transient behavior of the LMS algorithm. The transient performance of the steepest descent algorithm corresponds to the mean transient behavior of the weights and a lower bound on the transient behavior of the excess mse for the LMS algorithm. Although the curves in Fig. 4.3 all converge to zero (in general, to $\frac{J_{\min}}{\sigma_j^2}$), the steady-state performance of the LMS algorithm is nonzero for all but the optimal method, as seen in Fig. 4.1. The implication of Fig. 4.3 for the performance of the LMS algorithm is not the value to which the curves converge, but in the rate of convergence, since the transient performance of the steepest descent algorithm is the same as the mean behavior of the LMS weights. For example, for the traditional method with input TJR $= -10$ dB, the jammer gain starts at unity and converges to a steady-state value near 0.01 (-20 dB). The ensemble average of performance curves for different input samples with the same parameter values will exhibit transient behavior with the shape of the traditional method curve in the top panel of Fig. 4.3, but will converge to the steady-state value of 0.01.

With this understanding, it is possible to make several observations by comparing Figs. 4.1 and 4.3. First, in general, the conditions producing poorer steady-state performance (the output method at low TJR and the traditional method at high TJR) converge faster that those that produce more favorable steady-state performance. This is a direct result of the fundamental tradeoff inherent in selection of

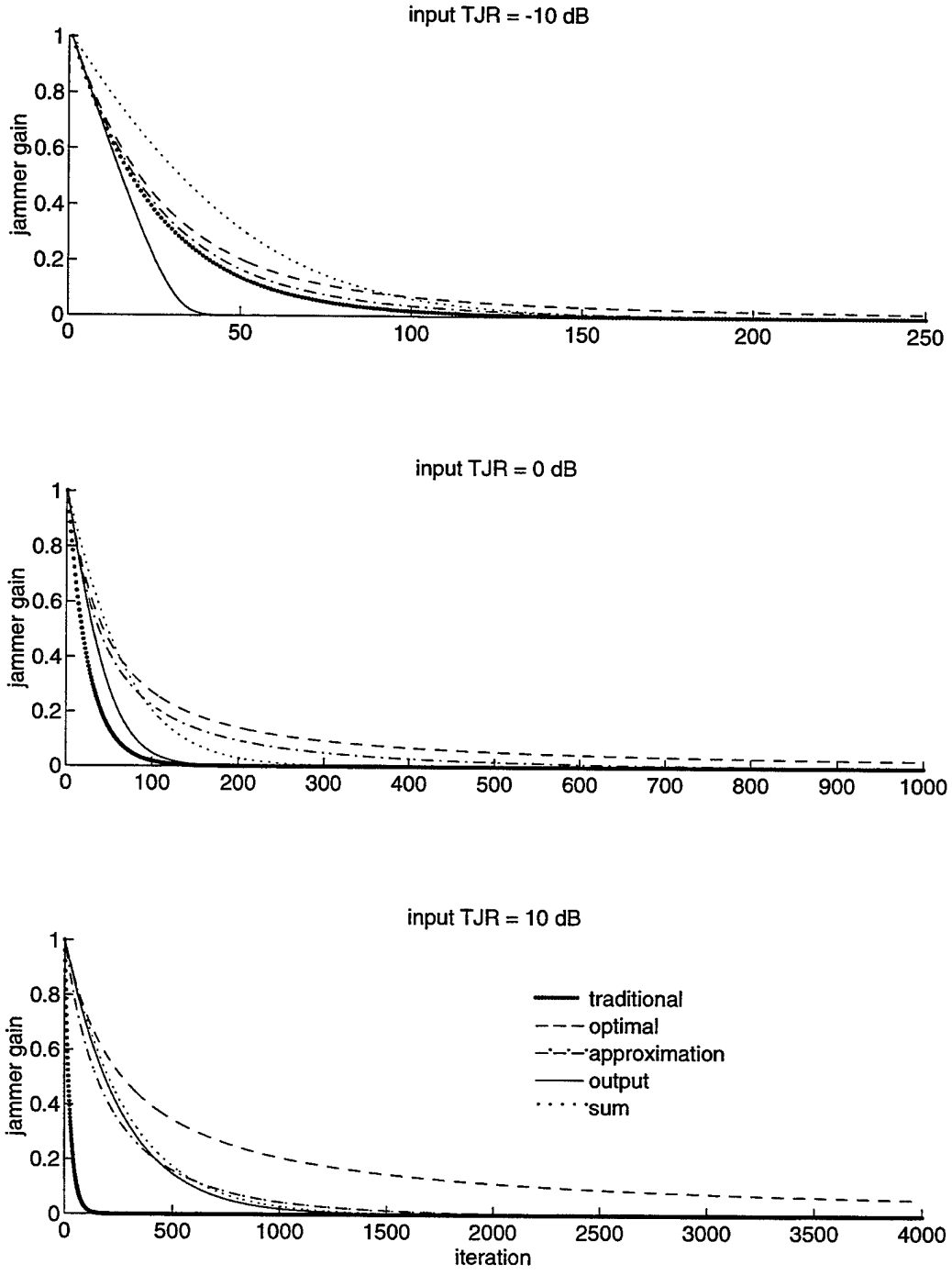

Figure 4-3: Transient behavior for five methods of computing the step-size parameter. The curves are based on substituting the appropriate expression for computing the step-size parameter into (4.72). The three panels show the behavior for input TJRs of -10, 0, and 10 dB.

the dimensionless step-size parameter, α. Second, despite the sometimes rapid initial convergence of the optimal method, it always exhibits the slowest convergence overall. This is because of the presence of the excess mse in the numerator of the optimal step-size parameter given by (4.40). As the excess mse converges, the step-size parameter is gradually reduced, and the convergence slows as it progresses. Finally, for a practical system, at high TJR the transient behavior is similar for the sum, output, and approximation-to-optimal methods. At low TJR, the sum method converges slightly slower than the traditional and approximation-to-optimal methods, but that disadvantage is insignificant compared to the improved steady-state performance obtained with the sum method.

Although the curves in Fig. 4.3 were computed for the case of equal eigenvalues, similar results are obtained when the eigenvalues are not equal. Unequal eigenvalues cause the different modes to converge at different rates, and the overall convergence is the sum of the modes. For a single eigenvalue, the transient behavior of the corresponding mode is of the form of Fig. 4.3 to within a scaling of the abscissa. Therefore, the transient behavior of the total excess mse corresponds to the sum of such scaled curves, and the relative performance for the different methods will follow the trends shown in Fig. 4.3.

Estimates of the convergence time based on an exponential decay can be obtained for particular situations by making additional assumptions. This will be demonstrated in the following derivation for the sum method, the practical method with the most promising steady-state performance. Similar derivations can be performed to gain insight into the transient performance of the other methods under particular conditions.

The relation described by (4.73) does not represent a sum of simple exponential decays, due to the presence of the quantity $J_{\text{ex}}(n)$ in the denominator. If the excess mse is small relative to the power of the other signals in the normalization ($J_{\text{ex}}(n) \ll \sigma_x^2 + \sigma_t^2 + J_{\min}$), then the effect of $J_{\text{ex}}(n)$ in the denominator of (4.73) is negligible

and the decay associated with each mode will be exponential with time constant

$$\tau_i \approx \frac{L(\sigma_x^2 + \sigma_t^2 + J_{\min})}{2\alpha\lambda_i} \tag{4.74}$$

for $\alpha\lambda_i \ll L(\sigma_x^2 + \sigma_t^2 + J_{\min})$. On the other hand, if the excess mse is large relative to the uncancellable signal powers ($J_{\text{ex}}(n) \gg \sigma_t^2 + J_{\min}$),[7] then (4.73) becomes

$$J_{\text{ex}}(n+1) = \sum_{i=1}^{L} J_{\text{ex},i}(n+1) \approx \sum_{i=1}^{L} \left(1 - \frac{\alpha\lambda_i}{L(\sigma_x^2 + J_{\text{ex}}(n))}\right)^2 J_{\text{ex},i}(n), \tag{4.75}$$

and the effect of $J_{\text{ex}}(n)$ in the denominator cannot be ignored. At the beginning of the adaptive process, the initial excess mse can be approximated by the primary jammer power, which is roughly equal to the power of the reference input ($J_{\text{ex}}(0) \approx \sigma_j^2 \approx \sigma_x^2$). Substituting σ_x^2 for $J_{\text{ex}}(n)$ in the last term of (4.75) reveals that the excess mse associated with each mode *initially* decays with a time constant given by

$$\tau_i \approx \frac{L\sigma_x^2}{\alpha\lambda_i} \tag{4.76}$$

for $\alpha\lambda_i \ll 2L\sigma_x^2$. As the excess mse decays from its initial value, $J_{\text{ex}}(n)$ becomes smaller than σ_x^2, the second term in the denominator of (4.73) decreases, and the excess mse decays more rapidly than indicated by (4.76). Therefore (4.76) provides a conservative estimate of the time constant.

Figure 4.4 shows the transient performance for the sum method, computed from the recursive formula given in (4.73), together with decaying exponentials with time constants given by (4.74) and (4.76). The parameter values are the same as those used to generate Fig. 4.3. As expected, when the TJR is high (bottom panel of Fig. 4.4), the transient predicted by the recursive formula closely matches the exponential with decay given by (4.74). When the TJR is low (top panel of Fig. 4.4), the transient predicted by the recursive formula initially tracks the exponential with decay given

[7] It is *not* reasonable to assume that the excess mse is very much greater than the reference input power ($J_{\text{ex}}(n) \gg \sigma_x^2$). It is assumed that the reference input power (σ_x^2) is comparable to the primary jammer input power (σ_j^2), therefore this situation could only occur if the system provided considerable amplification of the jammer signal.

by (4.76). As the system converges, the transient predicted by the recursive formula converges faster than the exponential, as expected. Eventually, the excess mse converges to a level sufficiently low that the assumptions used to derive (4.76) are invalid, and at some point the assumptions used to derive (4.74) become valid. For this case of equal eigenvalues used to generate Fig. 4.4, the time constants given by (4.74) and (4.76) are equivalent when the reference signal power equals the sum of the target signal and the excess mse ($\sigma_x^2 = \sigma_t^2 + J_{\min}$). For the parameter values used here, this occurs at TJR = 0 dB (middle panel of Fig. 4.4). In that case, the two exponential curves coincide, and the performance predicted by (4.73) does not differ substantially.

4.4 Simulations

To verify the results derived in the previous section, an adaptive noise canceller was implemented in computer simulations with five methods of adjusting the step-size parameter. The five methods were based on the traditional (μ_{trad}), optimal (μ^*), approximation-to-optimal ($\widehat{\mu}^*$), output (μ_{out}), and sum (μ_{sum}) methods described by equations (4.19), (4.40), (4.44), (4.57), and (4.60), respectively. Implementation of the optimal method requires knowledge of the optimal values for the adaptive weights, $\mathbf{w}^*$, which is possible in a computer simulation but not in a real system. The results for the optimal method are presented as a benchmark of the performance and to confirm the analysis of the previous section. The other four methods rely only on quantities available to the adaptive processor and therefore can be implemented in a practical system.

The target and jammer signals were generated from two mutually independent, normally distributed noise sources, $t(n)$ and $z(n)$, with zero mean and unit variance. The primary and reference jammer signals, $j[n]$ and $x[n]$, were generated from $z(n)$ for two different cases. In Case 1, the jammer signal in the primary input was a delayed version of the jammer signal in the reference input, that is $j(n) = z(n - 2)$ and $x(n) = z(n)$. In Case 2, the jammer signals in the primary and reference inputs were generated from the sum and difference of a delayed signal according to

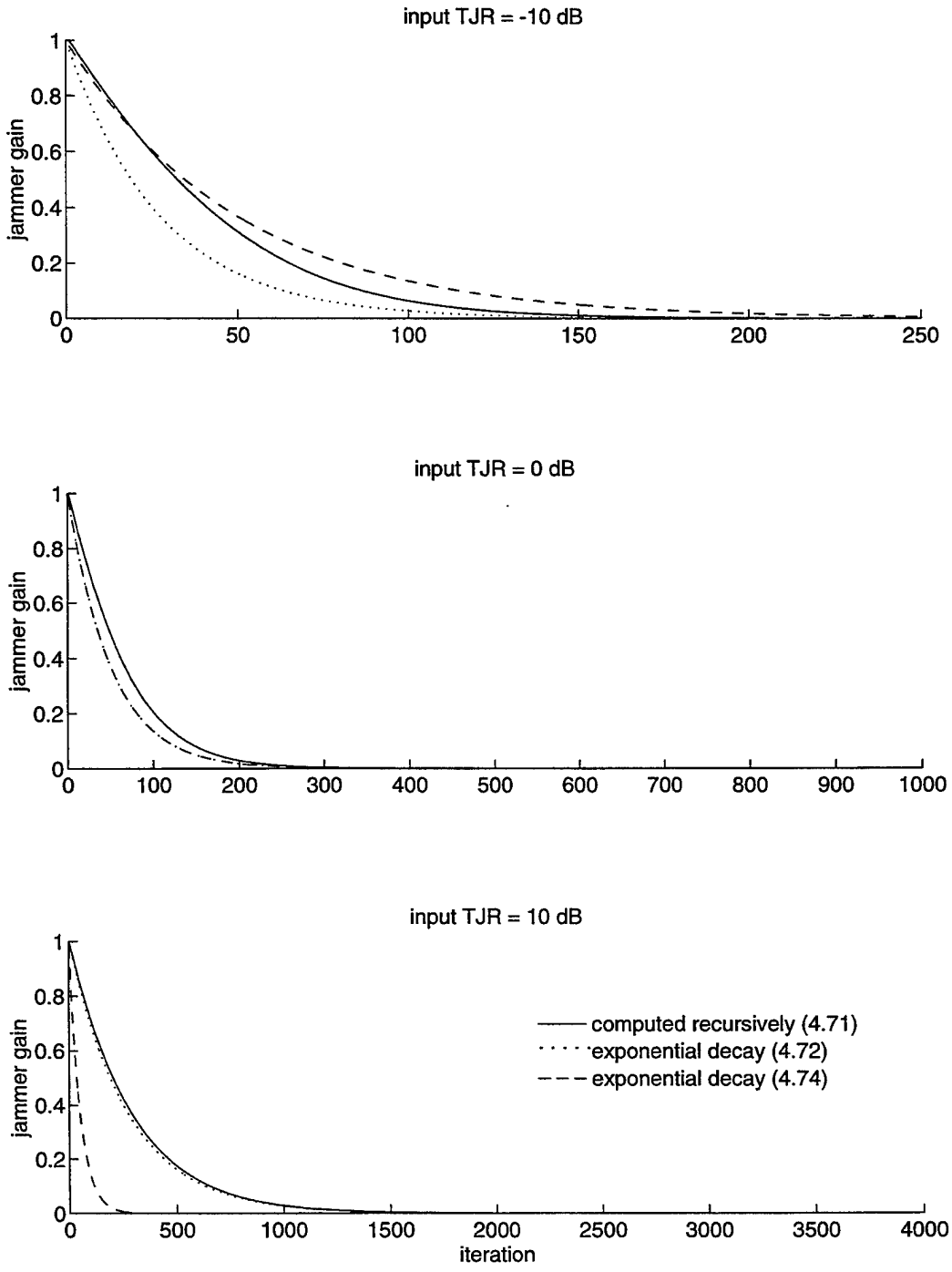

Figure 4-4: Transient behavior for the sum method of computing the step-size parameter. The solid curve is the true transient performance according to (4.73) and the dashed and dotted curves are exponential decays that approximate the transient behavior with time constants given by (4.74) and (4.76). The three panels show the behavior for input TJRs of -10, 0, and 10 dB.

$j[n] = \frac{1}{2}(z[n-2] + z[n])$ and $x[n] = \frac{1}{2}(z[n-2] - z[n])$.[8] The length of the adaptive filter was $L = 10$ and the normalized step-size parameter was $\alpha = 0.2$. With these parameter values, in Case 1, the minimum mse is $J_{\min} = 0$, and the eigenvalues of the autocorrelation matrix, $\mathbf{R}$, are $\lambda_i = \sigma_x^2$ for all i. In Case 2, the minimum mse is $J_{\min} = 0.33\sigma_x^2$, and the minimum and maximum eigenvalues are $\lambda_{\min} = 0.13\sigma_x^2$ and $\lambda_{\max} = 1.9\sigma_x^2$. For both Cases 1 and 2, the target signal was scaled to produce values of input TJR from -20 dB to $+20$ dB in increments of 10 dB. For each trial, the adaptive weights were initialized to the zero vector.

The required signal powers were calculated as follows. For the optimal method, the excess mse, $J_{\text{ex}}(n)$, was replaced by its instantaneous value, $[\mathbf{v}^T(n)\mathbf{x}(n)]^2$ in (4.40), and $E[y^2(n)]$ was computed according to (4.28), by summing the known values of σ_t^2 and σ_x^2 with the instantaneous value $[\mathbf{v}^T(n)\mathbf{x}(n)]^2$ instead of $J_{\text{ex}}(n)$. For the other methods, the signal powers σ_x^2, σ_{pri}^2, and $E[y^2(n)]$ were estimated by squaring and then filtering the reference input, primary input, and system output with a first-order recursive lowpass filter. For the approximation-to-optimal method, the time constant of the lowpass filter was 100 samples. For the sum and output methods, the time constant was equal to the filter length, $L = 10$.

Figures 4.5 and 4.6 show the simulation results (represented by discrete points) in terms of jammer gain as a function of input TJR, for Cases 1 and 2, respectively. The results were obtained by processing 300,000-sample source signals[9] and using the last 10,000 samples of the output to compute the steady-state error, $J(\infty)$, for each trial. For each condition, ten trials were performed with different samples of the target and jammer source signals, and the resulting steady-state error values were averaged over the ensemble of ten trials.

The smooth curves in Figs. 4.5 and 4.6 indicate the steady-state performance predicted by (4.31), (4.43), (4.51), (4.59), and (4.62), and are identical to the curves

[8]This relation between the primary and reference signals occurs when a simple two-microphone generalized sidelobe canceller is used to cancel a directional jammer signal that has a delay of two sampling periods between microphones.

[9]This length was selected to allow the optimal method to approach steady-state for the condition with the longest convergence time (Case 2 with input TJR = 20 dB).

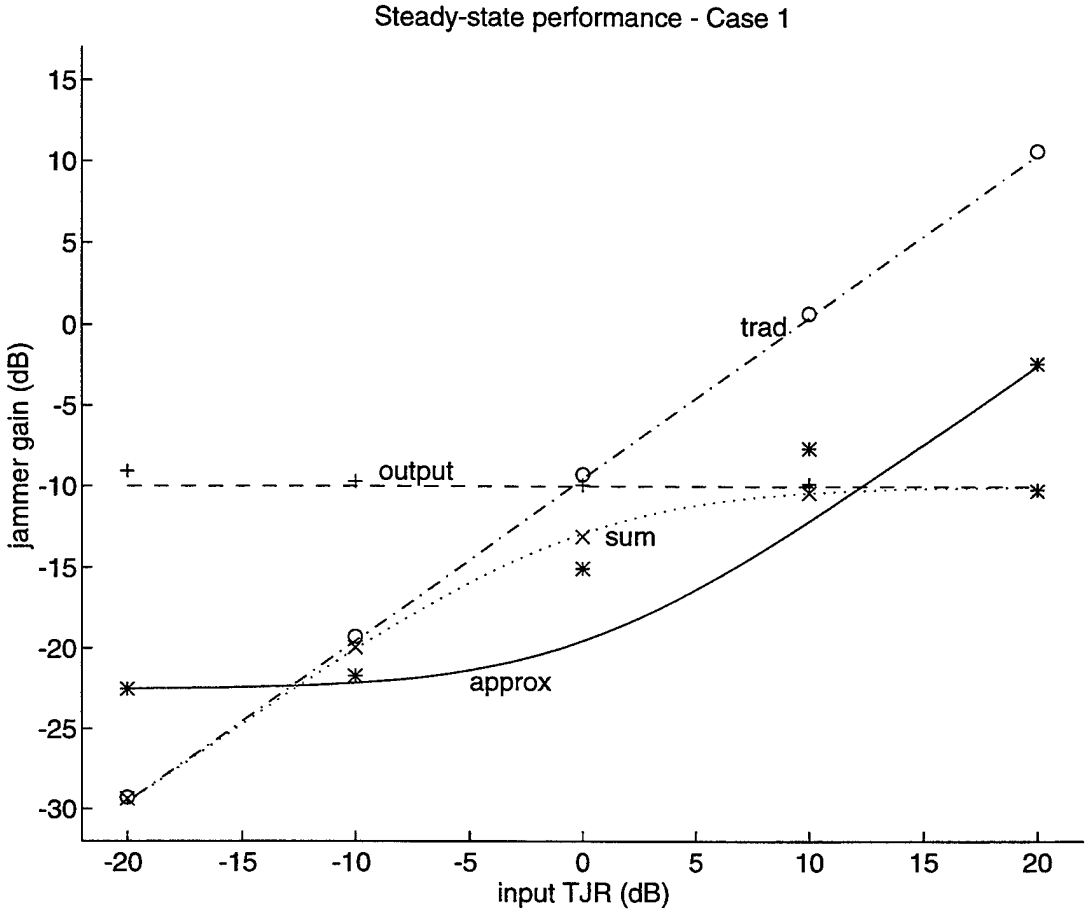

Figure 4-5: Steady state performance for four methods of computing the step-size parameter for Case 1. The plot shows the jammer gain due to the system as a function of the input TJR. The four methods are the traditional method, the approximation-to-optimal method, the output method, and the sum method. The simulation results are represented by discrete points, while the solid curves correspond to the analytical results shown in Fig. 4.1.

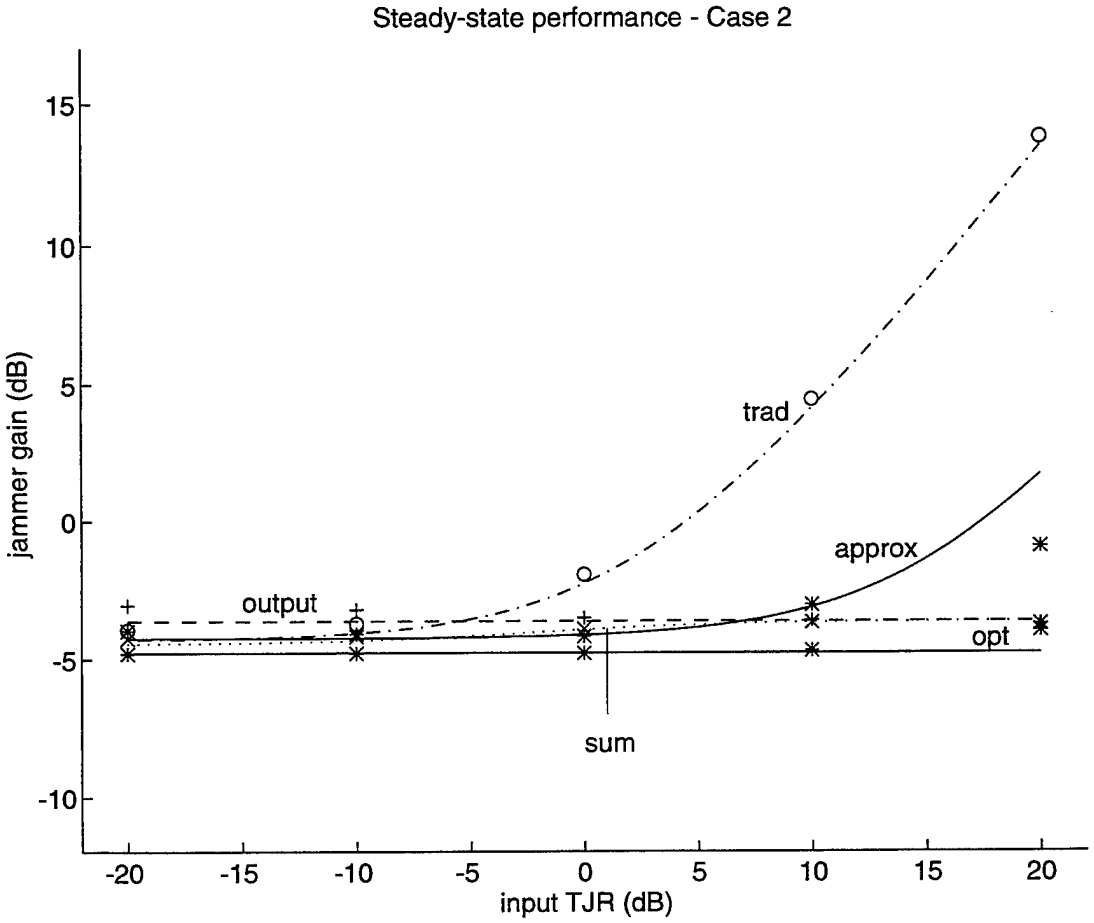

Figure 4-6: Steady state performance for five methods of computing the step-size parameter for Case 2. The plot shows the jammer gain due to the system as a function of the input TJR. The five methods are the traditional method, the optimal method, the approximation-to-optimal method, the output method, and the sum method. The simulation results are represented by discrete points, while the solid curves correspond to the analytical results shown in Fig. 4.2.

shown in Figs. 4.1 and 4.2. Again, values of $c_x = c_t = 0.05$ were used to calculate the estimation error, Δ, according to (4.54) for use in (4.51). Clearly, in steady state there is very good agreement between the simulations and the analytical results. Simulations of the optimal method for the parameter values used in Fig. 4.5 (not shown) confirmed that the steady-state performance converges to zero ($-\infty$ dB).

Figure 4.7 shows the transient behavior of the sum method for Case 1. The solid lines are the ensemble average of 50 simulation trials, and the dashed lines are exponential decays with time constants predicted by the analysis of Sec. 4.3.3. The dashed lines were generated assuming that the mse decays exponentially to the value of $J(\infty)$ predicted by (4.62), according to

$$J(n) = J(\infty) + [J(0) - J(\infty)]e^{-t/\tau} \tag{4.77}$$

This is in contrast to the transient behavior of the steepest descent algorithm shown in Figs. 4.3 and 4.4, where the mse decays to zero. For an input TJR of -10 dB (top panel of Fig. 4.7) the time constant is $\tau = 50$ samples, computed according to (4.76), and for an input TJR of 10 dB (bottom panel of Fig. 4.7) the time constant is $\tau = 275$ samples, computed according to (4.74). As expected, at low TJR, the exponential decay predicted by (4.76) gives a conservative estimate of the time constant; the actual convergence is slightly faster. At high TJR, the exponential decay predicted by (4.74) closely matches the simulation results. Overall, there is good agreement between the simulations and the analytical results.

4.5 Discussion

4.5.1 Summary of results

The preceding analysis determined an expression for the optimal time-varying step-size parameter for an adaptive noise canceller using the LMS algorithm to adjust the adaptive weights. The optimality criterion used was minimization of the total weight error power. When the algorithm reaches steady-state, this criterion is equivalent to

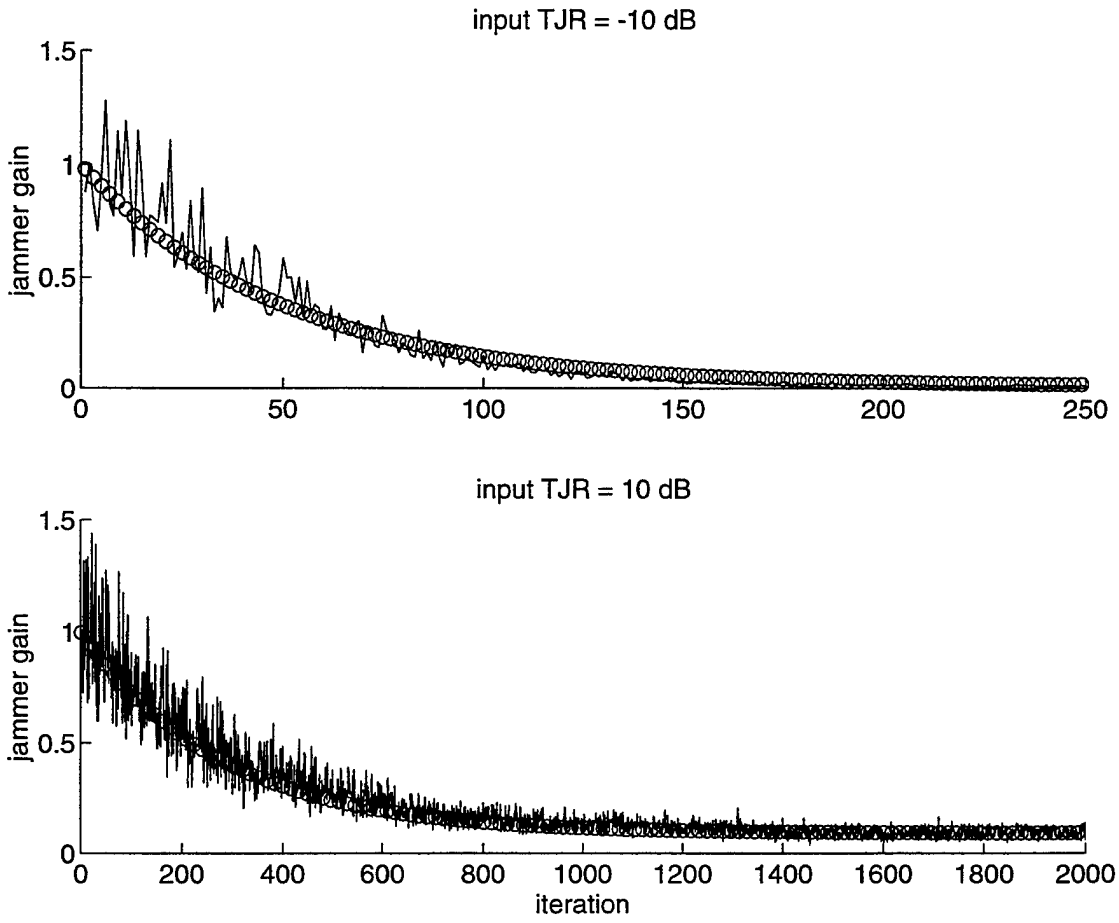

Figure 4-7: Transient behavior for the sum method of computing the step-size parameter for Case 1. The solid curve is the ensemble average from computer simulations, and the curve composed of circles is an exponential decay described by (4.77). The two panels show the behavior for input TJRs of -10 and 10 dB.

minimization of the excess mse due to the adaptive process. The resulting optimal method requires knowledge of quantities unavailable to the adaptive system. For implementation in a practical system, additional assumptions lead to three practical methods (approximation-to-optimal, output, and sum) for calculating the step-size parameter.

In terms of steady-state performance, the sum method is clearly preferable to the traditional, approximation-to-optimal, and output methods. The performance of the traditional method suffers in the presence of strong target signals because the excess mse is proportional to target power. The approximation-to-optimal method performs poorly at the extremes of target power due to its sensitivity to errors in the signal power estimates. The output method has excess mse independent of target power, which is unnecessarily high when the target signal is weak. The sum method provides the advantages of the traditional method in the presence of weak targets (excess mse proportional to the sum of the target power and the minimum mse) and of the output method in the presence of strong targets (constant excess mse).

Analysis of all five methods produced recursive formulas to characterize the transient behavior for known parameter values. It was shown that although methods that produce poor steady-state performance at the extremes of TJR converge more quickly, under conditions leading to good steady-state performance, the practical methods all exhibit similar transient behavior. Furthermore, a set of exponential decays were derived that can be applied to approximate the transient behavior of the sum method.

The surprisingly poor steady-state performance of the approximation-to-optimal method deserves some discussion. The problem with implementing the approximation-to-optimal method lies in the difficulty in obtaining good power estimates. The other methods are not as sensitive to errors in the power estimates because the estimates are only used to normalize the step-size parameter with respect to power levels. In the approximation-to-optimal method, the power estimates are subtracted with the goal of cancelling the target and input jammer powers and obtaining the excess error power. However, in most cases the powers to be cancelled by the subtraction are much

larger than the desired excess error power, and as a result, relatively large errors in the estimate of excess error power are likely. For the simulation results presented in Figs. 4.5 and 4.6, the time constant of the filter used to produce the power estimates was 100 samples. Additional simulations showed that using longer time constants did provide some improvement, but the performance was still proportional to target power.

In addition, the agreement between simulation and analytical results for the approximation-to-optimal method was not as good as for the other methods. That can be attributed to the restrictive assumptions about the form of the estimation error, Δ, that were required to simplify the analysis. Even so, the results of the analysis based on Δ successfully predict the basic trends of the simulation results.

4.5.2 Relation to other results

Some of the expressions derived above can be related to previous work concerned with the performance of adaptive echo-cancellers for the telephone network (Duttweiler, 1982; Sondhi and Berkley, 1980; Wehrmann et al., 1980; Höge, 1975). All of these works arrived at expressions for the optimal step-size parameter analogous to (4.39), and Wehrmann et al. (1980) and Höge (1975) considered ways of making approximations for practical implementation in a real system.

Duttweiler was primarily concerned with the use of nonlinearities in the correlation multiplier, that is, replacing the product $y(n)\mathbf{x}(n)$ in (4.17) with the product of arbitrary functions of $y(n)$ and $\mathbf{x}(n)$. A common variation on the LMS algorithm is to use the sign of $y(n)$, $\mathbf{x}(n)$, or both, in order to eliminate the need for multiplication in (4.17). Duttweiler's analysis showed that nonlinearities always impair performance relative to use of the true correlation multiplier.

To make the analysis tractable, Duttweiler made several assumptions similar to those of independence theory. Furthermore, Duttweiler assumed that the adaptive filter is long enough to completely model the echo path, so that $J_{\min} = 0$, and that samples of the input signal, $x(n)$, are independent, so that $\mathbf{R} = \mathbf{I}$. Under these assumptions, Duttweiler derived an expression for the evolution of the expected value of

the weight error power (equivalent to $\mathrm{tr}[\mathbf{K}(n)]$) for arbitrary nonlinearities. He evaluated that expression for the true multiplier, $y(n)\mathbf{x}(n)$, and for several nonlinearities, and then determined the optimal step-size parameter for each of those cases.

Three expressions from Duttweiler's analysis of the true correlation multiplier are directly related to expressions given in the current work. Making allowances for the different assumptions, Eqs. 48 and 50 from Duttweiler are closely related to (4.37) and (4.30), describing the evolution of the weight error power and the steady-state weight error power, respectively. In Eq. 85, Duttweiler gives the optimal step-size parameter for the true correlation multiplier, which, using the notation of the current work, is

$$\mu^* = \frac{1}{L\sigma_x^2}\frac{\sigma_{e_{\mathrm{ex}}}^2}{\sigma_y^2} \tag{4.78}$$

where $\sigma_{e_{\mathrm{ex}}}^2$ is the variance of uncancelled jammer signal, $e_{\mathrm{ex}}(n) = \mathbf{v}^T(n)\mathbf{x}(n)$, and σ_y^2 is the variance of the system output. Since $J_{\mathrm{ex}}(n) = E[e_{\mathrm{ex}}^2(n)]$, comparing (4.78) to (4.39) reveals that the two expressions are identical except for the use of variances in place of expected values based on ensemble averages. As is true of (4.39), (4.78) cannot be implemented in a real system, because $\sigma_{e_{\mathrm{ex}}}^2$ is unknown. Duttweiler points out that near-end speech detectors used on the telephone network can be seen as a crude approximation to (4.78).

In a review paper on echo cancellation for the telephone network, Sondhi and Berkley (1980) describe a similar result. Again, using assumptions similar to independence theory, they derive Eq. 34 to describe the evolution of the weight error power that is equivalent to (4.37) presented in this work. In Eq. 35, they present an expression for the step-size parameter that minimizes the weight error power, which is presumably obtained by taking the first derivative of Eq. 34 with respect to the step-size parameter. Correcting what appears to be a typographical error (lack of squaring the term in the numerator) and using the notation of the current work, their Eq. 35 is

$$\mu^*(n) = \frac{[\mathbf{v}^T(n)\mathbf{x}(n)]^2}{\mathbf{x}^T(n)\mathbf{x}(n)(\sigma_t^2 + J_{\min} + [\mathbf{v}^T(n)\mathbf{x}(n)]^2)}. \tag{4.79}$$

Noting that $E[(\mathbf{v}^T(n)\mathbf{x}(n))^2] = J_{\mathrm{ex}}(n)$ and that $E[\mathbf{x}^T(n)\mathbf{x}(n)] = L\sigma_x^2$ reveals that

(4.79) is equivalent to (4.39) except for the use of instantaneous values instead of expectations based on ensemble averages. With regard to (4.79), Sondhi and Berkley state that "this 'optimum' value can be estimated by assuming the x's to be i.i.d., and making some further simplifying assumptions." However, they do not explain what the simplifying assumptions are or how an approximation to (4.79) could be implemented in a real system.

The approach described by Sondhi and Berkley (1980) is based on work by Höge (1975). Using the notation of the current work, Höge (1975) reports that the optimal step-size parameter is given by

$$\mu(n)^* = \frac{\alpha}{L(\frac{1}{L}\mathbf{x}^T(n)\mathbf{x}(n) + \frac{\widehat{\sigma_t^2(n)}}{\widehat{\mathrm{tr}[\mathbf{K}(n)]}})} \tag{4.80}$$

where $\alpha = 1$ and $\widehat{\sigma_t^2}(n)$ and $\widehat{\mathrm{tr}[\mathbf{K}(n)]}$ are recursive estimates of the target signal power and the weight error power, respectively. Rearranging (4.80) yields

$$\mu(n)^* = \frac{\alpha\widehat{J_{\mathrm{ex}}}(n)}{L\sigma_x^2 E[\widehat{y^2}(n)]} \tag{4.81}$$

where the estimates $\widehat{J_{\mathrm{ex}}(n)} = \sigma_x^2\widehat{\mathrm{tr}[\mathbf{K}(n)]}$ and $E[\widehat{y^2(n)}] = \widehat{\sigma_t^2(n)} + \frac{1}{L}\mathbf{x}^T(n)\mathbf{x}(n)\widehat{\mathrm{tr}[\mathbf{K}(n)]}$ are based on (4.28) and the assumptions that $J_{\min} = 0$ and $\mathbf{R} = \sigma_x^2\mathbf{I}$. As a result of the latter assumption and (4.27), $J_{\mathrm{ex}}(n) = \sigma_x^2\mathrm{tr}\mathbf{K}(n)$. Comparing (4.40) to (4.81) reveals that the two expressions are the same if the estimates are replaced by their exact values. Höge proposes estimating σ_t^2 and $\mathrm{tr}[\mathbf{K}(n)]$ recursively from quantities available to the adaptive processor and from initial estimates of those values at $n = 0$.

Wehrmann et al. (1980) report that the optimal time-varying step-size parameter, using the notation of the current work, is

$$\mu^*(n) = \frac{1}{\mathbf{x}^T(n)\mathbf{x}(n)\left(1 + \frac{\sigma_t^2}{E[e^2(n)]}\right)}. \tag{4.82}$$

If $J_{\min} = 0$, using (4.28) in (4.82) and rearranging shows that

$$\mu^*(n) = \frac{J_{\text{ex}}(n)}{\mathbf{x}^T(n)\mathbf{x}(n)E[y^2(n)]}, \tag{4.83}$$

which is the same as (4.39) with $L\sigma_x^2$ estimated by $\mathbf{x}^T(n)\mathbf{x}(n)$ at each iteration.

Wehrmann et al. (1980) note that the optimal method cannot be implemented in a real system because the signals $e(n)$ and $t(n)$ are not available for calculating their expected values required in (4.82). They then propose an implementable method for calculating the "noise insensitive compromise (nic) step-size factor," which is analyzed in the next section.

4.5.3 Application to other proposed modifications of the LMS algorithm

The LMS algorithm is widely used because of its effectiveness, simplicity, and relative ease of implementation. It is therefore not surprising that many researchers have suggested modifications to the LMS algorithm. These modifications are intended for a variety of purposes, including reducing computational burden (Claasen and Mecklenbrauker, 1981; Mathews and Cho, 1987; Sullivan, 1993) and improving the fundamental tradeoff between convergence time and steady-state performance (Harris, et al., 1986; Karni and Zeng, 1989; Yasukawa and Shimada, 1993; Makino et al., 1993). Some of these modified LMS algorithms are based on rigorous analysis, while others are *ad hoc*. Furthermore, some of these methods are only effective in applications of the LMS algorithm where the target signal is weak or nonexistent.

The purpose of this section is to demonstrate how the methods of Sec. 4.3 can be applied to evaluate many of these proposed algorithms. Particular attention is given to the applicability of these modifications to configurations that require the algorithm to perform in the presence of strong target signals, such as the adaptive noise canceller. It should be noted, however, that not all modifications to the LMS algorithm can be evaluated using these methods. In order to analyze an algorithm using this framework, the modification must be expressable in terms of a time-varying

step-size parameter, $\mu(n)$, that is applied to the true correlation multiplier, $y(n)\mathbf{x}(n)$, in (4.17). Analysis of arbitrary nonlinear correlation multipliers is considerably more complicated (e.g., Duttweiler, 1982; Sullivan, 1993).

The following three examples illustrate how the analysis performed in Sec. 4.3 can be used to evaluate the noise insensitive compromise (nic) algorithm (Wehrmann et al., 1980), the signed-error LMS algorithm (Claasen and Mecklenbrauker, 1981; Mathews and Cho, 1987) and the LMS algorithm with adaptive damped convergence factor (Karni and Zeng, 1989).

Noise insensitive compromise (nic) algorithm

Wehrmann et al. (1980) propose the noise insensitive step-size factor, given by

$$\mu_{\text{nic}}(n) = \frac{\alpha}{X_{\max} \sum_{i=1}^{L} |x(n-i)|}, \tag{4.84}$$

where $X_{\max}$ is the maximum peak voltage of telephone speech. They provide simulation results using $\alpha = 2$ and show that it performs better than the traditional method when the target signal is present. Their simulation results are based on performance determined from a 200 ms segment taken after the system has adapted for 2 seconds, and they do not analyze the convergence time.

As is typical of telephone echo cancellers, they assume that the system will include a speech detector to suspend adaptation when the target signal, $t(n)$, consists of near end speech. As a result, when the system is adapting, the target signal consists only of line noise, and their simulations are restricted to values of TJR less than -20 dB. However, it is interesting to consider the performance of this method at high TJR as well.

The steady-state performance of the nic method can be determined by substituting (4.84) for μ in (4.30):

$$J_{\text{ex}}(\infty) = \frac{\alpha L \sigma_x^2 (J_{\min} + \sigma_t^2)}{2X_{\max} \sum_{i=1}^{L} |x(n-i)| - \alpha L \sigma_x^2}. \tag{4.85}$$

If the values of $x(n)$ are zero-mean Gaussian random variables, then $E[|x(n)|] = \sigma_x\sqrt{\frac{2}{\pi}}$ (Mathews and Cho, 1987). Using the Gaussian assumption, replacing $|x(n-i)|$ in (4.85) with its expected value and defining $B = \frac{\sigma_x}{X_{\max}}$ gives

$$J_{\text{ex}}(\infty) = \frac{\alpha B(J_{\min} + \sigma_t^2)}{2\sqrt{\frac{2}{\pi}} - \alpha B} \tag{4.86}$$

Comparing this expression to (4.31) shows that the steady state performance of the nic method is similar to the performance of the traditional method with the dimensionless step-size parameter, α, reduced by a factor, B, based on the ratio of actual reference input rms level to the maximum possible peak input.

For the nic method, the performance depends on both the TJR and the signal levels relative to $X_{\max}$. For example, the nic method will provide better performance when $\sigma_x^2 = \sigma_t^2 = \frac{X_{\max}^2}{16}$ $(B = \frac{1}{4})$ than when $\sigma_x^2 = \sigma_t^2 = \frac{X_{\max}^2}{4}$, $(B = \frac{1}{2})$ even though TJR = 0 dB for both cases. This is in contrast to the performance of the methods proposed in Sec. 4.3, which only depend on the input TJR. For the nic method, the worst case steady state performance occurs when the ratio, B, is largest, that is, when the input levels approach $X_{\max}$. Since the primary input must be less than $X_{\max}$ and it is assumed that $\sigma_x^2 = \sigma_j^2$, the worst case occurs when $\sigma_x^2 + \sigma_t^2 = X_{\max}^2$.

The worst case performance can be examined at the two extremes of TJR. At low TJR ($\sigma_x^2 \gg \sigma_t^2$), $B \approx 1$ and (4.86) becomes

$$J_{\text{ex}}(\infty) \approx \frac{\alpha(J_{\min} + \sigma_t^2)}{2\sqrt{\frac{2}{\pi}} - \alpha}, \tag{4.87}$$

which is similar to the performance of the traditional algorithm described by (4.31). At high TJR ($\sigma_x^2 \ll \sigma_t^2$), $B \approx \frac{\sigma_x}{\sigma_t}$ and (4.86) becomes

$$J_{\text{ex}}(\infty) \approx \frac{\alpha\sigma_x\sigma_t}{2\sqrt{\frac{2}{\pi}}} \tag{4.88}$$

where terms have been neglected based on the observations that $\sigma_t^2 \gg J_{\min}$ and $\sigma_t^2 \gg \alpha$. At high TJR, steady state performance is proportional to the square root of

the target power, which is considerably better than the steady state performance of the traditional method. However, the performance is not as good as that of the sum method, which approaches $\frac{\alpha\sigma_x^2}{2}$ at high TJR.

The above analysis is based on the worst case scenario for the signal levels and $X_{\max}$. Even though the performance at high TJR is proportional to the square root of the target power, for a wide range of signal levels the steady state performance will be better than that suggested by (4.87) and (4.88). The steady state performance of the nic method can always be improved by increasing the value of $X_{\max}$, but that is associated with slower convergence. The tradeoff between steady state performance and convergence time involved selecting an appropriate value for $X_{\max}$ is similar to that which occurs in selection of the dimensionless step-size parameter, α. Choosing a value of $X_{\max}$ that is small produces values of B close to unity, resulting in the steady state performance described by (4.87) and (4.88). Choosing a larger value of $X_{\max}$ produces better steady-state performance but proportionally longer convergence time, which will affect the low TJR cases more adversely. A reasonable choice of $X_{\max}$ can only be made if the range of input signal powers is known. This may be true not only for telephone lines, but also for digital systems that perform analog-to-digital conversion of the input data. In summary, the nic method has some potential for applications when enough information is available *a priori* to make a reasonable choice of $X_{\max}$ based on information about both the absolute power levels and the range of TJRs over which the system operates.

Signed-error LMS algorithm

When an application requires reduction in the computational complexity of the LMS algorithm, signed algorithms are often used to eliminate the multiplication required by the true correlation multiplier, $y(n)\mathbf{x}(n)$ in (4.17). Sullivan (1993) summarizes the following four signed algorithms, which use these functions to calculate the correlation multiplier:

- Signed product - sign$[y(n)x(n)]$

- Signed regressor - $y(n)\text{sign}[x(n)]$
- Signed error - $\text{sign}[y(n)]x(n)$
- Signed maximum - $\text{sign}[y(n)x(n)]\min(|y(n)||x(n)|)$.

The signed-error algorithm can be analyzed within the framework proposed here, because it can be expressed in terms of the traditional LMS algorithm in (4.17) with time-varying step-size parameter, $\mu(n)$, given by

$$\mu(n) = \frac{\alpha}{L\sigma_x^2|y(n)|} \tag{4.89}$$

Substituting (4.89) into (4.30) gives

$$J_{\text{ex}}(\infty) = \frac{\alpha(J_{\min} + \sigma_t^2)}{2|y(n)| - \alpha}. \tag{4.90}$$

If z is a Gaussian random variable with zero mean and variance σ_z^2, then the mean of its absolute value, $E[|z|]$, equals $\sqrt{\frac{2\sigma_z^2}{\pi}}$ (Mathews and Cho, 1987). Assuming that $y(n)$ can be modeled as a zero-mean, Gaussian process, applying this assumption to $E[|y(n)|]$ and substituting (4.28) gives

$$E[|y(n)|] = \sqrt{\frac{2E[y^2(n)]}{\pi}} \tag{4.91}$$

$$= \sqrt{\frac{2}{\pi}}\sqrt{\sigma_t^2 + J_{\min} + J_{\text{ex}}(n)}. \tag{4.92}$$

Replacing $|y(n)|$ in (4.90) with its expected value, substituting (4.92) and rearranging yields

$$(J_{\text{ex}}(\infty) + \sigma_t^2 + J_{\min})(\frac{8}{\pi}(J_{\text{ex}}(\infty))^2 - \alpha^2 J_{\text{ex}}(\infty) - \alpha^2(\sigma_t^2 + J_{\min})) = 0 \tag{4.93}$$

The positive solution to (4.93) is

$$J_{\text{ex}}(\infty) = \frac{\alpha^2 + \alpha\sqrt{\alpha^2 + \frac{32}{\pi}(\sigma_t^2 + J_{\min})}}{\frac{16}{\pi}}. \tag{4.94}$$

This result is equivalent to the steady-state excess mse for the signed error algorithm determined by Mathews and Cho (1987). This equivalence can be seen by substituting $\alpha = 2\alpha'\sqrt{\frac{2}{\pi}}$ into (4.94), giving

$$J_{ex}(\infty) = \frac{\alpha'^2 + \alpha'\sqrt{\alpha'^2 + 4(\sigma_i^2 + J_{min})}}{2}. \tag{4.95}$$

The expression given by (4.95) can be obtained from the steady-state standard deviation of the error given by Mathews and Cho (1987) by accounting for the target signal power, squaring their Eq. 39, and subtracting J_{min} to obtain the steady-state excess mse. In the presence of strong target signals, the steady state performance of the signed error algorithm is proportional to the square root of the target signal power. Thus, strong target signals affect the signed error algorithm less adversely than they affect the traditional algorithm, where the steady-state excess mse is proportional to the target signal power.

LMS algorithm with adaptive damped convergence factor

Karni and Zeng (1989) suggest a modification to the LMS algorithm intended to overcome the fundamental tradeoff between convergence time and steady-state error. Their method provides both rapid convergence and reduced misadjustment by allowing the step-size parameter to have a large initial value, and then progressively reducing the step-size parameter as the error signal converges. Specifically, they adjust the step-size parameter according to

$$\mu(n) = \frac{1}{L\sigma_x^2}(1 - e^{-\beta||\epsilon(n)\mathbf{x}(n)||}) \tag{4.96}$$

where $\epsilon(n)$ is the error signal, β is a damping parameter, and $||\ ||$ denotes the vector norm. They suggest that the vector norm can be replaced by the vector norm squared for ease of computation.

It appears that this approach will work as desired in applications with no (or weak) target signals. However, for the adaptive noise canceller, the error signal $\epsilon(n)$

is obtained from the system output, $y(n)$, which is a poor estimate of the output error in the presence of strong target signals. Therefore, strong target signals will cause the step-size parameter computed according to (4.96) to increase, leading to increased steady-state mse. In order to gain insight into the performance of this method in the steady-state, it is assumed that $y(n)$ and $\mathbf{x}(n)$ are uncorrelated (which is valid if the weights are converged to their optimal values so that $E[y^2(n)] \approx J_{\min} + \sigma_t^2$). Using the vector norm squared and replacing $||\mathbf{x}||^2$ with its expected value, $L\sigma_x^2$, yields

$$\mu_{\exp}(n) = \frac{1}{L\sigma_x^2}(1 - e^{-\beta y(n) L\sigma_x^2}) \tag{4.97}$$

Substituting (4.97) into (4.30) produces

$$J_{\exp}(\infty) = \frac{(1 - e^{-\beta y(n) L\sigma_x^2})(J_{\min} + \sigma_t^2)}{(1 + e^{-\beta y(n) L\sigma_x^2})}. \tag{4.98}$$

When the target signal is strong, so that the exponential term approaches zero, (4.98) becomes

$$J_{\exp}(\infty) = J_{\min} + \sigma_t^2. \tag{4.99}$$

Like the traditional method, this method of adjusting the step-size parameter causes the expected value of the excess mse to be proportional to the target signal power, leading to poor performance in the presence of strong target signals.

Chapter 5

Intermicrophone correlation for target-to-jammer ratio hypothesis test

5.1 Introduction

As discussed in Sec. 2.3.1, the performance of adaptive systems degrades at high target-to-jammer ratios. Greenberg and Zurek (1992) proposed computing a running measure of intermicrophone correlation, a metric related to the short-term TJR, and then inhibiting the adaptive process when the correlation exceeds some threshold. This is appropriate for the hearing-aid application because speech signals exhibit a high degree of power fluctuations, so the short-term TJR will contain pauses that allow adaptation even when the long-term TJR exceeds the threshold.

The purpose of this chapter is to investigate controlling adaptation based on the correlations between pairs of microphones. The basic idea is to compute running measurements of correlation for pairs of microphones for each iteration of the process. These correlation measures are combined and compared to a threshold value. If the correlation measure exceeds the threshold, then the decision is that the TJR is "high" and the adaptive weights remain at their previous values. If the correlation measure is less than the threshold, then the decision is that the TJR is "low" and the adaptive

weights are updated.

In this approach, the threshold is applied to the correlation measure, and the decision corresponds to whether or not the TJR falls within one of two ranges. This is a simpler problem than attempting to estimate the TJR from the correlation measure.

Other researchers have considered similar mechanisms to permit adaptation in intervals of low TJR and prevent adaptation in intervals of high TJR. Those methods rely on measures of the energy in the input signals to determine whether adaptation should be enabled or disabled. The methods proposed by Van Compernolle (1990a,b) and by Harrison et al. (1986) rely on the assumption that the long-term TJR is always positive. The methods described by Kaneda and Ohga (1986) and by Sondhi and Berkley (1980) are based on additional information about the presence or absence of the target signal that is not available in the hearing aid application.

Kompis (1993) proposed the *sigma-delta* method to control adaptation of a two-microphone generalized sidelobe canceller.[1] This method uses the ratio of power in the primary signal to the sum of the powers in the primary and reference signals. He evaluated this method and compared it to two other methods, the intermicrophone correlation used by Greenberg and Zurek (1992) and a *multidimensional correlation* method based on the cross-correlation function between the two microphone signals at time lags ranging from -0.8 ms to $+0.8$ ms. For the conditions used in the evaluation, the multidimensional correlation provides the best results, but also requires the most computation. In the remainder of his work, Kompis uses the sigma-delta method because it provides acceptable performance at low computational complexity.

This chapter investigates controlling adaptation at high TJR based on the correlation between microphones as proposed by Greenberg and Zurek (1992). It considers previously neglected issues such as criteria for selecting the correlation threshold, the effect of reverberation, and incorporating information from multiple pairs of microphones. The following section contains an analysis of the relationship between the intermicrophone correlation and the TJR; the intermicrophone correlation is used as a decision variable for choosing between the "low" and "high" TJR hypotheses. It is

[1]This method is also described in Dillier et al. (1993).

followed by simulations demonstrating its effectiveness.

5.2 Analysis of intermicrophone correlation for determining TJR

This section contains an analysis of the intermicrophone correlation as a means of determining TJR. It starts with a derivation of the probability density function (pdf) of the intermicrophone correlation for a single directional source arriving from a range of angles. The pdf for a single source is then used to derive the pdf for two directional sources arriving from different ranges of angles, conditioned on the relative strengths of the sources (TJR). It is assumed that within the ranges of angles defining target and jammer sources, all angles of incidence are equally likely. Next the effect of reverberation is included in the pdf. Then, binary hypothesis testing (Van Trees, 1968) is used to determine a threshold on the correlation that corresponds to the desired ranges of TJR. Several methods are proposed for combining the correlation measures from different pairs of microphones.

5.2.1 Probability density functions

Correlation of one directional source

To derive the pdf of the intermicrophone correlation for a single source, consider one source arriving from an unknown angle of azimuth in the horizontal plane, denoted θ. If it is assumed that all angles of incidence are equally likely, θ can be treated as a random variable with uniform density on the interval $\theta_1 < \theta < \theta_2$. Under this assumption, the probability density function is

$$f_{\theta_s}(\theta) = \frac{1}{(\theta_2 - \theta_1)} \tag{5.1}$$

for $\theta_1 < \theta < \theta_2$.

Assuming plane-wave propagation, the time delay between the signals arriving at

two microphones in free space is

$$\tau = \frac{d}{c} \sin\theta \tag{5.2}$$

where d is the intermicrophone spacing, c is the speed of sound, and θ is zero when the source is oriented broadside to the two microphones. The normalized correlation coefficient, ρ_s, between the two microphone signals for a pure tone source of frequency f arriving with time delay τ is

$$\rho_s = \cos(2\pi f \tau) \tag{5.3}$$

(Cremer and Müller, 1982), and substituting (5.2) gives

$$\rho_s = \cos\left(\frac{2\pi f d}{c} \sin\theta\right) = \cos(kd\sin\theta), \tag{5.4}$$

where the wavenumber k is

$$k = \frac{2\pi f}{c}. \tag{5.5}$$

The pdf for ρ_s can be derived from (5.1) and (5.4) using standard methods for deriving pdfs of functions of random variables. The resulting pdf for the intermicrophone correlation of a single narrowband directional source is

$$f_{\rho_s}(\rho) = \frac{1}{(\theta_2 - \theta_1)\sqrt{(kd)^2 - (\arccos\rho)^2}\sqrt{1-\rho^2}} \tag{5.6}$$

for $\cos(kd\sin\theta_2) < \rho < \cos(kd\sin\theta_1)$.

Now consider the cases of target and jammer individually. The target signal is defined as any source arriving at the microphones from a range of angles near straight ahead (zero degrees azimuth in the horizontal plane). Because the cosine function is even, positive and negative angles produce the same values of intermicrophone correlation. Therefore, negative angles can be ignored and the range of angles for the target signal is restricted to $0 < \theta < \theta_0$, where θ_0 is a relatively small angle. Substituting $\theta_1 = 0$ and $\theta_2 = \theta_0$ into (5.6) produces the pdf for a directional target

signal,

$$f_{\rho_t}(\rho) = \frac{1}{\theta_0\sqrt{(kd)^2 - (\arccos\rho)^2}\sqrt{1-\rho^2}} \tag{5.7}$$

for $\cos(kd\sin\theta_0) < \rho < 1$.

Similarly, the jammer signal is defined as any source arriving at the microphones from any direction outside the range of target angles. Because the correlation does not distinguish between signals arriving from the front and the rear, for this analysis, signals arriving within θ_0 of 180° are not included in the definition of jammer. Furthermore, because of the symmetry of the sine function, angles larger than 90° can be ignored along with the negative angles. Substituting $\theta_1 = \theta_0$ and $\theta_2 = \frac{\pi}{2}$ into (5.6) produces the pdf for a directional jammer signal,

$$f_{\rho_j}(\rho) = \frac{1}{(\frac{\pi}{2} - \theta_0)\sqrt{(kd)^2 - (\arccos\rho)^2}\sqrt{1-\rho^2}} \tag{5.8}$$

for $\cos(kd) < \rho < \cos(kd\sin\theta_0)$.

The pdfs for a single directional target and a single directional jammer described by (5.7) and (5.8) are shown in Fig. 5.1 for $\theta_0 = \arcsin(\frac{1}{4}) = 14.5°$ and for several values of kd.

Next, consider the case of two independent directional sources, one target and one jammer. The total intermicrophone correlation, ρ_d, is the normalized, weighted sum of the target and jammer correlations, given by

$$\rho_d = \frac{\sigma_t^2\rho_t + \sigma_j^2\rho_j}{\sigma_t^2 + \sigma_j^2} = \frac{Y\rho_t + \rho_j}{Y+1} \tag{5.9}$$

where σ_t^2 and σ_j^2 are the target and jammer signal powers, and $Y = \frac{\sigma_t^2}{\sigma_j^2}$, the target-to-jammer ratio. The pdf of the sum of two independent random variables is the convolution of their two pdfs. Since ρ_t and ρ_j are random variables with known pdfs, the pdf of ρ_d conditioned on Y, denoted $f_{\rho_d|Y}(\rho|Y)$, can be determined by convolving (5.7) and (5.8), with appropriate scaling by Y and $\frac{1}{Y+1}$. This is shown easily with

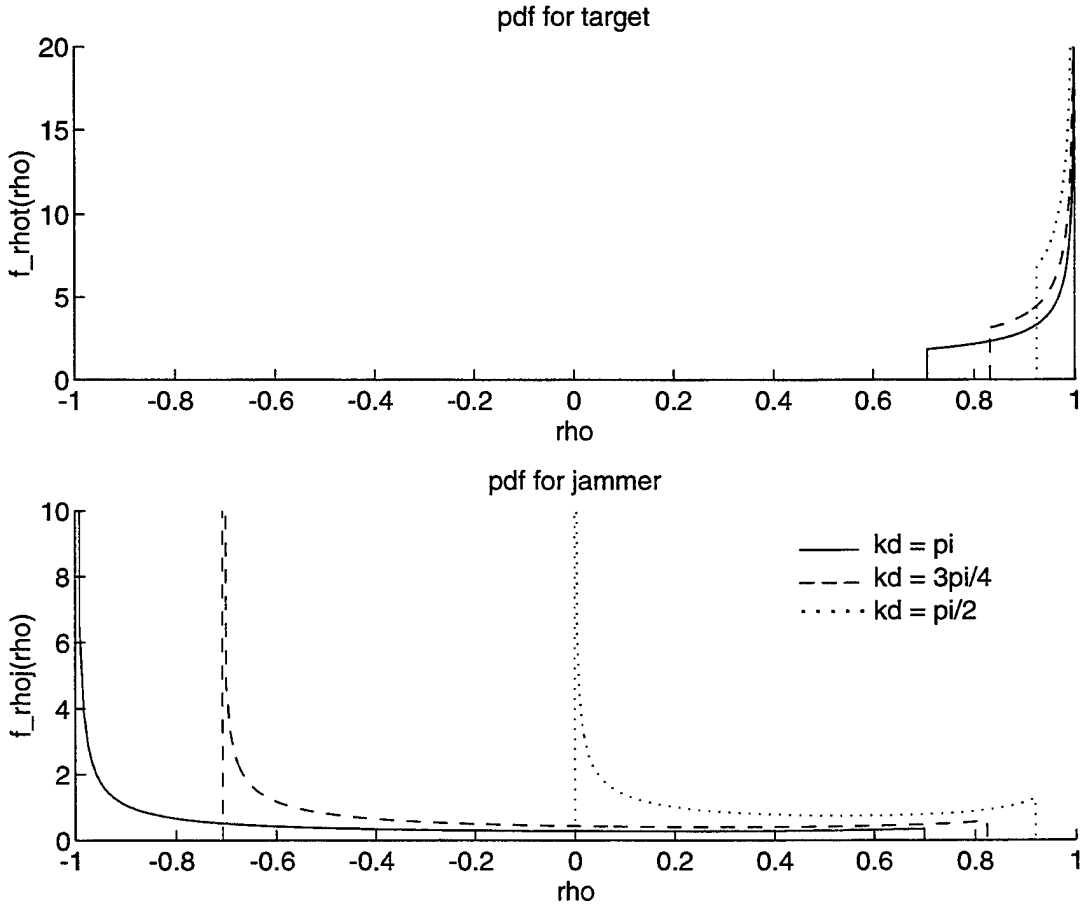

Figure 5-1: Probability density functions for the correlation of single source described by (5.7) and (5.8) for three values of kd.

the use of the intermediate variables:

$$\rho_t' = \frac{Y}{Y+1}\rho_t, \tag{5.10}$$

$$\rho_j' = \frac{1}{Y+1}\rho_j, \tag{5.11}$$

$$\rho_d = \rho_t' + \rho_j'. \tag{5.12}$$

Then the pdfs are

$$f_{\rho_t'|Y}(\rho|Y) = \frac{Y+1}{Y} f_{\rho_t}\left(\frac{Y+1}{Y}\rho\right), \tag{5.13}$$

$$f_{\rho_j'|Y}(\rho|Y) = (Y+1) f_{\rho_j}((Y+1)\rho), \tag{5.14}$$

and

$$\begin{aligned} f_{\rho_d|Y}(\rho|Y) &= f_{\rho_t'|Y}(\rho_1|Y) * f_{\rho_j'|Y}(\rho_2|Y) \\ &= f_{\rho_t}\left(\frac{Y+1}{Y}\rho\right) * f_{\rho_j}((Y+1)\rho). \end{aligned} \tag{5.15}$$

Closed form solutions could not be found for the integrals that result from substituting (5.7) and (5.8) into (5.15), so the following approximation was used. From Fig. 5.1, it can be seen that a reasonable approximation for $f_{\rho_t}(\rho)$ is given by a constant over the range $\cos(kd\sin\theta_0) < \rho < 1$ plus an impulse at $\rho = 1$. The constant is selected so that the area under the constant portion equals $\frac{1}{2}$ and the area of the impulse is $\frac{1}{2}$.[2] This approximation for the target pdf is given by

$$\hat{f}_{\rho_t}(\rho) = \frac{1}{2(1-\cos(kd\sin\theta_0))} + \frac{1}{2}\delta(\rho-1) \tag{5.16}$$

for $\cos(kd\sin\theta_0) < \rho \leq 1$, where δ is the unit impulse function. Figure 5.2 shows a comparison between this approximation and the pdf described by (5.7) for $\theta_0 = 14.5°$ and several values of kd.

The conditional pdf is obtained by substituting (5.16) and (5.8) into (5.15). The

[2]These values were chosen because the target pdf evaluated at the lower limit on ρ [$\rho_{t0} = \cos(kd\sin\theta_0)$] is close to $\frac{0.5}{(1-\rho_{t0})}$ for a range of values of θ_0 and kd. Specifically, $\frac{0.50}{1-\rho_{t0}} < f_{\rho_t}(\rho_{t0}) < \frac{0.55}{1-\rho_{t0}}$ for $10° < \theta_0 < 15°$ and $0 < kd < \pi$.

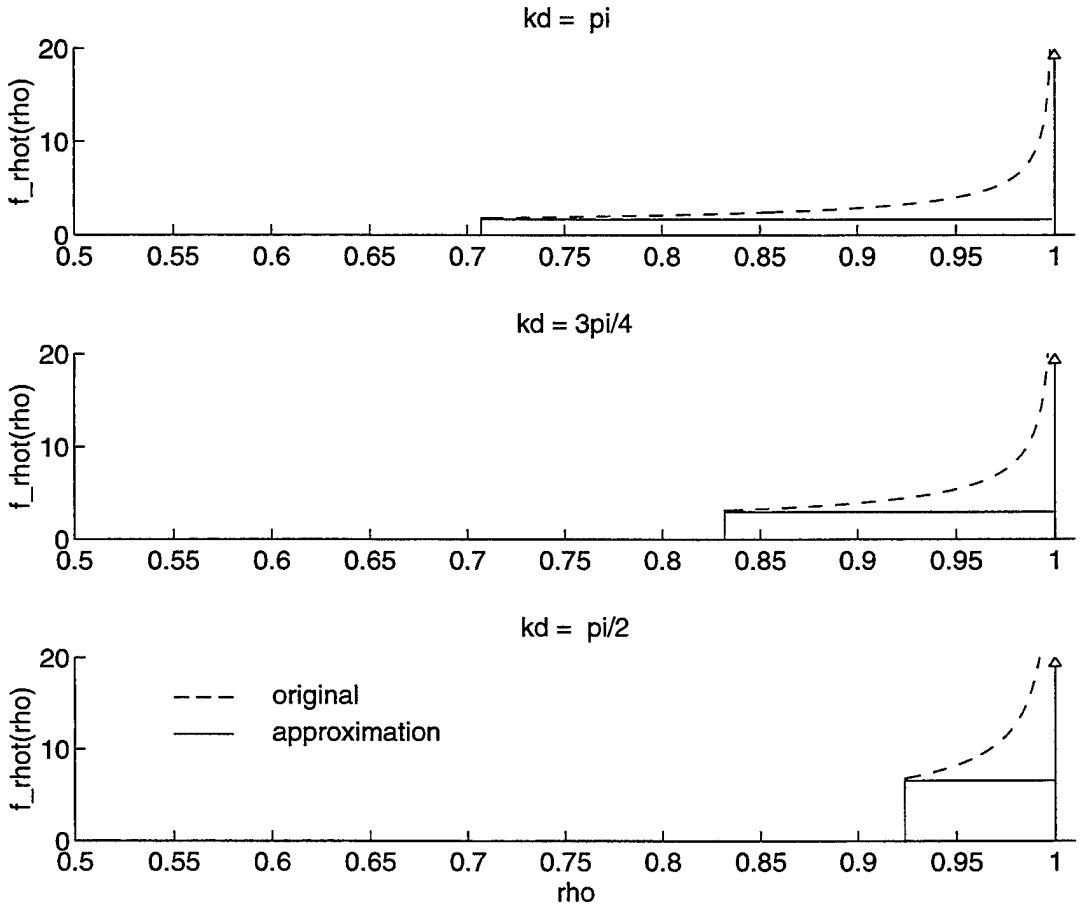

Figure 5-2: Original and approximate probability density functions for the target-source correlation described by (5.7) and (5.16) for three values of kd.

resulting convolution is performed in Appendix A, and the results are reproduced here:

$$
\begin{aligned}
&f_{\rho_d|Y}(\rho|Y) = \\
&\quad \frac{Y+1}{2Y(\frac{\pi}{2}-\theta_0)(1-\cos(kd\sin\theta_0))} \\
&\quad \left\{\left[\frac{\pi}{2} - \arcsin\left(\frac{\arccos((Y+1)\rho - Y\cos(kd\sin\theta_0))}{kd}\right)\right][u(\rho-\rho_1) - u(\rho-\rho_{2a})]\right. \\
&\quad + \left[\frac{Y(1-\cos(kd\sin\theta_0))}{\sqrt{kd^2 - (\arccos(\rho(Y+1)-Y))^2}\sqrt{1-(\rho(Y+1)-Y)^2}}\right. \\
&\quad + \arcsin\left(\frac{\arccos((Y+1)\rho - Y)}{kd}\right) - \arcsin\left(\frac{\arccos((Y+1)\rho - Y\cos(kd\sin\theta_0))}{kd}\right)\Big] \\
&\quad [u(\rho-\rho_{2a}) - u(\rho-\rho_{3a})] \\
&\quad + \left[\frac{Y(1-\cos(kd\sin\theta_0))}{\sqrt{kd^2 - (\arccos(\rho(Y+1)-Y))^2}\sqrt{1-(\rho(Y+1)-Y)^2}}\right. \\
&\quad \left.\arcsin\left(\frac{\arccos((Y+1)\rho - Y)}{kd}\right) - \theta_0\right][u(\rho-\rho_{3a}) - u(\rho-\rho_4)]\Big\}
\end{aligned}
\tag{5.17}
$$

for $Y < Y_0$ and

$$
\begin{aligned}
&f_{\rho_d|Y}(\rho|Y) = \\
&\quad \frac{Y+1}{2Y(\frac{\pi}{2}-\theta_0)(1-\cos(kd\sin\theta_0))} \\
&\quad \left\{\left[\frac{\pi}{2} - \arcsin\left(\frac{\arccos((Y+1)\rho - Y\cos(kd\sin\theta_0))}{kd}\right)\right][u(\rho-\rho_1) - u(\rho-\rho_{2a})]\right. \\
&\quad + \left(\frac{\pi}{2} - \theta_0\right)[u(\rho-\rho_{2b}) - u(\rho-\rho_{3b})] \\
&\quad + \left[\frac{Y(1-\cos(kd\sin\theta_0))}{\sqrt{kd^2 - (\arccos(\rho(Y+1)-Y))^2}\sqrt{1-(\rho(Y+1)-Y)^2}}\right. \\
&\quad \left.\arcsin\left(\frac{\arccos((Y+1)\rho - Y)}{kd}\right) - \theta_0\right][u(\rho-\rho_{3a}) - u(\rho-\rho_4)]\Big\}
\end{aligned}
\tag{5.18}
$$

for $Y > Y_0$, where

$$
Y_0 = \frac{\cos(kd\sin\theta_0) - \cos(kd)}{1-\cos(kd\sin\theta_0)}. \tag{5.19}
$$

Figure 5.3 shows the conditional pdf $f_{\rho_d|Y}(\rho|Y)$ given by (5.17) or (5.18) for several

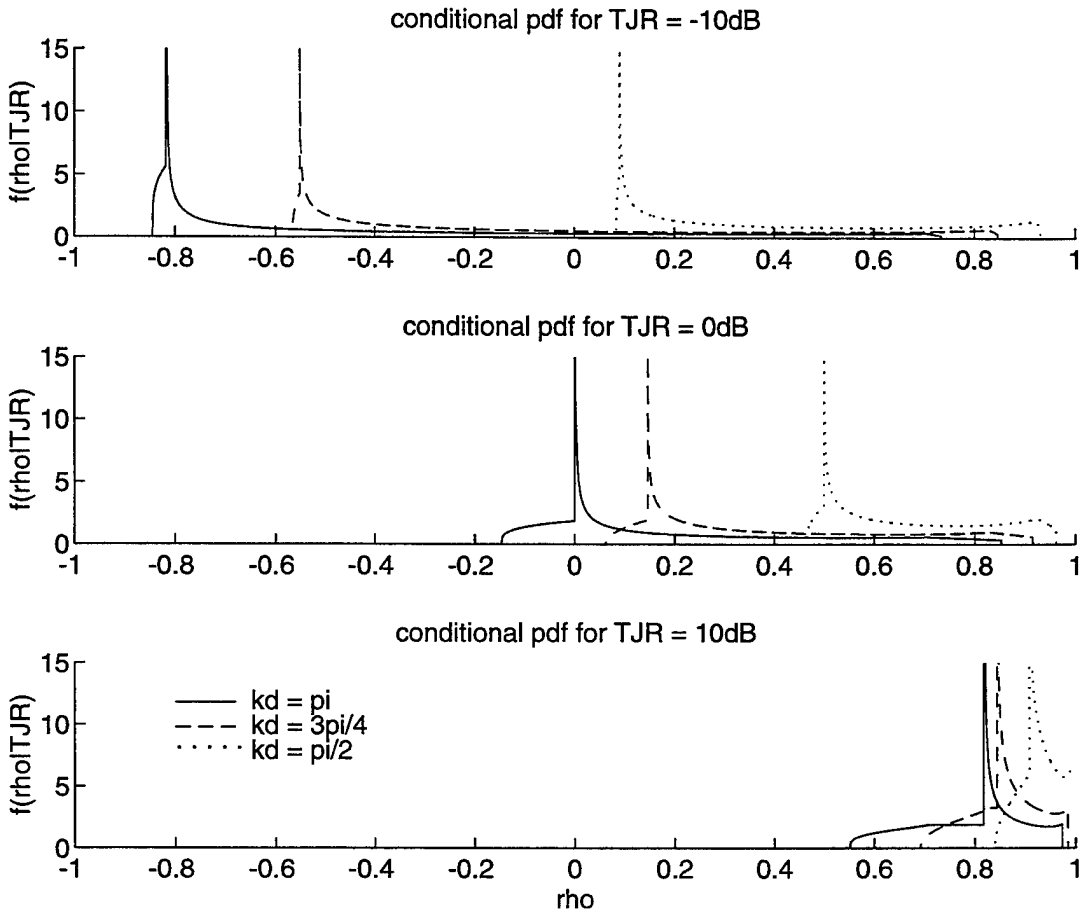

Figure 5-3: Probability density functions for the correlation of two sources described by (5.17) and (5.18), conditioned on TJR and for three values of *kd*.

values of Y and *kd*.

5.2.2 Correlation in reverberation

The above derivation of the pdfs only considered the direct target and jammer signals. The next step is to include reverberation.

As a first approximation, assume that the reverberant portion of the signals can be modeled as a diffuse sound field.[3] With this assumption, the direct and reverberant portions of the signal will be independent. As seen earlier for combining correlations of independent target and jammer, the total correlation, ρ_{tot}, is the normalized, weighted

[3]Note that this approach neglects early reflections.

sum of the direct and reverberant correlations, given by

$$\rho_{\text{tot}} = \frac{\sigma_d^2 \rho_d + \sigma_r^2 \rho_r}{\sigma_d^2 + \sigma_r^2} = \frac{W\rho_d + \rho_r}{W+1} \tag{5.20}$$

where σ_d^2 and σ_r^2 are the direct and reverberant signal powers, and $W = \frac{\sigma_d^2}{\sigma_r^2}$, the direct-to-reverberant ratio. The intermicrophone correlation of a diffuse sound field is

$$\rho_r = \frac{\sin(kd)}{kd} \tag{5.21}$$

(Cremer and Müller, 1982). Note that this applies to the reverberant portion of both the target and jammer signals. Furthermore, for a particular value of kd, the correlation of the diffuse field is a constant. Substituting (5.21) into (5.20) gives

$$\rho_{\text{tot}} = \frac{W\rho_d + \frac{\sin(kd)}{kd}}{W+1} \tag{5.22}$$

Treating the direct-to-reverberant ratio, W, as an unknown constant, the total correlation, ρ_{tot}, is a random variable with a conditional pdf related to the conditional pdf of the direct correlation ρ_d, given by (5.17) and (5.18). The effects of ρ_r and W are to shift the range of ρ_{tot} over which the pdf is nonzero by $\frac{\sin(kd)}{kd(W+1)}$ and to reduce the range of ρ_{tot} over which the pdf is nonzero by a factor of $\frac{W}{W+1}$.

Figure 5.4 shows the relationship between ρ_d and ρ_{tot} given by (5.22). Each plot in Fig. 5.4 shows the relationship between the direct correlation and the total correlation for a single value of kd and five values of W ranging from 0.1 to 10 (-10 dB to +10 dB). The slope of each line is $\frac{W}{W+1}$, which approaches zero for small W and approaches one for large W. For each value of kd, the lines for different values of W all intersect at $\rho_{\text{tot}} = \rho_d = \frac{\sin(kd)}{kd}$, which can be verified by substituting $\rho_d = \frac{\sin(kd)}{kd}$ into (5.22). This result has important implications for threshold selection, as discussed in the next section.

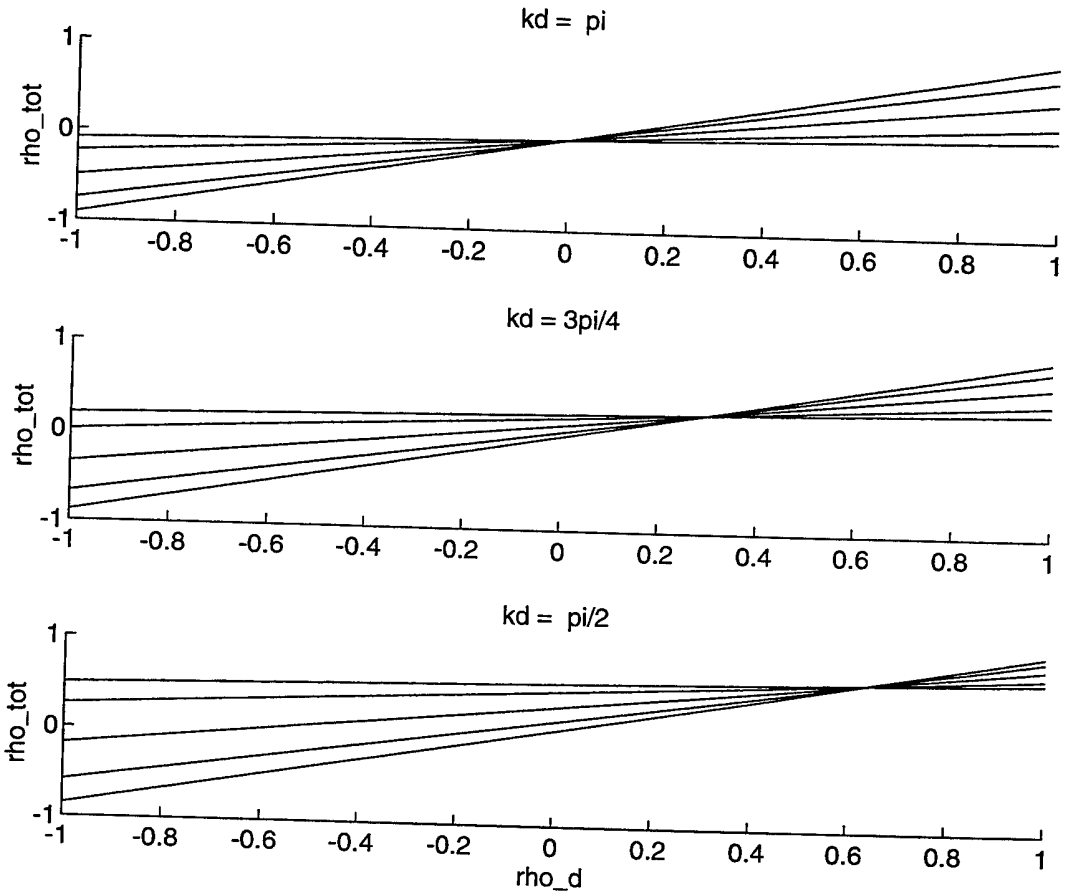

Figure 5-4: Relationship between correlation with and without reverberation as described by (5.22) for five values of direct-to-reverberant ratio (W = 0.1, 0.3, 1, 3, 10) and for three values of kd ($\frac{\pi}{2}, \frac{3\pi}{4}, \pi$).

5.2.3 Hypothesis testing

Binary hypothesis test

As discussed in Sec. 5.1, the goal is to use the correlation measure as the observation in a binary hypothesis test (Van Trees, 1968). The two hypotheses are TJR$<$ 0 dB (H0 = "low" TJR) and TJR$>$ 0 dB (H1 = "high" TJR), although the following approach could be applied to any pair of ranges of TJR. The cutoff is set to 0 dB because, as discussed in Sec. 2.3.1, the detrimental effects of misalignment and misadjustment are proportional to TJR and are typically noticeable at positive values of TJR.

Correctly determining that H0 is true (correctly saying TJR$<$ 0 dB) will be referred to as a detection and results in adapting under the desired circumstances. Incorrect determination of H0 (saying that TJR$<$ 0 dB when actually TJR$>$ 0 dB) is a false alarm and results in adapting when it is undesirable. Incorrect determination of H1 (saying that TJR$>$ 0 dB when actually TJR$<$ 0 dB) is a miss and results in not adapting under circumstances when adapting was desirable.

Of the two types of errors, false alarms are potentially more damaging than misses, because adapting when it is undesirable may degrade the signal, while not adapting when it is desirable only slows the convergence of the adaptive weights. Selecting the threshold on the correlation to distinguish between the two hypotheses controls the tradeoff between misses and false alarms.[4] Because of the nature of this tradeoff, it is difficult to quantify the costs associated with these two types of errors. Qualitatively, it is reasonable to permit a relatively high rate of misses in order to obtain a lower rate of false alarms.

In previous sections, the TJR, Y, has been considered an unknown constant, but in order to formulate the problem as a hypothesis test, it is necessary to assume a known distribution. Obviously, some degree of approximation is required in making such an assumption. Previous studies have shown that conversations in noisy environments often occur at long-term TJRs of 1–5 dB (Plomp, 1977; Teder, 1990). Short-term

[4]This tradeoff of convergence time versus error in the adaptive weights is similar to the tradeoff inherent in selection of the step-size parameter, μ, in (4.17), where smaller values of μ decrease misadjustment at the cost of longer convergence times.

fluctuations in speech level typically range from 18 dB above to 12 dB below the average power level (Kryter, 1962). In the following analysis, it is assumed that the TJR is evenly distributed on the range −20 dB to +20 dB, so that

$$f_{U_s}(U) = \frac{1}{40} \tag{5.23}$$

for $-20 \text{ dB} < U_s < +20 \text{ dB}$, where

$$U = 10 \log_{10} Y. \tag{5.24}$$

The sensitivity of the analysis to this assumption is considered below. Note that one result of this assumption is that the two hypotheses, H0 and H1, are equally likely.

First considering the case of no reverberation, the pdf of ρ_d conditioned on the two hypotheses H0 and H1 is found by integrating the conditional pdf given by (5.17) and (5.18), that is,

$$f_{\rho_d|H0}(\rho|H0) = \int_{-20}^{0} f_{\rho_d|Y}(\rho|Y)dU \tag{5.25}$$

$$f_{\rho_d|H1}(\rho|H1) = \int_{0}^{+20} f_{\rho_d|Y}(\rho|Y)dU \tag{5.26}$$

where $Y = 10^{U/10}$. These two integrations were performed numerically using the trapezoidal rule to produce the curves shown in Fig. 5.5.

For a particular threshold, ρ_0, the probability of detection is

$$P_d = \int_{-1}^{\rho_0} f_{\rho_d|H0}(\rho|H0)d\rho \tag{5.27}$$

Similarly, the probability of false alarm is

$$P_f = \int_{-1}^{\rho_0} f_{\rho_d|H1}(\rho|H1)d\rho, \tag{5.28}$$

while the probability of a miss is

$$P_m = 1 - P_f. \tag{5.29}$$

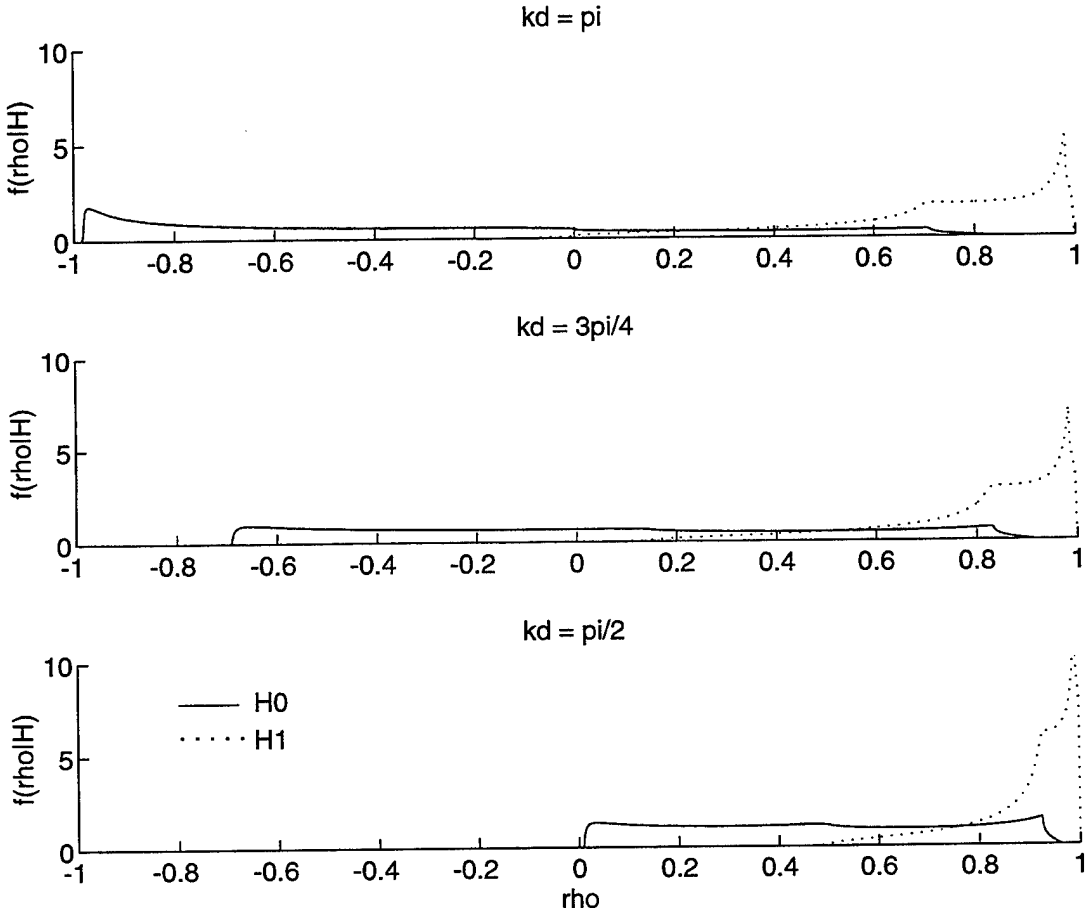

Figure 5-5: Probability density functions for the correlation of two sources described by (5.25) and (5.26), conditioned on the hypotheses H0 and H1 described in the text, for three values of kd.

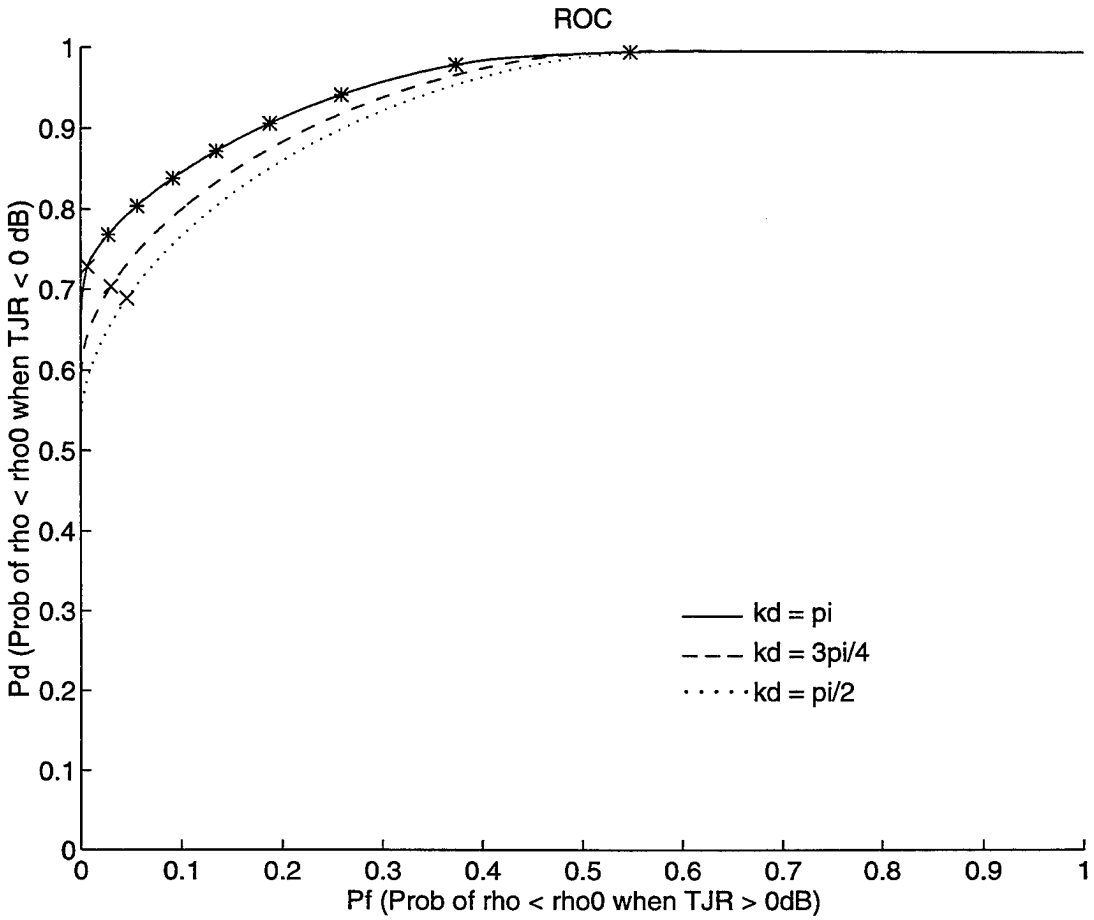

Figure 5-6: Receiver operating characteristic for binary hypothesis testing for three values of kd. The points labeled with 'x' indicate the performance when the threshold, ρ_0, is zero and the points labeled with '$*$' indicate the performance when $\rho_0 = 0.1, 0.2, \ldots, 0.8$.

Again performing these integrations numerically for values of ρ_0 in the range $-1 < \rho_0 < 1$ and plotting P_d versus P_f produces the receiver operating characteristic (ROC) curves shown in Fig. 5.6. Figure 5.6 shows that for any choice of threshold, the best performance is obtained with $kd = \pi$.

Substituting (5.5) into the choice of $kd = \pi$ and rearranging results in

$$f = \frac{c}{2d}. \tag{5.30}$$

For each microphone spacing, the correlation measure providing the most accurate

decision of the range of TJR is produced at a different frequency; for a microphone separation of $d = 7$cm, that frequency is $f = 2464$ Hz. Based on the ROC curves of Fig. 5.6, frequencies selected based on $kd = \pi$, and therefore (5.30), will be used in the remainder of this work.

Next, consider the effect of reverberation, as described by (5.22). The presence of reverberation causes the conditional pdfs shown in Fig. 5.5 to be shifted and scaled along the abscissa, because (5.25) and (5.26) are now integrals of a random variable shifted and scaled as in (5.22). However, since the magnitude of the scaling and shifting is identical for the pdfs corresponding to both hypotheses, the ROC curves in Fig. 5.6 are unchanged for any level of reverberation.[5] Therefore, if the level of reverberation is known, then the transformation between ρ_d and ρ_{tot} is known and it is possible to select a threshold, ρ_0, that will produce performance corresponding to a desired point on the ROC curve when applied to ρ_{tot}. However, when the level of reverberation is unknown, then a single threshold, ρ_0, applied to the total correlation, ρ_{tot}, maps to a range of values of ρ_d, corresponding to a range of values on the ROC curve. This issue is discussed in the next section.

Finally, the sensitivity of this analysis to the assumption that the TJR is evenly distributed between -20 and $+20$ dB is considered. The two curves in Fig. 5.7(a) show P_d and P_f versus threshold for $kd = \pi$. (The ROC curve in Fig. 5.6 was produced from the same values of P_d and P_f.) The curves in Fig. 5.7(b) show the probability that the correlation is below the threshold, versus threshold, for individual values of TJR. When the TJR is less than 0 dB, the curve corresponds to P_d for that value of TJR. Similarly, when the TJR exceeds 0 dB, the curve corresponds to P_f for that value of TJR. The two curves in Fig. 5.7(a) can be thought of as the integrals of all such single TJR curves within the two ranges of -20 dB $<$ TJR $<$ 0 dB and 0 dB $<$ TJR $<$ 20 dB. Because of the similar shapes of these curves and the relative symmetry of the contributions at positive and negative TJRs, the ROC curves shown

[5]Theoretically, this is true for any level of reverberation. In practice, in extreme reverberation (as the direct-to-reverberant ratio, W, approaches zero) the location on the ROC curve becomes increasingly sensitive to the threshold value, and the shape of the ROC curve becomes increasingly sensitive to the assumptions regarding the probability distributions.

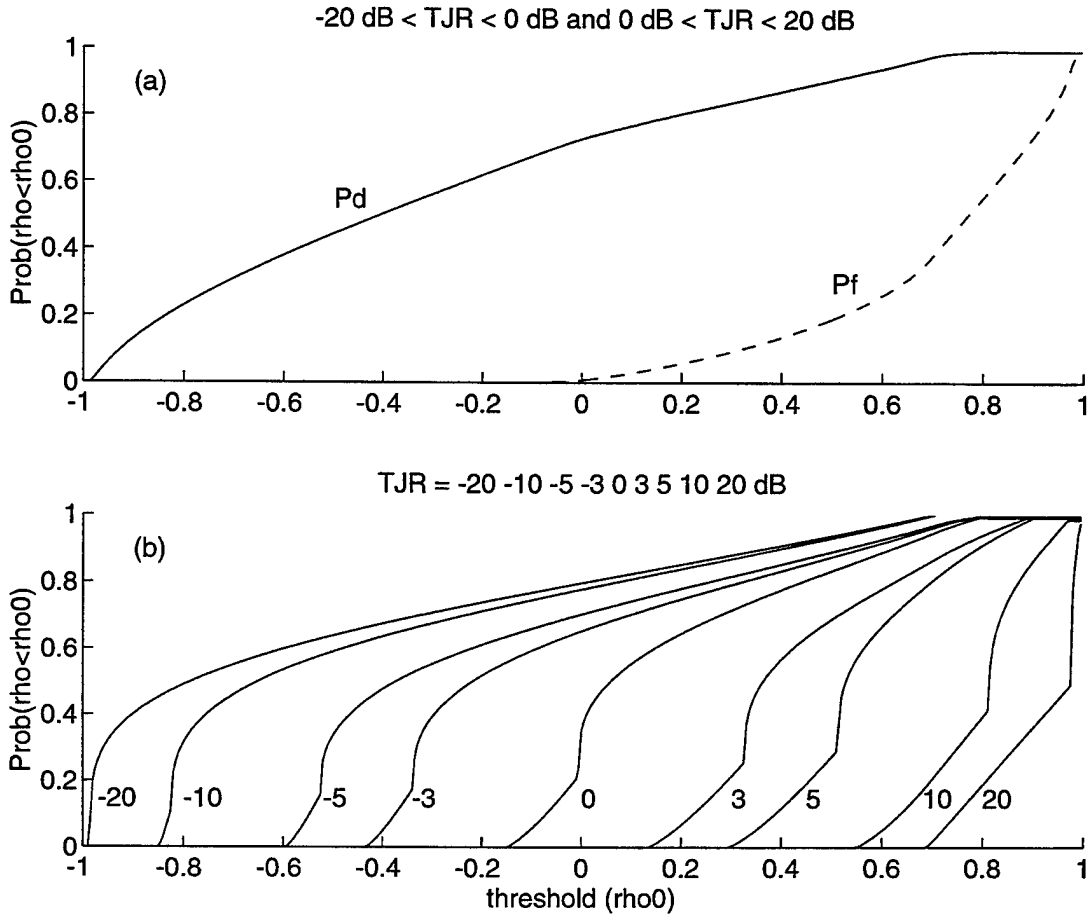

Figure 5-7: (a) Cumulative probability distributions for the correlation of two sources with two ranges of TJR: -20 dB<TJR<0 dB and 0 dB<TJR<20 dB. (b) Cumulative probability distributions for the correlation of two sources with specified TJR ranging from -20 dB to 20 dB.

in Fig. 5.6 are relatively robust to violations of the assumption that the TJR is evenly distributed between -20 and $+20$ dB.

Choice of threshold

Based on the above analysis, it is possible to select the threshold to achieve a desired result. Perhaps the most obvious option is to choose threshold $\rho_0 = \frac{\sin(kd)}{kd}$, because, as seen in Sec. 5.2.2, at that point ρ_d and ρ_{tot} are equal for any level of reverberation, so with that threshold, the performance will correspond to a single point on the ROC curve for all levels of reverberation. Each curve in Fig. 5.6 is labeled with 'x' at the

point corresponding to $\rho_0 = \frac{\sin(kd)}{kd}$.

One drawback to this approach concerns the distribution of errors as a function of jammer angle. Figure 5.6 shows that for $kd = \pi$ and $\rho_0 = \frac{\sin(kd)}{kd} = 0$, the detection rate is greater than 75%, so the system will miss more than 25% of the time when TJR < 0 dB. This would not be a problem if these errors were distributed more or less evenly over jammer angle, because, as discussed earlier, it is reasonable to permit some misses to obtain a low rate of false alarms. However, these misses are not evenly distributed, rather they are concentrated where correlation is high, which corresponds to small jammer angles.

To illustrate this, consider the correlation produced by a single jammer arriving from angle θ given by (5.4). With $kd = \pi$, $\rho = 0.69$ for $\theta = 15°$ and $\rho = 0$ for $\theta = 30°$. So with the threshold set to $\rho_0 = 0$ and with no target signal present, the system will not adapt in the presence of jammers arriving from angles between 15° and 30°. This range of angles is slightly higher for values of $kd < \pi$. And when the target signal is included, this range of angles extends beyond 30°, increasing with TJR.

In the remainder of this work, the threshold will be set to $\rho_0 = 0$ (that is, $\rho_0 = \frac{\sin(kd)}{kd}$ for $kd = \pi$), and it is accepted that the system will not adapt in response to jammers at angles below 30°. This is reasonable since the original choice of $\theta_0 = 14.5°$ was somewhat arbitrary and since little is known about how such systems will be affected by head movements when worn by human listeners. However, when real-time adaptive multiple-microphone systems are designed for field tests, it is suggested that a user input control the threshold selection. In this manner, the user can adjust the effective beamwidth of the system over some range, but the cost of narrower beamwidths is higher false alarm rates, resulting in potential degradations of the target signal at high TJR.

For these future systems, it will be useful to quantify the effect of increasing the threshold. This corresponds to moving to the right along the ROC curve, so that P_f increases together with P_d. The problem is that for unknown levels of reverberation, it is not possible to determine a mapping between the threshold and the location on the ROC curve. For example, if the threshold on ρ_{tot} is ρ_0, then with no reverberation,

performance is the same as for $\rho_d = \rho_0$, with a direct-to-reverberant ratio of 0 dB, performance is the same as for $\rho_d = 2\rho_0$, and with a direct-to-reverberant ratio of -10 dB, performance is the same as for $\rho_d = 11\rho_0$.

To illustrate this effect of reverberation on performance, in Fig. 5.6 the ROC curve corresponding to $kd = \pi$ is labeled with '$*$' at points corresponding to $\rho_0 = 0.1, 0.2, \ldots, 0.8$. As an example, if the threshold were set to $\rho_0 = 0.3$, then the maximum angle of an undetected jammer (with no target present) would decrease to 24°. The detection and false alarm rates would range from $P_d = 0.84$ and $P_f = 0.09$ (for $\rho_d = \rho_0 = 0.3$) in no reverberation to $P_d = 0.94$ and $P_f = 0.26$ (for $\rho_d = 2\rho_0 = 0.6$) with a direct-to-reverberant ratio of 0 dB. (direct-to-reverberant ratio of 0 dB). The false alarm rate would be much higher for direct-to-reverberant ratios below 0 dB. However, when the reverberation dominates, the effect of these errors may be less severe.

Furthermore, (5.22) suggests that as reverberation increases, the fluctuations in the correlation measure due to the direct target and jammer signals decreases. Therefore, if it were necessary to determine the direct-to-reverberant ratio of the acoustic environment, it might be possible to estimate that quantity from the variance of the correlation measurement over a reasonably long interval.

Determining broadband TJR

The preceding narrowband analysis has considered using a correlation measurement from one pair of microphones as a decision variable in the TJR hypothesis test for a particular frequency. However, the proposed method of controlling the adaptive process actually requires a single global decision as to the range of the broadband TJR. This raises two questions. First, if only two microphones are available, how accurately can the range of the broadband TJR be determined from a measure based on the narrowband analysis? Second, if more than two microphones are available, how can the information from different pairs of microphones be combined to generate the most accurate decisions concerning the range of broadband TJR?

In addressing the first question, it should be noted that the correlation measure-

ment corresponding to each microphone pair will not be based on a single frequency, rather, it will be computed for the portion of the signal in a relatively narrow band about the frequency, f, determined by (5.30). The sensitivity of the proposed method to varying bandwidth will be investigated in computer simulations in the next section.

For arrays of more than two microphones, a different correlation measurement can be obtained from each pair of microphones. If different pairs of microphones have different spacings, then they will provide correlation measurements based on different frequencies, according to (5.30). To address the second question, three methods of combining correlation measures are proposed. The first method, *voting*, consists of first comparing each correlation measurement to the threshold, and then using the majority of those decisions to determine the outcome. The second method, *averaging*, consists of first averaging the correlation measurements and then comparing the average to the threshold. The third method, *power-weighted averaging*, is the same as averaging except that each correlation measurement is first weighted by a running measure of the power in the corresponding frequency band. All three of these methods will be investigated in computer simulations in the next section.

5.3 Simulations

The simulations in this section are intended to illustrate the utility of the method analyzed in Sec. 5.2. A block diagram of the system for determining the range of short-term TJR is shown in Fig. 5.8. First, each pair of microphone signals is bandpass filtered. The arithmetic center frequency of the bandpass filter is determined from the microphone spacing and (5.30). Next, the instantaneous correlation is computed using a hard limiter, as in Greenberg and Zurek (1992), resulting in a binary quantity that is the product of the signs of the bandpass filtered signals.[6] The instantaneous correlation is then smoothed by a first-order recursive lowpass filter with

[6]The hard limiter is used to simplify the implementation in real-time systems. In addition to replacing multiplies with sign-bit comparisons, the hard limiting eliminates the need to divide by the square root of the signal powers, which would otherwise be needed for a normalized correlation measure.

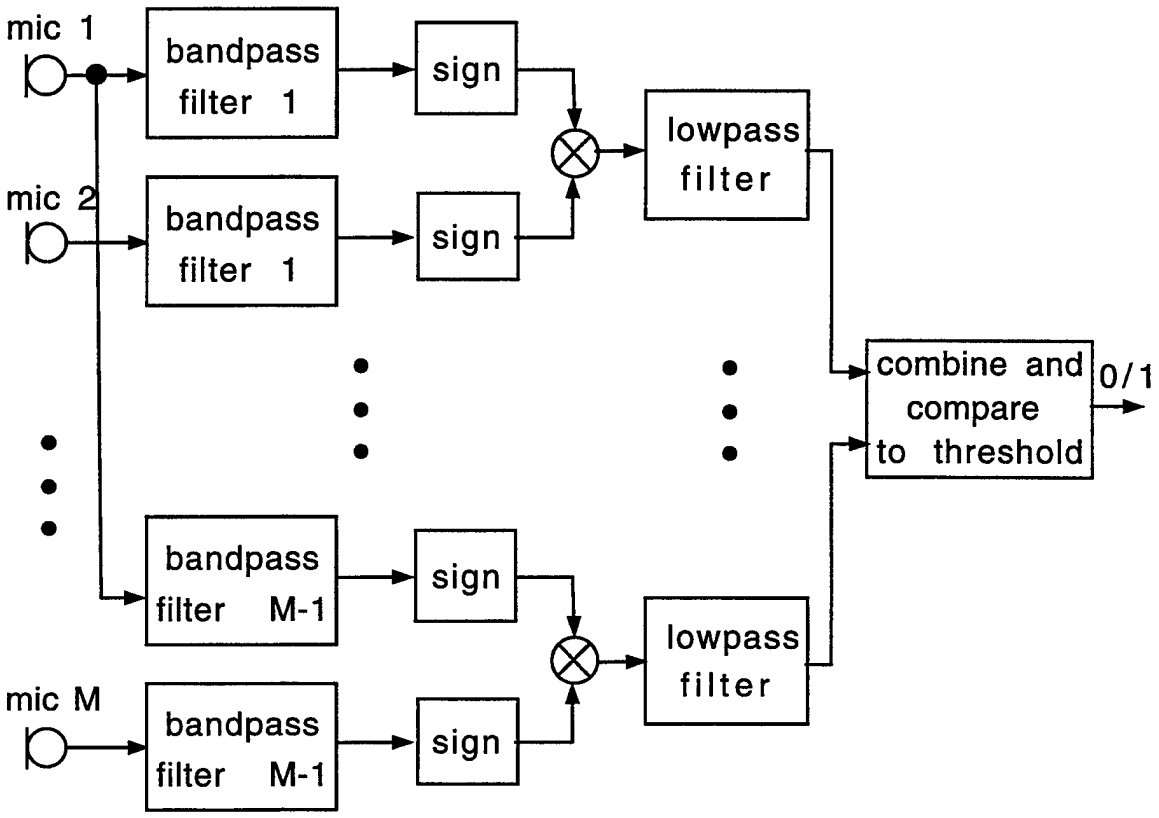

Figure 5-8: Block diagram of system to determine range of TJR. Each pair of microphone signals is bandpass filtered, the signs of the bandpass filtered signals are multiplied to produce the instantaneous correlation, and these values are smoothed by a first-order lowpass filter with a time constant of 10 ms. The lowpass filtered correlation values are combined and compared to the threshold by one of the three methods described in the text. The result is a binary decision about the range of TJR, TJR $<$ 0 dB or TJR $>$ 0 dB.

a time constant of 10 ms. This value was chosen because it is suitable for tracking the fluctuations in speech levels (Greenberg, 1989). Finally, the lowpass filtered correlation values from all frequency bands are combined and compared to the threshold according to one of the three methods (voting, averaging, or weighted averaging) described in Sec. 5.2.3. The result is a binary decision about the range of TJR, TJR $<$ 0 dB or TJR $>$ 0 dB, that determines whether or not the adaptive weights should be updated.

5.3.1 Noise

The first set of simulations are intended to verify the analysis of Sec. 5.2 and to investigate the robustness of the algorithm to variations in bandwidth.

For these simulations, the target and jammer sources were 14000 samples of zero-mean Gaussian noise. The jammer source had unit variance. The target source was scaled to produce a TJR that was constant over 1000-sample intervals, incrementing in 3 dB steps between -19.5 and 19.5 dB.

These source signals were convolved with anechoic source-to-microphone impulse responses generated by the room simulation described in Sec. 3.2. The array contained two microphones with 7 cm spacing. The target angle varied from 0 to 12 degrees and the jammer angle varied from 18 to 90 degrees, both in 4 degree increments. For all 76 combinations of target and jammer angles, the running correlation was computed as shown in Fig. 5.8 and compared to a threshold of $\rho_0 = 0$. For comparison, the running correlation was also computed without the hard limiter. The bandpass filter had a center frequency of 2464 Hz, computed from (5.30). The filter bandwidth varied from 10% to 180% of the center frequency (246 Hz to 4435 Hz), and was centered arithmetically.

For each sample point, the binary result of the processing was compared to the true TJR. Since TJR < 0 for the first half of the source signals and TJR > 0 for the second half, the detection rate was computed from the first 7000 points and the false alarm rate was computed from the last 7000 points. These values of P_d and P_f were averaged for all combinations of target and jammer angles. The results are shown in the left half of Fig. 5.9. For a wide range of bandwidths, $P_d \approx 0.7$ and $P_f < 0.1$.

The analysis in Sec. 5.2.3 indicates that for $\rho_0 = 0$ and $kd = \pi$ the probabilities of detection and false alarms are $P_d = 0.73$ and $P_f = 0.007$. This corresponds to the points marked with 'x' on the upper curve in Fig. 5.6 and with '$*$' in Fig. 5.9. In general, there is good agreement between the values predicted by the analysis of Sec. 5.2.3 and the results of the simulations. Several factors are responsible for both the discrepancies between the analysis and the simulation results and the trends in the simulation results. Those factors will be discussed after first summarizing the

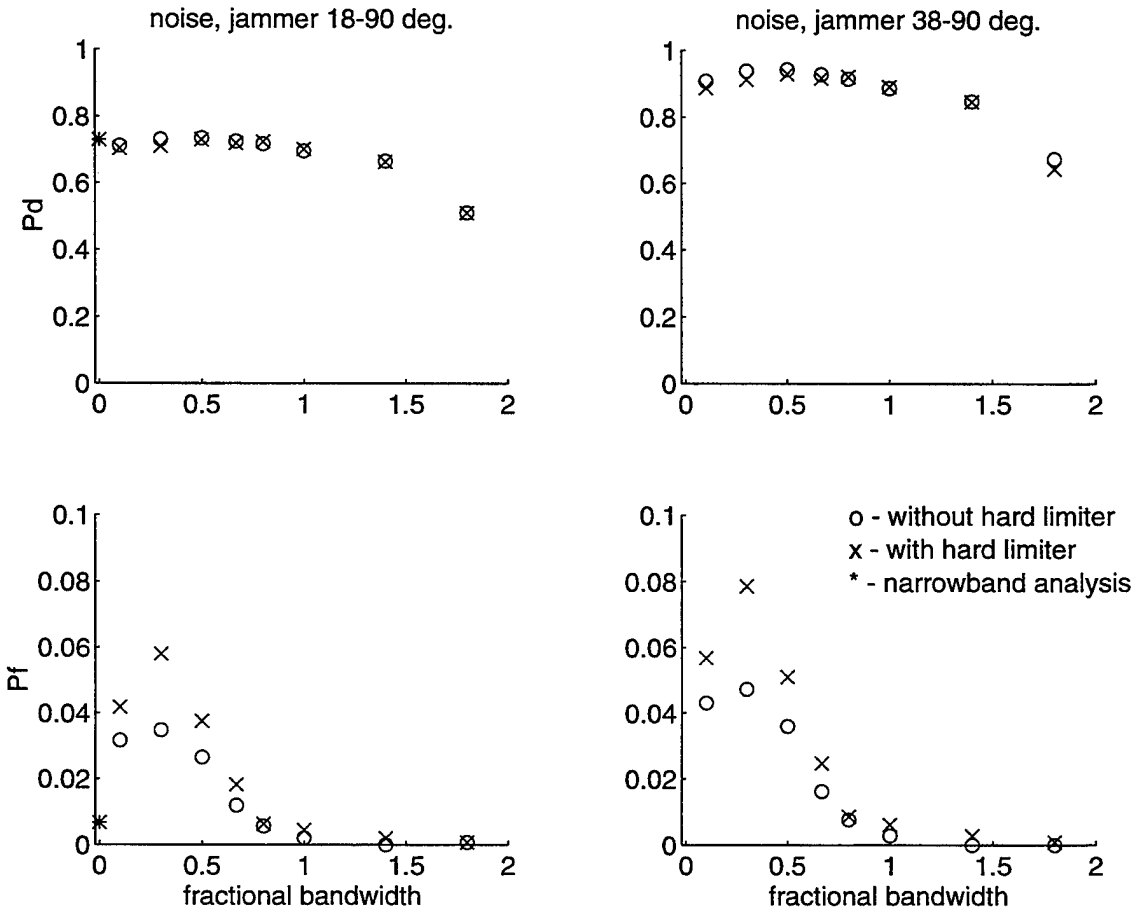

Figure 5-9: Simulation results showing rates of detection and false alarms, as a function of bandwidth, for noise received by two microphones in an anechoic environment. The points labeled with 'x' indicate the performance using the hard limiter (taking the sign of bandpass filtered signals as shown in Fig. 5.8), while the points labeled with 'o' indicate the performance without the hard limiter (the bandpass filtered signals are multiplied directly). The points labeled with '*' correspond to the values determined by the narrowband analysis of Sec. 5.2.3.

relationship between correlation measures, thresholds, and false alarm and detection rates.

The system shown in Fig. 5.8 is credited with a correct detection when the measured correlation is less than the threshold ($\rho < \rho_0$) and the true TJR < 0 dB. False alarms occur when $\rho < \rho_0$ and the true TJR > 0 dB. Increasing the threshold increases the rate of both detections and false alarms (moving to the right on the ROC curve), while decreasing the threshold decreases the rate of both detections and false alarms (moving to the left on the ROC curve). Any factor that causes the measured correlation, ρ, to decrease will have the same effect as raising the threshold, ρ_0, and conversely, anything that causes the measured correlation to increase will have the same effect as lowering the threshold.

The most striking discrepancy between the analysis and simulation results is the relatively low false alarm rate predicted by the analysis. This results from the approximation in (5.16) used for the target pdf. The approximation overrepresents $\theta_t = 0$ and underrepresents all other $0 < \theta_t < \theta_0$. This causes the analysis results to be biased towards $\theta_t = 0$, which contributes higher correlation values. The higher correlation values cause the analysis to predict lower rates of detection and false alarms. This approximation has much more of an impact on the false alarm rates, because it only affects the target signal's contribution to correlation, and false alarms occur when the target signal dominates (TJR> 0dB).

Figure 5.9 illustrates the effects of varying bandwidth. The original analysis was performed for narrowband sources. Obviously, using wideband signals will include additional frequencies in the computation of ρ. The effect of these frequencies depends on the source angle. For a rectangular band of noise arithmetically centered at f with bandwidth B, the mean correlation value is given by

$$\bar{\rho} = \cos(2\pi f\tau)\frac{\sin(\pi B\tau)}{\pi B\tau} \tag{5.31}$$

(McConnell, 1985). Substituting (5.2) and (5.30) into (5.31) gives the relationship between source angle and correlation for $kd = \pi$ for arbitrary bandwidth as a fraction

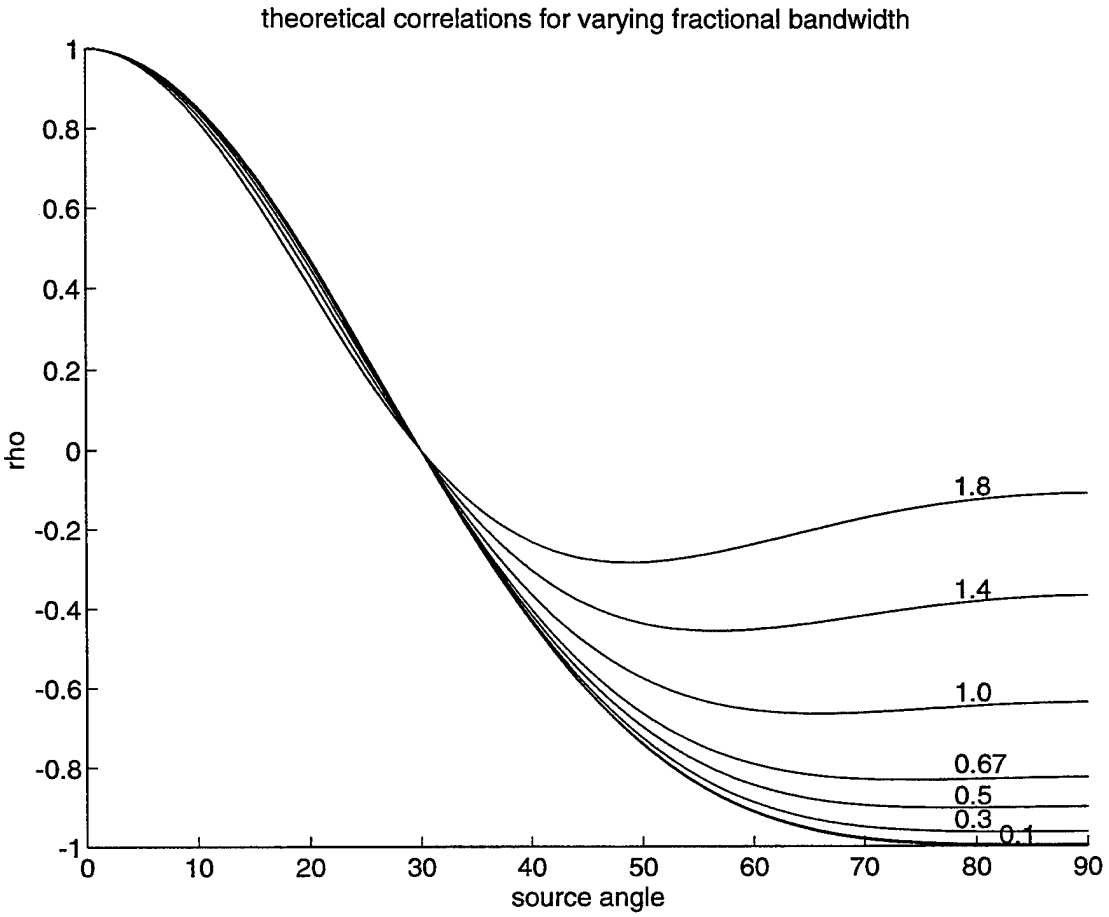

Figure 5-10: Theoretical relationship between correlation and source angle, for fractional bandwidths as indicated, ranging from 0.1 to 1.8.

of center frequency, that is,

$$\bar{\rho} = \cos(\pi \sin(\theta)) \frac{\sin(\pi \frac{b}{2} \sin(\theta))}{\pi \frac{b}{2} \sin(\theta)} \tag{5.32}$$

where b is the fractional bandwidth $\frac{B}{f}$. Figure 5.10 illustrates this relationship for several fractional bandwidths. In Fig. 5.10 the curve for $b = 0.1$ is indistinguishable from the pure cosine obtained for a narrowband source.

From (5.31) and Fig. 5.10 it is clear that the effect of increasing signal bandwidth is to decrease the magnitude of the correlation value. For source angles less than 30°, wideband signals provide smaller positive values while for source angles greater than 30°, they provide smaller negative values. Furthermore, the magnitude of this effect

is more pronounced for jammers ($15° - 90°$) than for targets ($0° - 15°$). Therefore, the effect of increasing the bandwidth is to increase the correlation measure, leading to lower rates of detection and false alarms.[7]

Another factor that affects the performance of the correlation measure is the use of a hard limiter to compute the instantaneous correlation. For Gaussian signals, the relationship between the hard-limited correlation and the true correlation is $\rho_{\text{hl}} = \frac{2}{\pi} \arcsin(\rho_{\text{true}})$ (Papoulis, 1984). The result of this arcsine transformation is to compress the relationship between TJR and ρ near $\rho = 0$, which may lead to more errors in both directions, that is, increased false alarms and decreased detections. Figure 5.9 shows the results of simulations with and without hard limiting. Although the effect of hard limiting is to increase errors, the increase is slight, and for many applications may be worth the savings in computational complexity.[8]

Finally, as discussed in Sec. 5.2.3, the errors are not distributed evenly as a function of jammer angle, rather, the "misses" are concentrated when jammer angle is small. The right half of Fig. 5.9 shows P_d and P_f when jammer angles between 18 and 34 degrees are ignored. For the range of jammer angles between 38 and 90 degrees, the overall performance is much better, with $P_d \approx 0.9$, and only a slight increase in P_f. To illustrate the dependence on jammer angle, Fig. 5.11 shows P_d and P_f as a function of jammer angle for a fractional bandwidth of 0.67. The four curves in each panel show the performance for the four target angles, $\theta_t = 0, 4, 8, 12°$. Again the

[7]This explains the general trend of decreasing P_d and P_f with increasing bandwidth, but not the initial increase seen in Fig. 5.9. Because the detection and false alarm rates described by (5.27) and (5.28) correspond to the area of the measurement's conditional pdf that is below the threshold, those values depend on the entire pdf, not just its mean. For the fractional bandwidths studied (0.1 to 1.8), the variance of the correlation value was observed to decrease with increasing bandwidth. This is because the wider bandwidths contain more frequencies, making the result less sensitive to the fluctuations of individual frequency components. For some conditions of target angle, jammer angle, and TJR, as the bandwidth increased, this secondary effect of decreasing variance was sufficient to cause increases in P_f and P_d, despite the increase in the mean of the correlation measure. This accounts for the non-monotonicity of the simulation results in Fig. 5.9.

[8]The purpose of the hard limiter is to replace multiplies with sign-bit comparisons and eliminate the need for normalizing the correlation measure. However, when the threshold is zero, only the *sign* of the correlation measure is relevant, and the normalization is not required, since it will not affect the sign of the resulting correlation measure. Therefore, *when the threshold is zero, it is possible to eliminate the hard limiter*, especially on hardware platforms that require the same resources for multiplication as for sign-bit comparison.

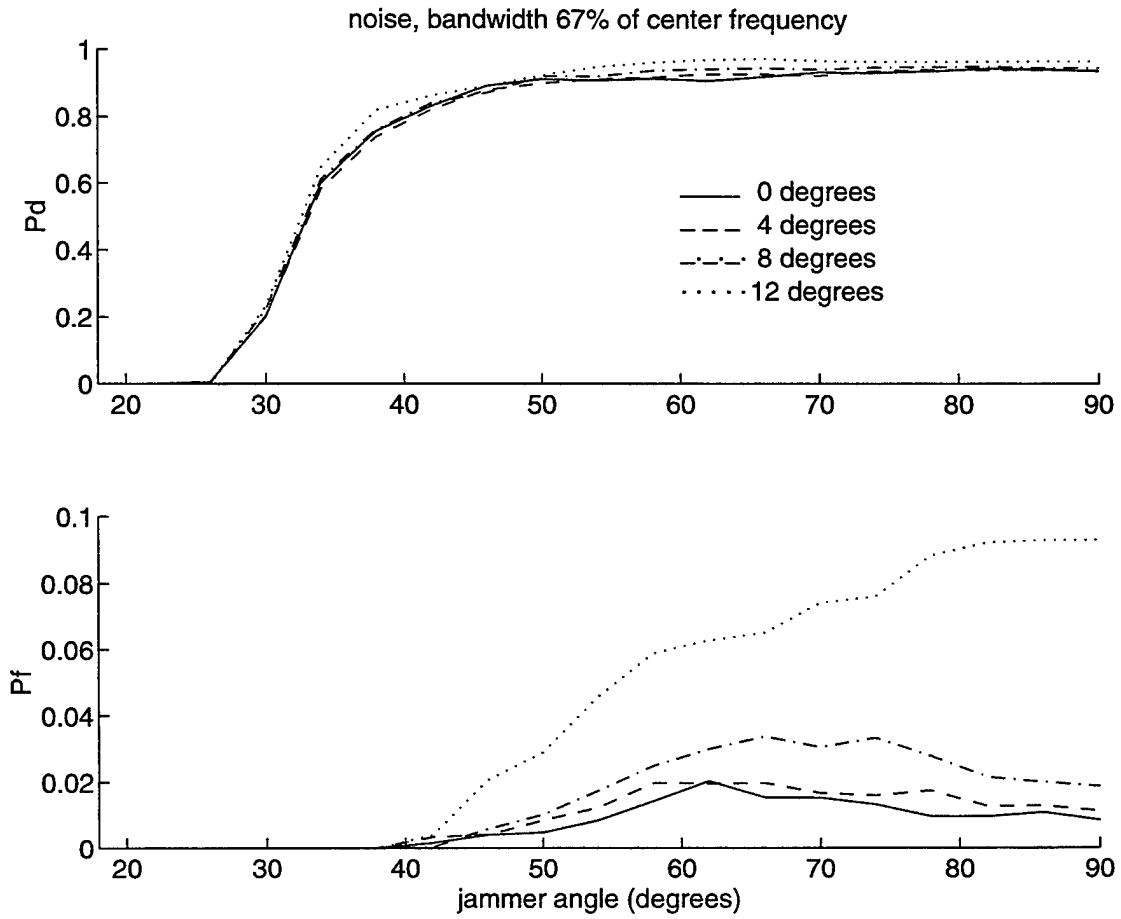

Figure 5-11: Simulation results showing rates of detection and false alarms, as a function of jammer angle, for noise received by two microphones in an anechoic environment. The fractional bandwidth was 0.67, and results are shown for four target angles, $\theta_t = 0$, 4, 8, and 12° .

TJR varied in 3 dB steps from -19.5 dB to 19.5 dB. Figure 5.11 shows that there is essentially no detection of TJR< 0dB when jammers are located at angles less than 30 degrees and a rapid transition in the detection of TJR< 0dB when the jammer angle changes from 30° to 40°. Similarly, the false alarm rate increases with increases in either target angle or jammer angle.

5.3.2 Speech

The second set of simulations are intended to investigate the effect of speech sources and reverberation. These simulations included both two- and five-microphone arrays.

The target and jammer sources were sentences and babble prepared as described in Sec. 3.1. The source signals were scaled so that the long-term TJR was 0 dB.

Two-microphone array

The 7-cm, two-microphone broadside array was evaluated using three sentences and babble for each of the 76 combinations of target and jammer angles. All of the processing was the same as for the noise sources in the previous section. The hard limiting was included in the processing.

The performance was evaluated by averaging the rates of detection and false alarms for all conditions and comparing to the true TJR. The true TJR was determined by squaring the target and jammer signals received at the leftmost[9] microphone, processing the squared signals with the same 10 ms lowpass filter used to smooth the correlation measure, and computing the ratio of the two filtered signals. The values of P_d and P_f were computed in two ways, by comparing the binary decision to the true broadband TJR, and by comparing it to the true bandpass TJR in the frequency band used to compute the correlation measure.

Figure 5.12 shows the results. The general trends in performance with speech signals follow the trends seen in Fig. 5.9 with noise. As would be expected, the performance is better (higher detection rate and lower false alarm rate) when it is referenced to the TJR in the frequency band used by the correlation measure than when it is referenced to the broadband TJR.

Comparing Fig. 5.12 with Fig. 5.9 does show some differences in the results obtained with speech and noise. The two most significant differences consist of a drastic reduction in detection rate at large bandwidths and an overall increase in the false alarm rate.

The lower detection rates for large fractional bandwidths is due to the difference between noise and speech source signals. Unlike the noise used in the previous section, the frequency components of speech are not evenly distributed within the band of interest. This makes the performance more sensitive to increased bandwidth, and

[9]when facing the target

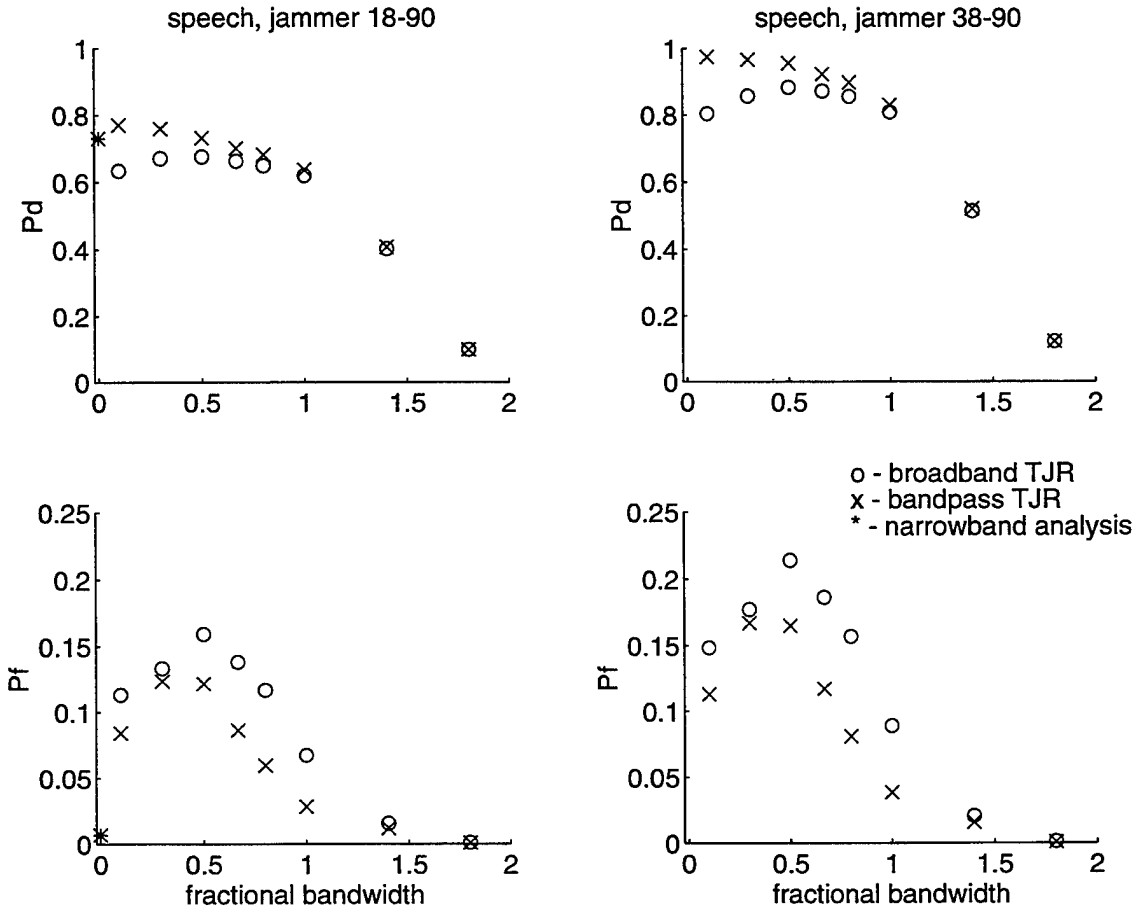

Figure 5-12: Simulation results showing rates of detection and false alarms, as a function of bandwidth, for speech and babble received by two microphones in an anechoic environment. The points labeled with 'x' indicate the performance referenced to the bandpass TJR, while the points labeled with 'o' indicate the performance referenced to the broadband TJR. The points labeled with '*' correspond to the values determined by the narrowband analysis of Sec. 5.2.3.

accounts for the low rate of detection for fractional bandwidths greater than unity.

The overall increase in the false alarm rate is due to the range of TJRs available in the signals. For the noise signals, the TJR varied in 3 dB steps that included -1.5 dB and 1.5 dB. For the speech signals, the short-term TJR varied continuously through a range of TJRs including 0 dB. Many of the false alarms occurred on these transitions. This can be seen in Fig. 5.13, which shows the true TJRs for one sentence along with the locations of misses and false alarms.

In order to investigate the usefulness of the correlation method in reverberation, a subset of the conditions described above were repeated for the reverberant source-to-microphone impulse responses described in Sec. 3.2. The target angle was either 0 or 12 degrees and the jammer angle was 38, 54, 70, or 86 degrees. For the eight combinations of target and jammer angles, the rates of detection and false alarm were computed as described above for the same three sentences and babble. For the reverberant conditions, the true TJRs used to assess performance were computed from the direct wave of target and jammer signals; reflections were not included.

The results are shown in Fig. 5.14.[10] The addition of reverberation lowers the detection rates overall and causes further reduction in detection rates with increasing bandwidth. The addition of reverberations causes no distinct trends in false alarm rates.

With a two-microphone array, only one correlation measure can be computed. As a result, bandwidth selection is governed by two conflicting goals. On one hand, it is desirable to use a wide frequency band, so that the correlation measure will reflect as much information as possible about the broadband TJR. On the other hand, the use of relatively wide bandwidths is limited by their negative impact on detection rates. This tradeoff can be seen in Figs. 5.12 and 5.14, where increasing bandwidth causes the broadband and bandpass results to converge, but also causes a substantial reduction in detection rates. In order to balance these two conflicting requirements, a fractional bandwidth of 0.67 (one octave) will be used with two-microphone arrays

[10]The two plots on the left contain results obtained with the anechoic room impulse responses for the same eight combinations of target and jammer angles, that is, the values were obtained by averaging a subset of the data points that were averaged to generate the values shown in Fig. 5.12.

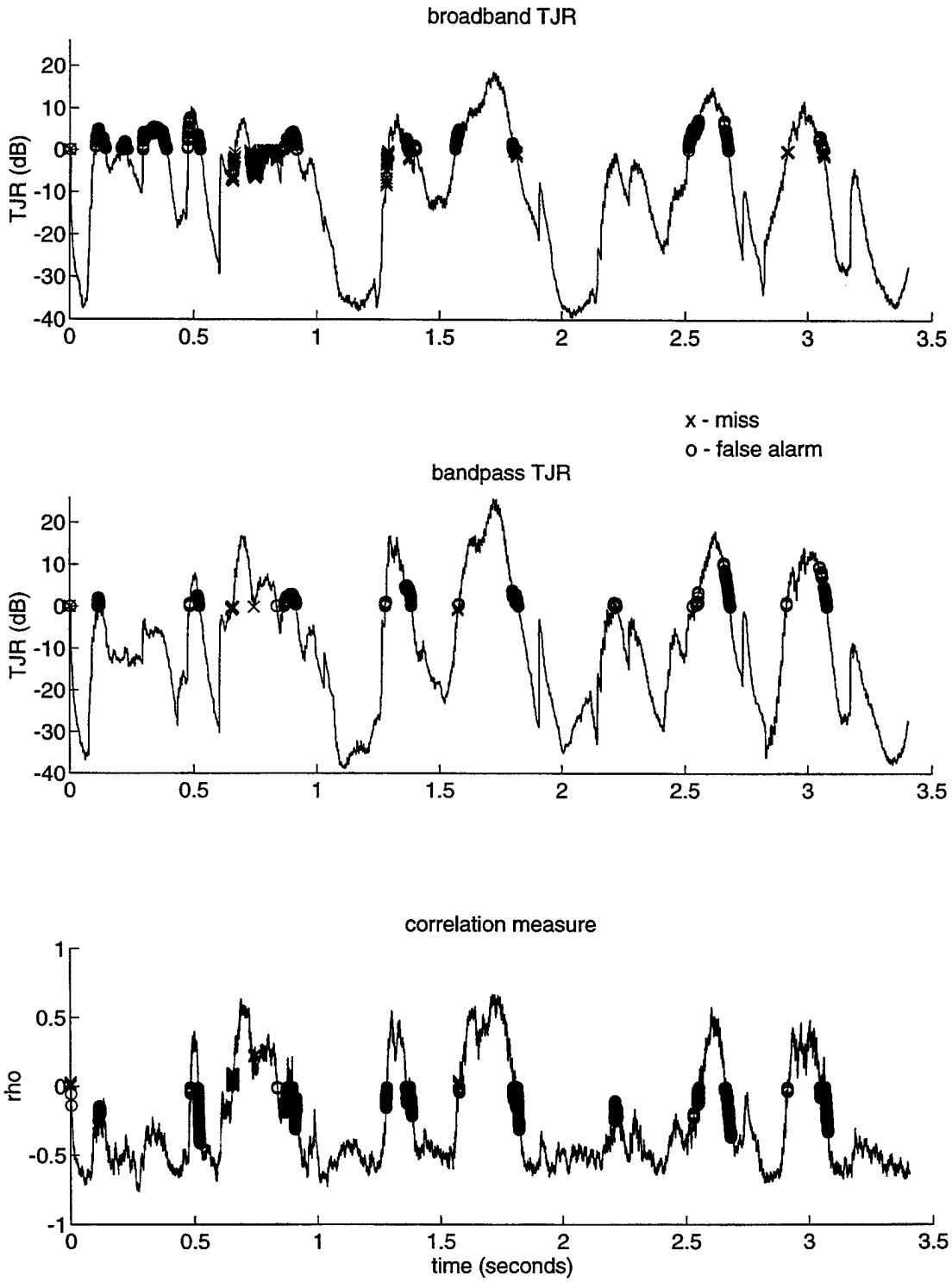

Figure 5-13: Simulation results showing true TJR, bandpass TJR, and correlation measure with locations of misses ('x') and false alarms ('o'), for speech and babble received by two microphones in an anechoic environment. The target and jammer angles are $\theta_t = 12°$ and $\theta_j = 90°$, with a fractional bandwidth of 0.67. The resulting detection and false alarm rates were $P_d = 0.95$ and $P_f = 0.30$ for the broadband TJR and $P_d = 0.99$ and $P_f = 0.15$ for the bandpass TJR.

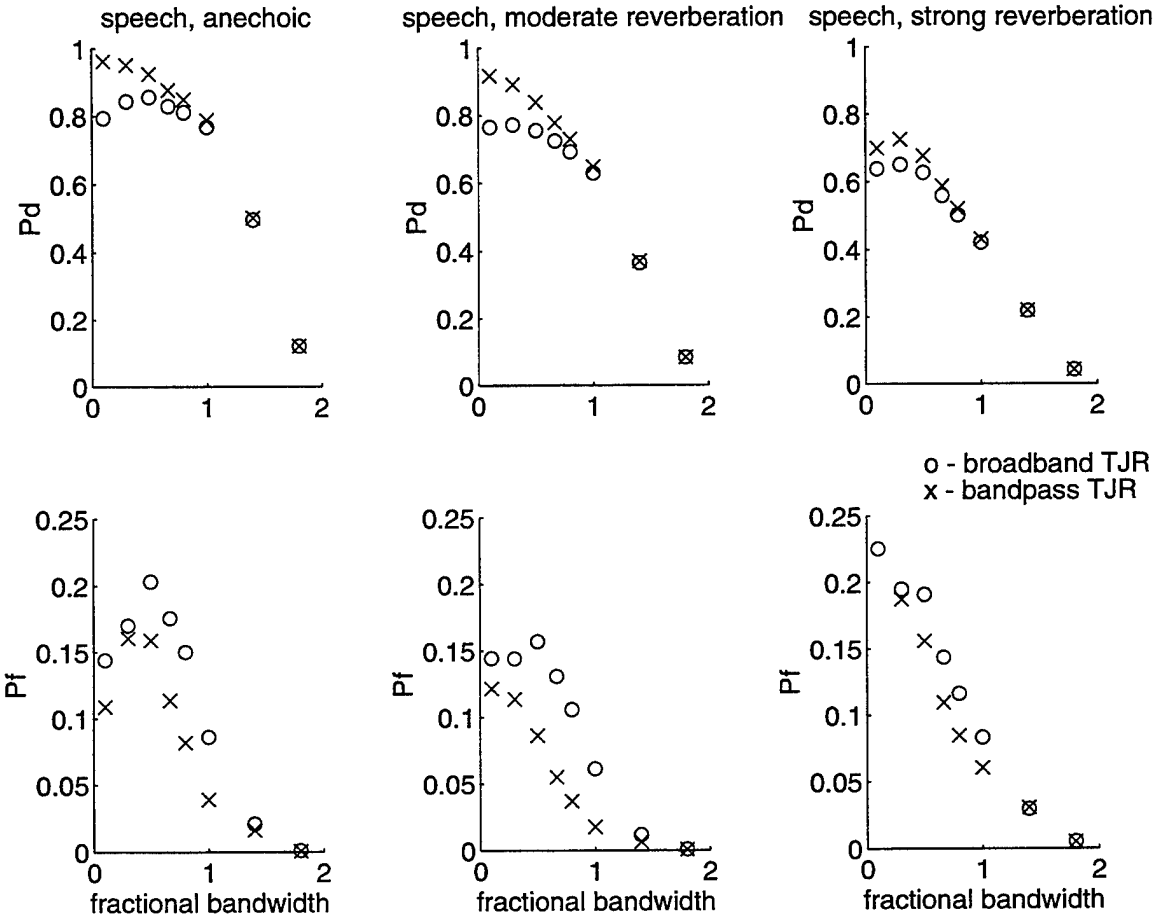

Figure 5-14: Simulation results showing rates of detection and false alarms, as a function of bandwidth, for speech and babble received by two microphones in anechoic and reverberant environments. The points labeled with 'x' indicate the performance referenced to the bandpass TJR, while the points labeled with 'o' indicate the performance referenced to the broadband TJR.

spacing (cm)	desired center frequency (Hz)	actual frequency band (Hz)
4	4313	3000–5000
8	2156	1700–3000
12	1438	1250–1700
16	1078	860–1250

Table 5.1: Frequency bands used with intermicrophone spacings obtained from a 16-cm, five-microphone array.

in the remainder of this work.

Five-microphone array

An M-microphone array has $\frac{M(M-1)}{2}$ possible pairs. If the array elements are evenly spaced, then those pairs represent $M-1$ distinct values of intermicrophone spacing. For a five-microphone array, there are 10 possible pairs with 4 distinct spacings. In contrast to the two-microphone case, obtaining adequate frequency coverage is not a problem because of the variety in microphone spacing. Instead, the issue is to determine the best method for combining the correlation measurements generated from different spacings and frequency bands.

The simulated five-microphone array was 16 cm long, with 4 cm spacing between microphones. The leftmost microphone was paired with each of the other four microphones to produce four smoothed correlation measures. The desired center frequency for each pair was determined according to (5.30). The actual cutoff frequencies were selected to provide bands roughly centered at the center frequencies without overlap between neighboring bands. The values used are given in Table 5.1.

The same processing used for the two-microphone array was applied to each pair of microphone signals to produce a smoothed correlation measure. Then those measures were combined using each of the three methods (voting, averaging, and power-weighted averaging) described in Sec. 5.2.3. The results obtained using those three methods were compared to the true broadband TJR to generate rates of detection and false alarms. For the voting method, ties were resolved by selecting H1 (saying

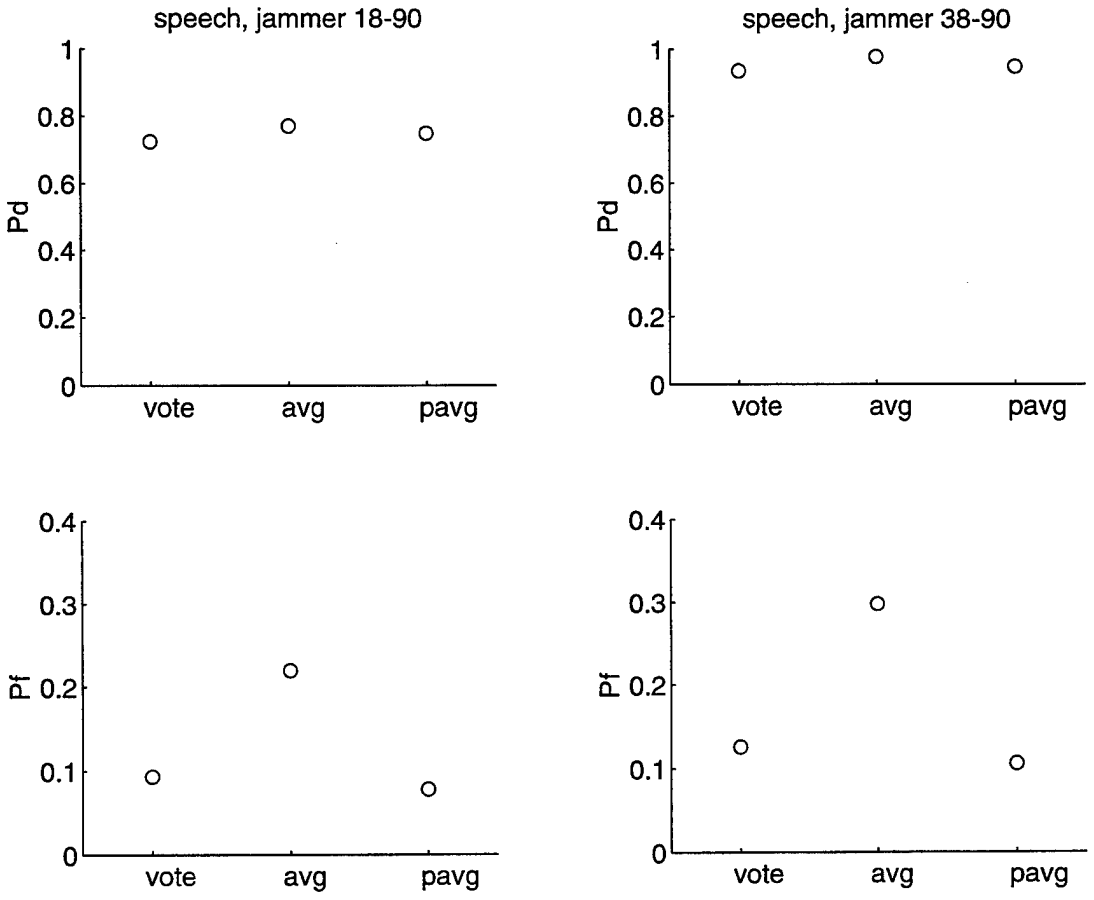

Figure 5-15: Simulation results showing rates of detection and false alarms for speech and babble received by five microphones in an anechoic environment. Results are shown for voting, averaging, and power-weighted-averaging methods described in the text, labeled *vote*, *avg*, and *pavg*, respectively.

TJR > 0 dB), resulting in lower rates of both detections and false alarms.

Figure 5.15 shows the results for the 5-microphone array in an anechoic environment. The values are averages of 76 pairs of target/jammer angles and three sentences. Comparing the three methods of combining correlation measures, the voting and power-weighted-averaging methods are comparable, while the averaging method has a relatively high rate of false alarms.

Comparing Fig. 5.15 to Fig. 5.12 reveals that in general, using four bands obtained from five microphones outperforms the one band obtained from two microphones. However, that improvement is modest compared to the more than four-fold increase

in computational requirements. Future investigations could quantify the incremental benefit obtained from each additional pair of microphones used to compute correlation measures. This would allow the system designer to select the number of microphone pairs and frequency bands needed for a particular application, trading relatively small reductions in performance for large reductions in computational complexity. For example, it is possible that combining correlation measures from two microphone pairs with appropriate spacing could provide performance comparable to that obtained with four microphone pairs shown in Fig. 5.15, at half the computational complexity.

Figure 5.16 shows results in reverberation for the same eight pairs of target and jammer angles considered for the two-microphone array. The performance of the five-microphone array in reverberation is consistent with the trends previously observed. The presence of reverberation reduces the detection rate, with no clear trends in the false alarm rate. Again, the voting and power-weighted-averaging methods are comparable, while the averaging method has a higher rate of false alarms. Although there appears to be a slight advantage to power-weighted averaging, it requires substantially more computation than the voting method. Therefore, the remainder of this work will use the voting method for combining multiple correlation measures.

5.4 Discussion

The purpose of this chapter is to investigate using quantities derived from the correlations between pairs of microphones as decision variables in a hypothesis test concerning the range of TJR. The proposed method was analyzed for narrowband signals with and without reverberation, and then implemented and evaluated in simulations with both noise and speech signals. Despite many violations of the assumptions used in the original analysis, the simulations show that the narrowband analysis provides useful insight to the more complicated case of broadband speech signals.

The analysis with narrowband signals revealed that the binary hypothesis test produces the best results when the relationship between microphone spacing and frequency is governed by $kd = \pi$. Furthermore, the uncertainties introduced by

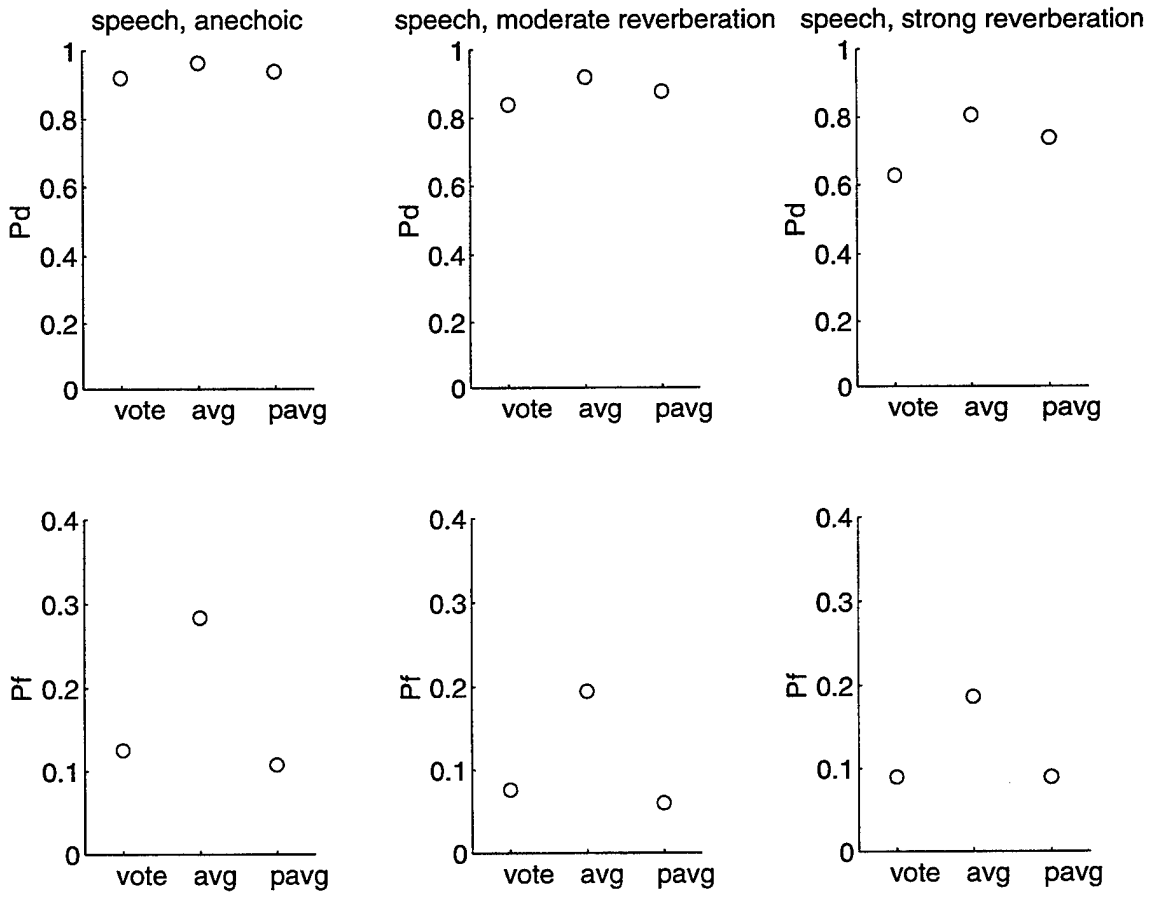

Figure 5-16: Simulation results showing rates of detection and false alarms for speech and babble received by five microphones in anechoic and reverberant environments. Results are shown for voting, averaging, and power-weighted-averaging methods described in the text, labeled *vote*, *avg*, and *pavg*, respectively.

varying levels of reverberation and the relative costs of the two types of errors indicates that a reasonable choice for the correlation threshold is $\rho_0 = 0$.

The simulations considered both two- and five-microphone arrays. For a two-microphone array, only one correlation measure can be computed. In this case, the conflicting demands of high detection rate and good frequency coverage are balanced by selecting an intermediate value such as 0.67 for the fractional bandwidth. For a five-microphone array, the multiple correlation measures from different frequency bands are best combined by using the voting method, so as to balance performance considerations with computational demand.

The approach proposed and evaluated in this chapter was based entirely on the correlation coefficient between microphone signals, that is, on the correlation with zero time lag. This was motivated by the need to develop a method with relatively low computational complexity. However, the overall approach analyzed and evaluated in this chapter could easily be extended to utilize values derived from the correlation function at nonzero lags.

Chapter 6

Effect of target reflections

6.1 Introduction

The LCMV beamformer assumes that the target direction is known and that the target and jammer signals are uncorrelated. As discussed in Sec. 2.3.2, target signal reflections violate one of these two assumptions. If the reflected target signal is considered target, then the assumption of known target direction is violated. On the other hand, if the reflected target is considered jammer, the assumption of uncorrelated target and jammer is violated. In either case, the result is that the reflections of the target signal arriving from directions other than that of the target source provide the beamformer with information that may be used to cancel the target signal.

The implications of a system that cancels reverberant target signals must be considered from the point of view of speech intelligibility. Clearly, if a system cancels the direct wave of the target signal, it will have a detrimental effect on intelligibility. However, if the system cancels reflections of the target signal, its effect is less obvious. In general, early reflections contribute to intelligibility while late reflections degrade intelligibility, where the distinction between early and late reflections is 50–95 ms after the direct wave (Cremer and Müller, 1982). Consequently, a system that cancels early target reflections would degrade intelligibility, while a system that cancels late target reflections would improve intelligibility. Unfortunately, within the structure of the generalized sidelobe canceller there is no way to distinguish between early and

late reflections.

Although the ultimate goal of this work is to improve intelligibility, which requires consideration of early and late target reflections, the work described in this chapter takes a simpler approach. This chapter considers the effect of target reflections on the performance of a two-microphone generalized sidelobe canceller, but the results also apply to adaptive noise cancellers and to systems with any number of microphones. The performance measures are the gain in powers of the direct and reflected target signals.

In order to determine the effects of several parameters on system performance, simple source-to-microphone impulse responses are created to account for a small number of reflections. In addition, system performance is examined for the simulated room impulse responses described in Sec. 3.2.

6.2 Background

Figure 6.1 shows a block diagram of the system considered in this chapter. It is based on a two-microphone version of the generalized sidelobe canceller shown in Fig. 2.4. Unlike that system, it does not include misadjustment or transient behavior due to the LMS algorithm. This is accomplished by replacing the adaptive filter weights by their optimal values. Furthermore, the environment differs in that no jammer source is present, because the target-only condition provides a worst-case assessment of target cancellation.

The target source, $t_s(n)$, is filtered by two source-to-microphone room impulse responses, $h_{t0}(n)$ and $h_{t1}(n)$. The two microphone signals are added and subtracted to produce the primary and reference signals, respectively. The primary signal is

$$z(n) = \frac{1}{2}(t_s(n) * (h_{t0}(n) + h_{t1}(n))) \tag{6.1}$$

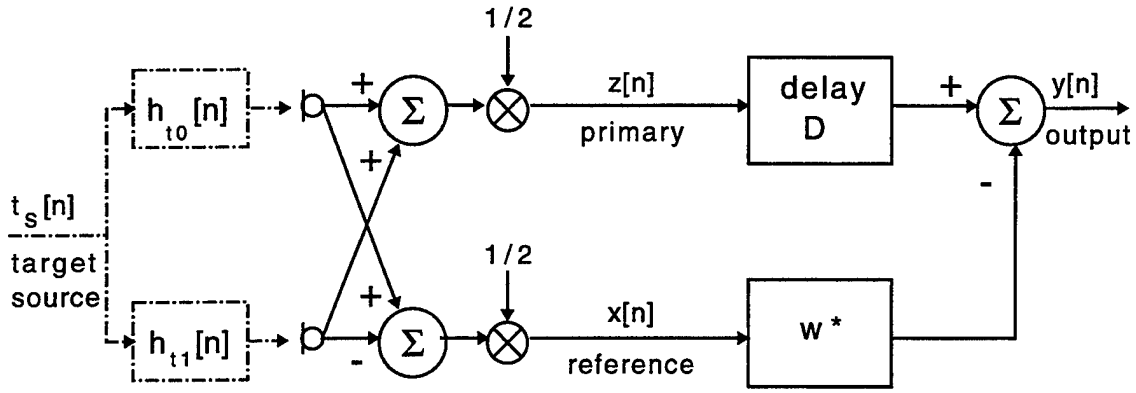

Figure 6-1: Block diagram of target-only system with optimal weights. The input is the target source, which is filtered by two source-to-microphone room impulse responses, $h_{t0}(n)$ and $h_{t1}(n)$. The two microphone signals are added and subtracted to produce the primary and reference signals, $z(n)$ and $x(n)$, respectively. The reference signal is filtered by the optimal weights, $\mathbf{w}^*$, determined according to (6.3) in the text. The result is subtracted from the primary signal, delayed by D samples, to produce the system output.

and the reference signal is

$$x(n) = \frac{1}{2}(t_s(n) * (h_{t0}(n) - h_{t1}(n))). \tag{6.2}$$

The reference signal is filtered by the optimal weights, which are determined according to (4.11),

$$\mathbf{w}^* = \mathbf{R}^{-1}\mathbf{p}, \tag{6.3}$$

where $\mathbf{R}$ is the autocorrelation matrix of the reference signal in the tapped delay line of the adaptive filter and $\mathbf{p}$ is the cross-correlation vector between the delayed primary signal and the reference signal in the tapped delay line. The filtered reference signal is subtracted from the primary signal, delayed by D samples, to produce the system output.

If the target source, $t_s(n)$ is stationary, zero-mean white noise, then the autocorrelation matrix, $\mathbf{R}$, and the cross-correlation vector, $\mathbf{p}$, can be determined from the impulse responses $h_{t0}(n)$ and $h_{t1}(n)$, the primary delay, D, and the filter length, L, after Zurek et al. (1990). This can be seen as follows. The autocorrelation matrix, $\mathbf{R}$,

is the $L \times L$ symmetric Toeplitz matrix with entries in the ith row and jth column given by

$$\mathbf{R}_{i,j} = r(i-j) \quad i = 1, \ldots, L \quad j = 1, \ldots, L, \tag{6.4}$$

where $r(k)$ is the autocorrelation function of the reference signal,

$$r(k) = E[x(n)x(n-k)]. \tag{6.5}$$

Similarly, the cross-correlation vector, $\mathbf{p}$, is the $L \times 1$ vector with the ith entry given by

$$\mathbf{p}_i = p(i-1-D) \quad i = 1, \ldots, L, \tag{6.6}$$

where $p(k)$ is the cross-correlation function between the primary and reference signals,

$$p(k) = E[z(n)x(n-k)]. \tag{6.7}$$

Substituting (6.1) and (6.2) into (6.5) and (6.7) and rearranging produces

$$\begin{aligned} r(k) &= \frac{1}{4}E[(t_s(n) * (h_{t0}(n) - h_{t1}(n)))(t_s(n) * (h_{t0}(n-k) - h_{t1}(n-k)))] \\ &= \frac{1}{4}r_t(k) * (h_{t0}(k) - h_{t1}(k)) * (h_{t0}(-k) - h_{t1}(-k)) \end{aligned} \tag{6.8}$$

and

$$\begin{aligned} p(k) &= \frac{1}{4}E[(t_s(n) * (h_{t0}(n) + h_{t1}(n)))(t_s(n) * (h_{t0}(n-k) - h_{t1}(n-k)))] \\ &= \frac{1}{4}r_t(k) * (h_{t0}(k) + h_{t1}(k)) * (h_{t0}(-k) - h_{t1}(-k)) \end{aligned} \tag{6.9}$$

where $r_t(k)$ is the autocorrelation function of the target source, that is,

$$r_t(k) = E[t_s(n)t_s(n-k)]. \tag{6.10}$$

If $t_s(n)$ is zero-mean white noise, then $r_t(k) = \delta(k)$ (the unit impulse), and the

functions $r(k)$ and $p(k)$ become

$$r(k) = \frac{1}{4}(h_{t0}(k) - h_{t1}(k)) * (h_{t0}(-k) - h_{t1}(-k)) \tag{6.11}$$

and

$$p(k) = \frac{1}{4}(h_{t0}(k) + h_{t1}(k)) * (h_{t0}(-k) - h_{t1}(-k)). \tag{6.12}$$

These expressions depend only on the source-to-microphone impulse responses, so, if the target source is zero-mean white noise, then the optimal weights, $\mathbf{w}^*$, can be computed from $h_{t0}(n)$, $h_{t1}(n)$, L, and D using (6.3), (6.4), (6.6), (6.11) and (6.12).

Assuming the source-to-microphone impulse responses $h_{t0}(n)$ and $h_{t1}(n)$ consist of a direct wave that is equal in the two microphones, and reflections that differ in the two microphones, their difference, $h_{t0}(n) - h_{t1}(n)$, depends only on the reflections. Examining (6.11) and (6.12) reveals that the autocorrelation function $r(k)$ consists only of terms related to the reflections, while the cross-correlation function $p(k)$ consists of terms related to both the direct wave and the reflections. The cross-correlation function $p(k)$ can be considered the sum of two components, the terms due only to the reflections, and those due to the direct wave and reflections.[1] Since the cross-correlation vector $\mathbf{p}$ consists only of the terms of $p(i - 1 - D)$ for $i = 1, \ldots, L$, the choice of D determines whether or not the terms of $p(k)$ including information about the direct wave are included in the optimal weights, $\mathbf{w}^*$.

In particular, examining (6.6) and (6.12) reveals that if no reflections occur within D samples of the direct wave, then $\mathbf{p}$, and consequently $\mathbf{w}^*$, depend only on the reflections. This has important implications for the performance of the system in the presence of target reflections. If D is less than the interval between the direct wave and the first reflection, the optimal weights will be the same as if no direct wave were present, and *no cancellation of the direct wave can occur*, despite the fact that the target reflections violate one of the two basic assumptions of LCMV beamformers. This is an extension of the observation that target cancellation due to target reflections can be avoided by setting $D = 0$ (Hoffman et al., 1994).

[1] Examples of this decomposition are given in Sec. 6.5.2.

The analysis leading to the important result in the previous paragraph was based on two assumptions, that the direct wave is equal in the two microphones and that the source is zero-mean white noise. Violation of the first assumption subjects the direct wave to cancellation due to misalignment, which is a problem regardless of the level of reverberation and supercedes the problem of cancellation due to reflections. (Making adaptive arrays robust to misalignment was a major motivation behind the modifications proposed in Chs. 4 and 5.) Violation of the second assumption complicates the analysis because the optimal weights, $\mathbf{w}^*$, cannot be determined solely from the source-to-microphone impulse responses and the parameters L and D. In this case, the optimal weights will also depend on the autocorrelation of the source signal, as indicated in (6.8) and (6.9). When the target signal is voiced speech (which is correlated for short lags), the above result must be modified to state that no significant cancellation of the direct wave can occur when D is less than the sum of two quantities — the interval between the direct wave and the first reflection and the maximum lag for which the source exhibits substantial correlation.

6.3 Methods

In order to study the effect of target signal reflections, several source-to-microphone room impulse responses are used. Two simple types of impulse responses are a direct wave with a single reflection and a direct wave with two reflections. In both cases, the direct wave is aligned in time and of equal amplitude in the two microphones, simulating a perfectly aligned array.

The single-reflection impulse responses consist of a direct wave of unit amplitude followed by a single reflection arriving at the microphones with a relative delay of one sample. The purpose of the relative delay is to make the reflection appear to arrive from a direction other than straight ahead.[2] This is similar to the simple case analyzed by Lu and Clarkson (1993) for an adaptive noise canceller. This case is

[2] A relative delay of one sample makes the reflection appear to arrive from the azimuthal angle $\theta = \arcsin(\frac{cT_s}{d})$, where c is the speed of sound, T_s is the sampling period, and d is the spacing between microphones.

described by the equations

$$h_{t0}(n) = \delta(n) + a\delta(n - d_1 - 1) \tag{6.13}$$

$$h_{t1}(n) = \delta(n) + a\delta(n - d_1). \tag{6.14}$$

An example of single-reflection impulse responses is illustrated in Fig. 6.2(a) for $d_1 = 50$ and $a = 0.2$.

The two-reflection impulse responses consist of a direct wave of unit amplitude followed by two reflections of the same amplitude but with different relative delays. This case is described by the equations

$$h_{t0}(n) = \delta(n) + a\delta(n - d_1 - 1) + a\delta(n - d_2 + 2) \tag{6.15}$$

$$h_{t1}(n) = \delta(n) + a\delta(n - d_1) + a\delta(n - d_2). \tag{6.16}$$

An example of two-reflection impulse responses is illustrated in Fig. 6.2(b) for $d_1 = 50$, $d_2 = 70$ and $a = 0.2$.

In addition to the simple impulse response described above, two additional pairs of impulse responses were studied. These impulse responses represent moderately reverberant and strongly reverberant rooms and are shown in Figs. 6.2(c) and 6.2(d). They were generated by the room simulation as described in Sec. 3.2.

For each pair of source-to-microphone impulse responses, the source-to-system-output impulse response was computed for the system shown in Fig. 6.1. The filter length was $L = 1000$ and the primary delay varied from $D = 0$ to $D = 990$ for each condition. The target source was assumed to be stationary zero-mean white noise. $\mathbf{R}$ and $\mathbf{p}$ were determined from (6.4), (6.6), (6.11) and (6.12), and the optimal weights were computed according to (6.3) using the Levinson algorithm (Golub and van Loan, 1983).

To assess the performance of the system for each condition, the source-to-system-output impulse response was compared to the source-to-primary impulse response. For each of these impulse responses the powers of the direct and reflected portions of

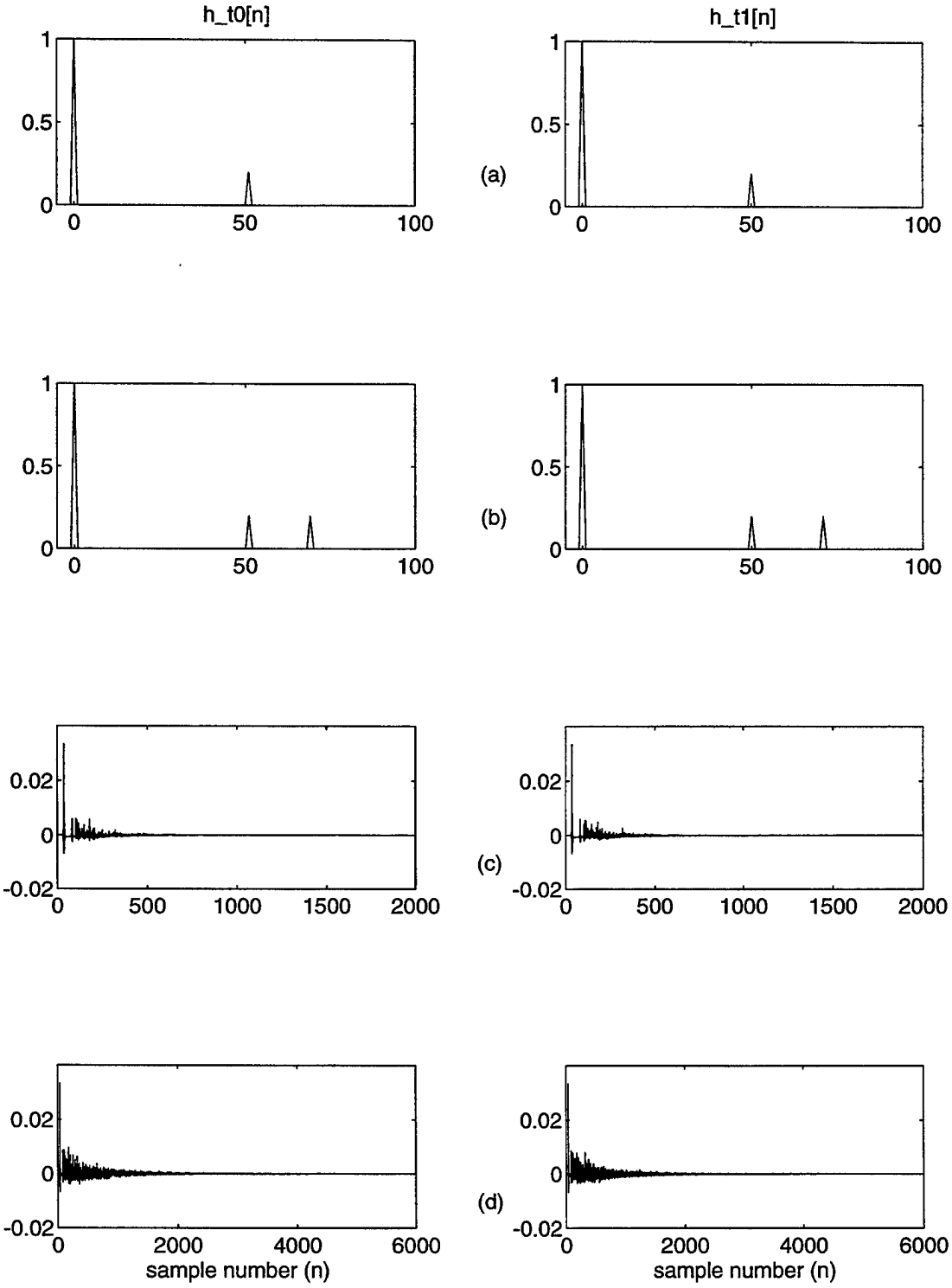

Figure 6-2: Examples of source-to-microphone impulse responses described in the text. (a) Single-reflection impulse responses described by (6.13) and (6.14), (b) two-reflection impulse responses described by (6.15) and (6.16), (c) simulated room impulse responses described in Sec. 3.2 with wall absorption of 0.6 (moderate reverberation), and (d) simulated room impulse responses described in Sec. 3.2 with wall absorption of 0.2 (strong reverberation).

the impulse response were calculated. The direct power was based on the power in the five samples of the impulse response surrounding the known index of the direct wave, while the reflected power was calculated based on the power in the remainder of the impulse response. The gain in direct wave power due to the system is computed from the ratio of direct wave power in the system output to direct wave power in the primary channel. This quantity is 0 dB when no direct wave cancellation occurs and negative when cancellation of the direct wave occurs. The gain in reflected power due to the system is calculated in a similar fashion, and negative values of the gain indicate attenuation of the target reflections.[3] These measures, based on the powers in segments of the impulse responses, differ from $\Delta\Gamma(T_d)$ and $\Delta\Gamma(T_r)$ defined in Sec. 3.3 and, unlike those measures, provide an accurate indication of the effect of the system even when the output includes cancellation of direct target based on target reflections.

6.4 Results

Figures 6.3 and 6.4 show the gains in direct and reflected powers for the four pairs of impulse responses. The solid lines in the left half of Fig. 6.3 show the gains in direct and reflected target powers, as a function of primary delay D, for the case of a single reflection described by (6.13) and (6.14) with $a = 0.2$ and $d_1 = 50$. As expected from the analysis in Sec. 6.2, when $D < d_1$ the direct wave is preserved and the system provides substantial cancellation of the reflection. When $D \geq d_1$, the system cancels both the direct wave and the reflection. The cancellation of the reflection is reduced because the system minimizes the total output power, and since the direct wave contributes more to the total output power, that quantity is minimized by providing more cancellation of the direct wave and less cancellation of the reflection. Except for the large change that occurs at $D = d_1$, the system performance is independent of D.

The solid lines in the right half of Fig. 6.3 show the gains in direct and reflected

[3]Note that these gains are based on a different reference than in the remainder of this work, where the gain is relative to a single microphone signal. Here the gain is relative to the primary signal, so that it does not include attenuation of reflections due to averaging the microphone signals.

target powers, as a function of primary delay D, for the case of two reflections described by (6.15) and (6.16) with $a = 0.2$, $d_1 = 50$ and $d_2 = 70$. As expected, when $D < d_1$ the direct wave is preserved, and when $D \geq d_1$, both the direct wave and the reflections are cancelled to some degree. Unlike the case of a single reflection, the degree of cancellation varies with D, in addition to the large change that occurs at $D = d_1$. The cause of these variations will be investigated in Sec. 6.5.2.

Figure 6.4 shows the gain in direct and reflected target powers, as a function of primary delay D, for the simulated room impulse responses shown in Figs. 6.2(c) and 6.2(d). The general trends in these results are similar to those seen in Fig. 6.3 with the simple room impulse responses. For both pairs of impulse responses, the first reflection occurs 46 samples after the direct wave, but it is aligned in time at the two microphones. The second reflection occurs 66 samples after the direct wave, and is not aligned at the two microphones. As expected, when $D < 66$ the direct wave is preserved and only the reflections are cancelled. When $D \geq 66$ both the direct wave and the reflections are cancelled.

The dotted lines in Figs. 6.3 and 6.4 show the effect of the system on the reflections *in the absence of the direct wave.* Because the reflections are signals arriving at the array from off-axis directions, the ability of the system to cancel target reflections is also indicative of its ability to cancel off-axis jammers. The dotted lines in Figs. 6.3 and 6.4 show that maximum cancellation of off-axis sources is obtained for a broad range of values of $D > 0$. Overall, the results shown in Figs. 6.3 and 6.4 show that there is a clear advantage to using values of D substantially greater than zero, but less than the delay to the first reflection.

Figure 6.5 shows the source-to-delayed-primary and source-to-system-output impulse responses for the simulated room with strong reverberation (Fig. 6.2(d)), for $D = 50$ and for $D = 500$. Clearly, for $D = 50$ the direct wave is preserved, and some reflections are noticeably attenuated. For $D = 500$, both the direct wave and the reflections are attenuated.

In order to investigate the variations in performance that occur with changes in the direct-to-reverberant ratio, modified source-to-microphone impulse responses were

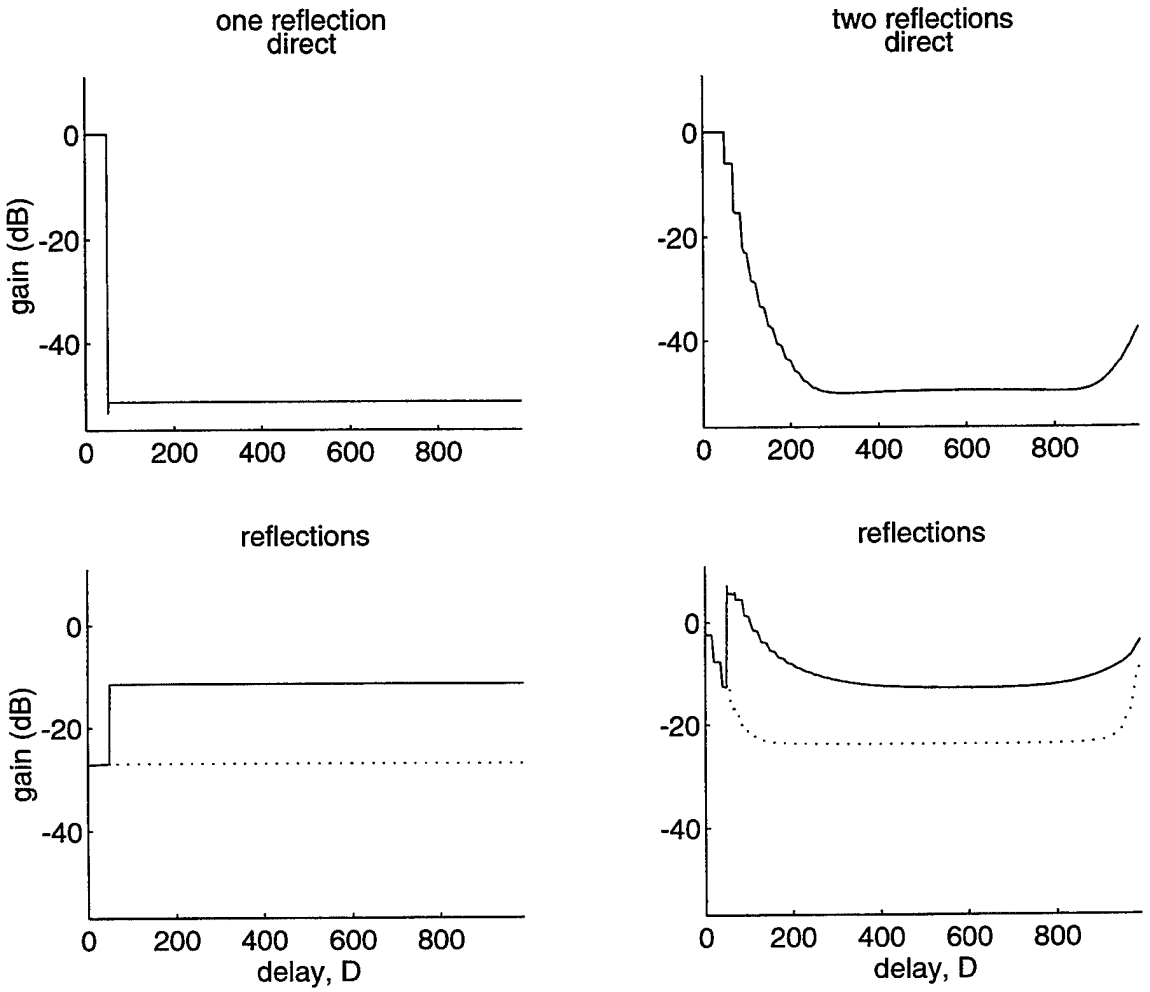

Figure 6-3: Gain of direct target and target reflections as a function of primary delay for impulse responses with a single-reflection (left) and with two reflections (right). Solid lines indicate results when both the direct and reflected components are present; dotted lines indicate results for reflected components alone.

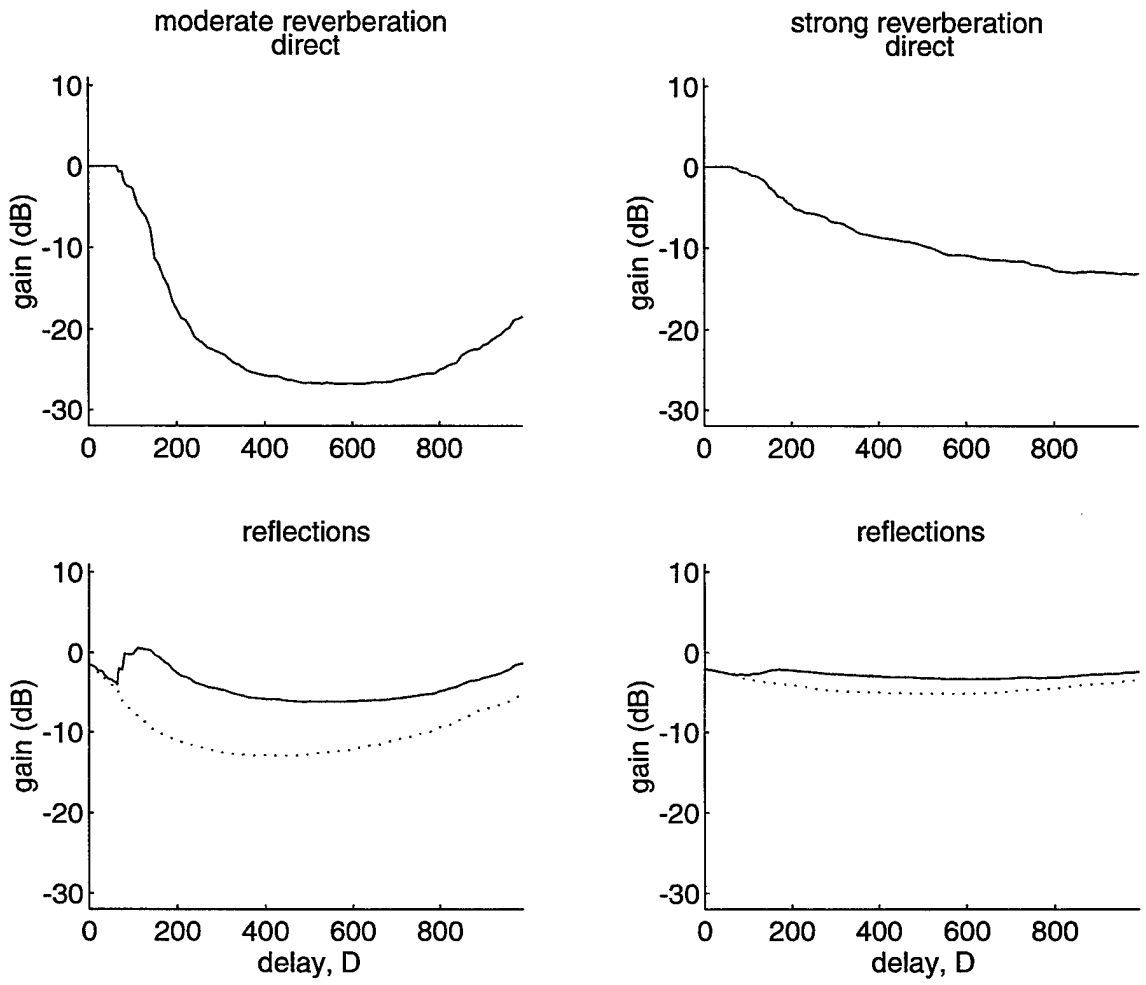

Figure 6-4: Gain of direct target and target reflections as a function of primary delay for simulated room impulse responses with moderate (left) and strong (right) reverberation. Solid lines indicate results when both the direct and reflected components are present; dotted lines indicate results for reflected components alone.

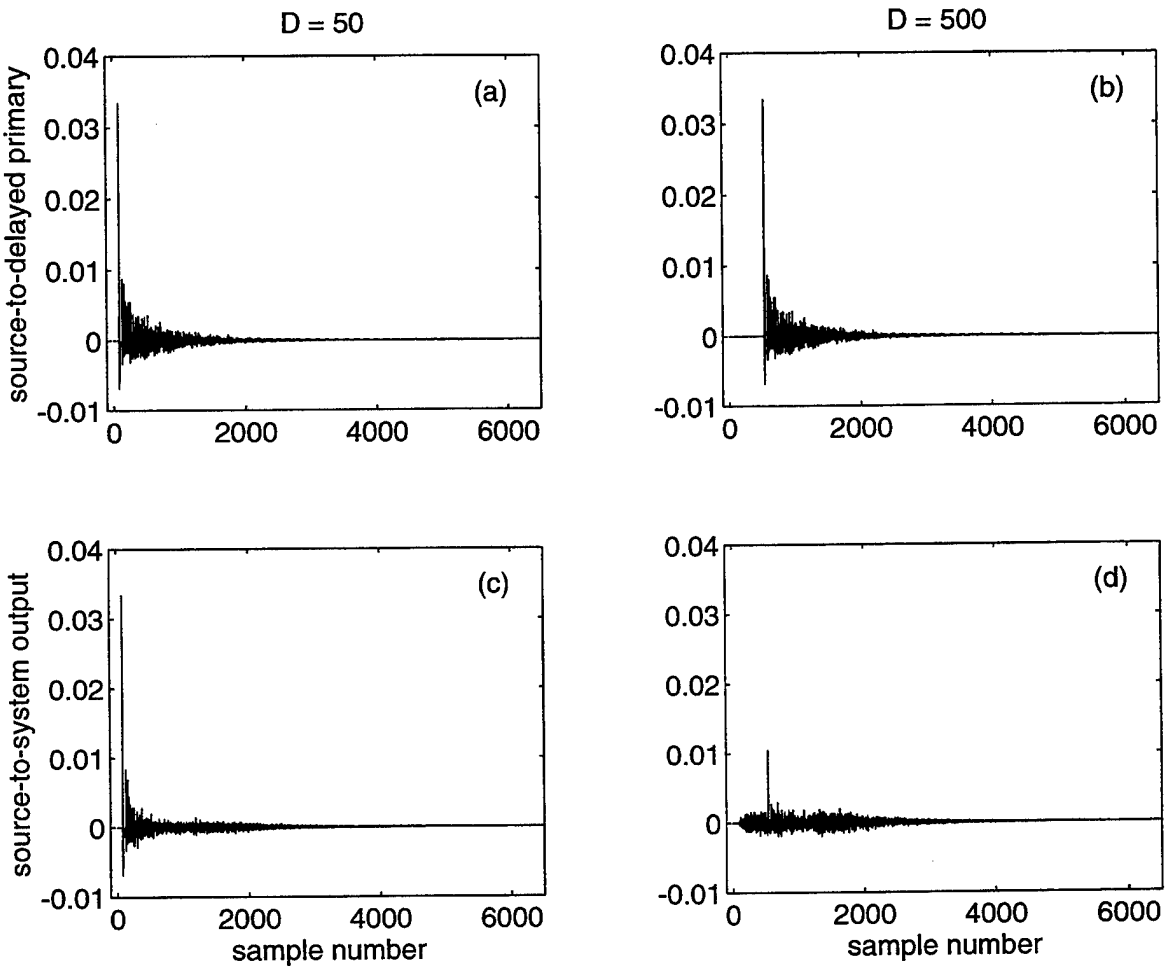

Figure 6-5: Source-to-delayed primary impulse responses for simulated room impulse responses with moderate reverberation for primary delays of (a) $D = 50$ and (b) $D = 500$. Source-to-system output impulse responses for simulated room impulse responses with strong reverberation for primary delays of (c) $D = 50$ and (d) $D = 500$.

developed based on the simulated impulse responses of the moderately reverberant room (Fig. 6.2(c)). Those impulse responses were separated into components consisting of either the direct wave or the reflections, and the direct-wave component was scaled before recombining with the reflections to produce impulse responses with the same structure, but different direct-to-reverberant ratios. Figure 6.6 shows the gain in direct and reflected target powers for these modified pairs of impulse responses. Because the optimal weights are selected to minimize the total output power, the results show relatively more cancellation of the stronger component, that is, more cancellation of reflections at the lower direct-to-reverberant ratio (dotted lines) and more cancellation of the direct wave at a high direct-to-reverberant ratio (solid lines). At the high direct-to-reverberant ratio, for some values of D, the system's attempt to minimize the stronger direct component results in amplification of the reflections (gain greater than 0 dB).

In addition to the results shown here, the gain in direct and reflected powers was computed for other impulse responses and for the addition of uncorrelated sensor noise in the two microphone signals. The general trends observed under a variety of conditions were similar to the results shown above.

6.5 Discussion

6.5.1 Summary

The results of the previous section suggest that a simple solution to the problem presented by reverberant target is to set the primary delay to zero, as suggested by Hoffman et al. (1994). However, the results also show that, in general, the cancellation of target reflections (and therefore cancellation of jammer signals) improves with increasing D. This improvement is because nonzero primary delays permit non-causal responses on the part of the adaptive filter, which was the initial motivation for including a primary channel delay (Widrow and Stearns, 1985). As a result, it is advisable to use a primary delay that is nonzero, but relatively small.

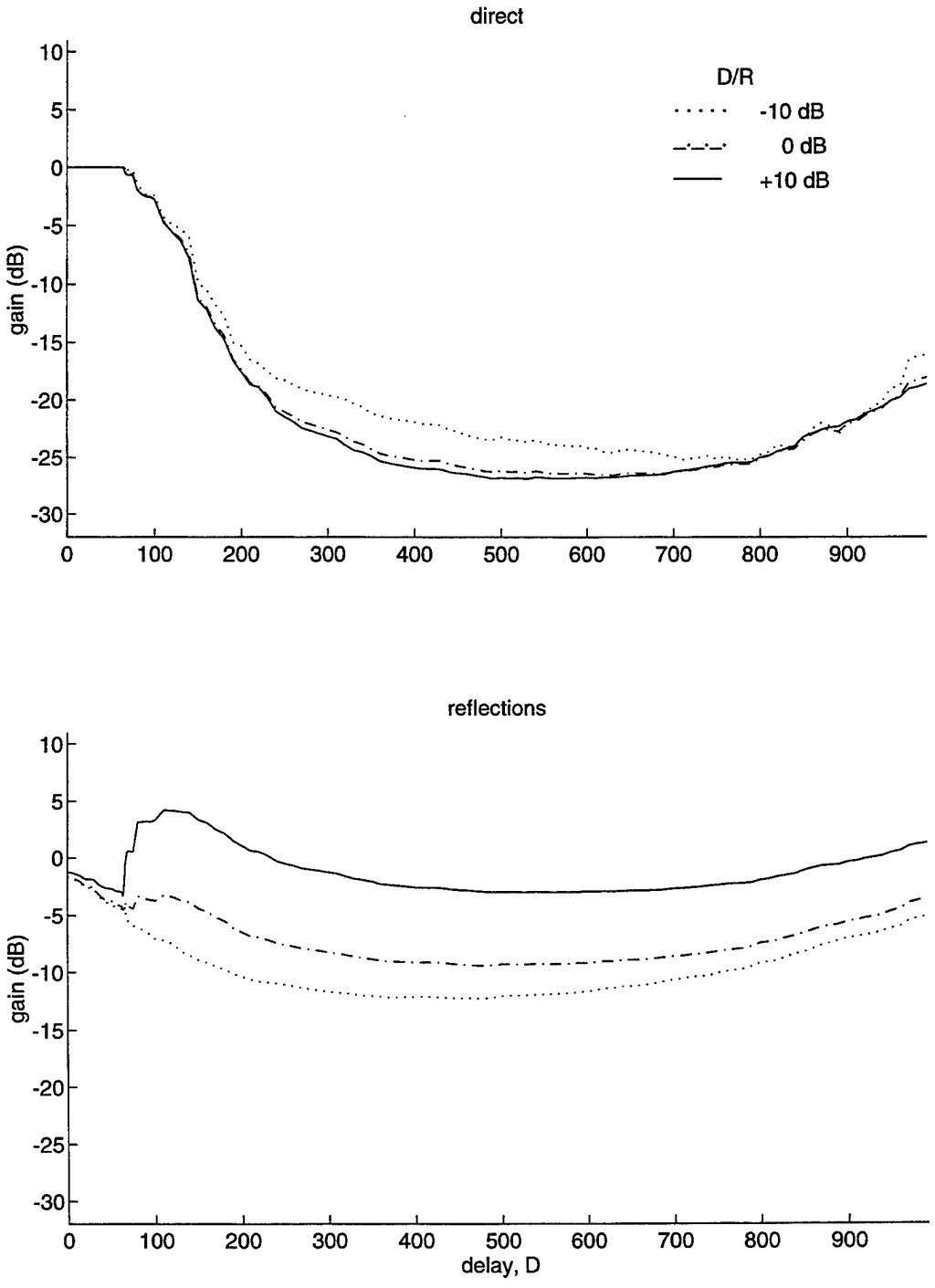

Figure 6-6: Gain of direct target and target reflections as a function of primary delay for modified impulse responses with direct-to-reverberant ratios of -10, 0, and $+10$ dB.

Ideally, the primary delay should always be less than the number of samples between the direct wave and the first reflection. However, since these systems must operate in a variety of acoustic environments, it is likely that, if D is nonzero, on some occasions early reflections will arrive at the array within D samples of the direct wave. Fortunately, when there are multiple reflections, the system is robust to some reflections within D samples of the direct wave. This robustness exists provided that there are additional reflections that arrive more that D samples within the direct wave. For example, there is relatively little cancellation of the direct wave in Fig. 6.4 for $66 \leq D \leq 120$. Those figures illustrate the worst case scenario for target cancellation, because no jammer signal is present and the filter weights are optimum.

Since the simulated room impulse responses have a 10 kHz sampling rate, reflections arriving at the microphones 50 – 66 samples after the direct wave corresponds to delays of 5.0 – 6.6 ms, or distances of roughly 2 meters at the speed of sound. Although earlier reflections can be expected in real rooms with furnishings, they will be few relative to the total reflections, and are not expected to change the general trends seen in Fig. 6.4.

Kompis and Dillier (1991) empirically optimized the delay, D, where the optimal parameter value was defined as that which provided the largest gain in TJR. They varied D for a single target/jammer configuration with various filter lengths in several reverberant rooms. They conclude that for $L < 128$, the value of the D has no great influence on performance, while for $L \geq 512$ the 'optimal' delay is 25–50% of the filter length. For the rooms that they studied, the time between the direct wave and first reflection is not known. However, their results are consistent with the current analysis. For relatively short filters, the delay does not matter because no reflections arrive within L samples of the direct wave. For relatively long filters, their suggested range of $\frac{L}{4} < D < \frac{L}{2}$ presumably results from the tradeoff between two factors that improve performance: relatively short D minimizes the number of reflections arriving within D samples of the direct wave and $D = \frac{L}{2}$ centers the non-causal impulse response.

Finally, to characterize the robustness of the system to some reflections within D

samples of the direct wave, it might be useful to quantify the relationship between the degree of direct wave cancellation and some measure of the reflections occurring within D samples of the direct wave and more than D samples after the direct wave. However, the following analysis shows that for room impulse responses with more than one reflection, other factors influence the relationship between D and system performance, and the performance cannot be explained solely on the basis of the reflections arriving within D samples of the direct wave.

6.5.2 Analysis

The lack of direct wave cancellation when D is less than the time between the direct wave and the first reflection was predicted in Sec. 6.2 and demonstrated in Sec. 6.4. Here, that result is analyzed for the cases of one and two reflections described in Sec. 6.3.

First, it will be useful to define some additional quantities. In Sec. 6.2, it was shown that if the direct wave is perfectly aligned in the two channels, the auto-correlation function $r(k)$, and consequently $\mathbf{R}$, consist only of terms related to the reflections, while the cross-correlation function $p(k)$ and vector $\mathbf{p}$ consists of terms related to both the direct wave and the reflections. It will be useful to decompose the function $p(k)$ into a component that depends only on the reflections ($p1(k)$) and a component that depends on both the direct wave and the reflections ($p2(k)$) by defining

$$p(k) = p1(k) + p2(k). \tag{6.17}$$

Then

$$\mathbf{p} = \mathbf{p1} + \mathbf{p2}, \tag{6.18}$$

where $\mathbf{p1}$ and $\mathbf{p2}$ are $L \times 1$ dimensional vectors based on $p1(k)$ and $p2(k)$ as in (6.6). Using (6.3), the optimal weights also consist of two components, that is,

$$\mathbf{w}^* = \mathbf{R}^{-1}\mathbf{p} = \mathbf{R}^{-1}\mathbf{p1} + \mathbf{R}^{-1}\mathbf{p2} = \mathbf{w}_1^* + \mathbf{w}_2^*, \tag{6.19}$$

where the weight vector $\mathbf{w}_1^*$ is only based on the reflections. In fact, the vector $\mathbf{w}_1^*$ is equivalent to the weights that would result if the direct wave were absent and the source-to-microphone impulse responses consisted solely of off-axis reflections.

In addition to the fact that $\mathbf{R}$ depends only on the reflections, the matrix $\mathbf{R}$ determined according to (6.4) and (6.11) does not depend on the primary delay, D. On the other hand, the cross-correlation vector, $\mathbf{p}$, determined according to (6.6) and (6.12) does depends on the direct wave and D.

For the case of a single reflection, substituting (6.13) and (6.14) into (6.12) gives

$$\begin{aligned} p(k) &= \frac{1}{4}(2\delta(k) + a\delta(k-d_1-1) + a\delta(k-d_1)) \\ &\qquad *(a\delta(k+d_1+1) - a\delta(k+d_1)) \\ &= \frac{a}{4}(2\delta(k+d_1+1) - 2\delta(k+d_1) + a\delta(k+1) - a\delta(k-1)), \end{aligned} \tag{6.20}$$

which can be separated into the two terms

$$p1(k) = \frac{a^2}{4}(\delta(k+1) - \delta(k-1)) \tag{6.21}$$

and

$$p2(k) = \frac{a}{2}(\delta(k+d_1+1) - \delta(k+d_1)). \tag{6.22}$$

For any value of D in the range $0 < D < L-1$, $\mathbf{p1}$ has two nonzero entries that occur in positions D and $D+2$. If $0 < D < d_1$, then $\mathbf{p2} = 0$ and $\mathbf{w}^* = \mathbf{w}_1^*$ (the optimal weights for cancelling reflections alone). If $D \geq d_1$, then $\mathbf{p2}$ is nonzero, and the resulting weights depend on (and cancel) both the direct wave and the reflections.

Therefore, for the case of a single reflection, the dependence of performance on the primary delay D observed in the left half of Fig. 6.3 is completely explained by whether or not a particular value of D results in a cross-correlation vector $\mathbf{p}$ that includes nonzero elements of $p2(k)$, which contain information about the correlation between the direct wave and the reflections. However, this result does not generalize to the case of two or more reflections, as shown below.

For the case of two reflections, separating the direct wave from the reflections and

substituting (6.15) and (6.16) into (6.12) gives

$$\begin{aligned} p1(k) &= \frac{a^2}{4}(-\delta(k+d_2-d_1)-\delta(k+d_2-d_1-1) \\ &\quad +\delta(k+d_2-d_1-2)+\delta(k+d_2-d_1-3) \\ &\quad -\delta(n+2)+\delta(n+1)-\delta(n-1)+\delta(n-2) \\ &\quad +\delta(k-d_2+d_1+3)-\delta(k-d_2+d_1+2) \\ &\quad +\delta(k-d_2+d_1+1)-\delta(k-d_2+d_1)) \end{aligned} \tag{6.23}$$

and

$$p2(k) = \frac{a}{2}(-\delta(k+d_2)+\delta(k+d_2-2)+\delta(k+d_1+1)-\delta(k+d_1)) \tag{6.24}$$

The twelve terms in (6.23) are clustered into three groups of four impulses. For any value of D in the range $1 < D < L - d_2 + d_1 - 1$, **p1** has at least eight nonzero entries, corresponding to the last eight terms in (6.23). If $D \geq d_2 - d_1$, then all twelve terms of (6.23) occur as nonzero entries in **p1**. Therefore, it is expected that the system will show a change in the performance near $D = d_2 - d_1$.[4]

The four terms in (6.24) comprise two groups of two impulses. If $0 < D < d_1$, then $\mathbf{p2} = 0$ and $\mathbf{w}^* = \mathbf{w}_1^*$ (the optimal weights for cancelling reflections alone). If $d_1 < D < d_2$, then **p2** contains two nonzero terms, and the resulting weights depend on (and cancel) both the direct wave and the reflections. If $D > d_2 + 1$, then **p2** contains four nonzero terms, and the resulting weights will cancel the direct wave more effectively than in the previous case.

For the case of $d_1 = 50$ and $d_2 = 70$, the above analysis predicts an improvement in cancellation of reflections near $D = d_2 - d_1 = 20$, no direct cancellation for $D < 50$, some direct wave cancellation when $50 < D < 70$, and increased direct wave cancellation when $D > 70$. The performance observed in the right half of Fig. 6.3 is

[4]When $d_2 - d_1 - 3 \leq D < d_2 - d_1$, **p1** has between nine and eleven nonzero entries. For simplicity, when impulsive terms of cross-correlation functions occur in clusters, the details of such transitions will be ignored. Hence the change in performance is expected *near*, but not exactly at, $D = d_2 - d_1$.

in accordance with these predictions.

However, the right half of Fig. 6.3 shows that there are additional changes in performance of magnitude similar to those predicted by the analysis, occurring at $D = 40$ and at intervals of 20 starting with $D = 90$. This dependence of performance on D cannot be attributed to the inclusion of additional terms in **p1** and **p2**. Rather, it is due to the fact that varying D affects the position of the nonzero entries in **p1** and **p2**, which determines which columns of the matrix $\mathbf{R}^{-1}$ are used to produce the filter weights. The structure of $\mathbf{R}^{-1}$ depends only on the reflections, and the filter length L, not on the direct wave or the primary delay D.

Therefore, this section concludes with the observation that, although the presence or absence of direct target cancellation can be predicted based on the presence or absence of reflections within D samples of the direct wave, it is not possible to predict other general variations in performance with D when multiple reflections exist.

6.6 Conclusion

The effect of reflections of the desired target source on the performance of a two-microphone generalized sidelobe canceller was studied. Simple source-to-microphone impulse responses were created to account for a small number of reflections. In addition, performance was studied using the simulated room impulse responses described in Sec. 3.2.

The results show that the primary channel delay, D, has a large impact on the system's ability to cancel the direct target based on target reflections. Direct target cancellation is eliminated entirely when the primary delay is shorter than the interval between the arrival of the direct wave and the arrival of the first reflection at the microphone array. Direct target cancellation due to target reflections is most pronounced when there are a small number of reflections and those reflections arrive at the array within the time window determined by the primary delay. Direct target cancellation is less severe when there are a large number of reflections and only a small fraction of the reflections arrive within the time window determined by the

primary delay, and other benefits derived from using nonzero values of the primary delay suggest that it is advisable to use a primary delay that is nonzero, but relatively small.

An attempt was made to quantify the robustness of the system when a small fraction of the total number of reflections occur within D samples of the direct wave. However, when more than one reflection exists, the relationship between system performance and primary delay depends on the structure of the inverse of the autocorrelation matrix, and the system performance cannot be explained solely on the basis of the reflections arriving within D samples of the direct wave.

Chapter 7

Simulation Results

7.1 Introduction

The purpose of this chapter is to evaluate adaptive-array hearing aids in a variety of acoustic environments. The systems considered are based on the generalized sidelobe canceller proposed by Griffiths and Jim, described in Sec. 2.1. These systems are implemented in computer simulations and evaluated using G_I, the physical measure of intelligibility-weighted gain described in Sec. 3.3.

The results of these simulations will provide answers to the following questions:

1. Are the modifications suggested in Chs. 4 and 5 effective against the problems of misadjustment and misalignment when integrated into a complete system?

2. What level of performance can be expected with practical systems in a variety of acoustic environments?

3. How is performance in various environments affected by design parameters such as filter length and number of microphones?

7.2 Processing

The first step required for the computer simulations is to generate signals received by the microphone arrays for processing by the systems under consideration. This

was accomplished by convolving the source materials described in Sec. 3.1 (IEEE sentences and SPIN babble sampled at 10 kHz) with the source-to-microphone impulse responses described in Sec. 3.2. To simulate perfectly aligned arrays, the target source was located at 0° and the jammer source was at 45° azimuth.[1] To simulate misaligned arrays, the target source was located at 10° and the jammer source was at 55° azimuth. Two configurations were simulated, a 7-cm array of two omnidirectional microphones and a 16-cm array of five omnidirectional microphones, as described in Sec. 3.2. Three levels of wall absorption were used to generate one anechoic and two reverberant conditions. The two reverberant conditions had direct-to-reverberant ratios of +6 dB and −2 dB, and will be referred to as moderate and strong reverberation, respectively. The relative level of the target and jammer sources was varied to produce three target-to-jammer ratios of −20, 0, and +20 dB.

These signals were processed by two- and five-microphone adaptive systems using yoked processors (Sec. 3.3) to determine the effect of the system on each of three signal components: the jammer, the direct target, and the target reflections. The algorithms evaluated included four combinations of processing options based on modifications suggested in Chs. 4 and 5, so that each condition was tested with the sum method of normalizing the step-size parameter, with the correlation method of controlling adaptation, with both of these modifications, and with neither modification. Based on the results of Ch. 6, the primary delay was set to $D = 50$. Two adaptive filter lengths were considered, $L = 100$ and $L = 1000$, corresponding to 10 ms and 100 ms at the 10 kHz sampling rate.

Figure 7.1 shows a block diagram of the complete system with both modifications. The sum method, described and analyzed in Ch. 4, consists of normalizing the adaptive weights according to (4.17) and (4.60). For comparison, the processor was also tested using the traditional method (4.19). For both methods, the dimensionless step-size parameter was $\alpha = 0.25$. The signal powers required by (4.19) and (4.60) were obtained by squaring the reference input and system output and then processing

[1]Previous work has shown that the performance obtained with a jammer located at 45° is representative of performance obtained with a single jammer at other angles (Greenberg, 1989).

with first-order recursive lowpass filters. The time constant of the lowpass filter used on the reference input equaled the length of the adaptive filter (10 ms or 100 ms) in order to account for the power of the signal in the tapped delay line. The time constant of the lowpass filter used on the system output was 10 ms, which was found to be a good value for tracking power fluctuations in speech.

The correlation method of controlling adaptation was implemented as described in Sec. 5.3. For the two-microphone array, the bandpass filter cutoff frequencies were 1643 Hz and 3286 Hz, one octave about the center frequency, 2464 Hz, determined by (5.30). For the five-microphone array, the bandpass filter cutoff frequencies were those given in Table 5.1. All of the bandpass filters were 10^{th}-order Butterworths. The hard limiter was included in computing the instantaneous correlation, and the instantaneous values were smoothed by a first-order recursive lowpass filter with 10-ms time constant. The threshold correlation value was $\rho_0 = 0$. For the five-microphone system, the voting method was used.

For each combination of acoustic condition and processing option, the system adapted on the same sequence of 40 IEEE sentences paired with 40 matching-length segments of SPIN babble. The lengths of the sentences varied from 22656 to 38912 samples, with a mean of 29242 samples. When the source signal levels were adjusted to produce a TJR of 0 dB over all 40 sentences, the TJRs for individual sentences ranged from -2.5 to 1.9 dB. For processing, the sentences and babble segments were concatenated to produce a single set of source signals of 117 sec duration. For evaluation, the performance measures were calculated individually for each sentence-plus-babble segment. The intelligibility-weighted gain, G_I, was computed based on the system output and the input signal received at one microphone; the two-element array used the leftmost microphone to obtain the input levels and the five-element array used the center microphone.

For each condition, the steady-state performance was determined by averaging the performance measures (in dB) obtained from the last five sentences (36–40).[2] Com-

[2]These five sentences had lengths of 26880, 27648, 25856, 24448 and 31616 samples and TJRs of 1.4, 1.9, -0.6, -0.5, and 0.9 dB when scaled for TJR=0 dB over all 40 sentences.

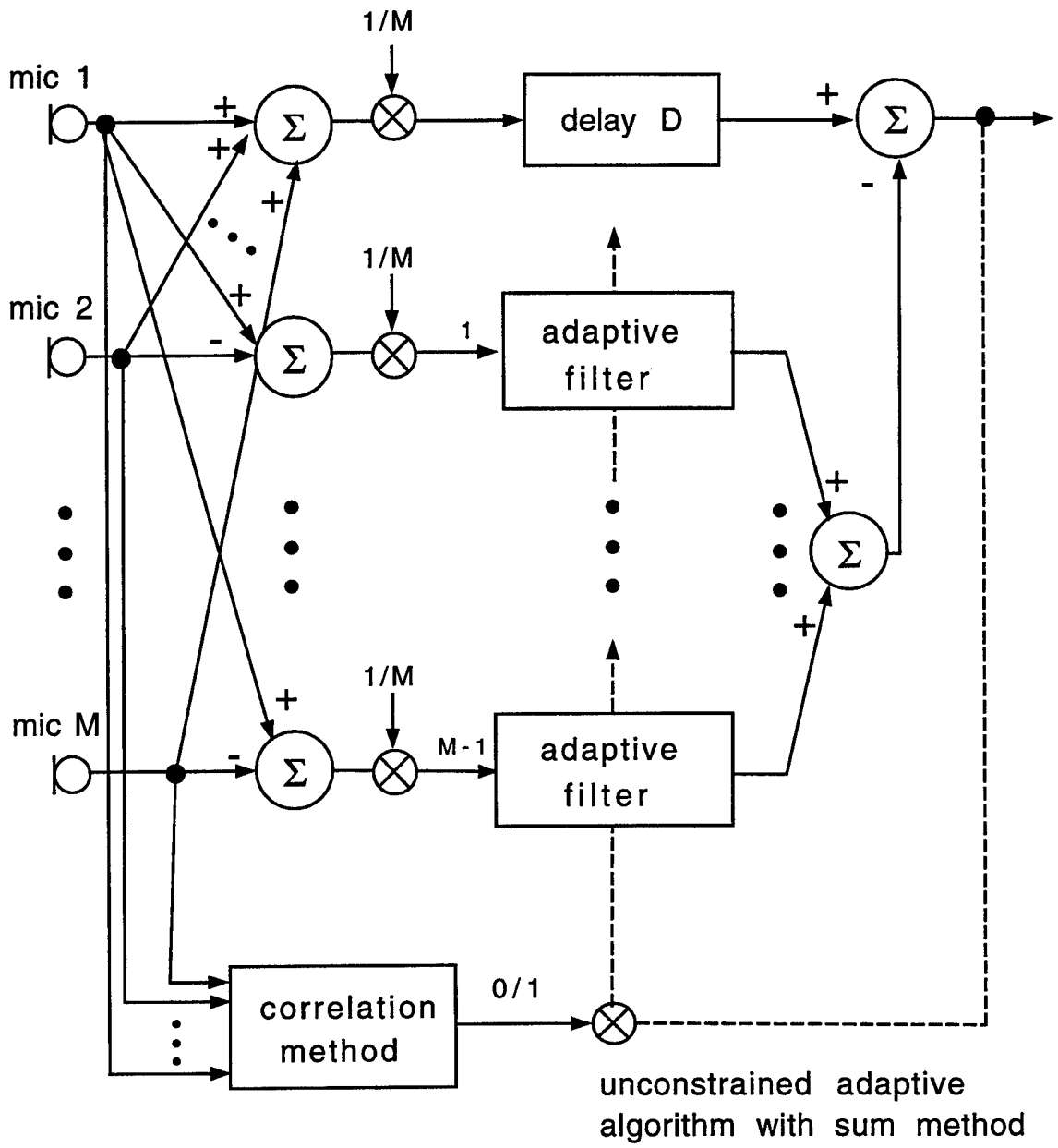

Figure 7-1: Block diagram of the generalized sidelobe canceller modified by the correlation method of controlling adaptation (details shown in Fig. 5.8). The adaptive filter weights are updated according to (4.17) using either the traditional method (4.19) or the sum method (4.60) of normalizing the step-size parameter. The system has M microphones and $M-1$ adaptive filters, each with L taps.

paring these performance measures to values obtained by averaging the preceeding five sentences (31–35) showed a difference of less than 2 dB for all conditions. Therefore, the results presented below are not sensitive to minor variations in the speech materials.

For most of the conditions considered, the system converged rapidly, and the performance was roughly constant over all 40 sentences. However, a few of the conditions considered had much longer convergence times, and for one condition (five-microphone array with 1000-point filters), the system had not reached steady-state even after 40 sentences. The steady-state performance measures based on the last five sentences are presented in the next section, while the transient performance will be discussed in Sec. 7.4.

7.3 Steady-state performance

7.3.1 Effect of modifications

Figures 7.2 and 7.3 show the steady-state performance with and without the modifications. Each plot in these figures shows the intelligibility-weighted gain, G_I, versus the direct-to-reverberant ratio for all four processing options (sum method of normalizing the step-size parameter, correlation method of controlling adaptation, both modifications, and neither modification). Figure 7.2 shows the results for 0 dB input TJR, and Fig. 7.3 shows the results for +20 dB input TJR. Results are not shown for input TJR of −20 dB because the modifications have little or no effect at low TJR.

As explained in Sec. 3.3, positive G_I values indicate improved intelligibility (amplification of the target or attenuation of the jammer), while negative G_I values indicate degraded intelligibility (attenuation of the target or amplification of the jammer). Figure 7.2 shows that for 0 dB input TJR, the unmodified algorithm provides moderate gains for all conditions. Performance improves with the addition of either modification, and adding both modifications provides the best performance. The largest improvements occur in the anechoic environment, but the modifications also provide

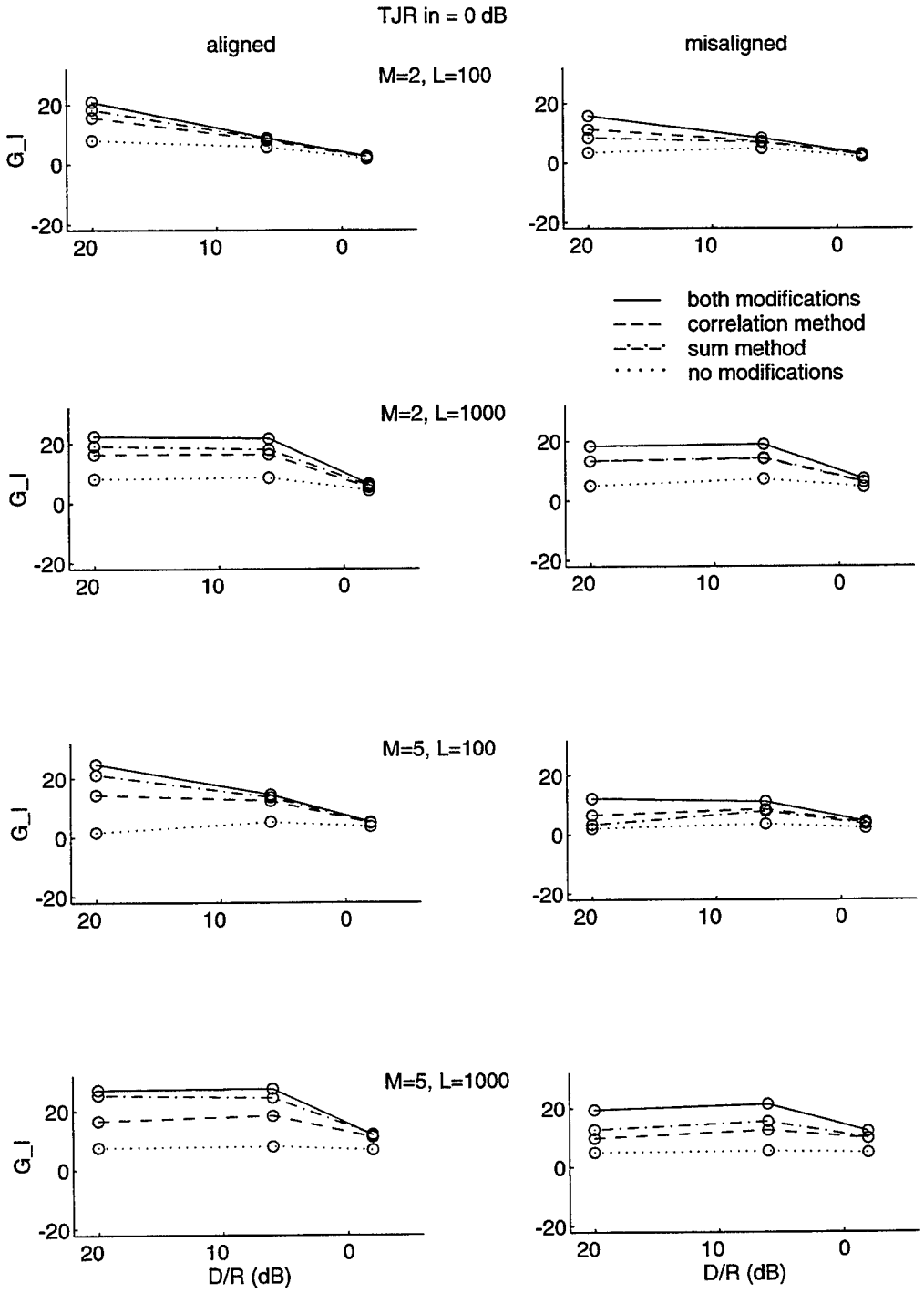

Figure 7-2: Intelligibility-weighted gain, G_I, versus direct-to-reverberant ratio showing steady-state performance with and without the two modifications. Anechoic results are shown at a direct-to-reverberant ratio of +20 dB. The input TJR was 0 dB. The arrays were either perfectly aligned to the straight-ahead target or misaligned by 10°. The systems tested were two- and five-microphone arrays with 100- and 1000-point adaptive filters.

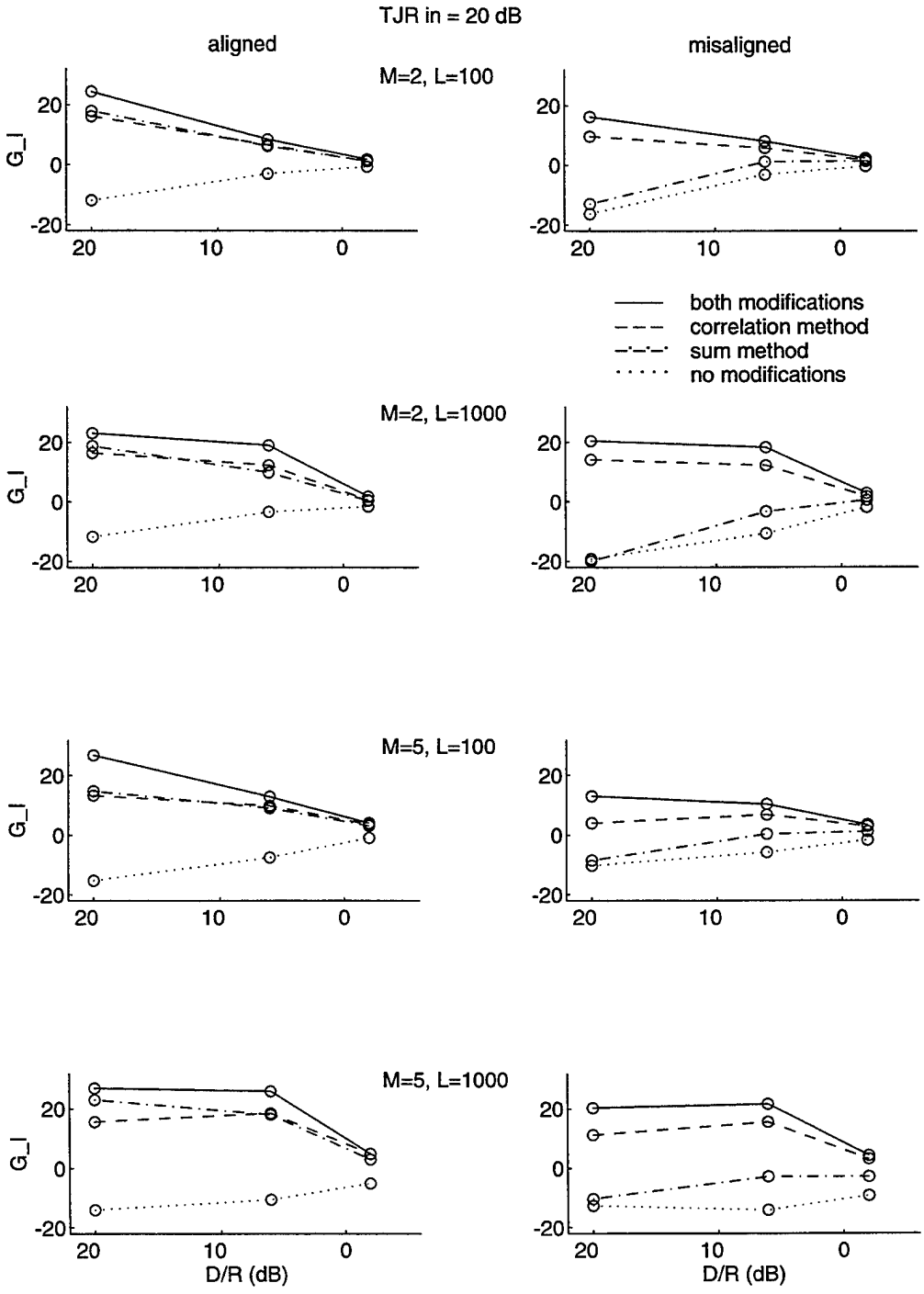

Figure 7-3: Intelligibility-weighted gain, G_I, versus direct-to-reverberant ratio showing steady-state performance with and without the two modifications. Anechoic results are shown at a direct-to-reverberant ratio of +20 dB. The input TJR was +20 dB. The arrays were either perfectly aligned to the straight-ahead target or misaligned by 10°. The systems tested were two- and five-microphone arrays with 100- and 1000-point adaptive filters.

substantial improvements in moderate reverberation.

Figure 7.3 demonstrates the need for the modifications when the input TJR is high. In this case, the unmodified algorithm performs poorly, with values of G_I as low as -20 dB. Again, the best performance is obtained with both modifications, the largest improvements occur in the anechoic environment, and the modifications also provide substantial improvements in moderate reverberation. Although performance generally improves with either modification, for the misaligned conditions the correlation method alone provides much larger benefits than the sum method alone. While the sum method alone effectively reduces misadjustment when the array is aligned, it permits substantial target cancellation when the array is misaligned. The interactive effects of the two modifications on misadjustment and target cancellation have been explained previously (Greenberg and Zurek, 1992).

From the results shown in Figs. 7.2 and 7.3, it is clear that the system always performs better with both modifications than it does with either modification alone or with no modifications. This was shown previously for two microphones with $L = 100$ in an anechoic environment (Greenberg and Zurek, 1992). The current results indicate that *the modifications are effective in anechoic and reverberant environments, for arbitrary filter lengths, and for five as well as two microphones.*

The next section summarizes steady-state performance results for the algorithm utilizing both modifications. The transient performance of all four processing options will be considered in Sec. 7.4.

7.3.2 Performance with both modifications

This section considers in more detail the performance of the algorithm with both modifications; it examines the effect of design parameters (adaptive filter length, L, and number of microphones, M), as well as variations in the acoustic environment (degree of reverberation, TJR, array alignment). In presenting these results, it will be useful first to consider the intelligibility-weighted gain, G_I, and then to examine the components that compose G_I.

Intelligibility-weighted gain

Figure 7.4 shows the steady-state performance for systems using both modifications. As before, the steady-state performance was determined from the average value of G_I for the last five sentences. The values shown for TJR=0 dB and TJR=20 dB are repeated from Figs. 7.2 and 7.3.

Each plot in Fig. 7.4 shows G_I versus the direct-to-reverberant ratio for three input TJRs. Comparing the three curves in each plot shows that the best performance is obtained when the input TJR is low, but very good performance is obtained for all input TJRs. For all values of input TJR, G_I is positive, indicating that the systems always provide some benefit. Furthermore, comparing the right and left sides of Fig. 7.4 reveals that the systems are robust to misalignment. Comparison with Figs. 7.2 and 7.3 indicates that the combination of the two modifications are responsible for this robustness to misalignment and high input TJR.

The results in Fig. 7.4 show that the best performance is obtained in anechoic environments and performance decreases with increasing reverberation. In moderate reverberation, the longer filters provide substantial benefits over the shorter filters. In strong reverberation, G_I approaches a small, positive value regardless of filter length. These results are consistent with previously reported trends of performance for a two-microphone system in reverberation for the limited case of no target signal (Greenberg and Zurek, 1992).

For the conditions studied here, the five-microphone array shows a slight performance advantage over the two-microphone array. However, these two arrays perform comparably because there is only one directional jammer. The two-microphone array can form one independent broadband null, while the five-microphone array can create four independent broadband nulls. Therefore, the five-microphone array will have a substantial advantage over the two-microphone array in the presence of multiple directional jammers. The number of microphones required in a practical system will be discussed in Sec. 8.2.

The points marked by 'x' in Fig. 7.4 indicate the performance of a fixed beamformer with uniform weights, that is, the system shown in Fig. 7.1 with the adap-

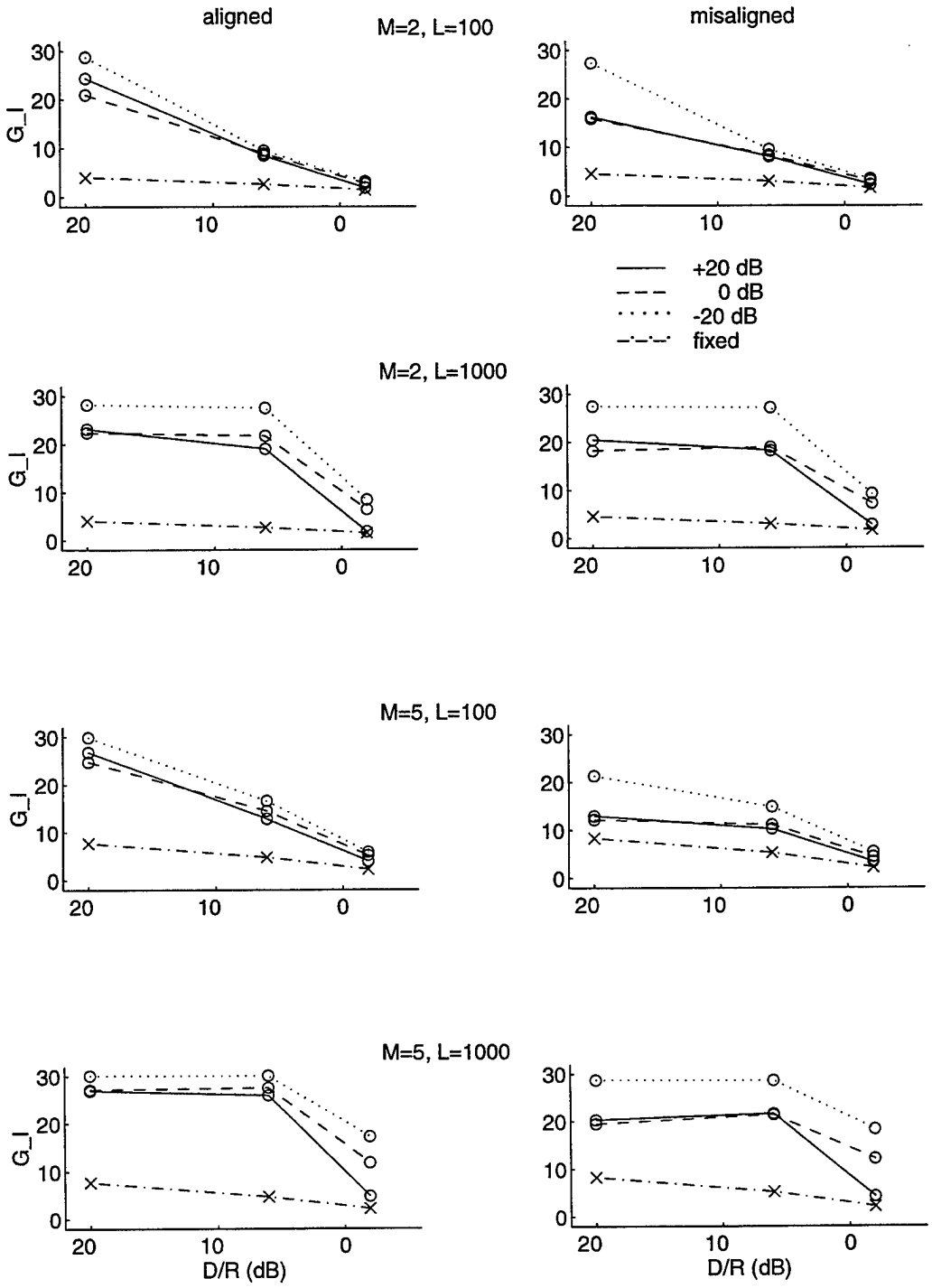

Figure 7-4: Intelligibility-weighted gain, G_I, versus direct-to-reverberant ratio showing steady-state performance with both modifications for three input TJRs. Anechoic results are shown at a direct-to-reverberant ratio of +20 dB. The arrays were either perfectly aligned to the straight-ahead target or misaligned by 10°. The systems tested were two- and five-microphone arrays with 100- and 1000-point adaptive filters. Also shown are results of the underlying fixed system, described in the text.

tive filter disconnected. In extreme reverberation, the performance of the system approaches that of the underlying fixed system, that is, the output is simply the primary signal because the adaptive filter weights approach zero. This was demonstrated previously for a two-microphone system with no target signal (Greenberg and Zurek, 1992). The most reverberant condition simulated here (−2 dB direct-to-reverberant ratio) has sufficient directional components so that the adaptive filter weights are nonzero and the performance may exceed that of the underlying fixed beamformer. Even so, the current results demonstrate that with both modifications, this trend toward 'graceful failure' of the adaptive algorithm is extended to cases including both target and jammer signals, as expected.

Components of intelligibility-weighted gain

Considering the intelligibility-weighted measures that contribute to G_I, discussed in Sec. 3.3, provides additional understanding of the behavior of the system. Figures 7.5–7.8 display values of $\Delta\Gamma(T_d)$, $\Delta\Gamma(T_r)$, $\Delta\Gamma(T)$, and $\Delta\Gamma(J)$ derived from the same output signals used to produce the values of G_I shown in Fig. 7.4.

Under ideal conditions, the generalized sidelobe canceller should exactly preserve the direct target signal, that is $\Delta\Gamma(T_d)$ should equal 0 dB. Under nonideal conditions, misalignment and target reflections are the two possible causes of direct target cancellation. In accordance with the results of Ch. 6, all of the systems evaluated used a relatively short primary delay of $D = 50$ (5 ms). As discussed in Sec. 6.4, for these source-to-microphone impulse responses, the first off-axis reflection arrives at the microphones 66 samples after the direct wave. Therefore, for aligned arrays, the simulation results should show no cancellation of direct target due to target reflections.

Figure 7.5 shows the effect of the systems on the direct target. As expected, for the two-microphone array, the direct target signal was completely preserved. The five-microphone system showed slight cancellation of the direct target (-1.2 dB $<$ $\Delta\Gamma(T_d) < 0$ dB) due to level and phase differences at pairs of microphones placed asymmetrically with respect to the direction of propagation. This can be considered

a form of misalignment due to the fact that the room simulation produces spherical radiation, so the target signal at the array was not an ideal plane wave.

For misaligned arrays, target cancellation is possible because the system is constrained to preserve sources arriving from 0°, but the target source actually arrives from 10°. Despite this violation of the assumption of known target direction, with both modifications the two-microphone arrays exhibit very little direct target cancellation (less than 2 dB). However, the five-microphone array shows significant cancellation of the direct target, particularly in an anechoic environment. This is because the five-microphone system can steer four independent broadband nulls. Even though the modifications prevent adaptation when the target signal is strong, the system can steer multiple nulls and therefore directs one at the jammer and another at the misaligned target. Without the modifications, this additional null would be much deeper. This illustrates one of the major differences between the two- and five-microphone arrays; it will be discussed more thoroughly in Sec. 8.2.

Two additional features of the results in Fig. 7.5 for the five-microphone array deserve mention. First, the most extreme direct target cancellation occurs at 0 dB input TJR. This effect was reported previously (Greenberg and Zurek, 1992) and occurs because the correlation method is more accurate and therefore more effective against misalignment at higher input TJR. Second, it appears that the shorter filter results in more target cancellation than the longer filter. This misleading result is due to the fact that even after 40 sentences, the five-microphone array with 1000-point filters has not converged completely. This long convergence time will be discussed in Sec. 7.4. For now, it is sufficient to note that performance obtained by such long convergence times is irrelevant in a practical device.

Figure 7.6 shows the effect of the systems on target reflections for the two reverberant conditions. The values of $\Delta\Gamma(T_r)$ shown in Fig. 7.6 range from -4 dB to $+1$ dB. Positive values of $\Delta\Gamma(T_r)$ only occur for -20 dB input TJR, in which case the slight amplification of target reflections is a side effect of weights which have adapted to cancel the dominant jammer signal. Negative values of $\Delta\Gamma(T_r)$ indicate some cancellation of target reflections. In general, target reflections are subject to increased

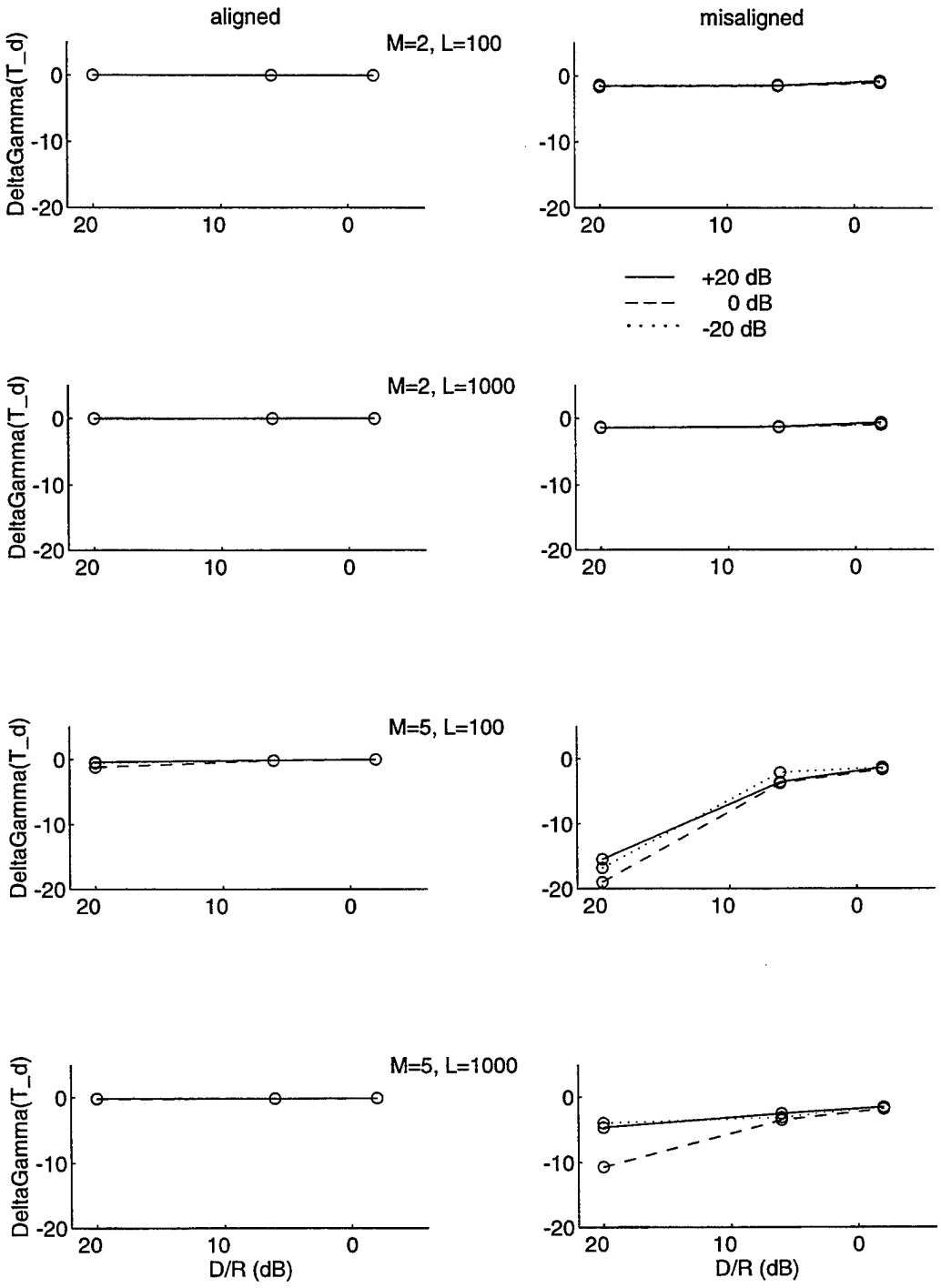

Figure 7-5: Effect of systems on direct target, $\Delta\Gamma(T_d)$, versus direct-to-reverberant ratio with both modifications for three input TJRs. Anechoic results are shown at a direct-to-reverberant pratio of +20 dB. The arrays were either perfectly aligned to the straight-ahead target or misaligned by 10°. The systems tested were two- and five-microphone arrays with 100- and 1000-point adaptive filters.

cancellation at high TJR, at lower direct-to-reverberant ratio, with longer filters, and with more microphones. These correspond to situations when the reflections are stronger and when the system has the capability to cancel them.

Figure 7.7 shows the effect of the systems on the total target signal, and Fig. 7.8 shows the effect of the systems on the jammer signal. Comparing the relative magnitudes of the values shown in Figs. 7.7 and 7.8 indicates that $\Delta\Gamma(J)$ is the dominant component of the values of G_I shown in Fig. 7.4. The only exception to this is the misaligned, five-microphone array in an anechoic environment. In this case, the system produces significant cancellation of the direct target, as discussed above. This target cancellation is undesirable, but for these conditions the system provides even more cancellation of the jammer signal. For example, with $L = 100$ and the input TJR = 0 dB, $\Delta\Gamma(T) = -19$ dB and $\Delta\Gamma(J) = 31$ dB, producing $G_I = 12$ dB. A real system will require automatic gain control to maintain output levels, so such target cancellation is tolerable as long as jammer cancellation exceeds target cancellation. The disadvantage is that requiring additional gain to restore the output levels also amplifies any uncorrelated noise, including microphone noise. It is also important to note that this target cancellation only occurred for the anechoic condition, and is drastically reduced in moderate reverberation. It is anticipated that this will not be a problem with real systems operating in real environments.

Polar patterns

Additional insight into the behavior of adaptive arrays is obtained by considering the magnitude response of the arrays as a function of frequency and source angle for distant plane-wave sources. For broadside arrays of omnidirectional microphones in free space, these responses are cylindrically symmetric about the array axis (90° – 270°) and therefore completely specified by their response in the horizontal plane. The magnitude response of the array is generated by computing the response of the generalized sidelobe canceller to pure tones traveling as ideal plane waves with wavefronts orthogonal to the horizontal plane for each azimuthal angle. This results in a response that is a function of both angle and frequency. The broadband response

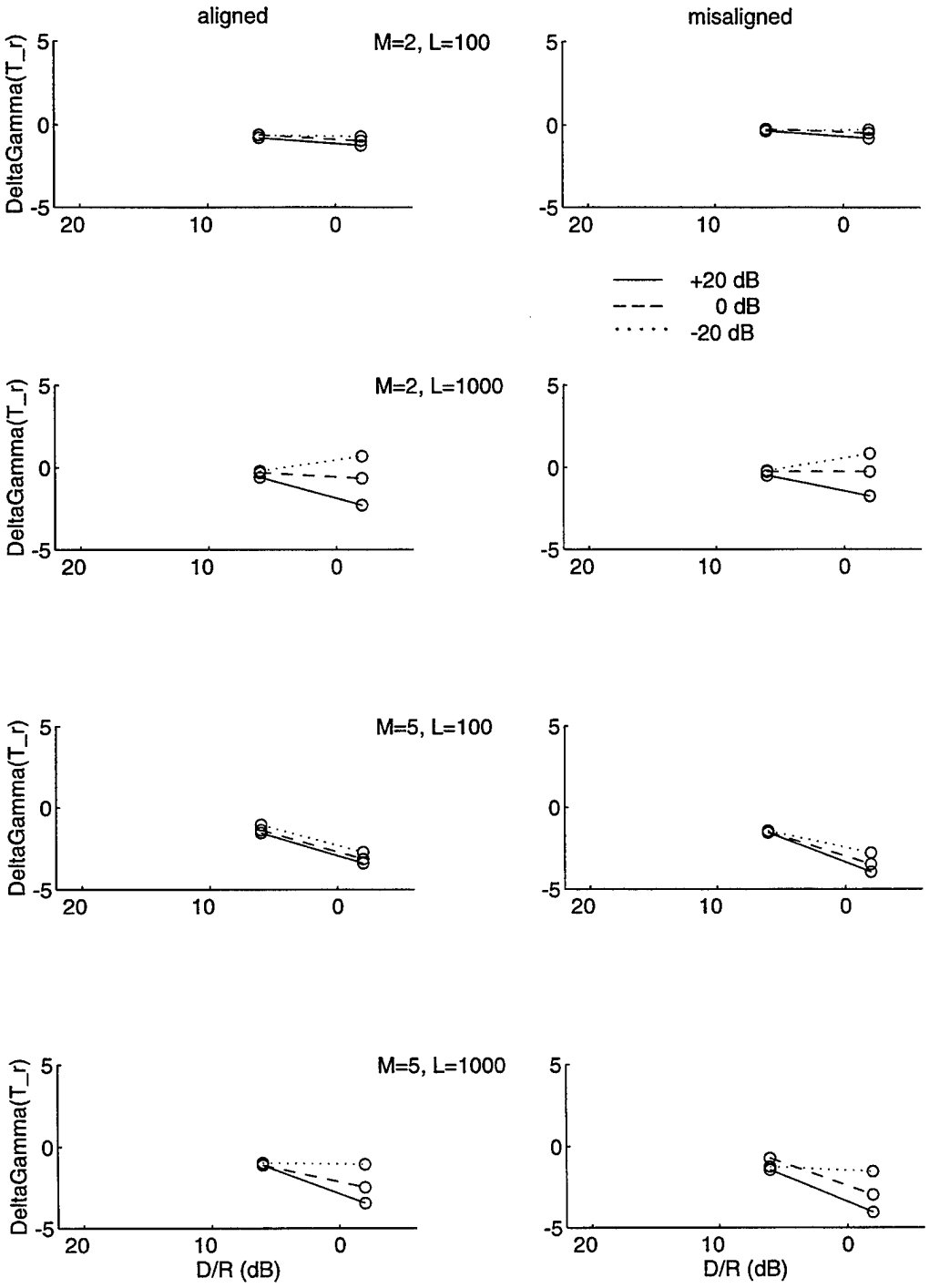

Figure 7-6: Effect of systems on reflected target, $\Delta\Gamma(T_r)$, versus direct-to-reverberant ratio with both modifications for three input TJRs. Anechoic results are shown at a direct-to-reverberant ratio of +20 dB. The arrays were either perfectly aligned to the straight-ahead target or misaligned by 10°. The systems tested were two- and five-microphone arrays with 100- and 1000-point adaptive filters.

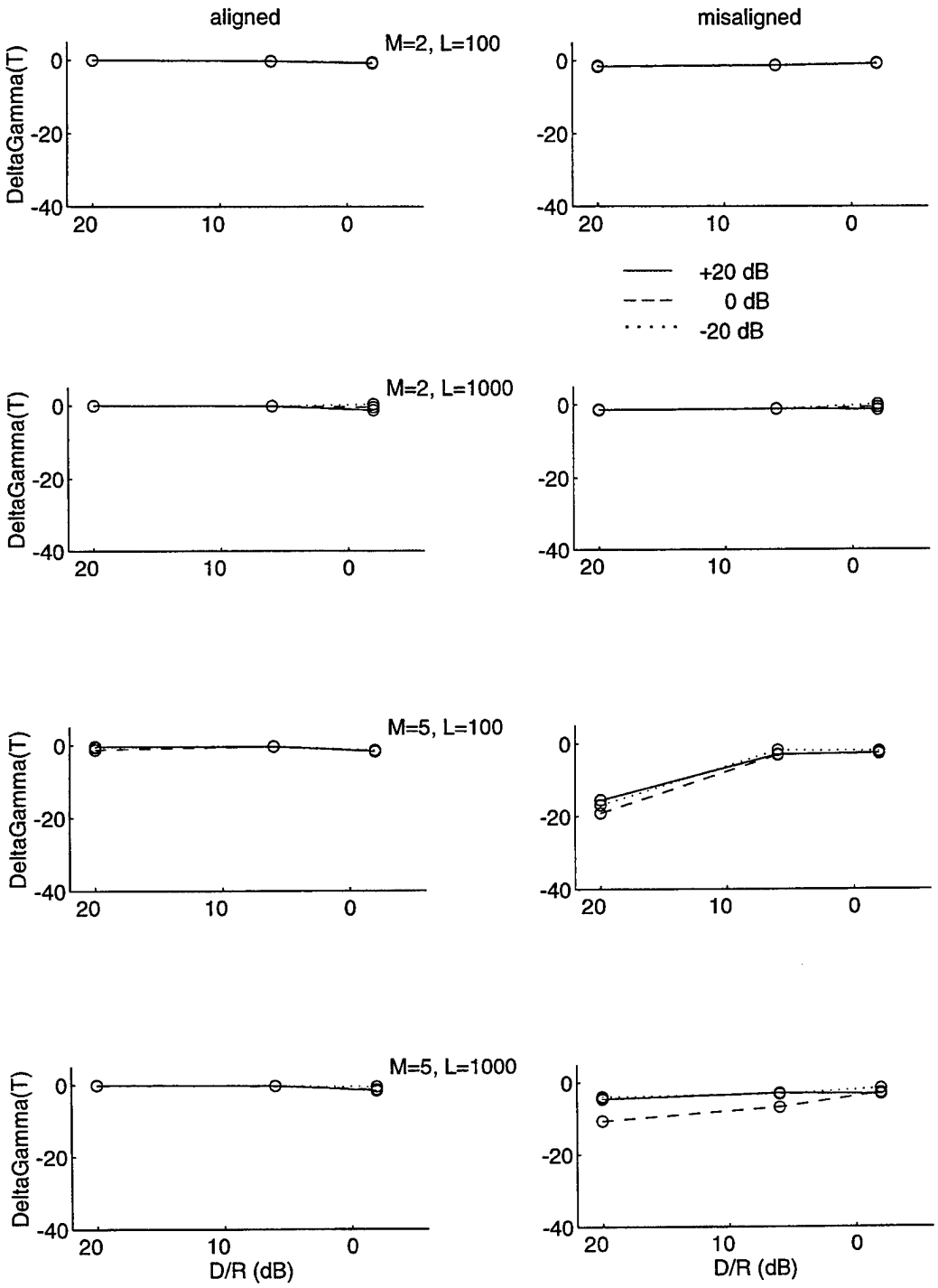

Figure 7-7: Effect of systems on total target, $\Delta\Gamma(T)$, versus direct-to-reverberant ratio with both modifications for three input TJRs. Anechoic results are shown at a direct-to-reverberant ratio of +20 dB. The arrays were either perfectly aligned to the straight-ahead target or misaligned by 10°. The systems tested were two- and five-microphone arrays with 100- and 1000-point adaptive filters.

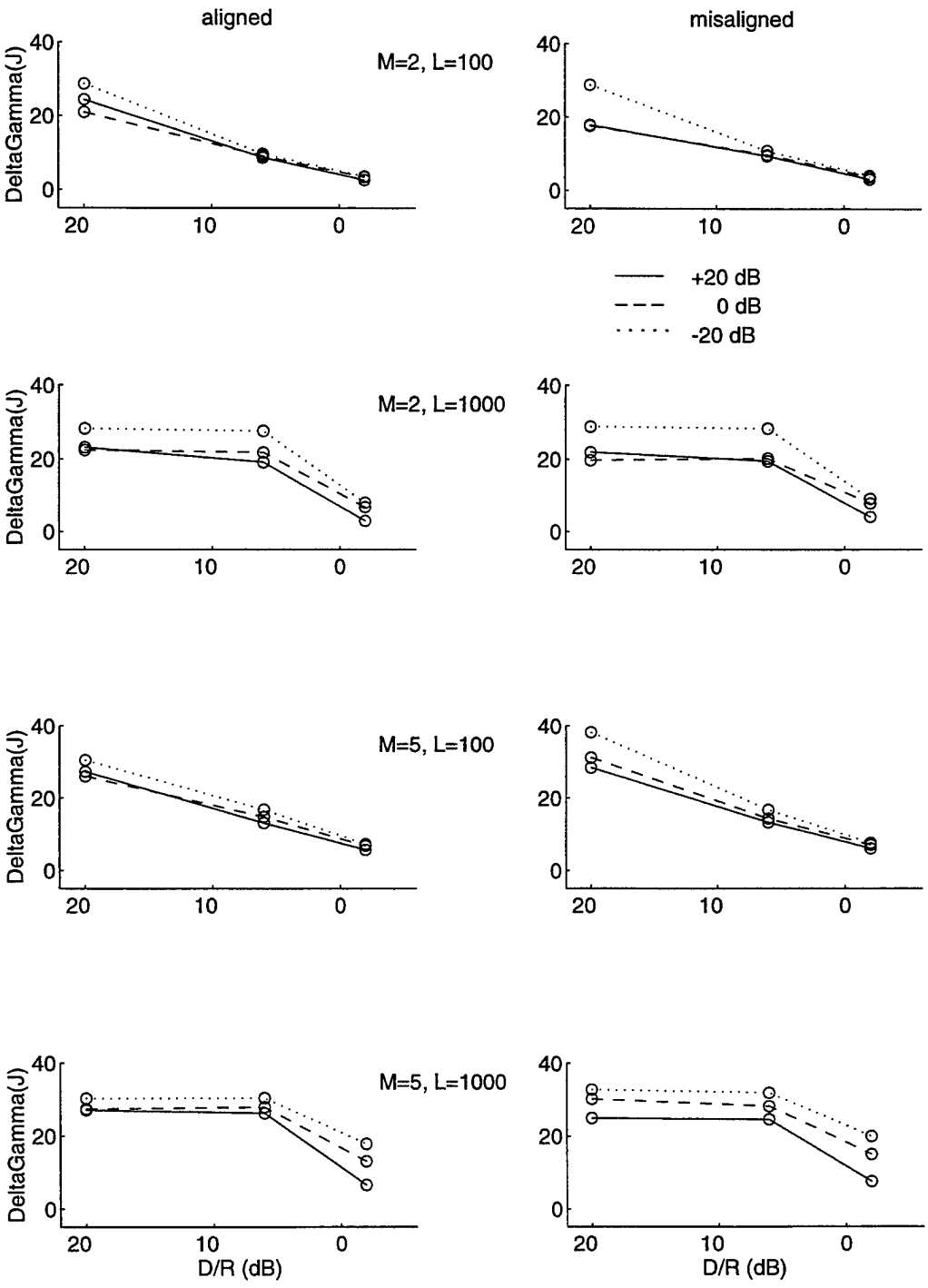

Figure 7-8: Effect of systems on total jammer, $\Delta\Gamma(J)$, versus direct-to-reverberant ratio with both modifications for three input TJRs. Anechoic results are shown at a direct-to-reverberant ratio of +20 dB. The arrays were either perfectly aligned to the straight-ahead target or misaligned by 10°. The systems tested were two- and five-microphone arrays with 100- and 1000-point adaptive filters.

is produced using intelligibility-weighted averaging, that is, taking the magnitude squared at the center frequency of each one-third-octave band, computing the level in dB, and applying Articulation Index weights to combine bands, as in (3.1).

Figures 7.9–7.14 show the intelligibility-weighted polar patterns[3] for the 24 conditions (two filter lengths, two array sizes, two array orientations, three levels of reverberation) with 0 dB input TJR shown in Fig. 7.4. In addition, the corresponding value of G_I from Fig. 7.4 is shown below each plot. Each polar pattern was computed from a single snapshot of the adaptive weights obtained after the system adapted on the entire sequence of 40 sentences and babble.

Figure 7.9 shows responses of the two-microphone array in an anechoic environment. The system has unity gain to signals arriving from 0°, as constrained by the generalized sidelobe canceller structure, and has formed a null in the direction of the jammer signal (45° for the aligned array and 55° for the misaligned array). Because the two-microphone system has one broadband degree of freedom, it can create one independent null. The second null (at 135° or 125°) is a result of the cylindrical symmetry of the broadside array. The polar pattern indicates that sources arriving from angles between 180° and 360° are slightly amplified by the system. However, these adaptive weights were obtained with no signals arriving at the array from those directions, so there was no reason for the system to prevent amplification of signals arriving from those directions.

Figure 7.10 shows polar patterns for the five-microphone array in an anechoic environment. For the most part, these patterns are similar to those seen in Fig. 7.9. One notable difference occurs in the misaligned case, where the five-microphone system steers a second independent null in the direction of the misaligned target (10°). This second null was discussed previously as the cause of the target cancellation seen in Fig. 7.5.

In Figs. 7.9 and 7.10, the depth of the nulls in the jammer direction is not exactly equal to the corresponding values of $\Delta\Gamma(J)$ shown in Fig. 7.8. This is because the

[3]According to the convention for polar plots, positive angles progress *counterclockwise* from zero degrees. These plots are consistent with the definition of positive angles given in Sec. 3.2 if they are interpreted as being viewed from *below* the array.

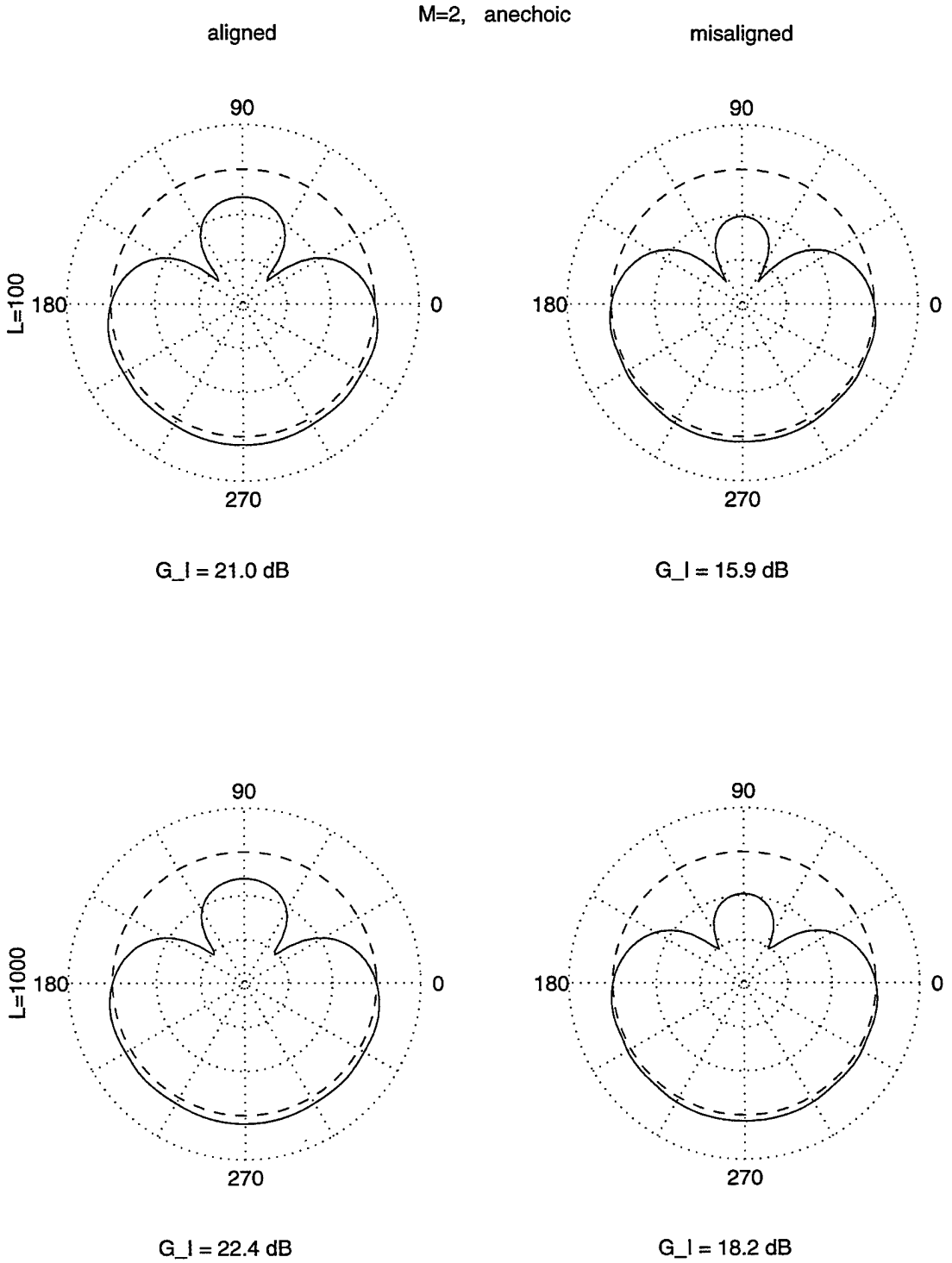

Figure 7-9: Polar patterns showing the intelligibility-weighted response of the two-microphone system in an anechoic environment. The input TJR was 0 dB. Radial grid lines are in 10 dB increments, and the dashed line indicates 0 dB. Values of G_I are from corresponding conditions in Fig. 7.4.

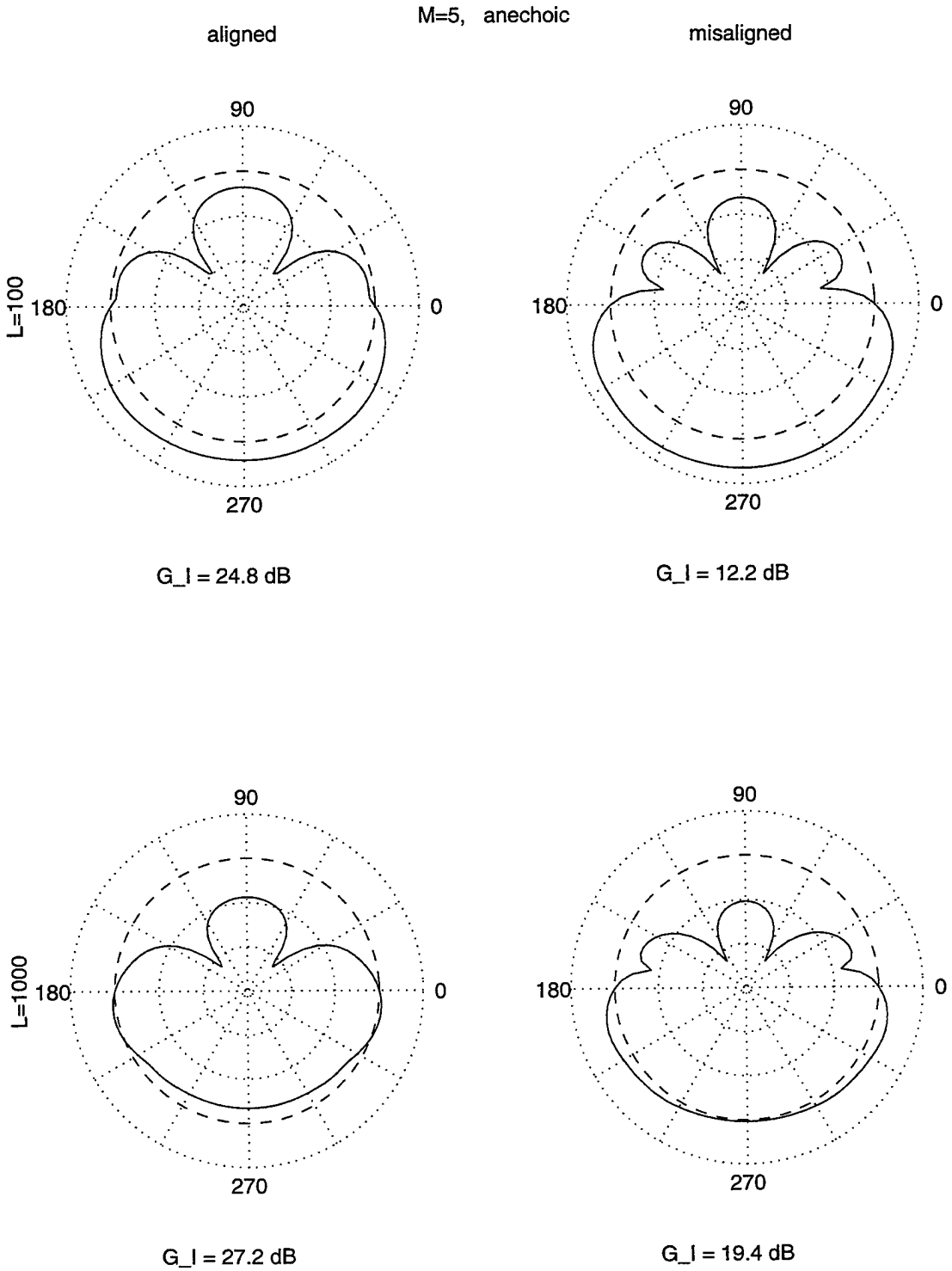

Figure 7-10: Polar patterns showing the intelligibility-weighted response of the five-microphone system in an anechoic environment. The input TJR was 0 dB. Radial grid lines are in 10 dB increments, and the dashed line indicates 0 dB. Values of G_I are from corresponding conditions in Fig. 7.4.

polar pattern is based on a single snapshot of the adaptive weights, while $\Delta\Gamma(J)$ is determined from the spectra of output signals obtained while the adaptive weights were fluctuating.

Figures 7.11–7.14 show polar patterns for the two- and five-microphone arrays in two reverberant environments. In interpreting these polar patterns, it is important to realize that the responses shown are for *independent* sources arriving from each angle, but that while adapting in reverberation, the weights are adjusted to minimize total output power, which may be accomplished by coherent addition of correlated sources (reflections) arriving from multiple angles. Comparing the two filter lengths in Figs. 7.11–7.14 reveals that shorter filters have deeper nulls, but the results in Fig. 7.4 indicate that the longer filter are associated with larger values of G_I. This is because the short filter minimizes the total output power by forming a null in the direction of the direct jammer, while the longer filter obtains additional benefits by using the adaptive weights to add coherent signals (arriving from different directions) out of phase, thereby cancelling the direct jammer as well as some jammer reflections.

This is verified in Fig. 7.15, which shows impulse responses for the two-microphone, aligned array in moderate reverberation. The top panel shows the jammer-source-to-microphone impulse response for the left microphone. The amplitude of the direct wave is 0.04; it was clipped in the figure to show the reflections in more detail. The middle and bottom panels show the source-to-system-output impulse responses for 100- and 1000-point filters, respectively, computed with the same snapshot of the adaptive weights used to generate the left half of Fig. 7.11. These impulse responses indicate roughly equal cancellation of the direct wave for the two filter lengths, and superior cancellation of reflections for the longer filter.

In a hearing aid, motion of the listener's head will cause the array position to vary with respect to the sound sources. The width of the nulls shown in Figs. 7.9–7.14 indicate that cancellation of the direct wave will be robust to slight head movements. However, as discussed previously, the longer filters provide improved cancellation in reverberation by adding coherent reflections out of phase. Cancellation of this type may be adversely affected by even slight head movements. Future evaluations with a

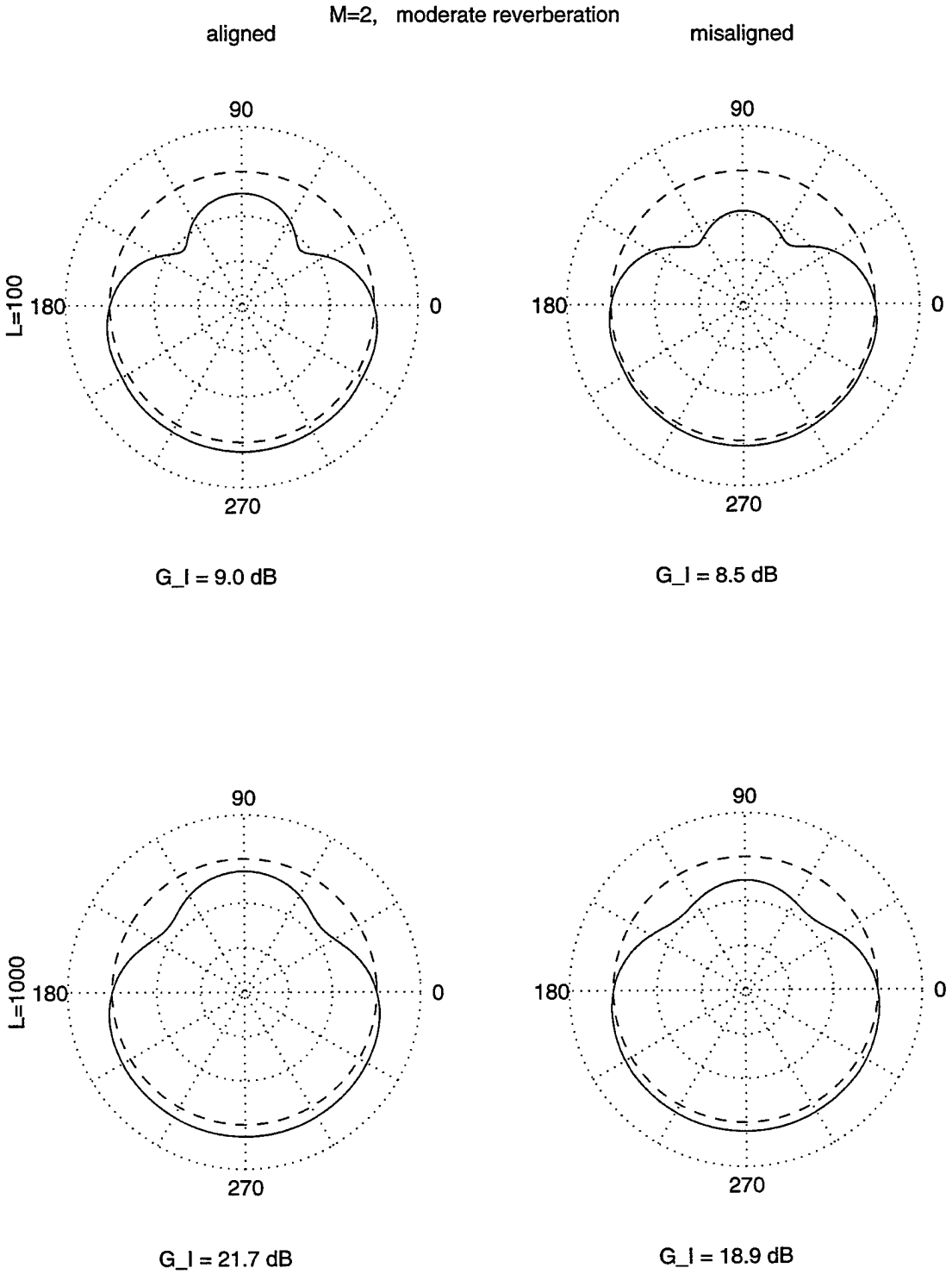

Figure 7-11: Polar patterns showing the intelligibility-weighted response of the two-microphone system in moderate reverberation. The input TJR was 0 dB. Radial grid lines are in 10 dB increments, and the dashed line indicates 0 dB. Values of G_I are from corresponding conditions in Fig. 7.4.

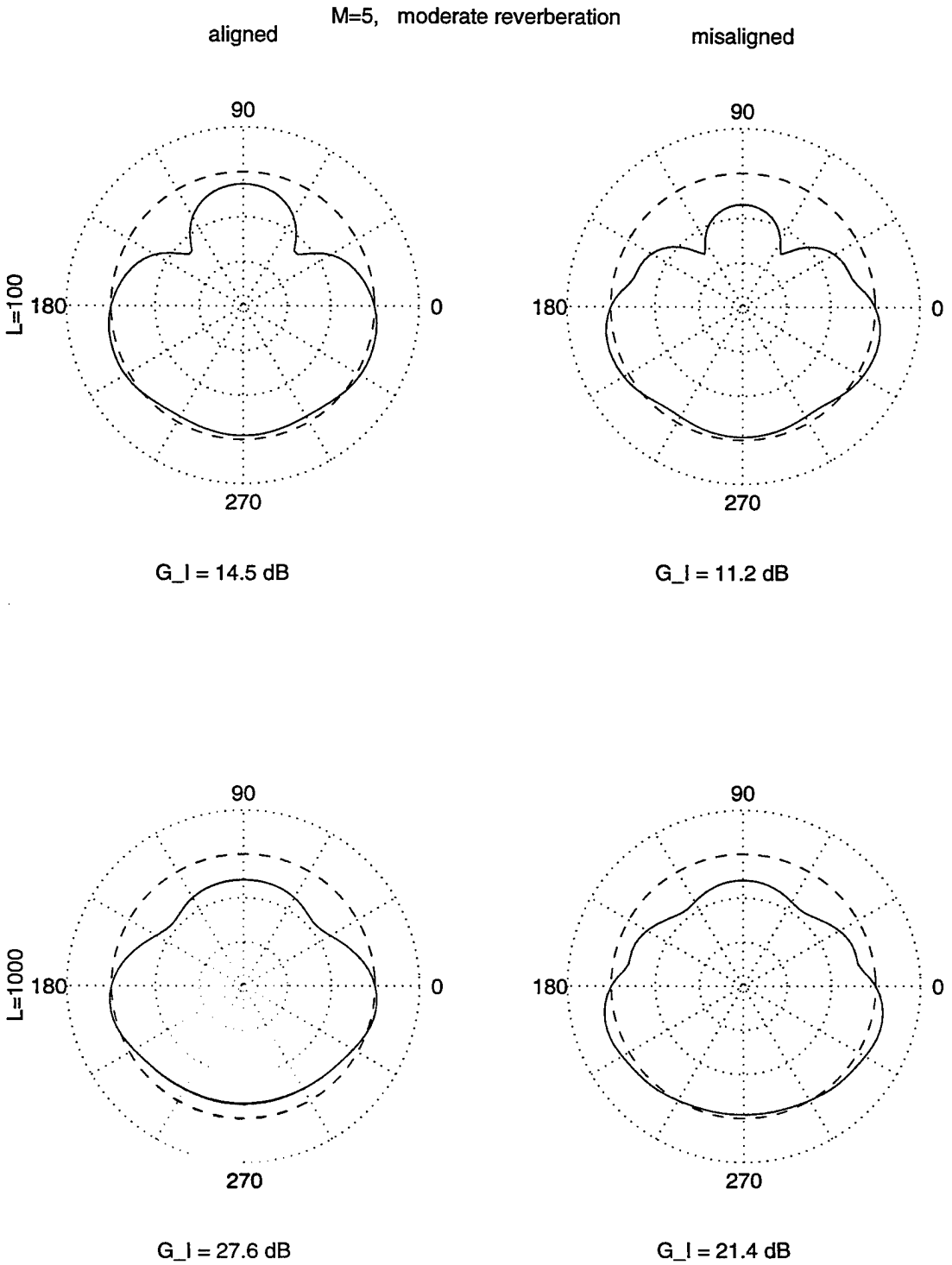

Figure 7-12: Polar patterns showing the intelligibility-weighted response of the five-microphone system in moderate reverberation. The input TJR was 0 dB. Radial grid lines are in 10 dB increments, and the dashed line indicates 0 dB. Values of G_I are from corresponding conditions in Fig. 7.4.

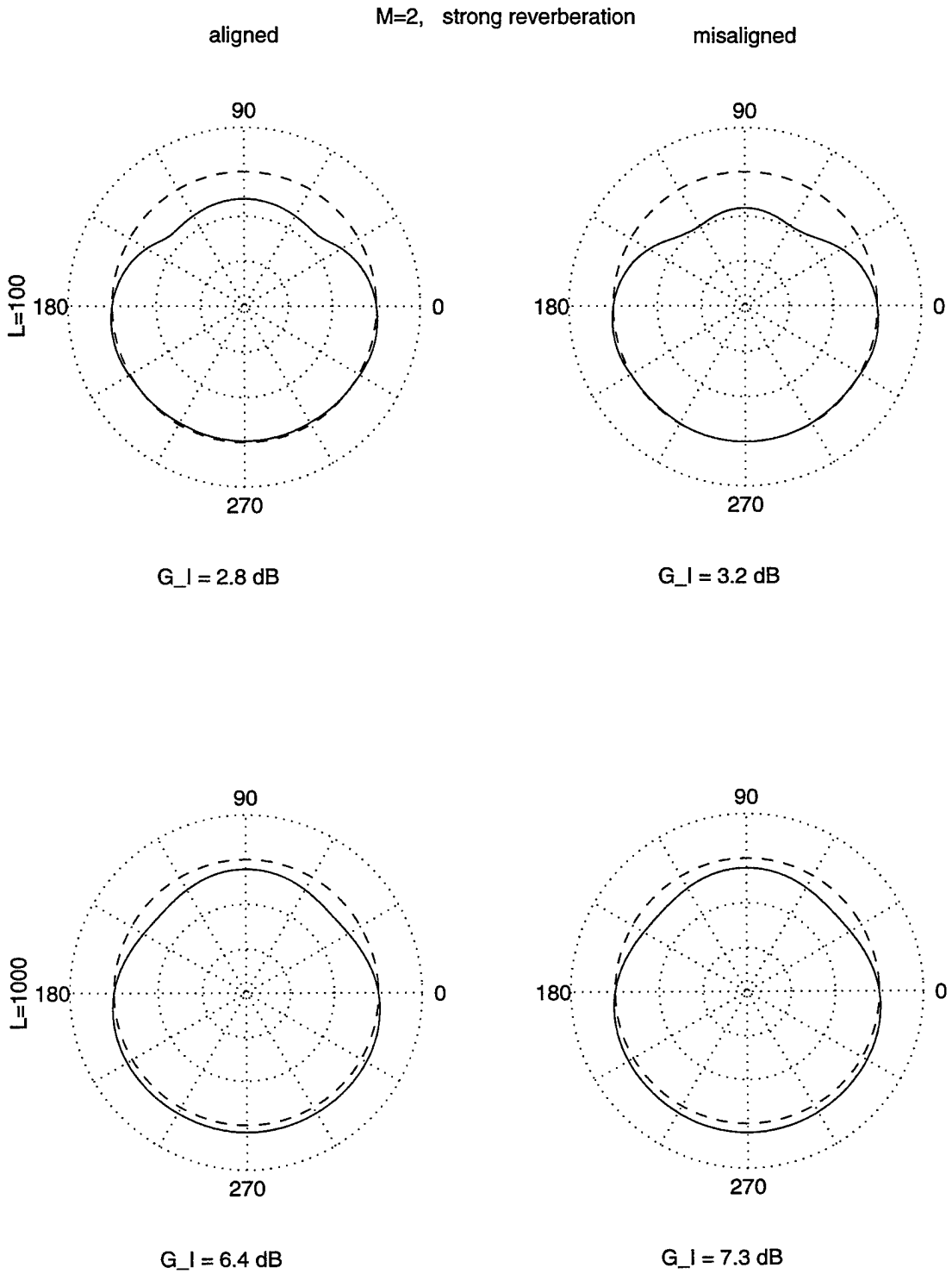

Figure 7-13: Polar patterns showing the intelligibility-weighted response of the two-microphone system in strong reverberation. The input TJR was 0 dB. Radial grid lines are in 10 dB increments, and the dashed line indicates 0 dB. Values of G_I are from corresponding conditions in Fig. 7.4.

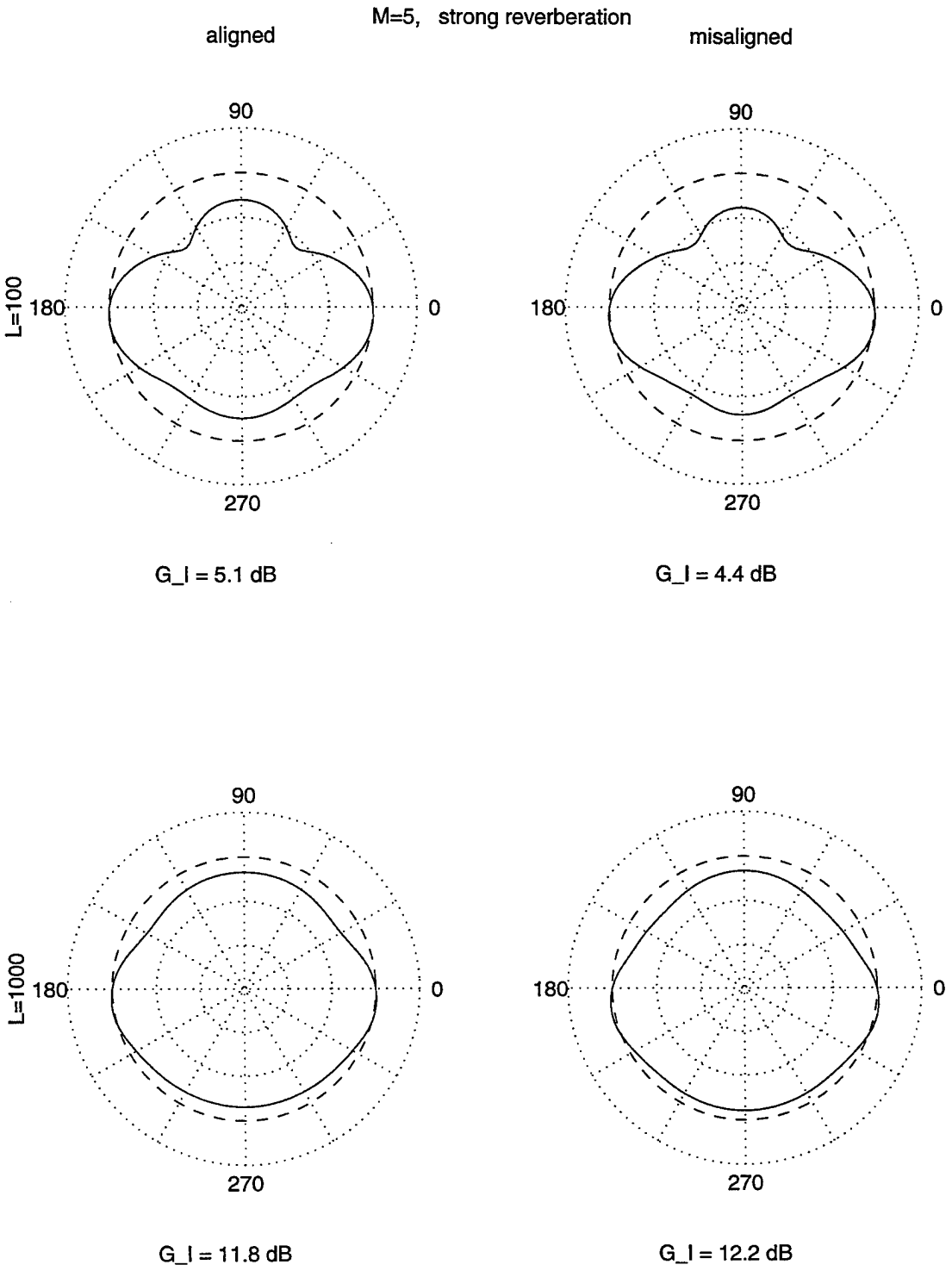

Figure 7-14: Polar patterns showing the intelligibility-weighted response of the five-microphone system in strong reverberation. The input TJR was 0 dB. Radial grid lines are in 10 dB increments, and the dashed line indicates 0 dB. Values of G_I are from corresponding conditions in Fig. 7.4.

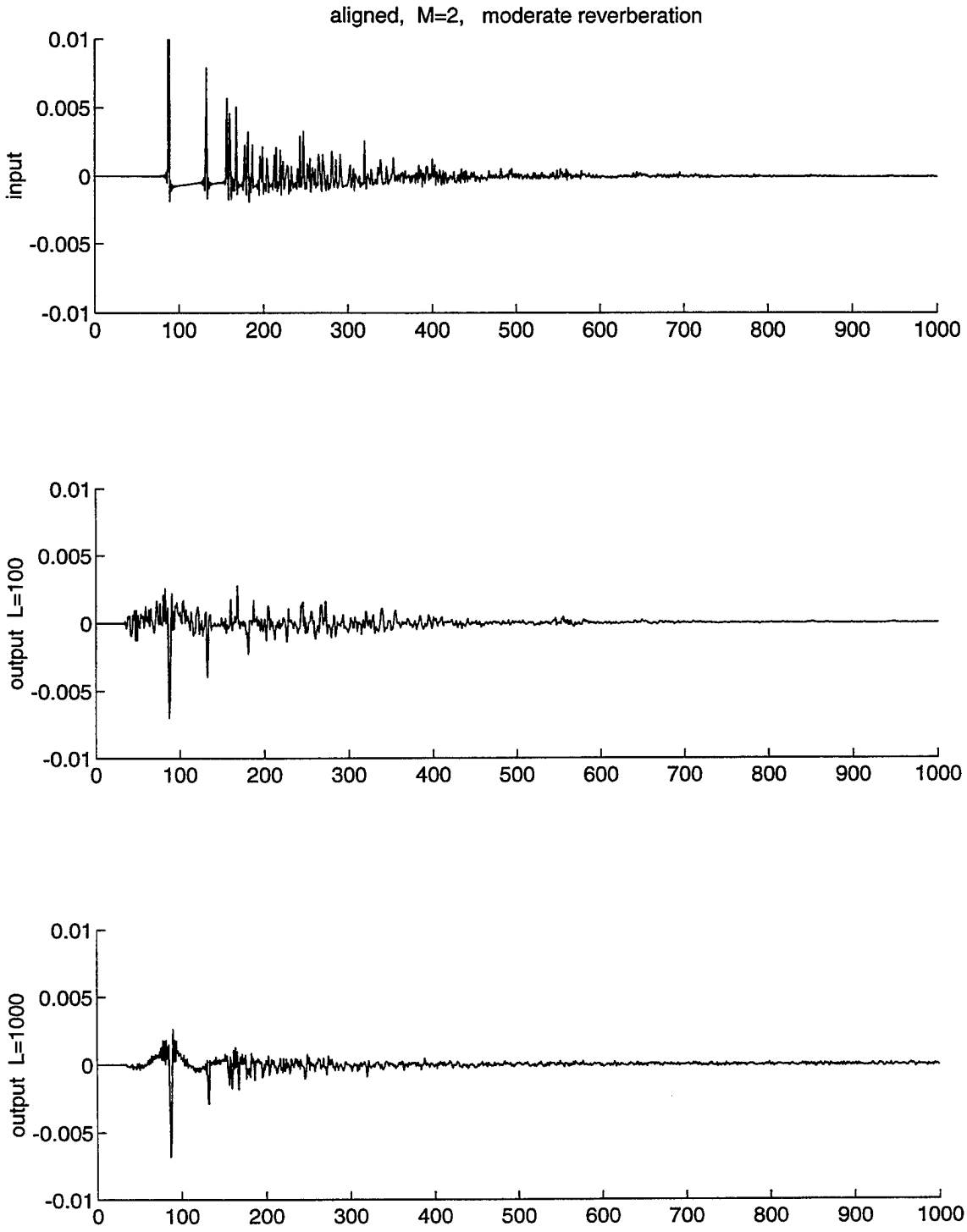

Figure 7-15: Impulse responses for two-microphone, aligned array in moderate reverberation. The top panel shows one jammer-source-to-microphone impulse response, with direct wave amplitude of 0.04 (clipped). The middle and bottom panels show the jammer-source-to-system output impulse responses for 100- and 1000-point filters, respectively.

real system should study the effects of head movements in order to assess the practical importance of the benefits of long filters in reverberation demonstrated here.

Figure 7.16 shows polar patterns for the responses of the underlying fixed systems. Included for comparison is a two-microphone array with the same span as the five-microphone array. These patterns are constant for all configurations of inputs. The polar plots show that the fixed systems are robust to misalignment (the main beam is fairly broad around 0°) and that in the presence of directional jammers, the two-microphone arrays provide gains of up to 5 dB, while the five-microphone array provides gains of up to 10 dB, where the actual attenuation depends on angle of arrival.

In extreme reverberation, the performance of the fixed system is characterized by its gain against isotropic noise, which is equivalent to its directivity index. The intelligibility-weighted directivity index (3.11) is $D_I = 1.7$ dB for the 7-cm two-microphone array, $D_I = 2.5$ dB for the 16-cm two-microphone array, and $D_I = 3.0$ dB for the 16-cm five-microphone array. It was found that two- and five-microphone arrays of the same length have similar values of D_I because at low frequencies, the two-microphone fixed array with uniform weights has a relatively narrow mainlobe, while at high frequencies, the five-microphone arrays have lower sidelobes. Both a narrow mainlobe and low sidelobes increase the directivity index. For the array dimensions and frequency ranges considered here, the weighted frequency averaging results in comparable values of D_I.

The performance of the underlying fixed system can be improved by using directional microphones (Soede et al., 1993a; Stadler and Rabinowitz, 1993). The fixed performance expected with directional microphones and the effect of directional microphones on the adaptive system will be discussed in Sec. 8.3.

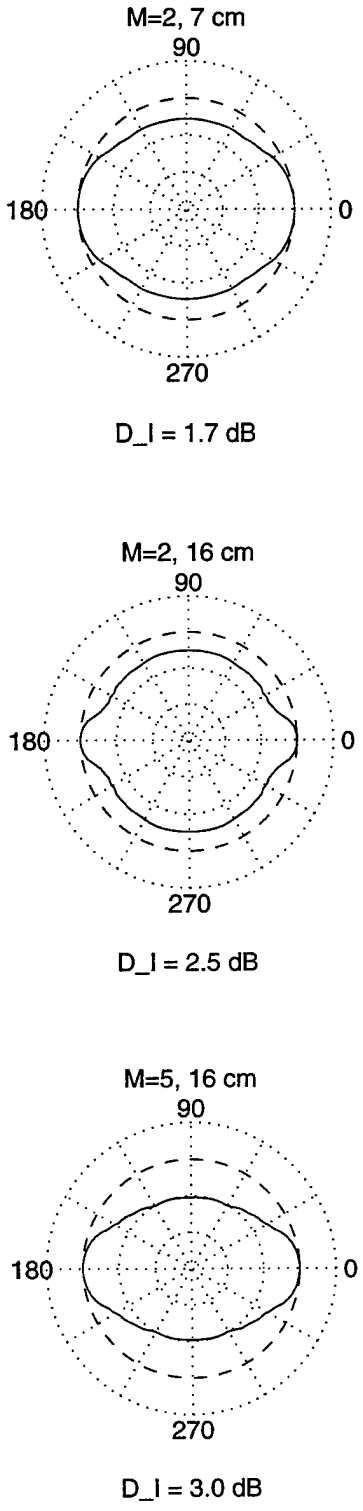

Figure 7-16: Polar patterns showing the intelligibility-weighted response of the underlying fixed systems for two- and five-microphone arrays.

7.3.3 Summary of steady-state performance

The steady-state performance of the systems investigated is summarized as follows:

- Using *both* modifications always gives better steady-state performance than using either modification alone or no modifications. Without the modifications, performance decreases dramatically with misalignment or increased TJR. With both modifications, the system is robust to misalignment and high TJR, and G_I is always positive.
- Using a short primary delay prevents cancellation of the direct target due to target reflections.
- With both modifications, the intelligibility-weighted gain, G_I decreases from 20–30 dB in an anechoic environment to 3–10 dB in strong reverberation.
- In an anechoic environment, performance is independent of filter length. In moderate reverberation, longer filters perform much better than shorter filters.
- For the single jammer case studied, the five-microphone array has only a slight advantage over the two-microphone array.

7.4 Transient performance

7.4.1 Effect of modifications

This section considers the transient performance of the algorithm with and without modifications. Initially, it is useful to summarize the following factors affecting convergence of the adaptive filters, many of which are derived from (4.70), (4.74), and (4.76).

- The convergence time is proportional to the total number of adaptive filter taps (the product of the filter length and one less than the number of microphones).

- Using the sum method of normalizing the step-size parameter slows the convergence. At low input TJR, the convergence is initially slower than the traditional method by a factor of 2, and at high input TJR the convergence is slower by a factor proportional to the TJR.

- Using the correlation method of controlling adaptation also slows convergence. Since the correlation method inhibits update of the adaptive weights on some iterations, the convergence time is longer by a factor equal to the reciprocal of the percentage of cycles for which the system actually adapted.

- The convergence time is inversely proportional to the dimensionless step-size parameter, α, which was held constant in these simulations.

- The convergence time is affected by the spread of the eigenvalues of the autocorrelation matrix of the reference signal.

Section 7.3 considered the steady-state performance after the system was allowed to adapt on a sequence of 40 sentences. Figure 7.17 shows the intelligibility-weighted gain, G_I, as a function of sentence number for all of the misaligned conditions with input TJR of 0 dB, and Fig. 7.18 shows results for the same conditions with input TJR of +20 dB.[4] Results are not shown for the aligned array, which demonstrated similar behavior except for predictable exceptions due to the ability of the system to cancel misaligned targets.

The four curves on each plot in Figs. 7.17 and 7.18 indicate the transient performance of the four processing options (sum method of normalizing the step-size parameter, correlation method of controlling adaptation, both modifications, and neither modification). Because the effect of each modification individually is to slow convergence, it is expected that the system using both modifications will converge most slowly. This is confirmed by the results in Figs. 7.17 and 7.18. For many conditions, the systems converged sufficiently rapidly that performance is constant over all

[4]The data for misaligned conditions shown in Figs. 7.2 and 7.3 correspond to the mean values of G_I for the last five sentences of the data shown in Figs. 7.17 and 7.18.

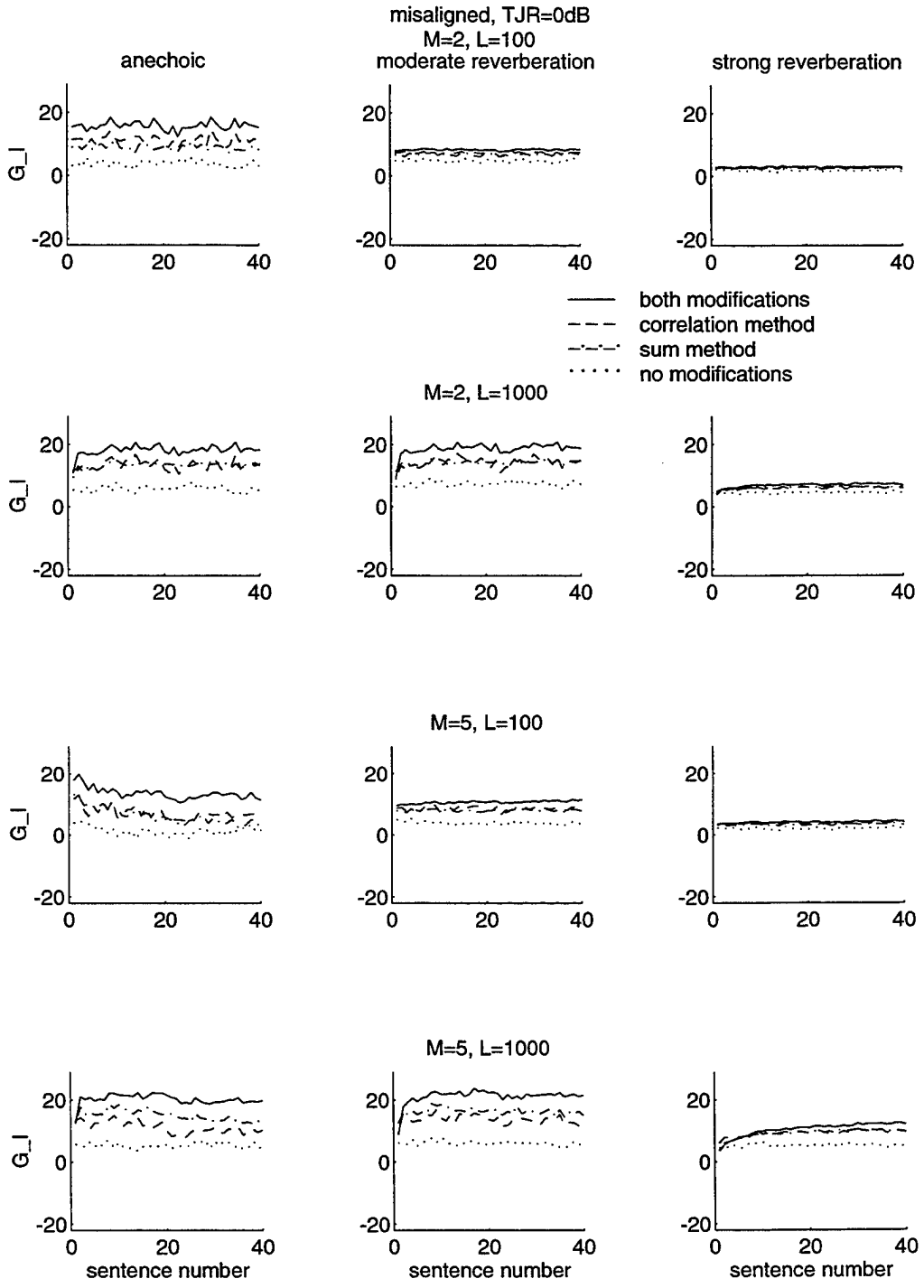

Figure 7-17: Transient performance shown by intelligibility-weighted gain, G_I, versus sentence number with and without the two modifications. The input TJR was 0 dB and the arrays were misaligned by 10°. Two- and five–microphone arrays were tested with 100- and 1000-point adaptive filters in three environments (anechoic, moderate reverberation, and strong reverberation).

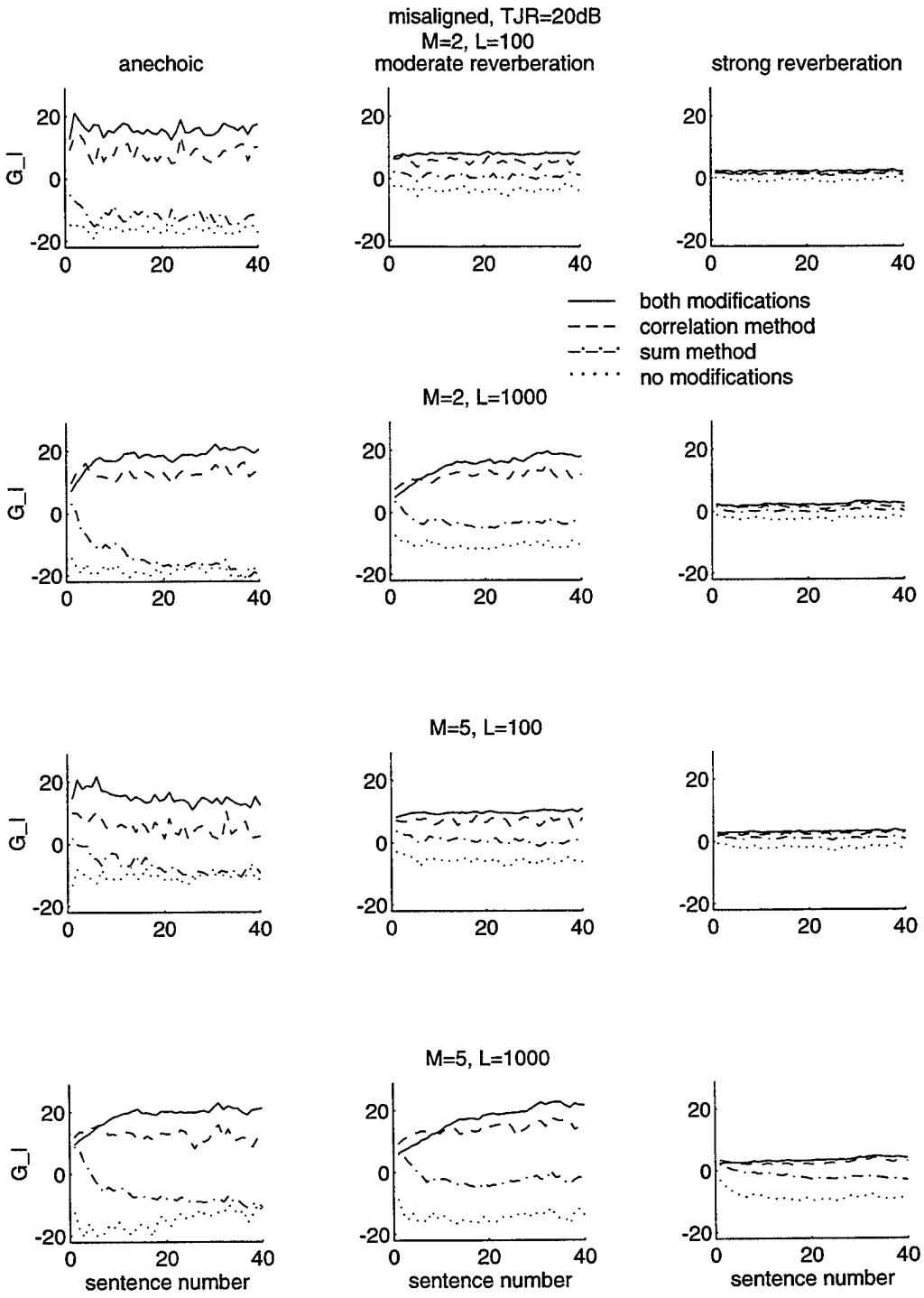

Figure 7-18: Transient performance shown by intelligibility-weighted gain, G_I, versus sentence number with and without the two modifications. The input TJR was +20 dB and the arrays were misaligned by 10°. Two- and five–microphone arrays were tested with 100- and 1000-point adaptive filters in three environments (anechoic, moderate reverberation, and strong reverberation).

40 sentences.[5] However, for those conditions where the convergence can be detected over successive sentences, the fastest convergence is obtained with no modifications, followed by one modification, and finally by the algorithm with both modifications, as expected.

Obviously, the goal of these systems is to obtain the best possible performance; there is no advantage in converging quickly to poor steady-state performance. Figures 7.2 and 7.3 showed that after converging to steady-state, performance is best with both modifications. Figures 7.17 and 7.18 show that even during the transients, use of both modifications provides the best performance for most conditions. The exception is two- and five-microphone arrays with 1000-point filters, when the input TJR is +20 dB. In this case, the correlation method alone initially has a slight advantage over both modifications. However, this is irrelevant for a practical system since it occurs when the input TJR is +20 dB and the unprocessed speech is already highly intelligible. Although systems using both modifications typically converge more slowly to superior steady-state performance, during the transient they performs at least as well as faster-converging systems without both modifications.

As stated above, the effect of the correlation method of controlling adaptation is to increase the convergence time by a factor equal to the reciprocal of the fraction of cycles for which the system actually adapted. These percentages can be obtained empirically for particular test conditions. Figure 7.19 shows percent of cycles for which the system adapted when the correlation method was used. The trends are roughly the same for two- and five-microphone arrays and for aligned and misaligned arrays. When the input TJR is −20 dB, the system typically adapts at least 80% of the time, and when the input TJR is 0 dB, the system typically adapts 50–70% of the time. Therefore, when the input TJR is 0 dB or lower, the correlation method increases the convergence time at most by a factor of 2. When the input TJR is +20

[5]The length of the first sentence is 3.4 seconds, and the average sentence length is 2.9 seconds. Although there was an onset transient within the first sentence, it was sufficiently short that it did not affect the average powers used to compute G_I for the entire sentence. For these conditions, quantifying the transient performance would require recomputing G_I for short segments of the first sentence. Individual inspection of the output waveforms for a number of these conditions revealed that systems using both modifications typically converged within one second.

dB, the system adapts on 20–30% of cycles.

Next it is useful to consider trends in the transient behavior of the system using both modifications (solid lines in Figs. 7.17 and 7.18). When the input TJR is 0 dB, the system's ability to adapt quickly to new interference sources is likely to have a large effect on intelligibility. Figure 7.17 shows that when the input TJR is 0 dB, the algorithm converges by the end of the first sentence for most conditions. The exception is the five-microphone array in an anechoic environment.

When the five-microphone array operates in the anechoic environment, the adaptive filter has two modes that converge at different rates and have competing effects on G_I. One mode converges more rapidly and cancels the jammer, while the other, slower mode adapts to cancel the misaligned target. Since this second mode of adaptation results in poorer performance, the fact that it converges slowly is actually an advantage. If temporal fluctuations of source and array locations in a real system prevented convergence of that second mode, it would actually be beneficial.

The competing effects of these two modes are seen for the five-microphone array with $L = 100$, and can be better understood by considering the values of the quantities that comprise G_I (not shown). For this condition, G_I is initially 20 dB due to $\Delta\Gamma(J)$. As time passes, the value of $\Delta\Gamma(J)$ rises to 30 dB, while the second mode converges to produce $\Delta\Gamma(T_d)$ of approximately -20 dB, resulting in G_I near 10 dB. For the five-microphone array with $L = 1000$, G_I is roughly constant, but the algorithm is not actually converged. Examination of $\Delta\Gamma(T_d)$ and $\Delta\Gamma(J)$ reveals that with the longer filter, both modes converge slowly and neither mode has reached steady-state at the end of 40 sentences.

Compared to Fig. 7.17, the results shown in Fig. 7.18 are considerably less important for a practical hearing aid. As stated earlier, when the input TJR is +20 dB, the unprocessed signals are already highly intelligible. In this case, the magnitude of G_I is relatively unimportant as long as G_I is positive. Figure 7.18 does show that with both modifications, both two- and five-microphone arrays with 1000-point filters have relatively long convergence times. In both anechoic and moderately reverberant rooms, the convergence time is on the order of 10 sentences (30 seconds). Since source

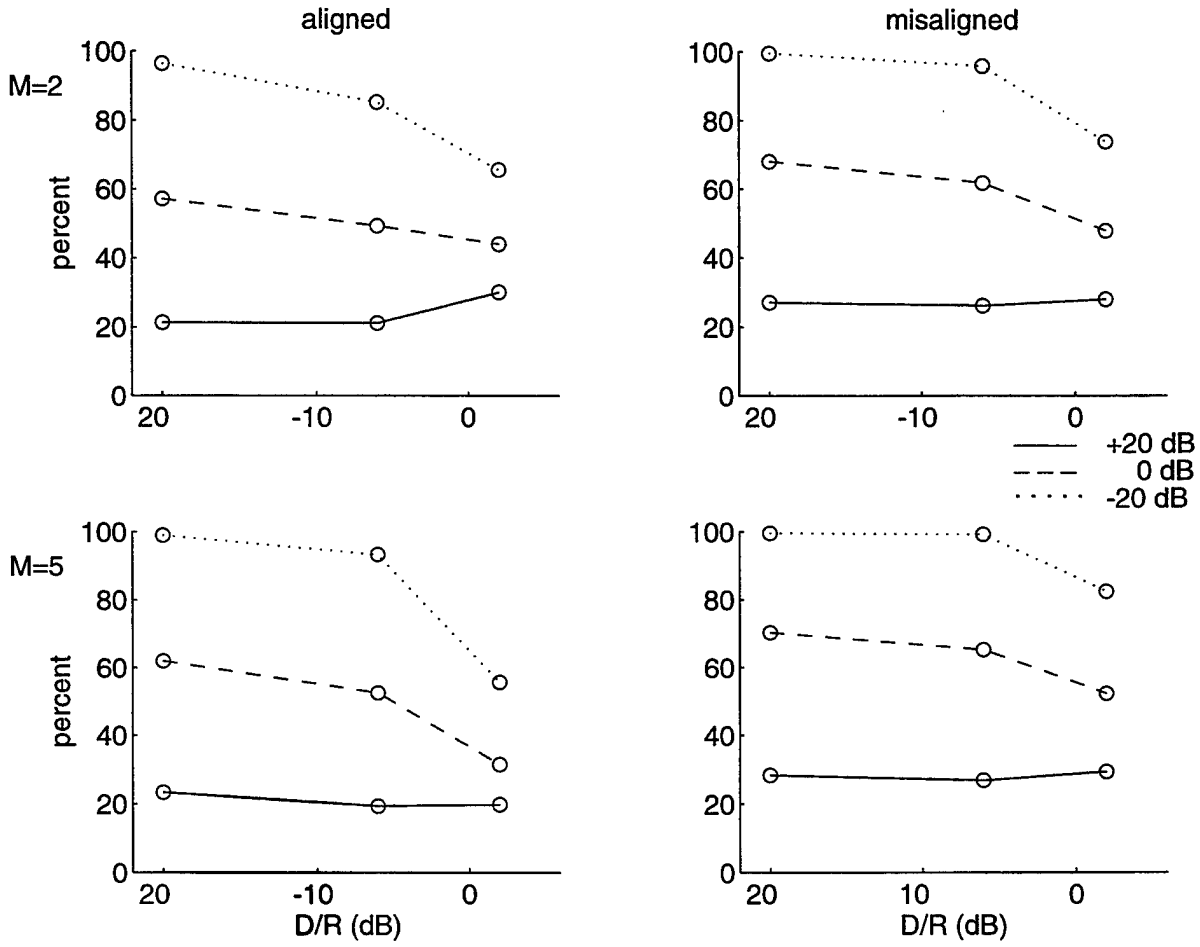

Figure 7-19: Percent of time the system adapted according to the correlation method, versus direct-to-reverberant ratio, for three input TJRs. Anechoic results are shown at a direct-to-reverberant ratio of +20 dB. The two- and five–microphone arrays were either perfectly aligned or misaligned by 10°.

and array locations may not remain constant for that long in a real system, the full benefits may not be realized at high input TJRs.

Because the convergence time is proportional to the total number of adaptive filter taps, it is expected that the 2-microphone array with 100-point filters will converge most quickly, followed by the 5-microphone array with 100-point filters, then the 2-microphone array with 1000-point filters, and finally the 5-microphone array with 1000-point filters. The simulation results match these expectations, best illustrated by the moderate reverberation conditions in Fig. 7.18.

The transient values of G_I shown in Figs. 7.17 and 7.18 are for one target and one jammer adapting from the initial condition with all of the weights equal to zero. A real system is likely to encounter situations where the weights have adapted to one jammer configuration and then an additional jammer appears. If the new jammer comes from a direction where the system's gain is greater than 0 dB (as seen in Fig. 7.9 and the upper half of Fig. 7.10), then this jammer may initially be more disruptive than it would be in the absence of the system. Therefore, there is some advantage to systems with a tendency to maintain the polar pattern less than 0 dB for all angles of incidence, for instance the five-microphone array with 1000-point filters as shown in the lower half of Fig. 7.10.

7.4.2 Summary of transient performance

The transient performance of the systems investigated is summarized as follows:

- For many of the conditions studied, the system converged in less than 3 seconds.
- Although the modifications appear to improve steady-state performance at the expense of slower convergence, even during transients the algorithm with both modifications performs at least as well as faster-converging algorithms without both modifications.
- Although some conditions have extremely long convergence times (30 seconds or longer) these correspond to situations when the benefits of the system may

not be required (very high TJR) and to situations when the slower converging mode is detrimental (target cancellation).

These results indicate that transient behavior of the modified algorithm appears to be sufficient for the current application, based on results of static test conditions. Of course the true test will come from field trials to see how listeners are affected by time-varying jammer configurations. If such tests indicate that the modified LMS algorithm developed here does not provide fast enough convergence, then it will be necessary to investigate other algorithms for adjusting the adaptive filter weights. A promising candidate is the fast affine projection algorithm (Gay, 1993) which provides relatively rapid convergence at low computational complexity. This algorithm is based on a generalization of NLMS and is implemented in the time domain, and therefore can be modified to include the correlation method derived in Ch. 5. Additional investigation is required to determine if this algorithm could also be modified to include the sum method derived in Ch. 4.

Chapter 8

Discussion

The simulation results presented in Ch. 7 provide answers to a number of important questions about the potential of adaptive microphone-array hearing aids. Clearly, these results indicate that the modified algorithm is sufficiently promising to warrant testing with normal-hearing and hearing-impaired listeners in laboratory tests and field trials. However, practical limitations, such as difficulty simulating headshadow, head movements and time-varying jammers, make the simulations inadequate for addressing additional important issues. Two of those issues include the use of *directional microphones* and the *number of microphones* needed in a head-sized array.

The discussion in this chapter first considers the interpretation of the intelligibility-weighted gain, G_I, used as a performance metric in Ch. 7. That is followed by discussions of the issues affecting the number of microphones needed in a head-sized array and the use of directional microphones. Finally, the nature of future laboratory and field tests are considered.

8.1 Interpretation of intelligibility-weighted gain

The intelligibility-weighted gain, G_I, is a useful measure for quantifying the effect of a speech transmission system (Greenberg et al., 1993). However, in judging systems intended for the hearing-aid application, it is necessary to consider the implications for speech intelligibility in interpreting the significance of improvements predicted by

G_I.

The intelligibility of the system output will depend on many factors, including the difficulty of the source material and the degree of reverberation. One very important factor is the intelligibility-weighted target-to-jammer ratio of the system output, $\mathrm{TJR}_{I,\mathrm{out}}$ defined in (3.7). This quantity reflects the intelligibility-weighted target-to-jammer ratio of the input and the intelligibility-weighted gain due to the system, that is,

$$\mathrm{TJR}_{I,\mathrm{out}} = \mathrm{TJR}_{I,\mathrm{in}} + G_I, \tag{8.1}$$

which is obtained from (3.8).

For normal-hearing listeners, target speech is typically intelligible for $\mathrm{TJR}_I = 0$ dB. As a result, when the input TJR[1] is -20 dB, G_I must be roughly $+20$ dB to make the output intelligible. On the other hand, when the input TJR is $+20$ dB, the signals will be highly intelligible without any processing. In that case, positive values of G_I are desirable because the system should not degrade intelligibility, but the magnitude of G_I is relatively unimportant in terms of the intelligibility of the output.

In the hearing-aid application, G_I and $\mathrm{TJR}_{I,\mathrm{out}}$ must be interpreted with respect to hearing-impaired listeners. Studies comparing speech reception thresholds of normal-hearing and hearing-impaired listeners have estimated that the disability of impaired listeners is equivalent to a reduction of 10–13 dB in TJR when the jammer consists of a single competing talker (Festen and Plomp, 1990; Larsby and Arlinger, 1994). Therefore, a system that produces a G_I of approximately 10 dB for moderate levels of input TJR is expected to provide significant benefit to hearing-impaired listeners.

8.2 Number of microphones

How many microphones should be used in a microphone-array hearing aid? There is no simple answer to this question because the number of microphones in the array

[1]Because the input signals were approximately whitened, the unweighted input TJR corresponds to $\mathrm{TJR}_{I,\mathrm{in}}$ within 1 dB for the signals used here.

has a significant impact on many issues. These issues include cancellation of directional sources, robustness of the underlying fixed system in extreme reverberation, complexity of implementation, and the cosmetic acceptability of a practical device.

8.2.1 Directional jammers

As discussed in Sec. 2.3.1, an M-microphone array can form $M-1$ independent broadband nulls. As a result, any array (two or more microphones) will be effective against one directional jammer. The simulation results presented in Ch. 7 show that in the presence of a single jammer source, there is only a slight benefit to having more than two microphones. Previous work has shown that for infinite length filters, once the number of microphones exceeds the number of jammers, little or no additional benefit is obtained by adding more microphones (Peterson, 1989). The current simulation results indicate that for one directional jammer, this is true for finite filters as well.

If the environment contains two independent jammers, an array with more than two microphones can steer nulls in the direction of both jammers, while the behavior of the two-microphone array depends on the relative jammer locations and levels. If the jammers have unequal powers, a two-microphone array will attenuate the stronger of the two jammers, because of the need to minimize total output power, but that attenuation is limited by the need to avoid substantial amplification of the weaker jammer. If the jammers are of equal power and are not located such that the single available null can effectively attenuate both sources, the two-microphone array will perform comparably to the underlying fixed beamformer.

In the presence of a large number of independent, directional jammers, these theoretical considerations suggest that increasing the number of microphones will always improve performance. However, for head-sized arrays and realistic levels of sensor noise, the incremental improvement is negligible beyond 4–6 microphones (Peterson, 1989). This is presumably because for the frequencies and dimensions of interest, additional microphones result in spatial oversampling. The current work considers five-microphone arrays due to this limitation and also to facilitate comparison with

other work on microphone arrays for hearing aids (Soede et al., 1993a,b; Hoffman et al., 1994; Stadler and Rabinowitz, 1993).

The simulation results presented in Ch. 7 also demonstrate one disadvantage of additional microphones. If the number of microphones exceeds the number of independent jammers by two or more, then the system has more degrees of freedom than required to direct nulls at all of the jammers. In this case, if the target is misaligned, an unused degree of freedom may be used to direct a null at the misaligned target.

The interaction between the number of microphones and the number of jammers discussed above could be demonstrated using multiple jammers in computer simulations similar to those described in Ch. 7. However, designing such simulations to provide results *meaningful to the hearing-aid application* is not possible due to a lack of information about commonly encountered acoustic environments. How often do listeners encounter more than one directional jammer? When multiple jammers do exist, what are their angular distributions and relative power levels? Future work should either address these questions before simulating multiple jammer environments or proceed directly to building portable microphone arrays for evaluation in a variety of real acoustic environments encountered in everyday activities.

8.2.2 Reverberation

It is also important to consider the effect of the number of microphones on performance in the presence of extreme reverberation. As discussed in Sec. 7.3.2, the performance of adaptive systems approaches that of the underlying fixed system with increasing reverberation. Also, for the array dimensions and frequency ranges considered here, the number of microphones alone does not have a substantial impact on the intelligibility-weighted directivity for broadside arrays with uniform weights. Therefore, in extreme reverberation, the adaptive system performance measured by G_I will approximate the fixed system performance predicted by D_I, which is not affected by the number of microphones.

A consideration neglected in the previous discussion of fixed array performance is the noise sensitivity, which is a measure of robustness of fixed systems (Stadler and

Rabinowitz, 1993). In general, when arrays with different numbers of microphones provide the same level of intelligibility-weighted directivity (D_I), the array with more microphones will have lower noise sensitivity. For broadside arrays of omnidirectional microphones with uniform weights[2] the noise sensitivity is $\frac{1}{M}$ for all frequencies, that is, -3 dB for the two-microphone array and -7 dB for the five-microphone array, relative to 0 dB for a single omnidirectional element. This indicates that the fixed five-microphone array is more robust to any noise that is uncorrelated between microphones, including internal sensor noise, gain mismatch, and microphone placement error. These sources of error were not considered in Ch. 7, although target misalignment was included in the simulations.

Another issue to consider is the robustness of the underlying fixed array in the presence of headshadow. The design and analysis of fixed arrays is based on the assumption that the array is in free space, while the application requires that the array be worn on the head. Soede et al. (1993a) showed that although polar patterns are substantially different for array responses measured in free space and on a mannikin, the frequency-dependent directivity indices are comparable. In particular, for a 10-cm endfire array of five cardioid microphones along the temple of eyeglass frames, the directivity index was about 1 dB lower when the array was on the head, relative to free space. For a 14-cm broadside array along the front of eyeglass frames, the directivity index was similar for measurements made in free space and on the head. For the broadside array, some frequencies showed improved directivity because the head provided additional attenuation of sources arriving from the rear. Future work should consider comparable two-microphone arrays to determine if the number of microphones affects the robustness of fixed arrays to headshadow effects.[3]

[2]This corresponds to the underlying fixed array for the systems considered in Ch. 7.

[3]It has been shown that two-microphone *adaptive* arrays are robust to the effects of headshadow (Greenberg and Zurek, 1992).

8.2.3 Summary of advantages of two- and five-microphone arrays

Based on the results of computer simulations, it is not possible to recommend the number of sensors required in a microphone-array hearing aid. However, the relevant issues are the following.

The five-microphone array is

- more effective against multiple jammers, and
- more robust in extreme reverberation (due to lower noise sensitivity of the underlying fixed beamformer).

The two-microphone array is

- less susceptible to target cancellation for the same number of jammers,
- simpler to implement (in both hardware and software), and
- more cosmetically acceptable (two ear-level devices rather than five elements on eyeglass frames or a headband).

Some of the advantages (and disadvantages) of two- and five-microphone arrays could be combined in a system that uses the average of five microphone signals for the primary channel, and the difference between two of those signals as the input to a single reference channel. Such a system would combine the robustness of a five-microphone fixed system with the resistance of the two-microphone system to target cancellation. It would also require less computation than the five-microphone system with four reference channels. However, it would still require the user to wear an array of five microphones and would not steer independent nulls against multiple directional jammers. Even so, such a system may be appropriate if future studies indicate that the increased robustness of a five-microphone array is required and that multiple directional jammers are rarely encountered in everyday listening environments.

8.3 Directional microphones

The motivation for using directional microphones in microphone-array hearing aids is the desire to improve jammer cancellation, particularly in extreme reverberation. Since the performance of an adaptive system approaches that of the underlying fixed system in extreme reverberation, an obvious approach is to maximize the directivity of the underlying fixed system. The design of fixed arrays for maximal directivity has been studied extensively in the context of the hearing-aid application (Soede et al., 1993a,b; Stadler and Rabinowitz, 1993; Kates, 1993). One way to improve the directivity of fixed arrays is the use of directional microphones. Other researchers have also considered the use of directional microphones in adaptive arrays (Weiss, 1987; Schwander and Levitt, 1987; McKinney and DeBrunner, 1994).

The theoretical polar patterns of cardioid, supercardioid, and hypercardioid microphones, which are independent of frequency, are shown in Fig. 8.1. The directional microphones provide a gain of 0 dB to straight-ahead target sources and attenuate jammers arriving from all other directions. For directional jammers, the amount of attenuation depends on the angle of arrival. Figure 8.1 shows that a jammer arriving from 45° is attenuated roughly 2 dB by all three directional microphones, while a jammer arriving from 90° is attenuated 6 dB, 9 dB, and 12 dB by cardioid, supercardioid, and hypercardioid microphones, respectively. For jammers approaching a diffuse field, such as in extreme reverberation, the amount of attenuation provided by a single microphone is given by its directivity: 4.7 dB, 5.6 dB, and 6.0 dB for cardioid, supercardioid, and hypercardioid microphones, respectively, where all values are relative to 0 dB for a single omnidirectional microphone.

Stadler and Rabinowitz (1993) studied fixed systems based on omnidirectional and directional microphones in 14-cm broadside arrays and 11-cm endfire arrays. They considered arrays of two to seven elements and various methods of selecting the fixed weights. Their results for broadside arrays show that regardless of the type of microphone, the more complex weighting schemes provide only slight improvements in directivity over uniform weights, and at a cost of increased noise sensitivity. That

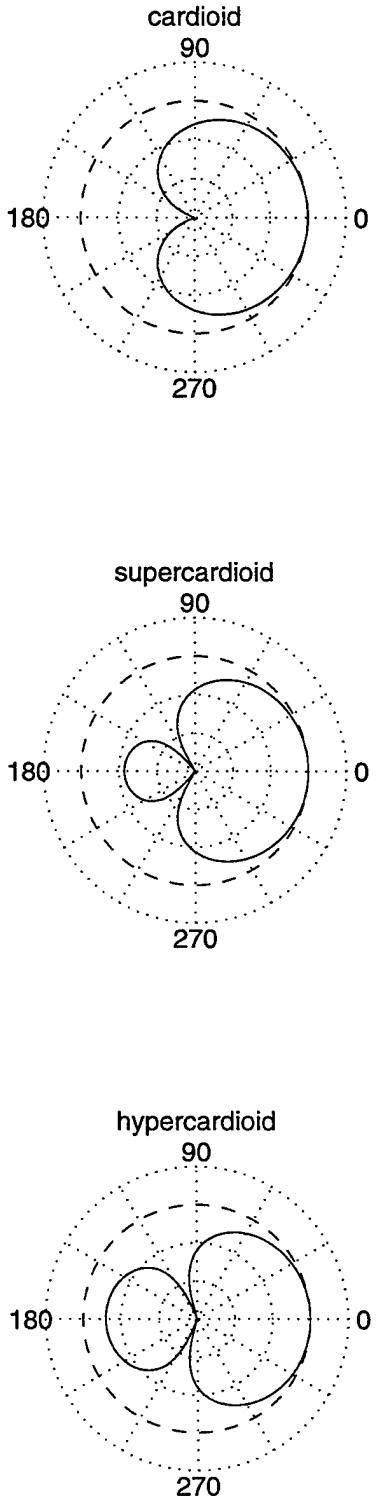

Figure 8-1: Polar responses of single directional microphones; cardioid (top), supercardioid (middle), and hypercardioid (bottom).

	number of microphones					
	1		2		5	
microphone type	D_I	Ψ_I	D_I	Ψ_I	D_I	Ψ_I
omnidirectional	0.0	0.0	2.5	−3.0	2.6	−7.0
cardioid	4.7	7.9	7.1	4.9	7.1	0.9
supercardioid	5.6	5.3	7.8	2.3	8.1	−1.7

Table 8.1: Values of intelligibility-weighted directivity, D_I, and intelligibility-weighted noise sensitivity, Ψ_I, both in dB, for a single microphone or a 14-cm broadside array with uniform weights. All values taken from Stadler and Rabinowitz (1993), except those for a two-microphone array of omnidirectional elements, which were computed using equivalent methods.

result indicates that obtaining the primary channel from the mean of the microphone signals (uniform weights) is sufficient in the current application.

Stadler and Rabinowitz (1993) calculated intelligibility-weighted directivities, D_I, and noise sensitivities, Ψ_I, for 14-cm broadside arrays of two and five elements using uniform weights with omnidirectional and directional microphones.[4] Table 8.1 summarizes values relevant to the current discussion. These results show that for fixed arrays of constant length, additional microphones have little effect on directivity, but do improve the noise sensitivity, as discussed in Secs. 7.3.2 and 8.2.2. Clearly, using either cardioid or supercardioid microphones instead of omnidirectional ones provides substantial improvements in directivity, with tolerable levels of noise sensitivity.

It is also necessary to consider the effect of directional microphones on the performance of the adaptive system against directional jammers. Obviously, the use of directional elements will have a large and beneficial effect against jammers arriving from behind, because they eliminate the front-back symmetry of broadside arrays. As discussed above, the directional elements have no effect on the target signal and attenuate directional jammers by an amount that depends on the angle of arrival. That attenuation is effectively a shift in the TJR of the input signals seen by the adaptive system. For jammers arriving from forward directions, directional elements will shift

[4]In that work, the microphones referred to as hypercardioids are actually supercardioids.

the input TJR by less than 6–12 dB, depending on the type of microphones used. However, since the modified algorithm based on the methods presented in Chs. 4 and 5 is robust to changes in input TJR, the use of directional microphones should not have a large effect on the performance of the adaptive system.

The computer simulations of Ch. 7 could be modified to incorporate directional microphones, but the results of those simulations can already be predicted. Because the jammer was located at either 45° or 55°, including directional microphones is equivalent to shifting the input TJR by 2 dB for the anechoic condition, and the results would not differ substantially from those obtained with omnidirectional microphones. For the reverberant conditions, the performance would improve to the extent that the directional microphones increase attenuation of reflections from all directions. In strong reverberation, the performance of the underlying fixed system would increase to roughly 7–8 dB, from the 1–3 dB shown by the rightmost 'x' in each plot in Fig. 7.4.

From the above discussion, it is clear that using directional elements in microphone-array hearing aids should have a beneficial effect on the performance in reverberation, with no cost in performance or processing. Therefore, arrays constructed for future evaluations should incorporate directional microphones.

8.4 Laboratory and field tests

The preceding sections have identified a number of issues that cannot be adequately investigated by computer simulations. Future work should focus on construction and evaluation of prototype systems with two- and five-microphone arrays of directional elements. The evaluations should be designed to study robustness to headshadow and head movements, to confirm the benefits predicted by the simulations, to assess the response in the presence of time-varying jammer sources, and to study the number of microphones required, that is, the number of independent jammers commonly encountered in real environments.

The first set of tests to be performed with a real system should consider robustness to headshadow via physical measurements. For evaluating the underlying fixed sys-

tem, testing should compare the polar patterns and directivities with the array in free space and on a mannikin, as measured by Soede et al. (1993a) for a five-microphone array of cardioid elements. Similar measurements of polar patterns in free space and on a mannikin head should be made for adaptive systems in the presence of directional jammers in anechoic environments and in moderate reverberation.

In addition, physical measurements should be made in the presence of head movements, to verify that the additional benefits of long adaptive filters can be obtained under realistic conditions, as discussed in Sec. 7.3.2. Previous work (Schwander and Levitt, 1987) has considered the effect of head movements on word recognition scores of normal-hearing subjects listening to speech processed by an adaptive noise canceller in a reverberant room. That system used an 800-point (80 ms) adaptive filter and obtained the reference input from a cardioid microphone mounted on the listener's head and facing toward the rear. Their results showed that although head movements reduce the effectiveness of the noise reduction process, that reduction is small relative to the benefit of the processing. Future work should include physical measurements to assess the effect of head movements on the generalized sidelobe canceller, in order to quantify the practical benefits of long filters in reverberation.

The next step is to perform intelligibility tests with normal-hearing and hearing-impaired listeners. These tests should confirm the improvements predicted by the simulations in a controlled environment, that is, with known direct-to-reverberant ratio, input TJR, number of jammers, and jammer locations. In addition to measuring intelligibility, these tests should solicit the subjects' subjective impressions and attempt to quantify any other effects of the processing, such as ease of listening, annoyance, etc. Introducing time-varying jammers under these controlled conditions will also allow assessment of the algorithm's transient behavior and its effect on both intelligibility and ease of listening.

Finally, construction of a battery-powered, wearable prototype will allow field tests with hearing-impaired listeners. These tests will assess the potential of the systems in real acoustic environments, rather than in a controlled laboratory setting. The listener will be exposed to time-varying jammers, various numbers of jammers, differ-

ent levels of reverberation, and a range of input TJRs. Quantifying the performance of systems outside of the laboratory will require developing a simple rating method for the listener to use. It will also be useful to develop a monitoring scheme that stores samples of the adaptive filter weights, the intermicrophone correlation, and other measures obtained by the system. This information can be used to determine how often the adaptive algorithm is significant[5] and to provide information about the types and frequency of acoustic environments encountered by the listener in everyday activities.

[5]When the weights are close to zero, the adaptive system performance is not substantially different from that of the underlying fixed system.

Chapter 9

Conclusion

This work is part of a larger project concerned with the development of microphone-array hearing aids. As described in Ch. 2, previous work consisted of computing theoretical performance limits (Peterson, 1989) and evaluating practical systems (Peterson et al., 1990; Greenberg and Zurek, 1992). Those evaluations revealed several problems with the generalized sidelobe canceller and led to the development of two *ad hoc* modifications to the adaptive algorithm. The current work uses both theoretical analysis and computer simulations to formalize previously proposed modifications, specifies a modified algorithm for use in an adaptive microphone-array hearing aid, and demonstrates the benefits of that algorithm in a variety of simulated acoustic environments. Concurrent work (Welker, 1994) has considered adaptive arrays with binaural outputs, to prevent "tunnel hearing" imposed by a directional hearing aid with a monaural output. Future work will consist of implementing the proposed systems in real-time for evaluations in laboratory and field trials.

The current work contains a thorough analysis of previously proposed methods for controlling adaptation and provides guidelines for parameter selection applicable in reverberation and for arbitrary numbers of microphones (Chs. 4 and 5). It also contains an analysis of the specific causes of target cancellation in reverberation and reveals that a simple parameter choice can solve this problem (Ch. 6). The results of Chs. 4–6 lead to specification of a modified algorithm for use in adaptive microphone-array hearing aids.

The modified algorithm was implemented and evaluated in computer simulations. Chapter 7 contains the results of those simulations, which serve three purposes. First, they demonstrate the effectiveness of the modifications and parameter choices determined in Chs. 4–6. Second, they illustrate the levels of performance provided by practical systems using different filter lengths, L, and numbers of microphones, M, in a variety of acoustic environments. Finally, they identify issues for further investigation with a real-time system in laboratory and field tests. Chapter 8 consists of a discussion of issues not resolved by the computer simulations and includes recommendations for future work.

The result of this work is the specification of a relatively simple and robust broadside adaptive array that is expected to provide a *minimum* of 7 dB interference reduction in a very reverberant sound field, and much greater reduction when the interference arrives predominantly via the direct path. In particular, this work supports the following conclusions:

- The modified adaptive algorithm makes the generalized sidelobe canceller robust to the problems of misalignment and misadjustment, which occur predominantly at high TJR (Sec. 7.3.1). The modifications consist of the sum method of normalizing the step-size parameter in the LMS algorithm (Ch. 4) and the correlation method of controlling adaptation (Ch. 5).

- Using a relatively short primary delay prevents cancellation of the direct target due to target reflections (Ch. 6).

- Very large intelligibility-weighted gains can be achieved in relatively anechoic environments; the size of the gains decreases with increasing reverberation. Substantial benefits are often provided in moderate reverberation, particularly if relatively long filters ($\sim$ 100 ms) are used. In extreme reverberation, the performance approaches that obtained using the underlying fixed system (Sec. 7.3.2). This asymptotic performance can be improved by using arrays of directional microphones (Sec. 8.3).

- In many realistic environments, convergence of the modified algorithm is sufficiently rapid for processing speech signals (Sec. 7.4).

- In the presence of a single jammer source, there is no advantage to using more than two microphones (Sec. 7.3.2). Additional investigations are required to determine whether more than two microphones are beneficial when operating in commonly encountered acoustic environments (Sec. 8.2).

- Real-time processors must be constructed to confirm the benefits predicted by the simulations and to permit evaluation by human listeners under realistic acoustic conditions that include headshadow, head movements, and time varying jammers (Sec. 8.4).

Appendix A

The problem addressed in this appendix is the convolution of the approximate target pdf given by (5.16) with the jammer pdf given by (5.8), according to (5.15). Those equations are reproduced here using the unit step function, $u(t)$, to indicate the ranges over which they are nonzero:

$$\hat{f}_{\rho_t}(\rho) = \frac{(u(\rho - \cos(kd\sin\theta_0)) - u(\rho - 1))}{2(1 - \cos(kd\sin\theta_0))} + \frac{1}{2}\delta(\rho - 1) \tag{A.1}$$

$$f_{\rho_j}(\rho) = \frac{(u(\rho - \cos(kd)) - u(\rho - \cos(kd\sin\theta_0)))}{(\frac{\pi}{2} - \theta_0)\sqrt{(kd)^2 - (\arccos\rho)^2}\sqrt{1-\rho^2}} \tag{A.2}$$

$$f_{\rho_d|Y}(\rho|Y) = \hat{f}_{\rho_t}\left(\frac{Y+1}{Y}\rho\right) * f_{\rho_j}((Y+1)\rho). \tag{A.3}$$

The two expressions to be convolved are determined by making the appropriate substitutions in (A.1) and (A.2):

$$\hat{f}_{\rho_t}\left(\frac{Y+1}{Y}\rho\right) = \frac{(Y+1)(u(\rho - \frac{Y}{Y+1}\cos(kd\sin\theta_0)) - u(\rho - \frac{Y}{Y+1}))}{2Y(1 - \cos(kd\sin\theta_0))} + \frac{1}{2}\delta\left(\rho - \frac{Y}{Y+1}\right) \tag{A.4}$$

and

$$f_{\rho_j}((Y+1)\rho) = \frac{(Y+1)(u(\rho - \frac{1}{Y+1}\cos(kd)) - u(\rho - \frac{1}{Y+1}\cos(kd\sin\theta_0)))}{(\frac{\pi}{2} - \theta_0)\sqrt{(kd)^2 - (\arccos((Y+1)\rho))^2}\sqrt{1-((Y+1)\rho)^2}}. \tag{A.5}$$

There are two cases that result from this convolution, with each case having three distinct regions. Case A occurs when the jammer pdf is wider than the target pdf,

that is, when

$$Y < \frac{\cos(kd\sin\theta_0) - \cos(kd)}{1 - \cos(kd\sin\theta_0)} = Y_0. \tag{A.6}$$

Case B occurs when the target pdf is wider than the jammer pdf, that is, when

$$Y > \frac{\cos(kd\sin\theta_0) - \cos(kd)}{1 - \cos(kd\sin\theta_0)} = Y_0. \tag{A.7}$$

For Case A, the three regions of interest are bounded by

$$\rho_1 = \frac{Y\cos(kd\sin\theta_0) + \cos(kd)}{Y+1} \tag{A.8}$$

$$\rho_{2a} = \frac{Y + \cos(kd)}{Y+1} \tag{A.9}$$

$$\rho_{3a} = \frac{Y\cos(kd\sin\theta_0) + \cos(kd\sin\theta_0)}{Y+1} = \cos(kd\sin\theta_0) \tag{A.10}$$

$$\rho_4 = \frac{Y + \cos(kd\sin\theta_0)}{Y+1}. \tag{A.11}$$

The conditional pdf is determined by substituting (A.4) and (A.5) into (A.3), giving

$$\begin{aligned} f_{\rho_d|Y}(\rho|Y) &= \int f_{\rho_j}((Y+1)\rho_0)\hat{f}_{\rho_t}\left(\rho - \frac{Y+1}{Y}\rho_0\right) d\rho_0 \\ &= \frac{Y+1}{2(\frac{\pi}{2} - \theta_0)} \\ &\quad \left\{ \int_{\frac{\cos(kd)}{Y+1}}^{\rho - \frac{Y}{Y+1}\cos(kd\sin\theta_0)} X(\rho,\rho_0)\, d\rho_0\, [u(\rho-\rho_1) - u(\rho-\rho_{2a})] \right. \\ &\quad + \int_{\rho - \frac{Y}{Y+1}}^{\rho - \frac{Y}{Y+1}\cos(kd\sin\theta_0)} X(\rho,\rho_0)\, d\rho_0\, [u(\rho-\rho_{2a}) - u(\rho-\rho_{3a})] \\ &\quad \left. + \int_{\rho - \frac{Y}{Y+1}}^{\frac{\cos(kd\sin\theta_0)}{Y+1}} X(\rho,\rho_0)\, d\rho_0\, [u(\rho-\rho_{3a}) - u(\rho-\rho_4)] \right\}, \end{aligned} \tag{A.12}$$

for $Y < Y_0$, where

$$\begin{aligned} X(\rho,\rho_0) &= \frac{1}{\sqrt{(kd)^2 - (\arccos((Y+1)\rho_0))^2}\sqrt{1-((Y+1)\rho_0)^2}} \\ &\quad \left(\frac{Y+1}{Y(1-\cos(kd\sin\theta_0))} + \delta\left(\rho - \rho_0 - \frac{Y}{Y+1}\right)\right). \end{aligned} \tag{A.13}$$

Integrating (A.13) produces

$$\int X(\rho,\rho_0)\,d\rho_0 = \frac{-\arcsin\left(\frac{\arccos((Y+1)\rho_0)}{kd}\right)}{Y(1-\cos(kd\sin\theta_0))} + \frac{1}{\sqrt{(kd)^2-(\arccos((Y+1)\rho-Y))^2}\sqrt{1-((Y+1)\rho-Y)^2}} + C \quad \text{(A.14)}$$

where C is any constant. Substituting (A.14) into (A.12) produces the result for Case A:

$$\begin{aligned}
f_{\rho_d|Y}(\rho|Y) = & \\
& \frac{Y+1}{2Y(\frac{\pi}{2}-\theta_0)(1-\cos(kd\sin\theta_0))} \\
& \left\{\left[\frac{\pi}{2}-\arcsin\left(\frac{\arccos((Y+1)\rho-Y\cos(kd\sin\theta_0))}{kd}\right)\right][u(\rho-\rho_1)-u(\rho-\rho_{2a})] \right. \\
& + \left[\frac{Y(1-\cos(kd\sin\theta_0))}{\sqrt{kd^2-(\arccos(\rho(Y+1)-Y))^2}\sqrt{1-(\rho(Y+1)-Y)^2}}\right. \\
& \left. + \arcsin\left(\frac{\arccos((Y+1)\rho-Y)}{kd}\right)-\arcsin\left(\frac{\arccos((Y+1)\rho-Y\cos(kd\sin\theta_0))}{kd}\right)\right] \\
& [u(\rho-\rho_{2a})-u(\rho-\rho_{3a})] \\
& + \left[\frac{Y(1-\cos(kd\sin\theta_0))}{\sqrt{kd^2-(\arccos(\rho(Y+1)-Y))^2}\sqrt{1-(\rho(Y+1)-Y)^2}}\right. \\
& \left.\left. \arcsin\left(\frac{\arccos((Y+1)\rho-Y)}{kd}\right)-\theta_0\right][u(\rho-\rho_{3a})-u(\rho-\rho_4)]\right\}. \qquad \text{(A.15)}
\end{aligned}$$

Similarly, for Case B, the three regions of interest are bounded by

$$\rho_1 = \frac{Y\cos(kd\sin\theta_0)+\cos(kd)}{Y+1} \quad \text{(A.16)}$$

$$\rho_{2b} = \cos(kd\sin\theta_0) = \rho_{3a} \quad \text{(A.17)}$$

$$\rho_{3b} = \frac{Y+\cos(kd)}{Y+1} = \rho_{2a} \quad \text{(A.18)}$$

$$\rho_4 = \frac{Y+\cos(kd\sin\theta_0)}{Y+1}. \quad \text{(A.19)}$$

The conditional pdf is again determined by substituting (A.4) and (A.5) into (A.3),

this time for $Y > Y_0$, giving

$$
\begin{aligned}
f_{\rho_d|Y}(\rho|Y) &= \int f_{\rho_j}((Y+1)\rho_0)\hat{f}_{\rho_t}\left(\rho - \frac{Y+1}{Y}\rho_0\right) d\rho_0 \\
&= \frac{Y+1}{2(\frac{\pi}{2}-\theta_0)} \\
&\quad \left\{ \int_{\frac{\cos(kd)}{Y+1}}^{\rho-\frac{Y}{Y+1}\cos(kd\sin\theta_0)} X(\rho,\rho_0)\, d\rho_0 \; [u(\rho-\rho_1) - u(\rho-\rho_{2b})] \right. \\
&\quad + \int_{\frac{\cos(kd)}{Y+1}}^{\frac{\cos(kd\sin\theta_0)}{Y+1}} X(\rho,\rho_0)\, d\rho_0 \; [u(\rho-\rho_{2b}) - u(\rho-\rho_{3b})] \\
&\quad \left. + \int_{\rho-\frac{Y}{Y+1}}^{\frac{\cos(kd\sin\theta_0)}{Y+1}} X(\rho,\rho_0)\, d\rho_0 \; [u(\rho-\rho_3) - u(\rho-\rho_{a4})] \right\}. \qquad \text{(A.20)}
\end{aligned}
$$

which is identical to (A.12) except for the limits on the second integral. Substituting (A.14) into (A.20) produces the result for Case B:

$$
\begin{aligned}
&f_{\rho_d|Y}(\rho|Y) = \\
&\frac{Y+1}{2Y(\frac{\pi}{2}-\theta_0)(1-\cos(kd\sin\theta_0))} \\
&\left\{ \left[\frac{\pi}{2} - \arcsin\left(\frac{\arccos((Y+1)\rho - Y\cos(kd\sin\theta_0))}{kd} \right) \right] [u(\rho-\rho_1) - u(\rho-\rho_{2a})] \right. \\
&+ \left(\frac{\pi}{2}-\theta_0\right) [u(\rho-\rho_{2b}) - u(\rho-\rho_{3b})] \\
&+ \left[\frac{Y(1-\cos(kd\sin\theta_0))}{\sqrt{kd^2 - (\arccos(\rho(Y+1)-Y))^2}\sqrt{1-(\rho(Y+1)-Y)^2}} \right. \\
&\left. \left. \arcsin\left(\frac{\arccos((Y+1)\rho - Y)}{kd} \right) - \theta_0 \right] [u(\rho-\rho_{3a}) - u(\rho-\rho_4)] \right\}. \qquad \text{(A.21)}
\end{aligned}
$$

References

Alexander, S. T. (1986). *Adaptive Signal Processing.* (Springer-Verlag, NY).

ANSI (1969). *American National Standard Methods for the Calculation of the Articulation Index,* ANSI S3.5-1969 (American National Standards Institute, NY).

Beranek, L.L. (1954). *Acoustics.* (American Institute of Physics, NY).

Bershad, N.J. (1987). "On the optimum gain parameter in LMS adaptation," IEEE Trans. Acoustics, Speech, and Signal Processing **35**, 1065–1068.

Brey, R.H., Robinette, M.S., Chabries, D.M., and Christiansen, R.W. (1987). "Improvement in speech intelligibility in noise employing an adaptive filter with normal and hearing-impaired subjects," J. Rehab. Res. Dev. **24**, 75–86.

Chabries, D.M., Christiansen, R.W., Brey, R.H., Robinette, M.S., and Harris, R.W. (1987). "Application of adaptive digital signal processing to speech enhancement for the hearing impaired," J. Rehab. Res. Dev. **24**, 65–74.

Chazan, D., Medan, Y., and Shvadron, U. (1987). "Evaluation of adaptive multimicrophone algorithms for hearing aids," J. Rehab. Res. Dev. **24**, 111–118.

Claesson, I., Nordholm, S.E., Begntsson, B.A., and Eriksson, P. (1991). "A multi-DSP implementation of a broad-band adaptive beamformer for use in a hands-free mobile radio telephone," IEEE Trans. Vehicular Technology **40**, 194–202.

Claasen, T.A.C.M. and Mecklenbrauker, W.F.G. (1981). "Comparison of the convergence of two algorithms for adaptive FIR digital filters," IEEE Trans. Acoustics, Speech, and Signal Processing **29**, 670–678.

Cox, H., Zeskind, R.M., and Kooij, T. (1986). "Practical supergain," IEEE Trans. Acoustics, Speech, and Signal Processing **34** 393–398.

Cremer, L. and Müller, H.A. (1982). *Principles and Applications of Room Acoustics,* translated by T. J. Schultz. (Applied Science Publishers, NY).

Dillier, N., Frölich, T., Kompis, M., Bögli, H., and Lai, W.K. (1993). "Digital signal processing (DSP) applications for multiband loudness correction digital hearing aids and cochlear implants," J. Rehab. Res. Dev. **30**, 95–109.

Dillon, H. and Lovegrove, R. (1993). "Single-microphone noise reduction systems for hearing aids: a review and an evaluation," in *Acoustical Factors Affecting Hearing Aid Performance*, second edition, edited by G.A. Studebaker and I. Hochberg. (Allyn and Bacon, Boston).

Drake, A.W. (1967). *Fundamentals of Applied Probability Theory.* (McGraw-Hill, New York).

Durlach, N.I. and Colburn, H.S. (1978). "Binaural phenomena," in E.C. Carterette and M.P. Friedman (eds.) *Handbook of Perception, Vol. 4: Hearing.* (Academic Press, NY), 360–466.

Duttweiler, D.L. (1982). "Adaptive filter performance with nonlinearities in the correlation multiplier," IEEE Trans. Acoustics, Speech, and Signal Processing **30**, 578–586.

Farassopoulos, A. (1992). *Speech enhancement for hearing aids using real time adaptive filtering techniques.* Ph.D. Thesis, Ecole Polytechnique Federale de Lausanne.

Festen, J.M. and Plomp, R. (1990). "Effects of fluctuating noise and interfering speech on the speech-reception threshold for impaired and normal hearing," J. Acoust. Soc. Am. **88**, 1725–1736.

Feuer, A. and Weinstein, E. (1985). "Convergence analysis of LMS filters with uncorrelated Gaussian data," IEEE Trans. Acoustics, Speech, and Signal Processing **33**, 222–230.

Fisher, B. and Bershad, N.J. (1983). "The complex LMS adaptive algorithm — Transient weight mean and covariance with applications to the ALE," IEEE Trans. Acoustics, Speech, and Signal Processing **31**, 34–44.

Flanagan, J.L., Berkley, D.A., Elko, G.W., West, J.E., and Sondhi, M.M. (1991). "Autodirective microphone systems," Acustica **73**, 58–71.

Frost, O.L. (1972). "An algorithm for linearly constrained adaptive array processing," Proc. IEEE **60**, 926–935.

Gardner, W.A. (1987). "Nonstationary learning characteristics of the LMS algorithm," IEEE Trans. Circuits and Systems **34**, 1199–1207.

Gay, S.L. (1993). "A fast converging, low complexity adaptive filtering algorithm," presented at IEEE Workshop on Applications of Signal Processing to Audio and Acoustics, Mohonk, NY.

Golub, G.H. and Van Loan, C.F (1983). *Matrix Computations.* (Johns Hopkins University Press, Baltimore, MD).

Goulding, M.M. and Bird, J.S. (1990). "Speech enhancement for mobile telephony," IEEE Trans. Vehicular Technology **39**, 316–326.

Greenberg, J.E. (1989). *A real-time adaptive-beamforming hearing aid.* S.M. Thesis, M.I.T.

Greenberg, J.E. and Zurek, P.M. (1992). "Evaluation of an adaptive-beamforming method for hearing aids," J. Acoust. Soc. Am. **91**, 1662–1676.

Greenberg, J.E., Peterson, P.M., and Zurek, P.M. (1993). "Intelligibility-weighted measures of speech-to-interference ratio and speech system performance," J. Acoust. Soc. Am. **94**, 3009–3010.

Grenier, Y. (1993). "A microphone array for car environments," Speech Communication **12**, 25–39.

Griffiths, L.J. and Jim., C.W. (1982). "An alternative approach to linearly constrained adaptive beamforming," IEEE Trans. Antennas and Propagation **30**, 27–34.

Harris, R.W., Chabries, D.M., and Bishop, F.A. (1986). "A variable step (VS) adaptive filter algorithm," IEEE Trans. Acoustics, Speech, and Signal Processing **34**, 309–316.

Harrison, W.A., Lim, J.S., and Singer, E. (1986). "A new application of adaptive noise cancellation," IEEE Trans. Acoustic, Speech, and Signal Processing **ASSP-34**, 21–27.

Haykin, S.S. (1986). *Adaptive Filter Theory.* (Prentice Hall, Englewood Cliffs, NJ).

Haykin, S.S. (1991). *Adaptive Filter Theory*, second edition. (Prentice Hall, Englewood Cliffs, NJ).

Haykin, S.S., ed. (1985). *Array Signal Processing.* (Prentice Hall, Englewood Cliffs, NJ).

Hoffman, M.W. (1992). *Robust microphone array processing for speech enhancement in hearing aids.* Ph.D. Thesis, University of Minnesota.

Hoffman, M.W., Buckley, K.M., Link, M.J., and Soli, S. (1991). " Robust microphone array processor incorporating headshadow effects," Proc. IEEE Int. Conf. Acoustics, Speech, and Signal Processing **ICASSP-91**, 3637-3640.

Hoffman, M.W., Trine, T.D., Buckley, K.M., and Van Tasell, D.J. (1994). "Robust adaptive microphone array processing for hearing aids: Realistic speech enhancement," J. Acoust. Soc. Am. **96**, 759–770.

Höge, H. (1975). "Analysis of an adaptive echo canceller with optimized gradient gain," Siemens Res. Dev. Rep. **4**, 127–131.

Horowitz, L.L. and Senne, K.D. (1981). "Performance advantage of complex LMS for controlling narrow-band adaptive arrays," IEEE Trans. Acoustics, Speech, and Signal Processing **29**, 722–736.

Houtgast, T., Steeneken, H.J.M., and Plomp, R. (1980). "Predicting speech intelligibility in rooms from the modulation transfer function. I. General room acoustics," Acustica **46**, 60–72.

Hsia, T.C. (1983). "Convergence analysis of LMS and NLMS adaptive algorithms", Proc. IEEE Int. Conf. Acoustics, Speech, and Signal Processing, **83**, 667–670.

IEEE (1969). "IEEE recommended practice for speech quality measurements," IEEE, NY.

Jeyendran, B. and Reddy, V.U. (1990). "Recursive system identification in the presence of burst disturbance," Signal Proc. **20**, 227–245.

Johnson, D.H. and Dudgeon, D.E. (1993). *Array Signal Processing.* (Prentice Hall, Englewood Cliffs, NJ).

Kalikow, D.N., Stevens, K.N., and Elliott, L.L. (1977). "Development of a test of speech intelligibility in noise using sentence materials with controlled word predictability," J. Acoust. Soc. Am. **61**, 1337–1351.

Kaneda, Y. and Ohga, J. (1986). "Adaptive microphone-array system for noise reduction," IEEE Trans. Acoustics, Speech, and Signal Processing, **34**, 1391–1400.

Karni, S. and Zeng, G. (1989). "A new convergence factor for adaptive filters," IEEE Trans. Circuits and Systems **36**, 1011–1012.

Kates, J.M. (1993). "Superdirective arrays for hearing aids," J. Acoust. Soc. Am. **94**, 1930–1933.

Kohlmeier, B., Peissig, J., Hohmann, V. (1993). "Real-time multiband dynamic compression and noise reduction for binaural hearing aids," J. Rehab. Res. Dev. **30**, 82–94.

Kompis, M. (1993). *Der adaptive Beamformer: Evaluation eines Verfahrens zur Störgeräuschunterdrückung für Hörgeräte.* Ph.D. Thesis, Eidgenössischen Technischen Hochschule Zürich.

Kompis, M. and Dillier, N. (1991). "Noise reduction for hearing aids: Evaluation of the adaptive beamformer approach," Proc. Int. Conf. IEEE Engineering in Medicine and Biology Soc., **13** 1887–1888.

Kryter, K.D. (1962). "Methods for calculation and use of the articulation index," J. Acoust. Soc. Am. **34**. 1689–1697.

Larsby, B. and Arlinger, S. (1994). "Speech recognition and just-follow-conversation tasks for normal-hearing and hearing-impaired listeners with different maskers," Audiology **33** 165–176.

Lim, J.S. and Oppenheim, A.V. (1979). "Enhancement and bandwidth compression of noisy speech," Proc. IEEE **67**, 1586–1604.

Link, M.J. (1994). *Experimental spatial filtering and array calibration for speech enhancement.* Ph.D. Thesis, University of Minnesota.

Link, M.J. and Buckley, K.M. (1993). "Prewhitening for intelligibility gain in hearing aid arrays," J. Acoust. Soc. Am. **93**, 2139–2145.

Lu, M.H. and Clarkson, P.M. (1993). "The performance of adaptive noise cancellation systems in reverberant rooms," J. Acoust. Soc. Am. **93**, 1122–1135.

Makino, S., Kaneda, Y., and Koizumi, N. (1993). "Exponentially weighted stepsize NLMS adaptive filter based on the statistics of a room impulse response," IEEE Trans. Speech and Audio Processing **1**, 101–108.

Mathews, V.J. and Cho, S.H. (1987). "Improved convergence analysis of stochastic gradient adaptive filters using the sign algorithm," IEEE Trans. Acoustics, Speech, and Signal Processing, **35**, 450–454.

McConnell, M.V. (1985). *A two-microphone speech enhancement system for monaural listening.* S.M. Thesis, M.I.T.

McKinney, E.D. and DeBrunner, V.E. (1994). "A directional adaptive LMS acoustic array for hearing enhancement," J. Acoust. Soc. Am. **95**, 2990.

Mikhael, W.B., Wu, F.H., Kazovsky, L.G., Kang, G.S., and Fransen, L.J. (1986). "Adaptive filters with individual adaptation of parameters," IEEE Trans. Circuits and Systems **33**, 677–685.

Monzingo, R.A. and Miller, T.W. (1980). *Introduction to Adaptive Arrays.* (Wiley, NY).

Nagumo, J. and Noda, A. (1967). "A learning method for system identification," IEEE Trans. Automatic Control **12**, 282–287.

Nehorai, A. and Malah, D. (1980). "On the stability and performance of the adaptive line enhancer," Proc. IEEE Int. Conf. Acoustics, Speech, and Signal Processing **ICASSP-80**, 478–481.

Owsley, N.L. (1985). "Sonar array processing", in *Array Signal Processing*, edited by S.S. Haykin. (Prentice Hall, Englewood Cliffs, NJ).

Papoulis, A. (1984). *Probability, Random Variables, and Stochastic Processes.* (McGraw-Hill, New York).

Parry, J. (1990). "Microphone arrays for desktop computers and speech recognition," Proc. IEEE Int. Conf. Acoustics, Speech, and Signal Processing **ICASSP-90**, 1149–1151.

Peterson, P.M. (1986). "Simulation of the impulse response between a single source and multiple, closely-spaced receivers in a reverberant room," J. Acoust. Soc. Am. **80**, 1527–1529.

Peterson, P.M. (1989). *Adaptive array processing for multiple microphone hearing aids.* Ph.D. Thesis, M.I.T.; available as Technical Report No. 541 of the Research Laboratory of Electronics, M.I.T.

Peterson, P.M., Wei, S.-M., Rabinowitz, W.M., and Zurek, P.M. (1990). "Robustness of an adaptive beamforming method for hearing aids," Acta Otolaryngologica Suppl.**469**, 85–90.

Plomp, R. (1977). "Acoustical aspects of cocktail parties," Acustica **38** 186–191.

Plomp, R. (1978). "Auditory handicap of hearing impairment and the limited benefit of hearing aids," J. Acoust. Soc. Am. **63**, 533–549.

Reddy, V.U., Paulraj, A., and Kailath, T. (1987). "Performance analysis of the optimum beamformer in the presence of correlated sources and its behavior under spatial smoothing," IEEE Trans. Acoustics, Speech, and Signal Processing **ASSP-35**, 927–936.

Schwander, T.J. and Levitt, H. (1987)."Effect of two-microphone noise reduction on speech recognition by normal-hearing listeners," J. Rehab. Res. Dev. **24**, 87–92.

Shan, T.J. and Kailath, T. (1985). "Adaptive beamforming for coherent signals and interference," IEEE Trans. Acoustics, Speech, and Signal Processing **ASSP-33**, 527–536.

Smedley, T.C. and Schow, R.L. (1990). "Frustrations with hearing aid use: Candid reports from the elderly," Hearing J. **43**, 21–27.

Soede, W., Berkhout, A.J., and Bilsen, F.A. (1993a). "Development of a directional hearing instrument based on array technology," J. Acoust. Soc. Am. **94**, 785–798.

Soede, W., Bilsen, F.A., and Berkhout, A.J. (1993b). "Assessment of a directional microphone array for hearing-impaired listeners," J. Acoust. Soc. Am. **94**, 799–808.

Sondhi, M.M. and Berkley, D.A. (1980). "Silencing echoes on the telephone network," Proc. IEEE **68**, 948–963.

Stadler, R.W. and Rabinowitz, W.M. (1993). "On the potential of fixed arrays for hearing aids," J. Acoust. Soc. Am. **94**, 1332–1342.

Steeneken, H.J.M. and Houtgast, T. (1980). "A physical method for measuring speech-transmission quality," J. Acoust. Soc. Am. **67**, 318–326.

Strang, G. (1988). *Linear Algebra and its Applications: Third Edition.* (Harcourt Brace Jovanovich, San Diego).

Sullivan, M.C. (1993). "A signed maximum correlation multiplier for LMS filter adaptation," IEEE Trans. Signal Processing **41**, 147–151.

Teder, H. (1990). "Noise and speech levels in noisy environments," Hearing Instruments **41**, 32–33.

Van Compernolle, D. (1990a). "Hearing aids using binaural processing principles," Acta Otolaryngologica Suppl. **469**, 76–84.

Van Compernolle, D. (1990b). "Switching adaptive filters for enhancing noisy and reverberant speech from microphone array recording," Proc. Int. Conf. Acoustics, Speech, and Signal Processing **ICASSP-90**, 833–836.

Van Compernolle, D., Ma, W., Xie, F., and Van Diest, M. (1991). "Speech recognition in noisy environments with the aid of microphone arrays," Speech Communication **9** 433–442.

Van Trees, H.L. (1968). *Detection, Estimation, and Modulation Theory.* (John Wiley and Sons, New York).

Van Veen, B.D. and Buckley, K.M. (1988). "Beamforming: A versatile approach to spatial filtering," IEEE ASSP Mag. (April), 4–24.

Wehrmann, R., Van Der List, J., and Meissner, P. (1980). "A noise-insensitive compromise gradient method for the adjustment of adaptive echo cancellers," IEEE Trans. Communications **28**, 753–759.

Weiss, M. (1987). "Use of an adaptive noise canceler as an input preprocessor for a hearing aid," J. Rehab. Res. Dev. **24**, 93–102.

Weiss, M. and Neuman, A.C. (1993). "Noise Reduction in Hearing Aids," in *Acoustical Factors Affecting Hearing Aid Performance*, second edition, edited by G.A. Studebaker and I. Hochberg. (Allyn and Bacon, Boston).

Welker, D.P. (1994). *A real-time binaural adaptive hearing aid.* S.M. Thesis, M.I.T.

Widrow, B., Duvall, K.M., Gooch, R.P., and Newman, W.C. (1982). "Signal cancellation phenomena in adaptive antennas: Causes and cures," IEEE Trans. Antennas Propag. **AP-30**, 469–478.

Widrow, B., Glover, J.R., McCool, J.M., Kaunitz, J., Williams, C.S., Hearn, R.H., Zeidler, J.R., Dong, E., and Goodlin, R.C. (1975). "Adaptive noise cancelling: Principles and Applications," Proc. IEEE **63**, 1692–1716.

Widrow, B., McCool, J.M., Larimore, M.G., and Johnson, C.R. (1976). "Stationary and nonstationary learning characteristics of the LMS adaptive filter," Proc. IEEE **64**, 1151–1162.

Widrow, B. and Stearns, S.D. (1985). *Adaptive Signal Processing.* (Prentice Hall, Englewood Cliffs, NJ).

Yassa, F.F. (1987). "Optimality in the choice of the convergence factor for gradient-based adaptive algorithms," IEEE Trans. Acoustics, Speech, and Signal Processing **35**, 48–59.

Yasukawa, H. and Shimada, S. (1993). "An acoustic echo canceller using subband sampling and decorrelation methods," IEEE Trans. Signal Processing **41**, 926–930.

Zoltowski, M.D (1988). "On the performance analysis of the MVDR beamformer in the presence of correlateed interference," IEEE Trans. Acoustics, Speech, and Signal Processing **ASSP-36**, 945–947.

Zurek, P.M, Greenberg, J.E, and Peterson, P.M. (1990). "Sensitivity to design parameters in an adaptive-beamforming hearing aid," Proc. IEEE Int. Conf. Acoustics, Speech, and Signal Processing **ICASSP-90**, 1129–1132.